Real-Time Flood Forecasting Using Rainfall Forecasts From Numerical Weather Prediction Models

GUNDAPUNENI VENKATA RAO
(Roll No: 717003)

DEPARTMENT OF CIVIL ENGINEERING
NATIONAL INSTITUTE OF TECHNOLOGY
WARANGAL, TELANGANA – 506004, INDIA

JUNE – 2022

Real-Time Flood Forecasting Using Rainfall Forecasts From Numerical Weather Prediction Models

Submitted in partial fulfilment of the requirements
for the award of the degree of

DOCTOR OF PHILOSOPHY
in
CIVIL ENGINEERING

by
GUNDAPUNENI VENKATA RAO
(Roll No: 717003)

Supervisor
Dr. VENKATA REDDY KEESARA
Associate Professor

DEPARTMENT OF CIVIL ENGINEERING
NATIONAL INSTITUTE OF TECHNOLOGY
WARANGAL, TELANGANA – 506004, INDIA

JUNE – 2022

Dedicated to My Dear Wife, Beloved Parents, and Family Members

Every challenging work needs self-efforts, hard work and guidance from elders

NATIONAL INSTITUTE OF TECHNOLOGY WARANGAL

CERTIFICATE

This is to certify that the thesis entitled **"REAL-TIME FLOOD FORECASTING USING RAINFALL FORECASTS FROM NUMERICAL WEATHER PREDICTION MODELS"** being submitted by **Mr. GUNDAPUNENI VENKATA RAO** for the award of the degree of **DOCTOR OF PHILOSOPHY** in the Department of Civil Engineering, National Institute of Technology, Warangal, is a record of bonafide research work carried out by him under my supervision and it has not been submitted elsewhere for award of any degree.

Dr. Venkata Reddy Keesara
Thesis Supervisor
Associate Professor
Department of Civil Engineering
National Institute of Technology
Warangal (T.S) – India

Dissertation Approval

This dissertation entitled **"REAL-TIME FLOOD FORECASTING USING RAINFALL FORECASTS FROM NUMERICAL WEATHER PREDICTION MODELS"** by **Mr. Gundapuneni Venkata Rao** is approved for the degree of **Doctor of Philosophy.**

Examiners

_____

_____

_____

Supervisor(s)

_____

_____

_____

Chairman

_____

Date: _____

Place: _____

DECLARATION

This is to certify that the work presented in the thesis entitled **"REAL-TIME FLOOD FORECASTING USING RAINFALL FORECASTS FROM NUMERICAL WEATHER PREDICTION MODELS"** is a bonafide work done by me under the supervision of **Dr. Venkata Reddy Keesara** and was not submitted elsewhere for the award of any degree. I declare that this written submission represents my ideas in my own words and where others' ideas or words have been included, I have adequately cited and referenced the original sources. I also declare that I have adhered to all principles of academic honesty and integrity and have not misrepresented or fabricated or falsified any idea / data / fact /source in my submission. I understand that any violation of the above will be a cause for disciplinary action by the Institute and can also evoke penal action from the sources which have thus not been properly cited or from whom proper permission has not been taken when needed.

_____

(GUNDAPUNENI VENKATA RAO)

(Roll No: **717003**)

Date: _____

Acknowledgements

Since a research requires ample resources, support and motivation, I would like to thank and extend my gratitude to the ***National Institute of Technology, Warangal (NITW), Virginia Tech University (VT), Blacksburg, USA,*** and the ***Space Application Center (SAC), Ahmedabad*** for giving me the opportunity to work with such wonderful people and their support to complete this thesis work.

First and foremost, I would like to express my deep sense of gratitude to my thesis supervisor ***Dr. Venkata Reddy Keesara***, Associate Professor, Department of Civil Engineering for his continuous monitoring, moral support, patience, encouragement and timely inputs throughout my doctoral study and research work. Despite all the challenges he went through, his guidance was invaluable at every stage of my research, such as organizing funds for attending GIAN program at the IIT Madras, field visit to study area for data collection, for doing internship at the SAC Ahmedabad, and for continuous assistance for our USA visit as a part of SPARC project. The present research would not have been possible without his continuous support. His dedication to research work will always be a source of inspiration for the rest of my life.

I am grateful to ***Ministry of Education (MoE)*** for funding the current research work through the ***Scheme for Promotion of Academic and Research Collaboration (SPARC)*** through project number P270. The funds from MoE under the SPARC scheme have been used to visit the Nagavali and Vamsadhara river basins for collecting field data and for research visit to Virginia Tech University, USA.

In addition to the support I received from my supervisor, I am indebted to ***Dr. Venkataramana Sridhar***, Associate Professor, Department of Biological Systems Engineering, Virginia Tech, Blacksburg, USA. He is the foreign co-PI of SPARC project. Since the first time I met him in 2019, his support and encouragement to complete my research work has been invaluable. Although his presence is remote, he is always willing to help at any time whenever I faced a research problem. I am very grateful for the support and care I received from him during my visit to Virginia Tech. His dedication to his research work and the way he balances his personal and professional life is always an inspiration for me.

It is my pleasure to work as a team member on the SPARC Project with ***Prof. Raghavan Srinivasan*** (Foreign-PI of SPARC Project), Director of the Texas A&M AgriLife Blackland Research and Extension Center, College Station, TX, 77843, USA. He continuously monitored the project and provided moral support, encouragement and timely inputs throughout my research work.

I am thankful to my Doctoral Scrutiny Committee: Chairman ***Dr. P Rathish Kumar***, Professor and Head, Department of Civil Engineering and members ***Dr. N V Umamahesh***, Professor, Department of Civil Engineering, ***Dr. M Shashi***, Assistant Professor, Department of Civil Engineering, and ***Dr. T Ramakrishnudu***, Assistant Professor, Department of Computer Science and Engineering for their continuous monitoring, keen interest, insightful comments and encouragement during active research period.

I am also thankful to ***Prof. Deva Pratap*** and ***Dr. B Umesh*** Department of Civil Engineering, NITW for the moral support given during the period of research work.

I am thankful to ***Dr. Satya Prakash Ojha***, Scientist, SAC-ISRO and ***Dr. Sathiyamoorthy***, Scientist, SAC – ISRO, Ahmedabad, for providing me the opportunity to work as a research trainee under the Satellite Meteorology and OceAnography Research and Training (SMART) programme.

The public access to rainfall and temperature data and best track of tropical cyclones provided India Meteorological Department (IMD), WRF model and GFS data provided by NCAR, streamflow data provided by Mahanadi & Eastern Rivers Organization (M&ERO) Central Water Commission (CWC), Bhubaneswar India, flood inundation maps provided by National Remote Sensing Center (NRSC) are gratefully acknowledged.

I am thankful to ***Dr. Deepak Gopalakrishnan***, Post-Doctoral researcher, New York University Abu Dhabi for all the help and support during the period of my research work.

I thank my fellow research scholars ***Mr. K Kumar, Mrs. K Sreelatha, Mr. K Satish Kumar, Mr. Sagar Banavath, Mrs. B Aneesha Satya, Mr. K Ramabrahmam, Mr. N Nageswara Reddy, Mr. A Ayyappa Reddy, Dr. P Naga Sowjanya, Dr. P Shirisha, Mr. B Eswar Sai, Mrs. K N Loukika, Mrs. S L S Vani Jayanthi, Mr. M Teja, Mr. V Guru Pratap, Dr. K V Koteswara Rao, Dr. Oggu Praveen, Dr. Kavin Kumar, Dr. P Chandra Sai and Mr. V Manikanta*** for their direct or indirect help throughout the period of research work and creating an enjoyable and fun work environment. Last but not the least I extend my biggest and whole hearted thanks to my parents ***Mr. Gundapuneni Venkata Ratnam*** and ***Mrs. Gundapuneni Ramadevi,*** family members ***Mr. Y Srinu, Mrs. Laxmi, Mr. P Mallikarjuna, Mrs. Anuradha, Ms. Sai Jahnavi, Ms. Harini, Mr. Lokesh, Mr. Janaki Ram, Mr. P Srinivasulu, Mrs. P Ravanamma, and Mr. P Praveen*** for standing with me in testing times and offering good moral support all these years. Thanks are due to my wife ***Mrs. P Bhargavi*** for her affection and encouragement throughout the research period.

Gundapuneni Venkata Rao
Roll No: 717003

Abstract

The intensity and frequency of rainfall extremes have increased all over the world as a result of climate change. The increase in intensity and frequency of rainfall extremes has significant impact on human life and infrastructure, particularly by contributing to floods. Floods are the most common natural disasters in India that have significant impact on human life and infrastructure. Due to lack of proper flood forecasting and warning system, authorities are frequently struggling to evacuate the people from the flood prone areas. If the information about floods and flood inundation extent is made available to the public with sufficient lead time, they can be better prepared to deal with floods. Therefore, it is necessary to understand the rainfall characteristics over the study basins and to develop an integrated hydrologic and hydraulic model based on rainfall forecasts from the Numerical Weather Prediction (NWP) models to forecast floods with sufficient lead time. In the present research work, Nagavali and Vamsadhara basin are considered as study area. These two medium sized east flowing basins in Peninsular India are prone to frequent flooding due to heavy rainfall in the monsoon season and tropical cyclones formed by low pressure depressions in the Bay of Bengal (BoB) during pre- and post-monsoon seasons. Based on the proposed objectives of the research work, detailed methodology for the research is developed. With the developed methodology, work has been carried out in five modules.

In the first module, trends in rainfall and rainfall extremes over Nagavali and Vamsadhara river basins are studied at three time steps (long-term (1901-2018), pre-1950, and post-1950) with four different Mann-Kendall (MK) tests using daily gridded India Meteorological Department (IMD) rainfall data of 118 years (1901–2018). The spatial patterns of the trends are evaluated with the kriging interpolation method. Magnitude in rainfall and rainfall extremes (Consecutive Dry Days (CDD), Consecutive Wet Days (CWD), annual total precipitation in wet days (PRCPTOT), annual count of days when rainfall is greater than 10 mm (R10MM), greater than 20 mm (R20MM), greater than 40 mm (R40MM), 95th percentile of rainfall on wet days (R95PTOT), monthly maximum 1-day rainfall (RX1DAY), and monthly maximum consecutive 5-day precipitation (RX5DAY)) are analyzed using the Sen's slope method. Except in the monsoon season, a decreasing trend is observed in all the rainfall extremes in post-1950 compared to pre-1950 period. Whereas, in the monsoon an increasing trend is observed for the extremes in post-1950 period. Overall period (i.e. 1901–2018) an increasing trend is observed for rainfall and rainfall extremes in pre-monsoon (March–May), monsoon (June–September)

seasons and a decreasing trend in winter season (December–February) for both basins. No obvious trends are evident in the post-monsoon season (October–November). At the annual scale, rainfall and rainfall extremes exhibited an increasing trend. Overall, Nagavali basin experienced more extreme rainfall events indicating the higher vulnerability of floods while the middle and lower portions of Vamsadhara basin shown increase in rainfall extremes. A vast majority of the people in both the basins are dependent on agriculture for their livelihoods, and the increasing trends in rainfall and rainfall extremes in the lower and middle portions of both basins are causing frequent floods. Therefore, this study deserves careful extension, especially in the lower and middle portions of both basins, to evaluate extreme hydrologic-hydraulic flow regimes.

In the second module, Advanced Research Weather Research and Forecasting (WRF) model is used to conduct, a total of 56 numerical experiments and to find a suitable microphysical scheme for the prediction of track and intensity of the Tropical Cyclones (TCs) over North Indian Ocean (NIO). The performance of seven microphysical schemes (Ferrier, Lin, Morrison, Thompson, WSM3, WSM5, and WSM6) are evaluated using error metrics, namely Mean Absolute Error (MAE), Mean Square Error (MSE), Skill Score (SS), Direct Positional Error (DPE) and average track error with respect to observations provided by IMD. From the sensitivity experiments, it is found that the WSM3 scheme can be used as a suitable microphysical scheme for the prediction of TCs over NIO. Along with the track and intensity, rainfall of TCs is well predicted by WRF model. Although WRF model is able to predict rainfall for TCs, the WRF model is sensitive to initial and boundary conditions, grid resolution, representation of physical parameterization schemes, and geographical location. Hence, to overcome the limitations of WRF model, rainfall forecasts from the National Center for Environmental Prediction - Global Forecast System (NCEP-GFS) model are used to forecast floods in the lower and middle portions of both basins.

In the third module, performance skill of the National Center for Environmental Prediction - Global Forecast System (NCEP-GFS) model is evaluated for day-1 to day-5 forecast with a threshold of 1 mm/day in Nagavali and Vamsadhara river basins. From the results, the model predicted the rainfall with a correlation coefficient of greater than 0.3 and probability of detection greater than 0.6 for day-1 and day-3 forecasts. The bias in rainfall prediction shifted from overestimation to underestimation by 30% as forecast lead time increased. The total mean error is decomposed into hit, false, and missed bias. The main sources of total mean error are hit bias and false bias. However, missed bias influenced total mean error as lead time increased.

Bias correction is applied for the rainfall events with a rainfall intensity greater than 12 mm/day. Root Mean Square Error (RMSE) improved by more than 18% for day-1 forecast in both Nagavali and Vamsadhara basins, and the improvement ranged between 3% to 9% for other days. In Nagavali basin, relative bias (BIAS) and Mean Error (ME) improved and ranged from 44% to 65% for day-1 to day-5 forecast, whereas in Vamsadhara basin, it ranged from 65% to 93%. This module helped to develop the bias correction factors for GFS forecast rainfall of Nagavali and Vamsadhara basins. Bias corrected GFS forecast rainfall is given as input to the integrated hydrology and hydraulic model developed in fourth module.

In fourth module of the research work, an integrated hydrologic and hydraulic modeling framework is developed with Soil and Water Assessment Tool (SWAT) model and the Two Dimensional (2D) Hydrological Engineering Centre – River Analysis System (HEC-RAS) model. Bias corrected NCEP-GFS rainfall forecasts with a 48-hour lead time are given as input to the integrated model and simulated the streamflow, flood area extent, and depth for the historical flood events (i.e., 1991 - 2018) with peak discharges of 1200 m^3/s in Nagavali basin and 1360 m^3/s in Vamsadhara basin. The integrated model predicted flood inundation depths are in good agreement with observed inundation depths provided by the Central Water Commission (CWC). The inundation maps generated by the integrated modeling system with a 48-hour lead time for cyclone Titli demonstrated an accuracy of more than 75%. The results from this module can be exported into Web-GIS based platform for the visualization and dissemination of flood inundation maps to the public.

In the fifth module of the work, a Web-GIS based user interface system has been developed by using various programming languages (HTML, CSS, and JavaScript) and software (Visual Studio Code and GeoServer) for the visualization and dissemination of flood inundation maps. The Web-GIS based user interface system displays the flood inundation information as spatial maps and depths in the legend. Finally, integrated model presented in this research work is automated using R and Python programming languages. Methodology developed in this research work can be extended for other river basins. The insights gained from this research are useful for the public and government agencies for dissemination of early warning during the flood events, resource mobilization to protect communities, and sustainable water resources planning and management.

Keywords: Automation, Flood Inundation Area, Flood Forecasts, HEC-RAS, Integrated Model, Rainfall Extremes, SWAT, WRF, and Web-GIS.

Table of Contents

List of Tables

List of Figures

Nomenclature

β	:	Sen's slope estimate
r_k	:	Lag-k autocorrelation coefficient
H_p	:	Hurst phenomenon
$\emptyset^{-1}$	:	Inverse of standard normal distribution function
P_s	:	Simulated value of parameter
P_o	:	Observed value of parameter
O_i	:	ith Observed rainfall value
S_i	:	ith Forecasted rainfall value
O_i^{obs}	:	ith Observed streamflow data
O_i^{sim}	:	ith Simulated streamflow data
O_{mean}^{obs}	:	Mean of observed streamflow data
SW_{ti}	:	Soil water content at the end of the day (mm)
SW_O	:	Amount of initial soil water content on day i (mm)
R_{dayi}	:	Amount of precipitation on day i (mm)
Q_{surfi}	:	Amount of surface runoff on day i (mm)
E_{ai}	:	Amount of evapotranspiration on day i (mm)
W_{seepi}	:	Amount of water entering the vadose zone from the soil profile on day i (mm)
Q_{gwi}	:	Amount of return flow on day i (mm)
$\frac{\partial u}{\partial t}$	:	Local acceleration with time
$c_f u$	:	Bed friction
fv	:	Coriolis effect
y	:	Flood discharge values
μ	:	Mean
σ	:	Standard deviation
R_i	:	Rank
K_T	:	Change point
p	:	Probability of Significance
S_h	:	Forecasted hit events`
O_h	:	Observed hit events

O_m	:	Observed miss events
S_f	:	Forecasted false events
SS_i	:	Skill score
$V(S)$	:	Variance of S
$C_n(H_p)$	:	Hurst matrix

Abbreviations

APSDMA	:	Andhra Pradesh State Disaster Management Authority
ARS	:	Agricultural Research Service
AS	:	Arabian Sea
BF	:	Bias Factor
BIAS	:	Bias
BMA	:	Bayesian Model Average
BMJ	:	Bettes-Miller-Janjic
BoB	:	Bay of Bengal
CC	:	Correlation Coefficient
CDD	:	Consecutive Dry Days
CMP	:	Cloud Microphysics
CPS	:	Cumulus Parameterization Scheme
CRA	:	Contiguous Rain Area
CRD	:	Climate Research Division
CSI	:	Critical Success Index
CSS	:	Cascading Style Sheet
CWC	:	Central Water Commission
CWD	:	Consecutive Wet Days
CyberFlood	:	Flood disaster CYBER-infrastructure platform
DEM	:	Digital Elevation Model
DPE	:	Direct Positional Error
DST	:	Decision Support Tool
DWE	:	Diffusive Wave Equations
ECMWF	:	European Center for Medium Range Weather Forecasts
EPS	:	Ensemble Prediction System
ETCCDI	:	Expert Team on Climate Change Detection and Indices
FAR	:	False Alarm Ration
FFA	:	Flood Frequency Analysis
FMM	:	Frequency Matching Method
FV3	:	Finite-Volume Cubed-Sphere
GD	:	Grell-Deveyani

GDAS	:	Global Data Assimilation System
GFS	:	Global Forecasting System
GIS	:	Geographical Information System
GSI	:	Grid point Statistical Interpolation
GSM	:	Global Spectral Model
GTS	:	Global Telecommunications System
HBV	:	Hydrologiska Byråns Vattenbalansavdelning
HEC-HMS	:	Hydrologic Engineering Center-Hydrologic Modelling System
HEC-RAS	:	Hydrologic Engineering Center-River Analysis System
HRU	:	Hydrological Response Unit
HTML	:	HyperText Markup Language
IFIS	:	Iowa Flood Information System
IHIP	:	Intelligent Hydro-Informatics Integration Platform
IMD	:	India Meteorological Department
ISRIC	:	International Soil Reference and Information Centre
JMA	:	Japan Meteorological Agency
JS	:	JavaScript
KF	:	Kain-Fritsch
LAFS	:	Limited area Analysis and Forecast System
LR	:	Logistic Regression
LTP	:	Long-Term Persistence
LULC	:	Land Use and Land Cover
M&ERO	:	Mahanadi & Eastern Rivers Organization
MAE	:	Mean Absolute Error
ME	:	Mean Error
MK	:	Mann – Kendall
MOS	:	Model Output Statistic
MSE	:	Mean Square Error
MSLP	:	Mean Sea Level Pressure
MSW	:	Maximum Sustained Wind
MWO	:	World Meteorological Organization
NCAR	:	National Center for Atmospheric Research
NCEP	:	National Center for Environmental Prediction

NCMRWF	:	National Center for Medium Range weather Forecasting
NCUM	:	NCMRWF Unified Model
NGFS	:	NCMRWF's Global Forecast System
NN	:	Neural Network
NOAA	:	National Oceanic and Atmospheric Administration
NRSC	:	National Remote Sensing Center
NWP	:	Numerical Weather Prediction
PBL	:	Planetary Boundary Layer
POD	:	Probability of Detection
PRCPTOT	:	Annual Total Precipitation in Wet Days
R10MM	:	Annual Count of Days When Rainfall > 10 mm
R20MM	:	Annual Count of Days When Rainfall > 20 mm
R40MM	:	Annual Count of Days When Rainfall > 40 mm
R95PTOT	:	95^{th} Percentile of Rainfall on Wet Days
RM	:	Running Mean
RMSC	:	Regional Specialized Meteorological Centre
RMSE	:	Root Mean Square Error
RRTM	:	Rapid Radiative Transfer Model
RX1DAY	:	Monthly Maximum 1-Day Rainfall
RX5DAY	:	Monthly Maximum Consecutive 5-Day Rainfall
SAS	:	Simplified Arakawa Schubert
SDSS	:	Spatial Decision Support System
SHyFT	:	Statkraft Hydrologic Forecasting Toolbox
SOS	:	Sensor Observation Service
SRTM	:	Shuttle Radar Topography Mission
SST	:	Sea Surface Temperature
SUFI - 2	:	Uncertainty in Sequential Uncertainty Fitting – 2
SWAT	:	Soil and Water Assessment Tool
SWE	:	Shallow Water Equations
TCs	:	Tropical Cyclones
TSS	:	True Skill Score
UIS	:	User Interface System
URL	:	Uniform Resource Locator

USDA	:	United States Department of Agriculture
USGS	:	US Geological Survey
VGI	:	Volunteer Geographic Information
WebFRIS	:	Web-based Flood Risk Information System
WFS	:	Web Feature Service
WMS	:	Web Map Service
WPS	:	WRF Pre-processing System
WRF	:	Weather Research and Forecasting
WRF-DA	:	WRF Data Assimilation
WSE	:	Water Surface Elevation
WSF	:	WRF Software Framework
WSM3	:	WRF Single Moment 3-Class
WSM5	:	WRF Single Moment 5-Class
WSM6	:	WRF Single Moment 6-Class
WSN	:	Wireless Sensor Networks
YSU	:	Yonsei University

Chapter - 1 Introduction

1.1 Background

Over the years, climate on the Earth has changed significantly in both space and time. The spatio-temporal variability of climate and climate drivers have caused changes in the frequency, magnitude, duration, spatial extent, and timing of weather and climate extremes such as floods, droughts, and tropical cyclones, which have significant impact on human life and infrastructure (Han and Coulibaly 2017). The extreme events caused by climate change over the past two decades have resulted in a direct loss of ₹ 265.5 trillion in terms of purchasing power parity and a human loss of more than 4.9 million across the globe (Mohanty 2020). Rainfall is one of the most important climate variable that vary both in space and time, and its response in modifying the basin scale hydrological processes are critical for water resources management. The uneven distribution of rainfall intensities leads to increased incidents of extreme events and their intensities often lead to floods or droughts (Roy and Balling 2004).

Floods are one of the most common natural hazards, causing significant damage to human lives, and infrastructure in both developing and developed countries in the world (Chowdhuri et al. 2020; Han and Coulibaly 2017; Sravani 2018). Flood is defined as "High-water stages in which water over flows its natural or artificial banks onto normally dry land, such as river inundating its floodplain" (Natarajan and Radhakrishnan 2020). The recently published World Disaster Report by International Federation of Red Cross and Red Crescent Societies "IFRC" reported that floods (41%) constituted the largest percentage of all known disasters between 2008 and 2017 all over the world and affected as many as 730 million people, which is over a third of the estimated 2 billion people affected by natural hazards (IFRC 2020).

Past experiences indicate that floods and their impact can be mitigated but cannot be eliminated completely. The measures of flood risk mitigation can be divided into three major categories: (i) structural measures (ii) non-structural measures and (iii) a combination of structural and non-structural measures. Structural flood protection measures such as dams, levees, embankments, and flood wall, emphasize modifying a flood characteristic to reduce peak evaluations and spatial extent (Sudheer et al. 2019). However, these measures will not completely eliminate the hydraulic risk due to the impossibility of building larger structures to handle extremely low probability events (Perumal et al. 2011). As a result, experts have advocated a shift away from

structural flood protection measures to non-structural flood protection measures that reduce flood exposure (Jain et al. 2018). Flood forecasting is an important non-structural measure for preventing flood damage and reducing flood-related deaths and it is only beneficial if accurate forecasts are made with sufficient lead time (Nanditha and Mishra 2021). In recent years, technological advancements have enhanced the accuracy of real-time flood forecasting and warning systems. The use of rainfall observations from satellites, weather radars, and Numerical Weather Prediction (NWP) models significantly improved the capability of flood forecasting and warning systems in detecting extreme rainfall events that may cause flooding and the warnings are issued several days ahead when compared to flood forecasting systems based on the observed rainfall and streamflow (Kumar et al. 2020).

1.2 Extreme Climate Scenarios in India

India, with its unique geophysical conditions, climatic conditions, and topography, frequency, magnitude, duration, spatial extent, pattern and timing of weather and climate extremes are changing and ranked among the top ten most vulnerable countries in the globe in terms of climate change (Eckstein et al. 2021). Over the past five decades, the annual mean temperature has risen by approximately 0.7° C, including an increase of 0.63°C for the warmest day and 0.4°C for the coldest night. The Sea Surface Temperature (SST) has risen by 1° C. Since 1951, summer monsoon rainfall has declined by 6% with an increase in frequent dry and wet spells (Krishnan et al. 2020). As a result of these changing phenomena, cyclones are occurring more frequently throughout the country, droughts are affecting more than half of the country, and floods of unprecedented magnitude are causing catastrophic damage to people and socio-economic aspects of the country (Krishnan et al. 2020). Figure 1.1 shows the various disaster prone areas in India. The major disasters in the country include droughts, floods, tropical cyclones, earthquakes, and hot and cold waves.

Over the past few decades, several researchers have reported an increase in extreme rainfall events across India on a national and regional scale (Bisht et al. 2018a,b; Deshpande et al. 2016; Dubey and Sharma 2018; Goswami et al. 2006; Jain et al. 2017; Guhathakurta et al. 2011; Krishnamurthy et al. 2009). In addition to that, the frequency and intensity of Tropical Cyclones (TCs) are also increasing over the years (Mohanty et al. 2012). The increasing trend in rainfall extremes and the frequency of TCs lead to severe flooding across the country.

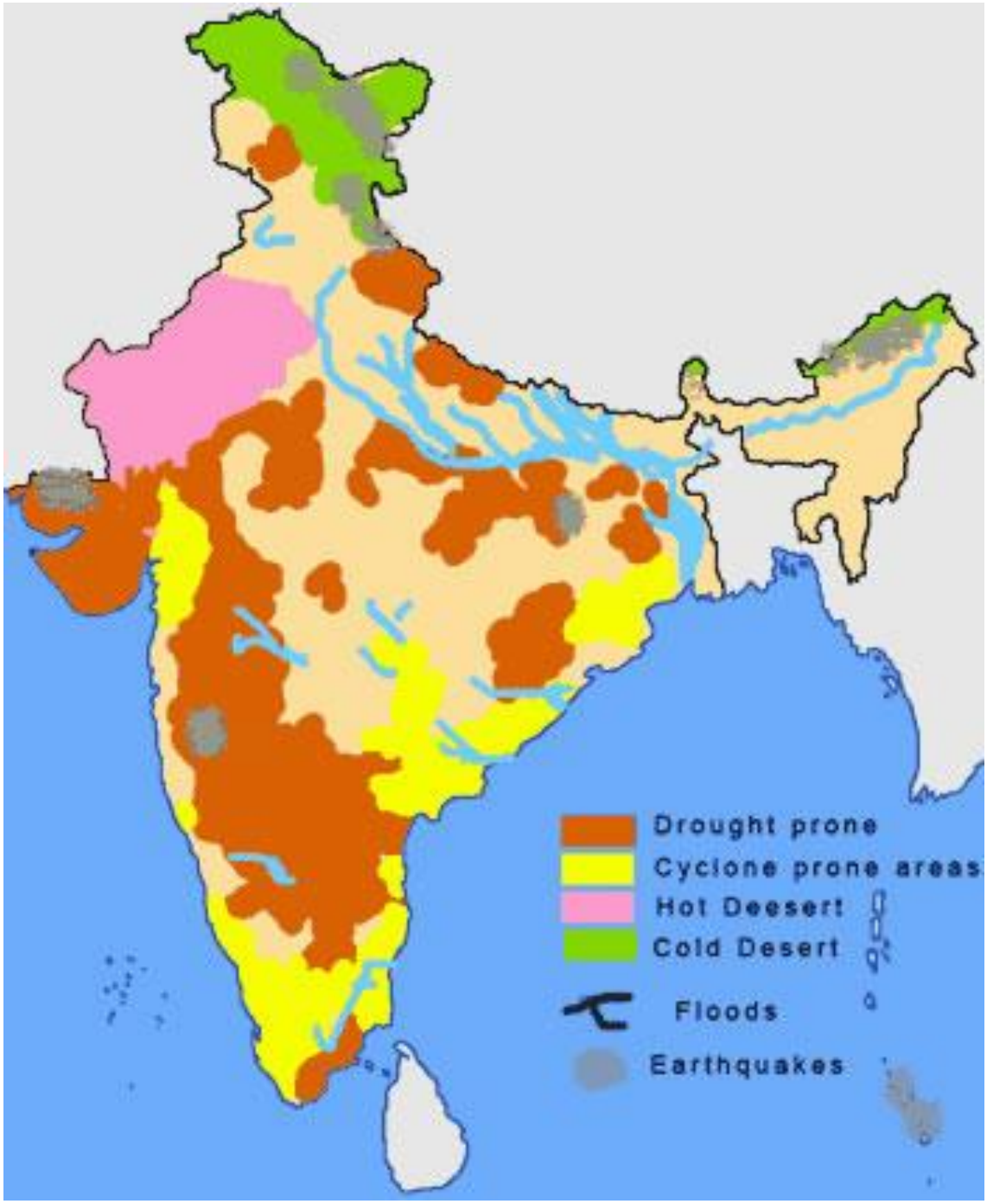

Figure 1.1 Natural hazard map of India (Source: MOI, 2022)

Among all the natural disasters, flooding is becoming more common in India as extreme weather events become very common, accounting for half of the natural disasters (Patankar 2020). Figure 1.2 shows the flood prone areas in the country (NDMA, 2022). Based on the flood patterns in India, the country has four distinct regions: the Brahmaputra river region, the North-West river region, the Ganges river region, and the Central India and Deccan region. Brahmaputra river region is located in the North-Eastern Parts of India. Continuous rainfall in this region has resulted in frequent floods. The frequent earthquakes and landslides in this area have disrupted the natural regime of river flow. As a result, regions that are expected to be flood-proof may not be so secure. North-West river region is located in the North-Western states of India. Compared to other regions of India, this region is relatively less prone to floods.

The Ganges river basin covers most of North India and a few states in Western India. This region is prone to severe floods due to heavy rainfall, river erosion, and massive sediment deposits. The Central India and Deccan river basins cover all states of southern India. The region is characterized by coastal states, which are prone to maritime flooding during cyclonic disturbances. In this region, most rivers have adequate water carrying capacity within the natural banks, except in the lower reaches and the delta area. In those areas, the overall slope of the bed is very low, which aggravates flooding problems, since the water cannot easily drain into the sea due to opposing tidal intrusion (Mohanty et al. 2020).

According to flood statistics from the Government of India, the flood-affected area in India has increased from 25 million hectares (Mha) in 1952 to 49.815 Mha in 2011 (Bhanduri 2019). Between 1953 and 2011, floods claimed 1,653 lives per year on average and caused ₹ 2709 billion in economic losses, includes housing, public property, and crop damage, according to government records (Joshi 2020). Flood damage is caused by a number of factors, including rapid population growth, rapid urbanization, increased development and other activities in flood plains, and global warming (Leon et al. 2014; Bhatt et al. 2017).

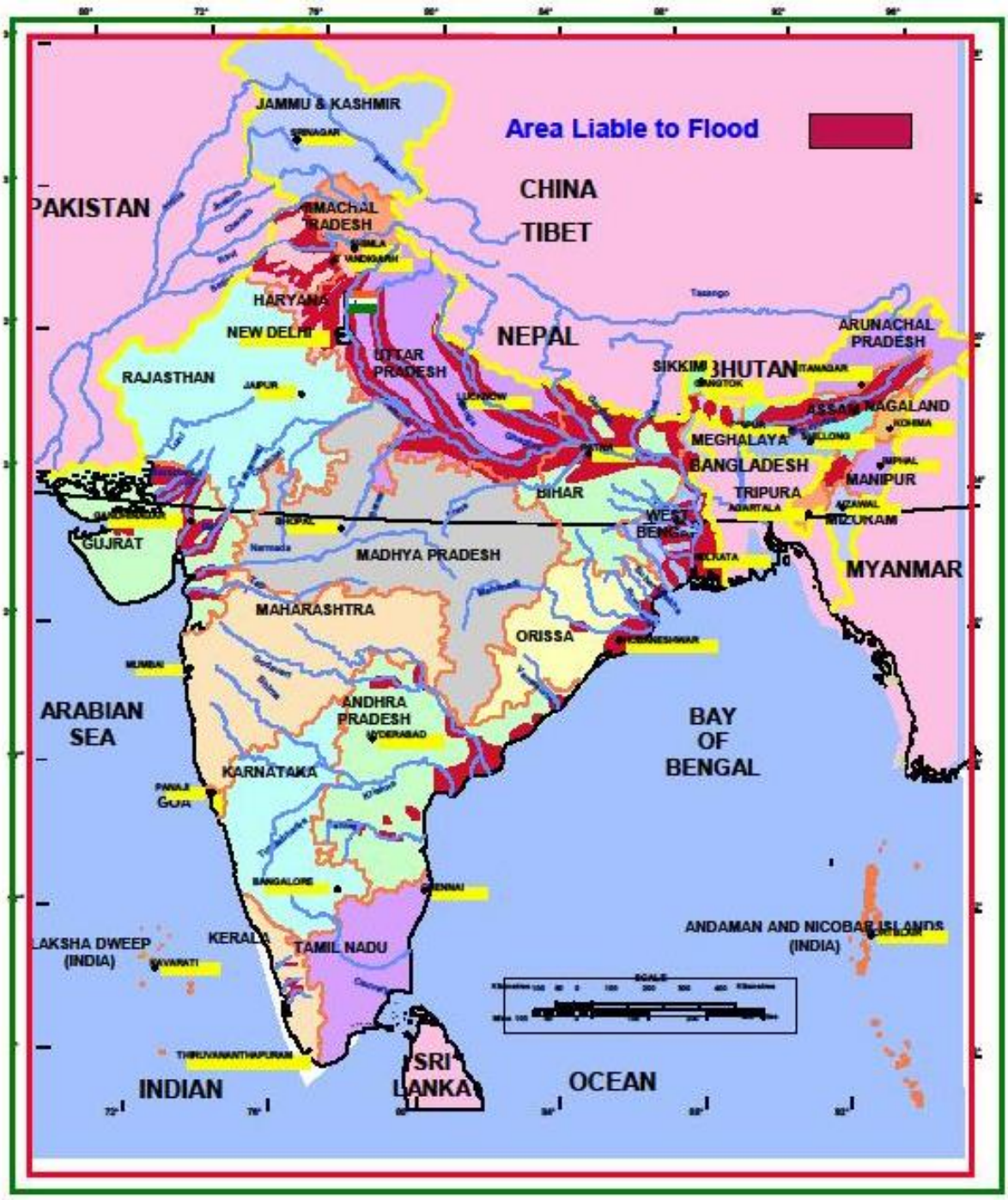

Figure 1.2 Flood prone area in India according to NDMA (Source: NDMA, 2022)

1.3 Rainfall forecasts from Numerical Weather Prediction (NWP) Models

Rainfall is the most important natural weather element required for an effective operational flood forecasting system in a catchment (Bisht et al. 2018a,b; Damrath et al. 2000; Deng et al. 2018; Ning et al. 2017; Prakash et al. 2018; Sun et al. 2017). Rainfall forecasts are currently provided using conventional methods such as satellite observations, weather radars, and NWP models. Among the observations, satellites and weather radars provide qualitative forecasts, while NWP models provide quantitative forecasts (Sridevi et al. 2020). Hence, quantitative rainfall forecasts from NWP models that represents land-atmospheric interactions continue to be the primary source of rainfall data for input into any hydrological model for flood forecasting, water management and disaster assessments among other applications (Sridhar et al. 2013; Shahrban et al. 2016; Sujatha and Sridhar 2017; Sridhar and Valayamkunnath 2018).

The NWP modeling is a method of forecasting future atmospheric conditions by solving a set of mathematical equations that describe the physical phenomenon of the atmosphere. Typical examples of these equations are equations of heat exchange, continuity equations, balance equations of water vapour, equations of motion, parameterizations for solar radiation, and laws of energy conservation, etc. Since 1946, NWP models are being used to forecast rainfall, temperature, and many other meteorological variables from the oceans to the top of the atmosphere (Shrestha et al. 2012). These models are available at both global and regional scales across the world. The global models are defined for the whole world, while the regional model is defined for a particular section of the atmosphere. Advanced Research Weather Research and Forecasting (WRF), Global Forecasting System (GFS), European Center for Medium-Range Weather Forecasts (ECMWF) are some examples of NWP models.

1.3.1 Advanced Research Weather Research and Forecasting (WRF) Model

The WRF modeling system has been in development for the past eighteen years. The current edition is Version 4, available since June 2018. The modeling software is in the public domain and freely available for community use. The Mesoscale and Microscale Meteorology Division of National Center for Atmospheric Research (NCAR) is currently maintaining and supporting a subset of the overall WRF code that includes the WRF Preprocessing System (WPS), WRF Software Framework (WSF), Advanced Research WRF (WRF) dynamic solver, WRF Data Assimilation (WRF-DA) system, and hybrid data assimilation capabilities.

WRF is designed to be a flexible, state-of-the-art atmospheric simulation system that is portable and efficient on available parallel computing platforms. WRF is suitable for use in a broad range of applications across scales ranging from meters to thousands of kilometers, including idealized simulations (e.g. les, convection, baroclinic waves), data assimilation research, parameterization research, forecast research, coupled-model applications, fire research, hurricane research, real-time NWP, regional climate research, and teaching, etc.. A detailed description about the model can be found at Wang et al. 2018.

1.3.2 Global Forecasting System

The Global Forecast System (GFS) of the National Center for Environmental Prediction (NCEP) is a medium range hydrostatic NWP model run by the U.S. National Weather Service (NWS). The GFS provides deterministic and probabilistic guidance on weather data for the next 16 days in GRIB2 format. The National Oceanic and Atmospheric Administration (NOAA) Grid point Statistical Interpolation (GSI) 3-D variational ensemble Kalman filter-variational hybrid system is used by the GFS modelling system for data assimilation (Mccorkle et al. 2018). The GFS files are available at a horizontal resolution of 0.25°×0.25° and can be downloaded from NCAR research data archive. The forecast is updated four times per day (00, 06, 12, and 18 UTC). One of the GFS model output variables is accumulated precipitation, where the precipitation forecasts are accumulations starting from the model runtime.

The GFS model went through a major upgrade, and its version 15 forecasts have been available since 12 June 2019. In version 15, the Finite-Volume Cubed-Sphere (FV3) dynamical core replaced the Global Spectral Model (GSM) as the core model. In the GSM model, the horizontal resolutions were T1543 (12.5 km), from 0 to 240 h (0–10 d), and T574 (~ 34 km), from 240 to 384 h (10–16 d). However, in the FV3 model, the horizontal resolution of the model is about 13 km for days 0–16. The model runs are re-gridded to produce precipitation forecasts at 0.25° resolution (NCEP, 2015).

1.4 Evaluation of NWP Model Forecasts

All the NWP models are based on the principle of hydrostatic equilibrium (Šaur 2017). With advancements in computational power, most of the NWP models are able to provide rainfall forecasts with a lead time of 1 – 15 days (Kumar et al. 2020). Accurate rainfall forecasts from NWP models will help in reducing the uncertainty in streamflow forecasts. However, the

rainfall forecasts from NWP models are subject to three types of error (i) Location, (ii) Timing, and (iii) Magnitude, which may limit their usefulness for streamflow forecasting, since hydrological models are sensitive to errors in rainfall forecasts (Sridevi et al. 2020). Therefore, the skill of NWP model rainfall forecasts needs to be verified before using them for any hydrometeorological applications.

Verification of a forecast involves comparing the forecast value with an observation of what actually occurred or with some reasonable estimate of the actual value. It can be qualitative or quantitative. In either case, it should provide information about the nature of the forecast error. Verification of forecast is important to monitor and improve the forecast quality, and to compare the quality of different forecast systems.

To verify the NWP model forecasts, several methods are available (i) eyeball method (ii) dichotomous method (iii) multi-category method (iv) continuous verification method and (v) probabilistic forecast method. The eyeball method is the oldest and most reliable method for verifying data. Data is presented as time series plots and spatial maps, and the degree of agreement between the observed and forecast data is evaluated using the human eye. However, this method is not quantitative and is prone to human errors. The dichotomous method returns 'Yes' if the model predicts rainfall and 'No' if there is no rain. In this method contingency table is used to verify the forecast which includes a large variety of contingency statistics including Probability of Detection (POD), False Alarm Ration (FAR), Critical Success Index (CSI), and True Skill Score (TSS), etc. Multi-category methods also start with a contingency table that shows the frequency of forecast and observed values in different bins. The advantage of this method is that it allows quick identification of forecast error. However, it is difficult to condense the results into a single value. Continuous verification method measures the difference between the forecast value and the observed value using several statistical indices such as Correlation Coefficient (CC), Mean Error (ME), Root Mean Square Error (RMSE), Bias (BIAS) etc. This method needs a set of values to verify the forecast (Broorks et al. 2017).

1.5 Hydrologic and Hydraulic Models for the Simulation of Floods

A hydrological model represents the natural hydrological cycle in a simplified form and is mainly used for understanding, forecasting and managing water resources. The best hydrologic model is the one which is less complex and uses minimum amount of data to produce results that are similar to the observed values. The hydrologic model converts the rainfall into run-off

by considering various hydrological processes including rainfall, evapotranspiration, and surface and sub-surface water flow. The input data required for hydrologic model includes rainfall, temperature, relative humidity, solar radiation, wind speed, Land Use and Land Cover (LULC), Digital Elevation Model (DEM) data, and soil data (Godara and Bruland 2019).

Over the past few decades, several hydrological models have been developed such as Hydrologiska Byråns Vattenbalansavdelning (HBV), MIKE SHE, Statkraft Hydrologic Forecasting Toolbox (SHyFT), Hydrologic Engineering Center-Hydrologic Modelling System (HEC-HMS), TOPMODEL, Soil and Water Assessment Tool (SWAT), etc. for effective management of water resources. Among all the models SWAT is a physically based semi-distributed watershed-scale hydrological model developed by the United States Department of Agriculture (USDA) Agricultural Research Service (ARS). The model is designed to predict the impact of land management practices on hydrology, sediment and contaminant transport in large and complex catchments at the Hydrological Response Unit (HRU) level. For the SWAT model to produce accurate hydrologic predictions, only a small amount of direct calibration is required.

Hydraulic models compute open channel flow based on St. Venant equations. Most commonly used hydraulic models are one dimensional or two dimensional or a combination of both (1D-2D). The hydraulic model converts the run-off into flood inundation levels. The input data required for hydraulic model includes runoff, LULC, soil characteristics, upstream and downstream boundary conditions. Most commonly used hydraulic models include Hydrologic Engineering Center-River Analysis System (HEC-RAS), MIKE 1D and 2D, BreZO, LISSFLOOD-FP, FLO-2D, etc. Among these models, HEC-RAS is one of the most comprehensive and efficient event-based model for preparing flood inundation maps. It can perform 1D, 2D, and combined 1D and 2D modelling. In 2D modelling, HEC-RAS can solve shallow water or diffusive wave equations, allowing the model to run more quickly and have increased stability. The algorithms used in HEC-RAS 2D unsteady flow modelling are capable of handling sudden release of water, supercritical, subcritical, and mixed flow regimes without enabling any additional options.

1.6 Flood Forecasting and Warning System

Flood forecasting and early warning is one of the most effective flood risk management strategies to minimize the negative impact of floods (ESCAP 2017). A typical flood forecasting and warning system is composed of three major elements: (i) flood detection (ii) flood forecasting and warning and (iii) flood response. The schematic representation of flood forecasting and warning system is shown in Figure 1.3.

Flood detection involves the continuous monitoring of hydrometeorological data from the catchment of interest. Flood forecasting involves the use of hydrologic and hydraulic models. Hydrological models are used to convert rainfall into runoff through a set of mathematical equations, while hydraulic models convert runoff into flood extent. Flood warnings are issued at this stage to the people and public agencies to plan rescue operations (Jain et al. 2018).

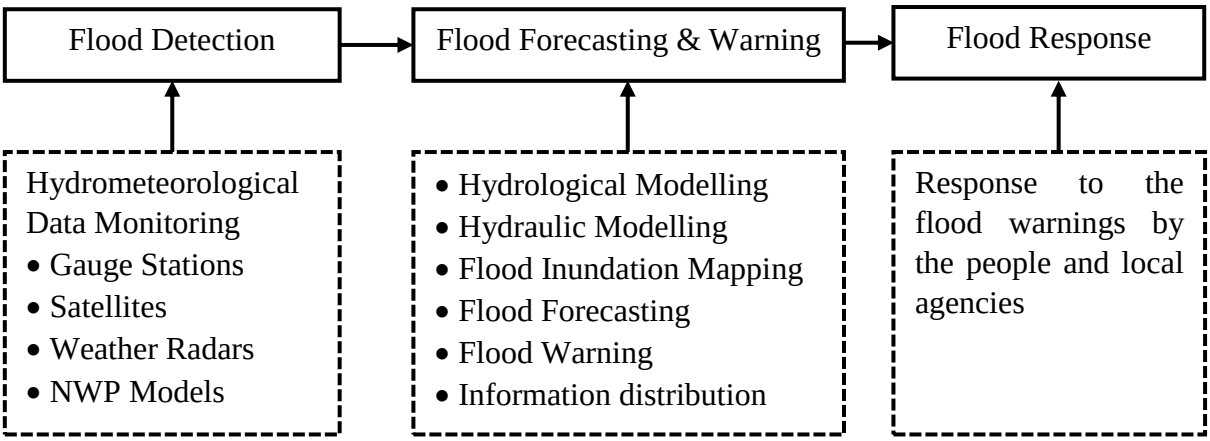

Figure 1.3 Schematic diagram of flood forecasting and warning system (Source: Jain et al. 2018)

1.7 Web-GIS for Dissemination for Flood Inundation Information

A User-Interface System (UIS) is an integrated set of software and hardware components that are used for collection, organization, storage, processing and communication of information among the users. Geographical Information System (GIS) is an information system that can acquire, store, and process spatial data. Combining GIS with web technologies enables users to process spatial data, perform spatial analysis and display generated results in the form interactive maps or graphs through the web browser (Mishra et al. 2020). Web-GIS is a distributed open source technology that provides a graphical user interface for accessing spatial data, performing spatial analysis, and visualizing web-services through a web browser. There are several technology levels to publish map data on the web, ranging from sites that simply

public static web maps to more sophisticated sites which support dynamic and interactively customizable maps. Web-GIS technologies are useful to publish flood inundation data and disseminate information to the public.

1.7.1 Web-GIS Architecture

The architecture of the Web-GIS is similar to the typical client/server three-tier architecture and is shown in Figure 1.4. Three tier architecture is one in which an interface is stored on the client side, the application on the server side, and a database on database server. The client side typically consists of a web browser while the server side consists of a web server, map server, web GIS software and a database. The web server communicates between the client and the map server. The map server provides the web server with the map content generated from the database. A web interface is required to take inputs from user interactions and display the requested data.

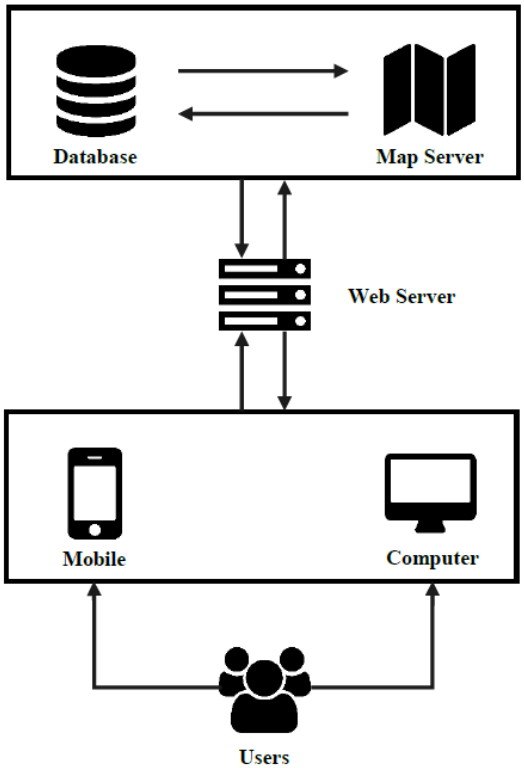

Figure 1.4 A typical Web-GIS Architecture (Source: Olaya 2018).

1.7.2 Web-GIS systems for flood data dissemination

The goal of flood risk communication is to provide flood related information to wide range of users, ranging from the general public at local level to administrative bodies at governance level. In recent years, Web-GIS based platform has been recognized as a powerful tool for data distribution, as it is cheap, reliable, interactive, and can easily reach people in a short period of time. Researchers have developed Web-GIS platforms for dissemination of flood inundation information in different parts of the world, including Iowa Flood Information System (IFIS) (Demir et al. 2018), Flood disaster Cyber-infrastructure platform (CyberFlood) (Wan et al. 2014), Spatial Decision Support System (SDSS) (Horita et al. 2015), geospatial Decision Support Tool (DST) (Knight et al. 2015), Intelligent Hydro-Informatics Integration Platform (IHIP) (Chang et al. 2018) , Web-based Flood Risk Information System (WebFRIS) (Mohanty and Karmakar 2021), and many others to provide real-time information about floods.

National Remote Sensing Center (NRSC) in India is the nodal agency for distributing natural disasters related information. NRSC developed a web application called Disaster Management Support Services under Bhuvan to provide forecasts and issue early warning about the natural disasters such as floods, droughts, forest fires, earthquakes, landslides, and cyclones across the country.

1.8 Research Motivation

The intensity and frequency of rainfall extremes have changed as a result of climate change, which has a significant impact on human life and infrastructure, particularly by contributing to floods. Floods are the most common natural disasters in India that have significant impact on human lives and infrastructure. In recent years, India has been hit by some of the most unusual extreme precipitation events, resulting in flooding and significant loss of life. On 26th July 2005, Mumbai received 994 mm of rainfall in 24 hours, leading to flash floods and landslides that claimed 419 lives and damaged 16000 cattle. During the floods, more than 100000 residential and commercial establishments as well as 30000 vehicles were damaged (Gupta 2007). In 2007, Bihar state received unprecedented rainfall of more than 300 to 400% than in normal days in the second half of July. The same was repeated in August and simultaneously heavy rainfall in the upper catchments led to severe floods in the state and claimed 519 lives and more than 20 million people got affected causing an economic damage of ₹ 150 billion (FMISC 2007). Heavy rainfall in October 2009 in the Krishna river basin resulted in severe floods in Kurnool city that

claimed more than 40 lives and caused significant damage to infrastructure (Ramachandraiah 2011). During 16-18 June 2013, Uttarakhand experienced an extreme rainfall event with a rainfall intensity of more than 200 mm/day, resulting in large floods that killed over 6000 people and caused economic losses of more than ₹ 285 billion (Nandargi et al. 2016). In December 2015, Chennai and its suburbs experienced extremely heavy rainfall (490 mm/day), inundating the coastal districts of Chennai, Kancheepuram, and Tiruvallur, affecting over 4 million people causing economic damages of approximately ₹ 225 billion (Narasimhan et al. 2016). A multi-day extreme precipitation event (200 mm/day) in Kerala in August 2018 caused massive flooding, killing 483 people and causing an economic loss of more than ₹ 3975 billion (Mishra et al. 2018). Because of a tropical depression that formed over the Bay of Bengal (BoB) in October 2020, Musi River received 192 mm of rainfall in 24 hours, caused flooding in Hyderabad, killing more than 30 people and caused an economic loss of ₹ 6717 million (Somasekhar 2020). If information on floods and flood inundation extents is available to the public with sufficient lead time, people and government agencies will be able to deal with floods in a more effective way.

1.9 Need for the flood forecasting model and information dissemination to the public

The Central Water Commission (CWC) is the nodal agency in India for providing deterministic flood forecasts based on observed precipitation and streamflow across major rivers and their tributaries. Currently, CWC provides flood warnings at 324 stations, including 128 reservoir inflow forecasts and 196 water level forecasts (CWC 2020). During extreme weather events, local agencies use CWC water level forecasts to plan rescue operations (Harsha 2020). However, water level estimates at a point are inconsistent and sparse over large areas, resulting in uncertainty in estimating flood inundation area and flood depth, making rescue operations difficult for local agencies. This is especially true following the recent floods in Assam, Tripura, Karnataka, Tamil Nadu, and Kerala (CWC-FRMD 2020). Local administrations can make better decisions and be better prepared if they have flood forecasts with inundation areas rather than deterministic flood forecasts. Countries such as the United States, the European Union and Japan have already shifted their focus to flood forecasting and inundation areas (Harsha 2020). In India, public and government officials have limited information about the flood inundation extent and depth. As a result, there is a need for development of integrated hydrologic and hydraulic models with enough lead time to provide flood forecasts as well as flood inundation

extent and depth. The results from the integrated hydrologic and hydraulic model can be exported into Web-GIS compatible formats using GIS software for visualization and analysis in the web-based platform (Santillan et al. 2020).

Nagavali and Vamsadhara are two east flowing medium sized river basins that are prone to flooding due to heavy rainfall in the monsoon season and TCs formed by low pressure depressions in the BOB during the pre- and post-monsoon seasons. In both basins, an increase in annual average rainfall of 100 mm has been observed over the previous two decades. The uplands of these basins are hilly, resulting in frequent flooding of low-lying areas due to extreme rainfall events. Over the last few decades, the frequency of prolonged floods has increased, causing severe damage to crops, life, and property in both basins' delta regions. According to the Andhra Pradesh State Disaster Management Authority (APSDMA), the Nagavali basin experienced more than 12 flood events, while the Vamsadhara basin experienced nine flood events. Authorities frequently struggle to evacuate villagers during floods due to a lack of a weather and flood forecasting system in the area. Hence, in the present research work it is proposed to develop an integrated hydrologic and hydraulic model and to apply it on Nagavali and Vamsadhara river basins to forecast floods and inundation area extent.

1.10 Aim and Objectives of the Study

The aim of the present research work is to develop an integrated hydrologic and hydraulic model that forecasts streamflow and generates flood inundation extent based on rainfall forecasts which will be published in Web-GIS based user interface system for the public use. Based on the aim of the research work, the objectives are framed as follows:

- Identification of trends in rainfall characteristics over the study area.
- Assessment of microphysical schemes on the track, intensity and rainfall prediction of tropical cyclones using Numerical Weather Prediction Models.
- Evaluation of rainfall forecasts available in the public domain from standard modelling mechanism.
- Development of an integrated modelling framework to forecast floods with well-established hydrologic and hydraulic models.
- Development of Web-GIS based framework for flood forecast data visualization and dissemination.

1.11 Organization of the Thesis

This thesis has seven chapters which include introduction, literature review, methodology, study area and database preparation, model set-up, results and discussions, and summary and conclusions. The research motivation, problem statement, and research objectives are presented in the introduction chapter. Literature review on rainfall extremes, floods due to extreme rainfall events, prediction of track and intensity of tropical cyclones by NWP model, evaluation of GFS rainfall forecasts, importance of integrated hydrologic and hydraulic models and flood forecasting, and development of Web-GIS have been presented in second chapter. The research methodology is presented in third chapter. The details about study area, data used, database preparation, and various model set-ups such as WRF, SWAT, and HEC-RAS for predicting tropical cyclones, simulating streamflow, and generation of flood inundation maps, respectively are presented in fourth chapter. Results and discussions are given in fifth and sixth chapters, while summary, conclusions, and limitations of the present research are explained in the concluding chapter.

Chapter - 2 Literature Review

2.1 General

Rainfall extremes in the Indian sub-continent are expected to be more often because of global warming. The increase in extreme events causes flooding in India, which has significant impact on human life and infrastructure. CWC is the nodal agency in India that provides deterministic flood forecasts across major rivers and their tributaries. However, the water level estimates at a point are not consistent or dense enough over large areas, and often lead to uncertainty in estimating the flood inundation area and flood depth, making rescue operations difficult for local agencies. Hence, there is a clear need for the modeling framework that can provide data about the present and future state of occurring floods. In this chapter, literature pertaining to rainfall and rainfall extremes, prediction of TCs using WRF model, and performance evaluation of rainfall forecasts from NWP models is presented. The literature required to develop an integrated hydrologic and hydraulic model to forecast floods and development of Web-GIS based data distribution system for the real-time distribution of flood inundation areas has been discussed in the following sections.

2.2 Trends in Rainfall and Rainfall Extremes over India

The spatio-temporal variations in rainfall in India may lead to natural disasters like floods and droughts which have adverse impact on human life and socioeconomic aspects of the country. Hence, there is a need to understand the characteristics of rainfall and rainfall extremes in a river basin to enhance water resources management strategies. Rainfall and extreme rainfall events have been extensively studied in India at regional and national scales using gridded rainfall data provided by India Meteorological Department (IMD) and these have drawn different conclusions (Bisht et al. 2018b,a; Roy and Balling 2004; Goswami et al. 2006; Guhathakurta and Rajeevan 2008; Deshpande et al. 2016; Rajeevan et al. 2008; Ghosh et al. 2012; Guhathakurta et al. 2011, 2015, 2017). Some studies reported no clear trend in rainfall over a period of longer than a century at monthly, seasonal, and annual scales over India (Ghosh et al. 2012; Rajeevan et al. 2008). However, Kumar et al. (2010), reported an increase in the magnitudes of winter, pre, and post monsoon rainfall and decrease in annual and monsoon rainfall at the national scale.

Roy and Balling (2004) studied the annual trends in seven extreme rainfall measurements, including total rainfall, 1, 5, and 30-day cumulative rainfall, and total rainfall at the 90^{th}, 95^{th}, and 97.5^{th} percentiles, at 129 gauge stations distributed across India. They found that, out of 903 time series data sets, 61 showed decreasing trend, and 114 showed increasing trend. The increasing trend in rain extremes has been widely distributed across the country, from the northwest Himalayas to the Deccan Plateau in the south, whereas a decreasing trend has been mostly found in the eastern parts of the Gangetic Plain and parts of Uttaranchal. Goswami et al. (2006) found an increasing trend in the frequency and magnitude of extreme rainfall events accompanied by a decreasing trend in the frequency of moderate rainfall events and no trend was found in seasonal mean rainfall over Central India. The increasing trends in extreme rainfall events at annual and decadal over central India may be attributable to variations in SST over the tropical Indian Ocean (Rajeevan et al. 2008). Guhathakurta and Rajeevan (2008) investigated rainfall patterns across 36 meteorological subdivisions in India. They reported that, the contributions from June, July, and September rainfall were decreasing for a few sub-divisions while August rainfall contributions were increasing to the annual rainfall. This is an indication that the frequency and magnitude of heavy rainfall events are increasing in the August month across the country. Dash et al. (2009) studied the characteristics of rainfall events in India. Based on the intensity of rainfall events, a decreasing trend was observed in low and moderate rainfall events in the hilly region and west central India, but increasing trends in heavy rain events in North-East India. On the basis of the duration of rainfall events, the rainfall event was classified as short, long, wet, dry, and prolonged dry spell. In terms of trends, a decreasing trend in the long spell events and an increasing trend in other categories was observed. The decreasing trend in the long spell events was observed in the west central region of India and increasing trends in other categories were observed in the hilly region, west central region and peninsular India.

Guhathakurta et al. (2011) studied the impact of climate change on extreme rainfall events. They reported that the trends in heavy rainfall events were increasing in peninsular, east and north east India while decreasing in Central and North India. Ghosh et al. (2012) found that the trends in extreme rainfall events within the country were not uniform. Vittal et al. (2013) also found similar results. At a national level, rainfall extremes reported an upward trend whereas at a regional scale, rainfall extremes were exhibited a non-uniform trend. The authors also noted a significant difference in rainfall characteristics (intensity, frequency, and duration) before and after 1950. Guhathakurta et al. (2015) analyzed trends in monsoon rainfall in India as a whole

and four homogeneous regions. The trends in rainfall exhibited multi-decadal variability of rainfall in the country as well as in the regions. However, the phases of multi-decadal variability were different between the country and regions. The change point for all India southwest monsoon was observed in 1965, while the change points for Central, Northwest, Peninsular, and Northeast India were 1926, 1942, 1946, and 1961, respectively. During the southwest monsoon in India, moderate rainfall events (5 mm/day to 100 mm/day) decreased significantly, whereas rainfall events with intensity greater than 100 mm/day were unaffected. Deshpande et al. (2016) examined the temporal changes in rainfall and temperature extremes over major river basins in India. The extreme weather events were defined using thresholds of 10 cm for rainfall and 40°C and 10°C for maximum and minimum temperatures. They found that the number of dry days (zero rainfall) increased across the river basins except at some portions in the Krishna and Peninsular river basins. The rivers in the central part of India show an increasing trend for heavy rainfall events. An increase in the monthly maximum temperature has also been observed in Krishna, Peninsular, and West coast river basins, whereas no such trend was found with regarded to minimum temperature.

Dubey and Sharma (2018) used 19 climate extreme indices based on rainfall and temperature data from regional climate models to analyze the historical and future climate predictions for Banas river basin in Rajasthan. They observed a significant trend in the number of warm days and nights, and a significantly decreasing trend in the number of cold days and nights. The total annual precipitation and the number of days with precipitation intensity greater than 10 mm/day and 20 mm/day in the basin have shown a decreasing trend, while consecutive dry days demonstrate an increasing trend for the historical and future periods. Bisht et al. (2018a, b) analyzed trends in rainfall and rainfall extremes at seasonal and annual scales of over 85 river basins in India from 1901 to 2015. They found that rainfall and rainfall extremes showed an increasing trend for most of the river basins. The Authors found that trends in rainfall and rainfall extremes showed significant difference during pre and post urbanization. Based on the aforementioned literature, it is clear that the patterns and variability rainfall characteristics have been widely investigated at national and regional scales and have drawn different conclusions. Some authors suggested that it is important to carry out trend analysis for rainfall characteristics for a basin at regional level rather than at national level for making better decisions, while others have not been so enthusiastic with the idea.

2.3 Evaluation of NWP Model Forecasts

Increasing rainfall and extreme rainfall events are causing frequent floods in the Indian subcontinent and coastal regions in particular are at high risk for tropical cyclones which form over the BoB. Using NWP models will improve the forecast capability of rainfall and tropical cyclones. WRF is the most commonly used NWP model for predicting the track and intensity of tropical cyclones. In addition to the WRF model, several NWP models are also used for forecasting rainfall. However, the NWP model rain forecasts are subject to three types of errors: location, timing, and magnitude, which may limit their applicability for hydrometeorological applications. Therefore, the skill of NWP model forecasts needs to be evaluated before using them for any hydrometeorological application.

2.3.1 Prediction of Tropical Cyclones over Indian Region using WRF Model

The WRF model has excellent ability to forecast extreme weather events on a high-resolution grid for the research and operational purposes (Moya-Álvarez et al. 2019). However, the ability of the WRF model to predict weather events depends on the initial and boundary conditions, representation of physical parameterization schemes, grid resolution, and geographical location (Di et al. 2015). Accurate representation of cloud processes in NWP models is crucial for the prediction of weather events, particularly for the track and intensity prediction of TCs. Representation of cloud processes plays an important role for the production and distribution of heat, mass, and momentum in the atmosphere in both horizontal and vertical directions based on precipitation, winds, and turbulence. The representation of physical parameterization schemes in NWP model is important, when the cloud processes and their effects are unresolved by the model (Deshpande et al. 2012; Sandeep et al. 2018). In the past two decades, based on several assumptions, researchers have developed a number of physical parameterization schemes for the prediction of weather events. Among all the physical parameterization schemes, Cloud Microphysics (CMP), Cumulus Parameterization Scheme (CPS), Planetary Boundary Layer (PBL), radiation (longwave and shortwave), and land-surface schemes are being used for weather predictions (Jandaghian et al. 2018). The cloud process in the model can be implicitly treated by CPS and explicitly treated by CMP schemes. CPS reduces convective instability in a model through the redistribution of temperature and moisture in a grid column (Wang and Seaman 1997). CMP schemes represent cloud and precipitation processes (e.g. condensation, nucleation, coalescence, phase changes, etc.) according to atmospheric conditions in terms of

temperature, wind, and moisture. Both CPS and CMP schemes control the spatio-temporal variations of rainfall and yield different profiles of moistening and heating in the atmosphere. Without double counting the thermo-dynamical impact, both types of schemes represent the convective activity (Deshpande et al. 2012; Sandeep et al. 2018).

Numerous studies have been conducted to assess the impact of physical parameterization schemes on the prediction of track and intensity of TCs using WRF model. Among all schemes in the WRF model, convective processes play an important role in the development of TCs and boundary layer dynamics in intensification (Chandrasekar and Balaji 2012; Deshpande et al. 2012; Pattanayak et al. 2012; Raju et al. 2011). Microphysical schemes have significant impact on the track prediction of TCs (Raju et al. 2011). Pattanaik and Rama Rao, (2009) found that the movement of Nargis cyclone was captured well with a landfall error of 30 to 40 kilometers (km) by WRF Single Moment 3-Class (WSM3) CMP scheme along with Grell-Deveyani (GD) CPS, Yonsei University (YSU) PBL schemes. (Raju et al., 2011, 2012) conducted 11 sensitivity experiments with different combinations of CPS, CMP, and PBL schemes to find a suitable combination of physical schemes for the track and intensity prediction of Nargis cyclone. They reported that Nargis cyclone was simulated well by Ferrier CMP scheme in combination with Kain-Fritsch (KF) CPS, and YSU PBL schemes. The best set suitable schemes were further used to predict multiple cyclones over the BoB. The experiments revealed that the best suitable schemes predicted the track, intensity, and timing of landfall reasonably well with a mean track error of 98 km at the time of landfall. Pattanayak et al. (2012) found that the track and intensity of TC Nargis was simulated well by Ferrier CMP scheme along with YSU PBL, Simplified Arakawa Schubert (SAS) CPS schemes. With the same CPS and PBL schemes, Kessler CMP scheme provided better results for TC Vardah (Sandeep et al. 2018). Kanase and Salvekar (2015) showed that WSM6 scheme in combination with Bettes-Miller-Janjic (BMJ) CPS and YSU PBL schemes simulated better results for TC Laila. Based on the sensitivity experiments conducted by Srinivas et al. (2013) and Lakshmi and Annapurnaiah (2016), the Lin scheme improved the results for TCs Sidr, Nisha, Tane, Jal, Nargis, and Hudhud along with a combination of Kain-Fritsch (KF) CPS and YSU PBL schemes. With the same combination of CMP and PBL schemes, Choudhury and Das (2017) (Choudhury and Das 2017) suggested the Goddard scheme and Ferrier scheme by Raju et al. (2011) and Reddy et al. (2014) for the prediction of TCs. Osuri et al. (2012) and Mahala et al. (2015) reported that TCs over NIO were simulated well by WRF Single Moment-3 (WSM3) scheme with the same CPS and PBL schemes.

Based on the previous studies, it may be difficult to identify a suitable microphysical scheme for the prediction of TCs over NIO region. Therefore, it is necessary to conduct numerical experiments to revalidate the suggested microphysical schemes for the prediction of TCs over NIO region.

2.3.2 Verification of GFS Model Forecasts

Several studies examined the skill of rainfall forecast by various NWP models: these models include Limited area Analysis and Forecast System (LAFS) (Bhowmik et al. 2007), the Global Spectral Model (GSM) running at National Center for Medium Range weather Forecasting (NCMRWF) (Mandal et al. 2007), the NCEP-GFS (Dube et al. 2014; Durai and Bhowmik 2014; Durai et al. 2010; Mukhopadhyay et al. 2019; Prakash et al. 2016b; Sharma et al. 2015; Sridevi et al. 2020, 2018; Ganai et al. 2021), the Regional Meso-Scale Weather Simulation Model (Singh et al. 2014), and the UK Met Office Unified Model (Dube et al. 2014; Durai et al. 2015; Satyanarayana and Kar 2016; Sharma et al. 2017; Ashrit et al. 2020) over the Indian region.

Durai et al. (2010) evaluated the skill of GFS five-day rainfall forecasts during the monsoon season of the year 2008 against the observed rainfall based on gauge measurements and Kalpana – 1 satellite using various accuracy and skill measures. They found that around the 25 mm/day forecast threshold, expect for day-1 forecast, the bias for rainfall prediction moved from overestimation to underestimation. When there were rainfall thresholds of more than 10 mm/day, the model's accuracy plummeted dramatically. Despite its bias in rainfall prediction, the model was far better at predicting the presence of rain than the magnitude and location of peak values. Dube et al. (2014) verified rainfall forecasts from GFS/T574 and NCMRWF Unified Model (NCUM) for heavy rainfall observed over Uttarakhand region of India on June 17 -18, 2013 using Contiguous Rain Area (CRA) method. They reported that the NCUM model captured the circulation features more realistically than GFS model prediction. However, the NCUM model’s skill in forecasting rainfall was reasonable up to 3 days and forecast skill decreased as lead time increased (Satyanarayana and Kar 2016).

Durai and Bhowmik (2014) verified the prediction skill of GFS T574 and GFS T1534 models over the Indian region for the 2011 summer monsoon season. They reported that both the models were capable of predicting rainfall, specific humidity, and lower tropospheric wind circulation. However, the magnitude of error for these parameters increased as the forecast lead time increased. Sharma et al. (2015) evaluated the medium range rainfall forecasts of

NCMRWF's Global Forecast System (NGFS) over Indian regions during monsoon seasons from 2010 to 2013 using feature based Contiguous Rain Area (CRA) method. The error in rainfall forecast was decomposed into rainfall pattern, location, and volume. They reported that the pattern error contributed more to rainfall forecast error than rainfall volume. Durai et al. (2015) verified quantitative precipitation forecasts from four operational Ensemble Prediction System (EPS) of ECMRWF, UKMO, NCEP, and Japan Meteorological Agency (JMA) over India in the short to medium range time scales. They found that EPS could reproduce seasonal mean rainfall over climatologically heavy rainfall regions. The forecast skill of NCEP and UKMO appeared to be similar to the ensemble mean forecast of EPS. Prakash et al. (2016) evaluated the skill of GFS T574 and GFS T1534 models over South Asia during peak monsoon months. They reported that GFS T1534 performed marginally better than GFS T574. Similar findings were reported for India by Sridevi et al. (2020, 2018). Mukhopadhyay et al., (2019) verified the skill of GFS T1534 model over Indian subcontinent during monsoon seasons in 2016 and 2017 using averaged gauge observations from IMD and rainfall from TRMM satellite data. The model accurately predicted moderate rainfall events. It overestimated rainfall events with light intensity and underestimated rainfall with heavy intensity. The spatio-temporal variations in rainfall were reasonably well captured. The authors suggested further development in the model with adequate input in initial conditions and data to enhance the model's skill in forecasting heavy rainfall events. Similar findings were reported by Ganai et al., (2021). Ashrit et al., (2020) evaluated the capabilities of different numerical models from the NCMRWF in forecasting extreme rainfall event across Kerala during August 2018. They reported that the model forecasts were accurate for short-term lead times (up to 3 days) mainly in terms of timing and to some extent in terms of rainfall intensity.

Based on previous studies, it is clear that the skill of rainfall forecasts from NWP models has been verified across India, and that the models are capable of capturing rainfall over various climatological regions. Though the models are able to capture rainfall, the accuracy in predicting location and magnitude varies considerably which causes systematic bias in forecasting rainfall. Hence, post-processing of rainfall forecasts to reduce bias may be required for operational purposes. The most commonly used post-processing methods are Neural Network (NN) method, Logistic Regression (LR), Bayesian Model Average (BMA), Model Output Statistic (MOS) method, Running Mean (RM), etc. (Durai and Bhradwaj 2014; Fan and Van 2011; Yang et al. 2020; Zarei et al. 2021). Although every bias correction method has its advantages and disadvantages, there is no perfect method for bias correction. For instant, MOS

requires long training periods from a static model, while NN and BMA require extensive computational resources. Furthermore, NWP model centers make frequent changes to numerical procedures, physical parameterizations and model resolutions (Durai and Bhradwaj 2014). To overcome the ever changing NWP model base, Ebert (2001) introduced the concept of Frequency Matching Method (FMM). The method can apply dynamic bias correction and requires fewer computational resources. Since 2004, FMM has been implemented to bias correct GFS provided rainfall forecasts at NCEP in the United States (Zhu and Toth 2004). Many studies have demonstrated that, FMM is good enough to bias correct rainfall forecasts over the region of interest (Wang et al. 2020; Zhu and Luo 2015; Yang et al. 2020; Guo et al. 2021). Wang et al. (2020) suggested that applying bias correction to rainfall forecasts at basin level may improve forecast accuracy. Hence, for any hydrometeorological applications, the NWP model forecasts at the basin level need to be verified rather than at country level to use in modeling applications.

2.4 Flood Forecasting and Warning System

Flood forecasting and early warning is one of the most effective flood risk management strategies to minimize the negative impacts of floods (ESCAP 2017). The CWC is the nodal agency in India that provides deterministic flood forecasts based on observed precipitation and streamflow across the major rivers and their tributaries (CWC 2020). During extreme weather events, local agencies use CWC water level forecasts to plan rescue operations (Harsha 2020). However, water level estimates at a point were inconsistent and sparse over large areas, resulting in uncertainty in estimating flood inundation area and flood depth, making rescue operations difficult for local agencies. As a result, there is a need for integrated hydrologic and hydraulic models to be developed with enough lead time to provide flood forecasts as well as inundation extent and depth.

2.4.1 Integrated Hydrologic and Hydraulic Models

Integrating hydrologic and hydraulic models can be a powerful method of modeling extreme hydrometeorological events using current computing resources (Leon et al., 2014; Sridhar et al., 2019). Biancamaria et al., (2009) coupled an ISBA hydrologic model with a LISFLOOD-FP hydrodynamic model to simulate runoff in an ungauged Ob River basin in the Arctic region. The best modeling results were obtained with a river depth of 10 m and a Manning coefficient of 0.015. Bonnifait et al., (2009) coupled n-TOPMODEL hydrologic model with a CARIMA

one dimensional hydraulic model to reconstruct a flood event in the Gard region of France in 2002 for post-event surveys. They suggested that the coupled model was useful for critical analysis and extrapolation of discharge rating curves. Schumann et al., (2013) integrated the VIC model with LISFLOOD-FP for flood inundation forecasting over the Lower Zambezi River in Africa. The model simulated inundation extent showed an agreement of 86% when compared with the observed flood map. Grimaldi et al., (2013) proposed a hydrologic and hydraulic model for a small and ungauged watershed using WFIUH hydrologic model and FLO-2D hydraulic model. For peak flow estimation, the model was tested using an event-based approach, a semi-continuous approach, and a fully-continuous approach. They found that the fully continuous approach accurately predicted peak flows when compared to observed flows.

Nam et al., (2014) integrated the super-tank hydrologic model with the one-dimensional HEC-RAS model to study Vu Gia-Thu Bon River in central Vietnam. The model predicted flood inundation depth and extent which agreed well with field observations. Nguyen et al., (2016, 2015) developed HiResFlood-UCI, an integrated hydrologic and hydraulic model for flash flood modeling at decameter resolution by combining the NWS's hydrologic model (HL-RDHM) with the hydraulic model (BreZo). The model was able to produce spatially distributed, high resolution flow information while maintaining hydrograph quality. Mai and De Smedt, (2017) linked the WetSpa and HEC-RAS models for flood prediction in Vietnam. Hydrographs were accurately predicted, with Nash-Sutcliffe efficiencies greater than 0.8. In particular, the time of concentration and flow volumes of peak flows, were predicted accurately. They suggested that the model was suitable for predicting inundation and assessing flood risks. Duvvuri, (2019) integrated SWAT model with HEC-RAS model to generate flood inundation maps in the flood prone areas of Cauvery river basin in India. The model was able to produce spatially distributed high-resolution flood inundation areas. Loi et al., (2019) developed an integrated hydrologic and hydraulic model based on SWAT and HEC-RAS to provide flood forecasting and warnings in the Vu Gia – Thu Bon river basin, Quang Nam province, Vietnam. The results showed that the model was able to predict the magnitude and timing of peak floods. Sholichin and Qadri, (2020) integrated SWAT model with HEC-RAS to identify inundation areas in the Bila river basin in Indonesia. The authors reported that the integrated model was able to predict flood inundation areas. The flood inundation maps can be exported into Web-GIS based platforms for visualization and dissemination of flood related information in real-time.

2.5 Flood Area Visualization and Public Dissemination Systems

Visualization and public dissemination system based on Web-GIS provides a graphical user interface for accessing spatial data, performing spatial analysis, and visualizing web-services through a web browser. Auynirundronkool et al. (2012) developed a method for automatic real-time flood detection involving a data retrieval service, a flood Sensor Observation Service (SOS) and a web-based flood detection service in a sensor web environment. The methodology developed was tested in central Thailand. The results indicated that the proposed approach could be useful for automatic instant flooding detection. Wan et al. (2014) developed a global CyberFlood with cloud computing service integration and crowdsourcing data collection. The model allows the public to update information on new flood events through smartphones or the internet. It provides location-based flood alerts to the public and local agencies for planning rescue operations. Horita et al. (2015) developed SDSS for flood risk management based on Wireless Sensor Networks (WSN) and Volunteer Geographic Information (VGI) for the town of Sao Carlos in Brazil. SDSS was able to provide valuable information by combining WSN and VGI data for emergency agencies for rescue operations during floods.

Knight et al. (2015) developed a DST that helps operational users take better decisions during extreme weather events. Flood information from LISSFLOOD-FP and SWAB models was incorporated into DST tool. The user interface enables users to adjust the input parameters according to the current situation to get flood information. Lagmay et al. (2017) developed a Web-GIS interface based on mashups of freely available source code that provides real-time information about natural disasters such as floods, tropical cyclones, earthquakes, tsunamis, and volcanic eruptions. This tool is heavily used by the Philippine government to plan prevention and mitigation measures when extreme events occur. Chang et al. (2018) developed an IHIP that used machine learning, visualization, and system design techniques to create a user-friendly web interface for improving online forecast capabilities and flood risk management in the Tiwan City. The IHIP framework consists of five layers including data access, data integration, servicer, functional subsystem, and user applications, and one database for flood prediction. The IHIP provides information about rainfall and floods in real-time which helps the communities in making better decisions during the floods. Mohanty and Karmakar (2021) developed a WebFRIS for Jagatsinghpur district in India using various open source tools and packages. The WebFRIS provides crucial information to town planners, water professionals, local bodies, flood experts, and also public on flood risk management. In the above literature,

it has been observed that open source based Web-GIS frameworks are widely used for disseminating flood inundation areas.

2.6 Critical Appraisal of Literature Review

Changing climate has altered the frequency, magnitude, duration, spatial extent, and timing of weather and climate extremes such as tropical cyclones, floods, and droughts. Rainfall is one of the most important climate variables that varies both in space and time. Rainfall and rainfall extremes in the Indian sub-continent are expected to be impacted by warming climate in future (Ali et al. 2019). Recent studies by Bisht et al., 2018, Dubey and Sharma, 2018, Jain et al., 2017, reported a significant increasing trend in rainfall extremes across India at national and regional levels. However, the trends are not uniform across the country with regard to floods and droughts (Ghosh et al. 2012). Floods are the most common natural disasters in India causing significant damage to human lives and infrastructure. For instance, recent floods in Hyderabad in 2020, Kerala in 2018, and Chennai in 2015 caused huge damage to humans and property. Early information about floods will help the public and government officials to take necessary action during extreme flood events. Flood forecasting and early warning system is an effective tool to minimize the negative impact of floods (Harsha 2020). With advancements in computational resources, an integrated hydrologic and hydraulic model can be a powerful method in modeling such extreme hydrometeorological events (Sravani 2018). Members of the general public and government officials will make better decisions during extreme events, if information is available in real-time through Web-GIS based interface systems. Detailed methodology is presented in the subsequent chapters based on the objectives proposed in chapter-1 and the literature review of the proposed objectives.

Chapter - 3 Methodology

3.1 General

Based on the objectives presented in the chapter – 1 and literature review in chapter - 2, the overall research methodology is prepared which is shown in Figure 3.1. The overall methodology is divided into five major components that include analysis of trends and patterns in rainfall characteristics over the study area, forecasting rainfall using WRF model, bias correction of NCEP-GFS (hereafter GFS) based rainfall forecasts, development of an integrated hydrologic and hydraulic modeling system for forecasting floods, and development of an Web-GIS based graphical user interface for visualization and dissemination of flood inundation information.

Trends in rainfall and rainfall extremes (Consecutive Dry Days (CDD), Consecutive Wet Days (CWD), annual total precipitation in wet days (PRCPTOT), annual count of days when rainfall is greater than 10 mm (R10MM), greater than 20 mm (R20MM), greater than 40 mm (R40MM), 95^{th} percentile of rainfall on wet days (R95PTOT), monthly maximum 1-day rainfall (RX1DAY), and monthly maximum consecutive 5-day precipitation (RX5DAY)) are examined using four different Mann-Kendall (MK) tests to study the trends and patterns in rainfall characteristics and to identify critical areas that are prone to floods in the selected study area.

To forecast floods, rainfall forecasts from NWP models such as WRF and GFS have been used. The mechanism used by WRF model for weather forecasting is shown in Figure 3.2. A simple multiplication bias correction scheme is used to apply bias corrections to GFS rainfall forecasts. The Bias corrected NWP model forecasts are given as input to the calibrated and validated SWAT model to forecast streamflow with lead-time. The forecasted streamflow are given as upstream boundary condition in HEC-RAS model to determine the flood inundation extent.

An integrated hydrologic and hydraulic modeling system is developed based on SWAT and 2D HEC-RAS models to simulate floods using rainfall forecasts from NWP models. Geospatial data such as Digital Elevation Model (DEM), LULC, and soil maps are required to set-up SWAT model. The daily meteorological like rainfall, maximum, and minimum temperature are used to simulate the streamflow. Uncertainty in Sequential Uncertainty Fitting – 2 (SUFI-2) algorithm in the SWAT-CUP is used for calibration, validation, and sensitivity analysis. The observed streamflow at various gauge stations is used to calibrate and validate the SWAT model

on daily basis. Once the SWAT model calibration and validation is completed, the SWAT model will simulate the streamflow for the selected extreme events. The simulated streamflow will be given as upstream boundary condition for the generation of flood inundation extent. The flood inundation maps are further exported into GeoServer to publish the layers in Web-GIS platform. Two river basins (Nagavali and Vamsadhara) which are prone to frequent floods due to heavy rainfall in the monsoon season and tropical cyclones in the pre- and post-monsoon season are chosen as study areas for this research.

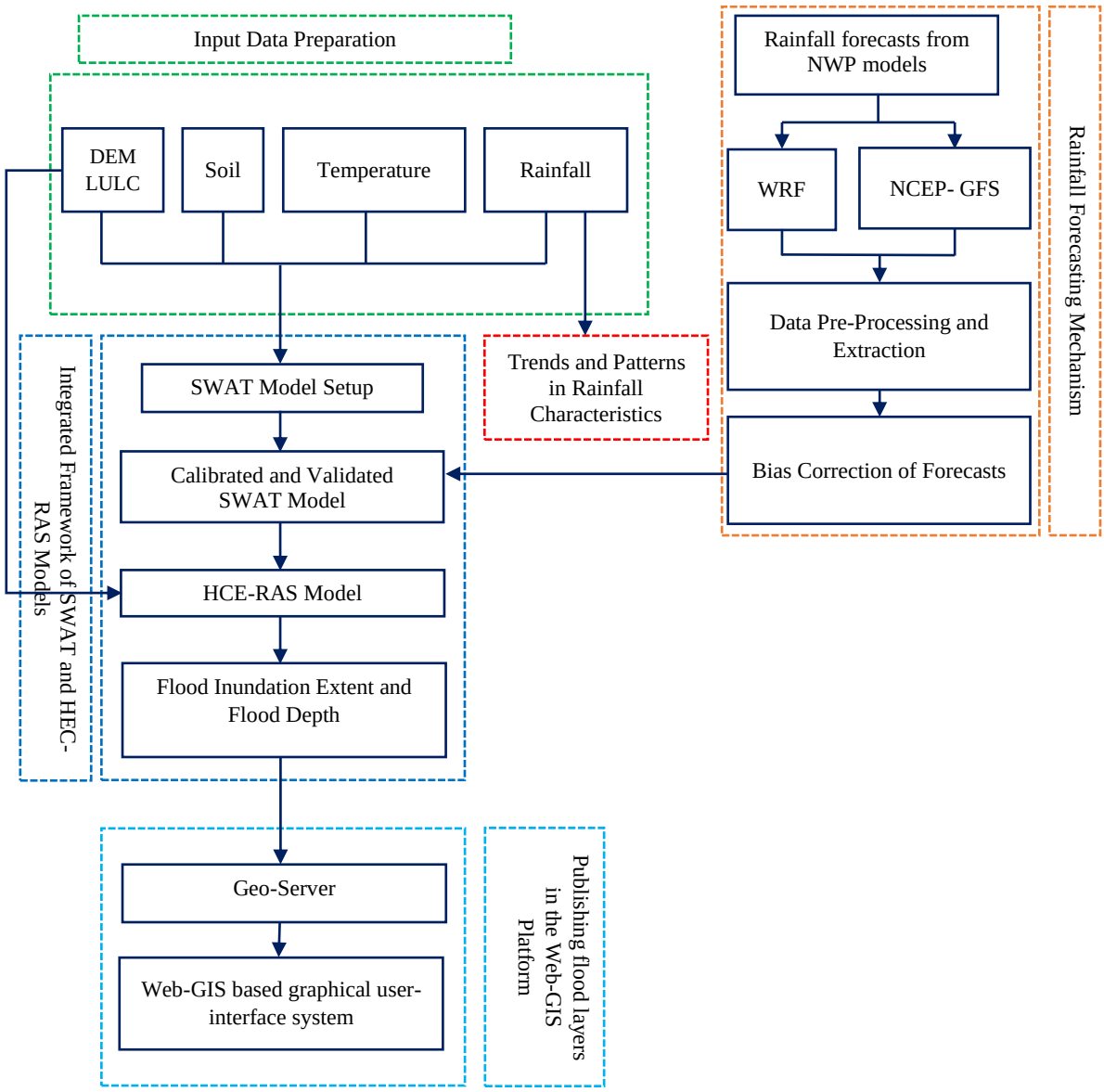

Figure 3.1 Overall methodology of the research work

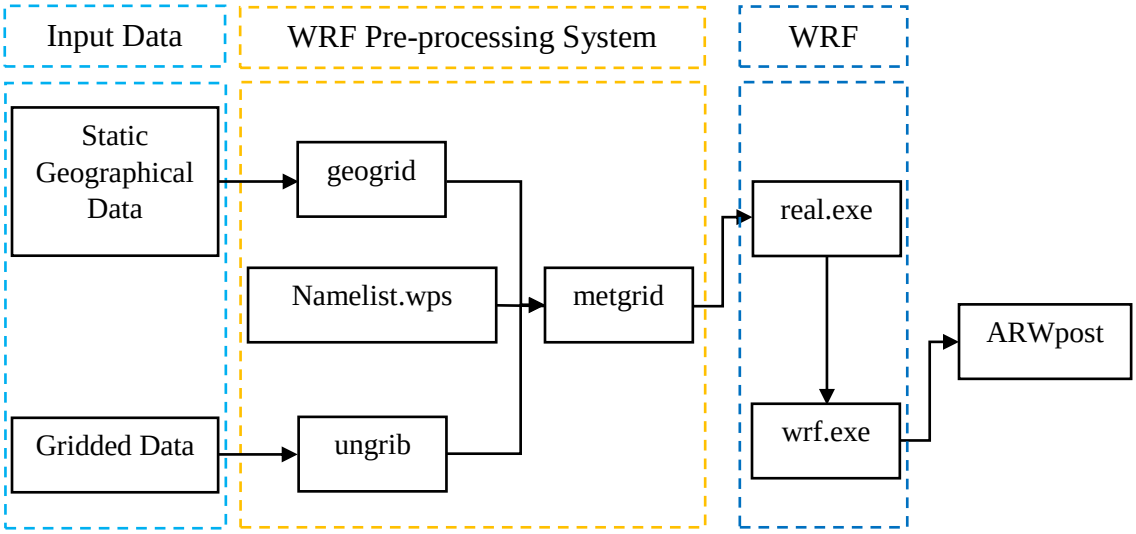

Figure 3.2 Mechanism used by WRF model to forecast weather parameters

3.2 Calculation of Rainfall Extremes

The rainfall extremes play an important role in understanding their hydrological impacts in a river basin. Based on the daily values of temperature and precipitation, the joint CCI/WCRP/JCOMM Expert Team on Climate Change Detection and Indices (ETCCDI) defined a total of 27 indices out of which 11 are for precipitation extremes and 16 for temperature extremes to gain insight into the changes in extremes (Yang et al. 2016). Among the 11 precipitation indices, 9 are selected to investigate the characteristics of rainfall extremes over Nagavali and Vamsadhara basins. The rainfall extremes are calculated at various temporal scales (i.e., monthly, seasonal, and annual) using RClimDex package in R developed and maintained by Xuebin Zhang and Yang Fang at Climate Research Division (CRD) or ETCCDI (Bronaugh 2019). It is the most commonly used package for calculating rainfall extremes. The package also conducts simple quality control on input data before calculating the rainfall extremes. The detailed description of rainfall extremes are presented in Table 3.1.

Table 3.1 Selected list of rainfall extremes in the present study and their definitions (Source: http://etccdi.pacificclimate.org/list_27_indices.shtml)

Extremes	Units	Definitions
CDD	Day	Maximum length of dry spell, Maximum number of consecutive days with RR < 1 mm. Count the largest number of consecutive days where RRij < 1 mm
CWD	Day	Maximum length of wet spell, Maximum number of consecutive days with rainfall ≥ 1 mm. Count the largest number of consecutive days where RRij ≥ 1 mm
PRCPTOT	mm	Total amount of rainfall in wet days. if i represents the number of days in j, then $\text{PRCPTOT} = \sum_{j=1}^{I} \text{RR}_{ij}$
R10MM	Day	Number of days when RR ≥ 10mm. Count the number of days where RRij ≥ 10mm.
R20MM	Day	Number of days when RR ≥ 20mm. Count the number of days where RRij ≥ 20mm.
RNNMM	Day	Number of days when RR ≥ nnmm. Count the number of days where RRij ≥ nnmm. (Where nn = User defined threshold)
R95PTOT	mm	Total rainfall when RR > 95p. Let RRwj be the daily precipitation amount on a wet day w (RR ≥ 1 mm) in period I and let RRwn be the 95th percentile of RR on wet days. If W represents the number of wet days in the period, then $\text{R95p}_j = \sum_{w=1}^{W} \text{RR}_{wj} \text{ where } \text{RR}_{wj} > \text{RR}_{wn}95$
RX1DAY	Day	Maximum 1-day rainfall. The maximum 1-day values for period j are RX1DAYj = max(RRij)
RX5DAY	Day	Maximum 5-day rainfall. Let RRkj be the rainfall amount for the 5-day interval ending k period j. The maximum 5-day values for period j are RX5DAYj = max(RRkj)

Note: *RR_{ij} is the daily rainfall amount on the day i in period j. For RNNMM, a threshold of 40 mm is chosen, and the extreme is R40MM

The data format for calculating rainfall extremes is presented in Table 3.2. For calculating CDD, the software counts the number of consecutive days with rainfall less than 1mm. For instance, CDD for the data provided in Table 3.2 is 4 days.

Table 3.2 Data format for computing rainfall extremes

Year	Jday	IMD Gridded Data
1901	1	0
1901	2	0
1901	3	0.7
1901	4	0
1901	5	3
1901	6	1.5
1901	7	2
1901	8	0

3.3 Trends in Rainfall and Rainfall Extremes

The most common method used for detecting trends in time series data is the original Mann-Kendall (MK) test. The MK test has proven to be useful in determining significant trends in hydrologic data at different probability levels (Yadav et al. 2014; Bisht et al. 2018a), which assumes spatial and temporal independence in hydrological time series data (Adarsh and Janga Reddy 2015; Deshpande et al. 2016; Dubey and Sharma 2018; Guhathakurta et al. 2015). It is well documented that the presence of either positive or negative autocorrelation influences the significance of trend (Kumar et al. 2009). The original MK test assumes no serial correlation in the hydrological time series data. However, most often, hydrological time series data are autocorrelated and lead to a disproportionate false rejection of null hypothesis (Hamed 2008; Hamed and Rao 1998; Yue et al. 2003). Similarly, the presence of long-term persistence can lead to underestimation of serial correlation and overestimation of significance of trends (Su et al. 2018). To overcome these effects, trend analysis is performed in this research using four kinds of MK tests i.e., the original Mann-Kendall test (MK1), Mann-Kendall test with trend-free pre-whitening (MK2), modified Mann-Kendall test (MK3), and Mann-Kendall test with long-term persistence (MK4). The detailed description of the four MK tests is provided in the following sections.

3.3.1 Mann-Kendall Test (MK1)

The original Mann-Kendall (MK) (Kumar et al. 2009) test is widely used for detecting trends in a hydrological time series dataset. If $x_1, x_2, x_3, \dots\dots\dots, x_n$ is the time series of length n, then the MK1 test statistics S is given by:

$$S = \sum_{i=1}^{n} \sum_{j=i+1}^{n} sign(x_j - x_i) \tag{3.1}$$

$$\text{Where, } sign(x_j - x_i) = \begin{cases} 1 & if\ (x_j - x_i) > 0 \\ 0 & if\ (x_j - x_i) = 0 \\ -1 & if\ (x_j - x_i) < 0 \end{cases} \tag{3.2}$$

Null hypothesis(H_0): There is no trend in a hydrological time series dataset. Alternate hypothesis(H_1): There exists an increasing or decreasing trend in a hydrological time series dataset. As S is normally distributed, the mean E(S) and variance of statistic S in eq. (3.1) is given below:

$$E(S) = 0 \tag{3.3}$$

$$V(S) = \frac{n\,(n-1)(2n+S)}{18} \tag{3.4}$$

The MK standardized test statistics Z is given by:

$$Z = \begin{cases} \dfrac{S-1}{(V(S))^{1/2}} & S > 0 \\ 0 & S = 0 \\ \dfrac{S+1}{(V(S))^{1/2}} & S < 0 \end{cases} \tag{3.5}$$

The negative values of S indicate decreasing trend and vice versa. The test statistic Z gives Significance Levels (SL) for rejecting null hypothesis. Confidence Level (CL) for rejecting the null hypothesis is given by:

$$CL = 1 - SL \tag{3.6}$$

The magnitude of trend is determined by Theil-Sen approach (TSA) (Kumar et al. 2009). The mathematical expression for TSA slope is given in eq. (3.7):

$$\beta = median\left[\frac{x_j - x_i}{j-i}\right] \text{ for all i < j} \tag{3.7}$$

If the condition $-Z_{k(1-\frac{\alpha}{2})} \leq Z_k \leq Z_{k(1+\frac{\alpha}{2})}$ is satisfied then H_0 is accepted at a significance level of α, otherwise, H_1 is accepted.

3.3.2 Mann-Kendall Test with trend-free pre-whitening (MK2)

Yue et al., (2003) showed that there will be an increase (decrease) in S value when autocorrelation is positive (negative) which is underestimated (overestimated) by the original variance $V(S)$. Thus, when trend analysis is conducted for the present data using MK1, it will show positive or negative trends when actually there is no trend. So, trend free pre-whitening treatment is adopted where lag-1 serial correlation components are removed from the series prior to applying MK test for trend detection. The following steps are used to determine trend analysis using MK-2 test. Calculate lag-1 (k = 1) autocorrelation coefficient (r_1) using eq. (3.8):

$$r_k = \frac{\frac{1}{n-k}\sum_{i=1}^{n-k}(x_i - \bar{x})(x_{i+k} - \bar{x})}{\frac{1}{n}\sum_{i=1}^{n}(x_i - \bar{x})^2} \tag{3.8}$$

If the condition $\frac{-1-1.645\sqrt{n-2)}}{n-2} \leq r_1 \leq \frac{-1+1.645\sqrt{n-2)}}{n-2}$ is satisfied, then the series is assumed to be independent at 10% significance level and there is no need of pre-whitening. Otherwise, pre-whitening is required for the series before applying MK1 test.

Eq. (3.9) is used to remove the trend in time series data to get detrended time series. The value of β is obtained from eq. (3.7):

$$x_i' = x_i - (\beta \times i) \tag{3.9}$$

Eq. (3.8) is used to calculate lag-1 autocorrelations for detrended time series given by eq. (3.9). To remove the lag-one autoregressive component from the detrended series to get a residual series will be the following expression:

$$y_i' = x_i' - r_1 \times x_{i-1}' \tag{3.10}$$

Yet again, $(\beta \times i)$ value is added to the residual series as follows:

$$y_i = y_i' + (\beta \times i) \tag{3.11}$$

MK1 test is applied to the blended series Y_i to determine the significance of the trend.

3.3.3 Modified Mann-Kendall test 3 (MK3)

Sometimes, removing lag-one autocorrelation is not enough for many hydrological time series datasets. Hamed and Rao, (1998) proposed a modified Mann Kendall test where the effect of all significant autocorrelation coefficients are removed from a data set. The modified variance of S is used i.e., $V(S)^*$ instead of $V(S)$ which is given as follows:

$$V(S)^* = V(S)\frac{n}{n^*} \tag{3.12}$$

Where $n^*$is effective sample size. Hamed and Rao (1998) proposed an equation for the calculation of $\frac{n}{n^*}$ which is given below:

$$\frac{n}{n^*} = 1 + \frac{2}{n(n-1)(n-2)}\sum_{i=1}^{n}(n-1)(n-i-1)(n-i-2)r_i \tag{3.13}$$

Where n is actual number of observations, r_i is lag-i significant autocorrelation coefficient of rank i of time series. After calculating $V(S)^*$, substitute it in place of $V(S)$ in eq. (3.4) when calculating Z from eq. (3.5).

3.3.4 Mann-Kendall test with long-term persistence (MK4)

In addition to the lag-one autocorrelation i.e. short-term persistence, the presence of Long-Term Persistence (LTP) or the Hurst Phenomenon (H_p) (Hurst, 1951) can considerably influence the significance of trends in hydrological time series dataset. To overcome LTP, Mann Kendall test with LTP is taken into consideration (Hamed 2008). The following steps are used to determine trend analysis using MK4 test. The procedure for calculating H_p is given as follows: A new time series x_i' is calculated from eq. (3.9). Using the ranks (R_i) of the detrended time series x_i', Z variate is calculated as follows:

$$Z_i = \emptyset^{-1}\left(\frac{R_i}{n+1}\right) \tag{3.14}$$

Where n is observation size, $\emptyset^{-1}$ is inverse of standard normal distribution function with zero mean and standard deviation is 1. For a given H, the elements of Hurst matrix are determined as follows:

$$C_n(H_p) = [\rho_{|j-1|}] \quad \text{for } i = 1{:}\,n, j = 1{:}\,n \tag{3.15}$$

Where ρ_l represents lag-l autocorrelation coefficient which is given below:

$$\rho_l = \frac{1}{2}[|l+1|^{2H_p} - 2|l|^{2H_p} + |l-1|^{2H_p}] \qquad \text{for } l > 1 \tag{3.16}$$

To calculate the exact value of H_p, the maximizing likelihood function is used as given below

$$logL(H_p) = -\frac{1}{2}\log|C_n(H_p)| - \frac{Z^T[C_n(H_p)]^{-1}Z}{2\gamma_0} \quad (3.17)$$

Where transpose of Z (Z^T) is obtained from MK-1 test, $C_n(H_p)$ is the Hurst matrix, γ_0 represents the variance. Eq. (3.17) is solved for different values of H ranging from 0.5 to 0.98 with 0.01 step interval and the H_p value which produces maximum $L(H_p)$ detected, as the answer.

The mean and Standard Deviation of H_p in terms of n (Hamed 2008) are as follows:

$$\mu_{H_p} = 0.5 - 2.87n^{-0.9067} \quad (3.18)$$

$$\sigma_{H_p} = 0.77654n^{-0.5} - 0.0062 \quad (3.19)$$

Then, calculate $Z_c\ as\ \frac{H_p - \mu_{H_p}}{\sigma_{H_p}}$ for a significance of trend at 10% significance level. For significant H, calculate the modified variance for S, recommended by Kumar et al (2009)

$$V(S)^{H'} = \sum_{i<j}\sum_{k<l}\frac{2}{\pi}sin^{-1}\left(\frac{\rho|j-l| - \rho|i-l| - \rho|j-k| + \rho|i-k|}{\sqrt{(2-2\rho|i-j|)(2-2\rho|k-l|)}}\right) \quad (3.20)$$

Where ρ_l is calculated from eq. (3.16). As the modified variance ($V(S)^{H'}$) is a biased estimator, correction is needed for bias as follows:

$$V(S) = V(S)^{H_p'} \times b \quad (3.21)$$

$$b = a_0 + a_1H_p + a_2{H_p}^2 + a_3{H_p}^3 + a_4{H_p}^4 \quad (3.22)$$

Where, a_0, a_1, a_2, a_3, and a_4 are coefficients which depends on the number of observations given by Kumar et al (2009). The modified variance $V(S)^{H_p'}$ obtained from eq. (3.20) is substituted in place of V(S) eq. (3.4) in MK1 test. The Mann Kendall Z statistics are tested for significance levels with the threshold values.

3.3.5 Pettit's Test

Pettit's test is commonly used for a significant change point in time series data. It tests H_0: The T variables follow one or more distributions that have the same location parameter (no change), against the alternative hypothesis: a change point exists. The non-parametric statistic is defined as:

$$K_T = max\left|U_{t,T}\right| \tag{3.23}$$

Where, $$U_{t,T} = \sum_{i=1}^{t}\sum_{j=t+1}^{T} sgn\left(X_i - X_j\right) \tag{3.24}$$

The change point in the time series is located at K_T, provided that the statistic is significant. The significance probability of K_T is approximated for $p \leq 0.05$ with the following equation:

$$p = 2\exp\left(\frac{-6\,K_T^2}{T^3 + T^2}\right) \tag{3.25}$$

3.3.6 Software Packages Used for Trend Analysis

Two open source packages in R Version (3.5.3) namely "modifiedmk" (Patakamuri and O'Brien 2019) and "HKprocess" (Tyralis 2016) are used to perform MK tests. The "modifiedmk" is used to perform MK1, MK2, and MK3 tests and Sen's slope test. Another package "HKprocess" is used to perform MK4 test. To get the spatial patterns of trends from point observations, kriging interpolation is applied using geospatial software.

3.4 Rainfall Forecasts from Numerical Weather Prediction (NWP) Models

The NWP modeling is a method of forecasting the future atmospheric conditions by solving a set of mathematical equations that describe the physical phenomenon of the atmosphere. The meteorological variable in the atmosphere change over time, so if the initial conditions are known, the governing equations in NWP models can be solved and new values of meteorological variables can be obtained. The simplest form of NWP model is given as follows:

$$\frac{\Delta A}{\Delta t} = F(A) \tag{3.26}$$

Where, ΔA gives the change in forecast variable at a particular location in space, Δt represents the change in time, and $F(A)$ represents the factors that are responsible for changes in the values of A. The mathematical expression for finding the forecast value of the meteorological variable is given in the following equation:

$$A^{Forecast} = A^{initial} + F(A) \tag{3.27}$$

Eq. (3.27) means that, the forecast value of any meteorological variable can be estimated by finding their initial values and then adding all the factors that are responsible for changes in the meteorological variable over a period of time. With advancements in computational power, most of the NWP models are able to provide rainfall forecasts with a lead time of 1

to 15 days. Accurate rainfall forecasts from NWP models will help in reducing the uncertainty in streamflow forecasts. However, the rainfall forecasts from NWP models are subjected to three types of errors (i) Location, (ii) Magnitude, and (iii) Timing, which may limit the usefulness for streamflow forecasting. Therefore, the skill of NWP model forecasts needs be evaluated before using them for any hydrometeorological applications.

3.4.1 Evaluation of WRF Model Forecasts

Statistical analysis is the most common method to find the uncertainty in model forecasts with respect to observations. The Direct Positional Error (DPE) has been calculated by using Haversine formula which gives the geographical distance between two points on a sphere. The mathematical expression for Haversine for any two points on a sphere is as follows:

$$Haversine\left(\frac{d}{r}\right) = haversine\,(\emptyset_2 - \emptyset_1) + \cos(\emptyset_1)\cos(\emptyset_2)\,haversine(\lambda_2 - \lambda_1) \quad (3.28)$$

Where, haversine is the haversine function which is given as follows:

$$haversine\,(\theta) = sin^2\left(\frac{\theta}{2}\right) \quad (3.29)$$

Where, d is the distance between the two points, r is the radius of the earth (6378 km), $\emptyset_1$ and $\emptyset_2$ are the latitudes of point2 1 and 2, λ_1 and λ_2 are longitudes of points 1 and 2. The value of d in eq. (3.28) can be obtained by using the following equation:

$$d = 2r\,arcsin\left(\sqrt{haversine\,(\emptyset_2 - \emptyset_1) + cos(\emptyset_1)\,cos(\emptyset_2)\,haversine(\lambda_2 - \lambda_1)}\right) \quad (3.30)$$

Mean Sea Level Pressure (MSLP) and Maximum Sustained Wind (MSW) are measured at each time step and evaluated against IMD observations. The Mean Absolute Error (MAE), Mean Square Error (MSE) have been calculated with respect to IMD observations. MAE is an average prediction error that is used to measure the forecast accuracy. MSE is a measure to determine the quality of a forecast with a positive value. If the value of MAE and MSE are close to zero, the quality of the forecast is better. The Skill Score (SS) of DPE, MSLP and MSW have been calculated with respect to reference forecast. The mathematical expressions for the MAE and MSE, SS for MAE, MSE and DPE are as follows:

$$\text{Mean Absolute Error (MAE)} = \frac{1}{n}\sum_{i=1}^{n}|P_s - P_o| \quad (3.31)$$

$$\text{Mean Square Error (MSE)} = \frac{1}{n}\sum_{i=1}^{n}(P_s - P_o)^2 \quad (3.32)$$

$$\text{Skill Score } (SS_i) = 1 - \frac{\text{MSE}_{\text{Simulation}}}{\text{MSE}_{\text{Reference}}} \quad (3.33)$$

$$\text{Skill Score } (SS_{DPE}) = 1 - \frac{\text{DPE}_{\text{Simulation}}}{\text{DPE}_{\text{Reference}}} \quad (3.34)$$

In the above equations, P_s is simulated value of parameter, P_o is observed value of parameter, and n is number of observations. SS is the relative accuracy score of a forecast over a reference forecast. The reference forecast has been chosen based on the numerical experiments conducted by Srinivas et al. (2013). By conducting 65 numerical experiments, Srinivas et al. (2013) suggested that Lin scheme provided better results for track and intensity prediction of 21 TCs over BoB. Hence, sensitivity experiments using Lin scheme considered are as a reference forecast and the skill score for all the other microphysical schemes are calculated. Positive values of SS indicate that the model is more skilled and vice-versa.

3.4.2 Evaluation of GFS Rainfall Forecasts

The verification of GFS model rainfall forecasts are carried out against IMD gridded rainfall data at the same resolution (0.25° × 0.25°). Model performance is evaluated using several accuracy and skill measures (Broorks et al. 2017) for day-1 to day-5 forecasts of 24-h accumulated rainfall over Nagavali and Vamsadhara basins.

3.4.2.1 Statistical Metrics

Statistical metrics such as CC, RMSE, ME, and BIAS are used to quantify the difference between GFS rainfall forecasts and observed data. CC refers to the degree of linear agreement between the forecasted and reference datasets. The absolute average error is measured using RMSE, which gives more weight to larger errors. ME refers to the averaged magnitude differences between the forecasted and reference datasets. Bias measures the average error trend in forecasted rainfall relative to observed rainfall. The mathematical equation for CC, RMSE, ME, and RBIAS are given as follows (Prakash et al. 2016a):

$$CC = \frac{\sum_{i=1}^{n}(O_i - \bar{O})(S_i - \bar{S})}{\sqrt{\sum_{i=1}^{n}(O_i - \bar{O})^2}\sqrt{\sum_{i=1}^{n}(S - \bar{S})^2}} \quad (3.35)$$

$$RMSE = \sqrt{\frac{1}{n}\sum_{i=1}^{n}(S_i - O_i)^2} \quad (3.36)$$

$$BIAS = \frac{\sum_{i=1}^{n}(S_i - O_i)}{\sum_{i=1}^{n} O_i} \times 100 \quad (3.37)$$

$$ME = \frac{1}{n}\sum_{i=1}^{n}(S_i - O_i) \quad (3.38)$$

Where, O is the observed rainfall data, S is the GFS forecasted rainfall data, $\bar{O}$ is the mean of observed rainfall, $\bar{S}$ is the mean of the forecasted rainfall, and n is the total number of observations.

3.4.2.2 Contingency Statistics

Due to the high spatial and temporal variability of rainfall, the standard method proposed by World Meteorological Organization (MWO) is insufficient for the verification of rainfall forecasts provided by NWP models (WMO 1977). For measuring the skill of the NWP model for rainfall forecasts, contingency statistics based on frequency of occurrence are more appropriate (Durai et al. 2010). Contingency statistics are used to evaluate the GFS model's skill to distinguish between dichotomous estimation. The dichotomous estimation will return 'Yes' if the model predicts rainfall and 'No' if there is no rain. A threshold value is always used to distinguish between rain and no-rain events. Therefore, a threshold of 1 mm/day is considered. The contingency statistics used in the present study are POD, FAR, CSI, and TSS. POD measures the fraction of observed rain events that are correctly forecasted by the model. FAR indicates the fraction of forecasted rain events that are observed to be no-rain events. CSI measures the fraction of rainfall events that are correctly diagnosed by the model. TSS measures the ability of the model to distinguish between the occurrence and non-occurrence of an event. The mathematical equations for POD, FAR, CSI, and TSS are given as follows (Sharma et al. 2021).

$$POD = \frac{H}{H + M} \quad (3.39)$$

$$FAR = \frac{F}{H + F} \quad (3.40)$$

$$CSI = \frac{H}{H + M + F} \quad (3.41)$$

$$TSS = \frac{(H \times CN) - (M \times F)}{(H + M) \times (F + CN)} \quad (3.42)$$

Where, H is the number of observed rain events that are correctly forecasted, F is the number of rainfall events forecasted but not detected, M is the number of observed rainfall events that are not forecasted, CN is the number of no rainfall events in both observed and forecasted data. The detailed information about$H$, F, M and CN are presented in Table 1. The rainfall threshold for calculating these statistics is set at 1mm/day. The day is considered to be dry if rainfall is less than 1 mm/day. A wet day is one in which the rainfall exceeds 1 mm/day.

Table 3.3 The contingency classification used to verify the forecasts by calculating POD, FAR, CSI, and TSS with a threshold of 1 mm/day

Forecast	Observed	
	Rain	No Rain
Rain	Hit (H)	False (F)
No Rain	Miss (M)	Correct Negative (CN)

3.4.2.3 Error Decomposition

Error decomposition analysis is used to evaluate the error components in precipitation estimates (Tian et al. 2009). The method divides mean error into three independent components: hit bias (HB), missed bias (MB), and false bias (FB). When the mean error is calculated across the entire dataset, it does not provide detailed information about the source of the error. When the mean error is decomposed, the three possible error sources can be distinguished. When rain events are correctly forecasted by GFS model, but rainfall intensity is incorrectly estimated, HB occurs. MB denotes the error caused by rain events that are incorrectly forecasted as no-rain events. The error caused by no-rain events that are incorrectly forecasted as rain events is referred to as FB. The value of HB can be either positive or negative, while MB is always negative and FB is always positive. The mathematical expressions for HB, MB, and FB are given as follows (Deng et al. 2018):

$$HB = \frac{1}{n}\sum_{h=1}^{H}(S_h - O_h) \tag{3.43}$$

$$MB = -\frac{1}{n}\sum_{m=1}^{M} O_m \tag{3.44}$$

$$FB = \frac{1}{n}\sum_{f=1}^{F} S_f \tag{3.45}$$

Total Bias (TB) or ME can be expressed as follows:

$$TB\ or\ ME = HB + MB + FB \tag{3.46}$$

Where, n is the total number of observations, H is the total number of hit precipitation events. M is the total number of missed precipitation events, and F is the total number of false events.

The sum of HB, MB, and FB is always equal to mean error. As MB and FB always have opposite signs, they may cancel each other out, resulting in a smaller mean error than individual components. Therefore, breaking down the mean error into independent components may aid us in better understanding the error nature of forecasted rainfall and the uncertainties of retrieval processes.

3.4.2.4 Bias Correction

Accurate rainfall estimates have the potential to reduce uncertainty in hydrological simulations. GFS rainfall forecast bias is corrected using a simple multiplication bias correction scheme. The Bias Factor (BF) is calculated as the ratio of gridded rainfall to GFS rainfall forecasts. To obtain bias corrected rainfall estimates, GFS rainfall forecasts are multiplied by BF. The mathematical expression for calculating BF is given in eq. (3.47) (Lekula et al. 2018):

$$BF = \frac{\sum_{i=1}^{n} O_i}{\sum_{i=1}^{n} S_i} \tag{3.47}$$

Where, i is the grid location and n is the total number of grids analyzed. Following bias correction, SS of BIAS, RMSE, and ME are calculated with respect to the reference value to find if there is any improvement in the model forecast. The mathematical expressions are given below for calculating SS for BIAS, RMSE, and ME:

$$SS_{BIAS} = 1 - \frac{BIAS_{after\ bias\ correction}}{BIAS_{before\ bias\ correction}} \tag{3.48}$$

$$SS_{RMSE} = 1 - \frac{RMSE_{after\ bias\ correction}}{RMSE_{before\ bias\ correction}} \tag{3.49}$$

$$SS_{ME} = 1 - \frac{ME_{after\ bias\ correction}}{ME_{before\ bias\ correction}} \tag{3.50}$$

3.5 Soil and Water Assessment Tool (SWAT)

Soil and Water Assessment Tool (SWAT) model works on a daily time step continuous simulating model for a long period. The model is a computationally efficient, physical based model and capable of simulating high-level spatial details by dividing the watershed into smaller sub-watersheds (Arnold et al. 2012). The HRU's are the percentages of sub-watershed area comprising homogeneous land use, management, and soil characteristics. SWAT model allows users to estimate the anticipated scenarios of a watershed by using different climate data and LULC patterns as inputs. In addition, it is capable of assessing the variability in stream flow by considering the future projected climate variables. SWAT model requires daily meteorological data i.e., either from a measured data set or generated by a weather generator model. The water balance equation, which governs the hydrological components of SWAT model, is as follows:

$$SW_{ti} = SW_O + \sum_{i=1}^{t}(R_{dayi} - Q_{surfi} - E_{ai} - W_{seepi} - Q_{gwi}) \quad (3.51)$$

Where, SW_{ti} is soil water content at the end of the day (mm), SW_O is the amount of initial soil water content on day i (mm), t is the time in days, R_{dayi} is the amount of precipitation on day i (mm), Q_{surfi} is the amount of surface runoff on day i (mm), E_{ai} is the amount of evapotranspiration on day i (mm), W_{seepi} is the amount of water entering the vadose zone from the soil profile on day i (mm) and Q_{gwi} is the amount of return flow on day i (mm).

3.6 Hydrological Engineering Centre - River Analysis System (HEC-RAS)

HEC-RAS is an integrated software designed to perform one-dimensional (1D), two-dimensional (2D), and combined one-dimensional and two-dimensional (1D/2D) hydraulic calculations for a full network of natural or constructed channels, overbank or floodplain areas, levee protected areas; etc. HEC-RAS model performs 1D and 2D computations using St. Venenat equations of conservation of mass and conservation of momentum. 1D model solves St. Venenat equations along one dimension, while 2D model solves St. Venenat equations in two dimensions. 1D modeling can be difficult in some rivers due to certain topographic and hydraulic features. These features include undefined boundaries between channels and overbanks, high-gradient flows in off-channel storage areas, unclear flow directions, flow direction that changes significantly, and river bends. The use of 2D modeling

will overcome the drawbacks of 1D modelling. HCE-RAS 2D modelling comprising several components including terrain data, LULC, 2D computational mesh, and unsteady flow data. 2D model performs the calculations based on Shallow Water Equations (SWE) or Diffusive Wave Equations (DWE). SWEs are also called as Navier-Stokes equations and are derived from conservation of mass as well as momentum equations. The mathematical expression for the SWE is as follows:

$$\frac{\partial u}{\partial t} + \left(u\,\frac{\partial u}{\partial x} + v\,\frac{\partial v}{\partial x}\right) = -g\,\frac{\partial H}{\partial x} + v_t\left(\frac{\partial^2 u}{\partial x^2} + \frac{\partial^2 v}{\partial x^2}\right) - c_f u + fv \qquad (3.52)$$

Where, $\frac{\partial u}{\partial t}$ is local acceleration with time, $u\,\frac{\partial u}{\partial x} + v\,\frac{\partial v}{\partial x}$ is advective acceleration, $g\,\frac{\partial H}{\partial x}$ is hydrostatic Pressure, $v_t\left(\frac{\partial^2 u}{\partial x^2} + \frac{\partial^2 v}{\partial x^2}\right)$ is viscosity, $c_f u$ is bed friction, and fv is Coriolis Effect. 2D DWE is the default option in HEC-RAS because it allows the computations to run faster and with greater stability. For DWE, the bottom fiction is equal to the pressure gradient. The water surface slope is balanced by the friction slope. This means the local and advective acceleration, viscosity and Coriolis Effect are not considered. The mathematical expression for DWE is as follows:

$$g\,\frac{\partial H}{\partial x} + c_f u = 0 \qquad (3.53)$$

3.7 Flood Frequency Analysis

Flood Frequency Analysis (FFA) is a technique used by hydrologists to predict flow values corresponding to specific return periods. FFA uses annual peak flow data to calculate statistical information such as mean, standard deviation and skewness for creating frequency distribution graphs. Several statistical distributions are available for FFA such as Normal, Log-Normal, Pearson, Log-Pearson, Gumbel, Exponential, and Weibull. Once the best distribution is selected, flood frequency curves are plotted. The flood frequency curves are then used to estimate the design flow values corresponding to specific return periods. In the present research, four 2-parameter distributions, namely, Log-Pearson Type-III, Log-Normal, Weibull, and Gumbel are used to calculate the return periods. The mathematical expressions for the distributions are as follows;

Log-Pearson Type – III

$$f_Y(y|\mu,\sigma) = \frac{1}{(\sigma^2\mu)^{1/\sigma^2}} \frac{y^{1/\sigma^2-1}\, e^{-y/(\sigma^2\,\mu)}}{\Gamma\left(1/\sigma^2\right)} \quad (3.54)$$

Log-Normal

$$f_Y(y|\mu,\sigma) = \frac{1}{\sqrt{2\pi\sigma^2}} \frac{1}{y} exp\left\{-\frac{[\log(y)-\mu]^2}{2\sigma^2}\right\} \quad (3.55)$$

Weibull

$$f_Y(y|\mu,\sigma) = \frac{\sigma y^{\sigma-1}}{\mu^\sigma} exp\left[-\left(\frac{y}{\mu}\right)^\sigma\right] \quad (3.56)$$

Gumbel

$$f_Y(y|\mu,\sigma) = \frac{1}{\sigma} exp\left[\left(\frac{y-\mu}{\sigma}\right) - exp\left(\frac{y-\mu}{\sigma}\right)\right] \quad (3.57)$$

Where, y is flood discharge values, μ is the mean, and σ is the standard deviation.

3.8 Development of Web-GIS based User Interface

The development of Web-GIS based user interface systems for flood visualization includes the use of various design and programming languages, as well as the use of mapping libraries, frameworks, GIS software, and web servers. In the current research, programming languages includes HyperText Markup Language (HTML), Cascading Style Sheet (CSS), and JavaScript (JS) are used. For mapping libraries and web servers, OpenLayers and GeoServer are used.

HTML is standard markup language that web browsers use to interpret and compose texts, images, and other material into visual and audible web pages and web applications. Default characteristics of every item of HTML markup are fed into the browser and these characteristics can be altered or enhanced by the use of CSS. Inclusion of CSS defines the look and layout of content. HTML can embed programs written in a scripting language such as JS which affect the behavior and content of web pages. Web browsers receive HTML documents from a webserver or from local storage and render them into multimedia web pages. The example scripts of HTML, CSS, and JavaScript used in the present research are shown in Figures 3.3, 3.4, and 3.5 respectively.

OpenLayers is a widely used open source JS mapping library for displaying map data in web browsers. It provides an API for building rich web-based geographic applications similar to Google and Bing maps. OpenLayers makes it easy to put a dynamic map on any web page. It can display map tiles, vector data, and markers loaded from various sources such as OSM,

MapBox, GeoServer, MapServer etc. The example script of OpenLayers is shown in Figure 3.6.

```
<!DOCTYPE html>
<html>
  <head>
    <meta charset="utf-8" />
    <title>Real-time Flood Forecastig</title>
    <meta
      name="viewport"
      content="initial-scale=1.0, user-scalable=no, width=device-width"
    />
    <link rel="stylesheet" href="https://openlayers.org/en/v6.12.0/css/ol.css" />
    <link rel="stylesheet" href="./dist/ol-style.css" />
    <link rel="stylesheet" href="style.css" />
  </head>
  <body>
    <div id="header">
      <div id="row1">
        <div id="column1">
          <a href="https://www.nitw.ac.in/" target="_blank">
            <img src="./img/NITW.png" alt="NITW" style="width: 100%;">
        </a>
        </div>
```

Figure 3.3 HTML script for Web-GIS based user interface system development

```
html,
body {
  height: 100vh;
  padding: 0;
  margin: 0;
  font-family: sans-serif;
  font-size: small;
}
#header {
  padding: 10px;
  background-color: beige;
}
#map {
  width: 98.7vw;
  height: 80vh;
}
#footer {
  background-color: bisque;
}
/* Limit the width of the layer-switcher */
```

Figure 3.4 CSS script for designing the appearance of Web-GIS based user interface system

```
(function () {
  var fullScreenControl = new ol.control.FullScreen();
  var zoomSliderControl = new ol.control.ZoomSlider();
  var scaleLineControl = new ol.control.ScaleLine();
  var updateLegend = function (resolution) {
    var graphicUrl = wmsSource.getLegendUrl(resolution);
    var img = document.getElementById('legend');
    img.src = graphicUrl;
  };
  var mousePositionControl = new ol.control.MousePosition();
  var map = new ol.Map({
    target: 'map',
    keyboardEventTarget: document,
    controls: ol.control.defaults().extend([
      fullScreenControl,
      //mousePositionControl,
      scaleLineControl,
      zoomSliderControl
    ]),
    layers: [
      new ol.layer.Group({
        title: 'Base maps',
        layers: [
```

Figure 3.5 JavaScript to add the content to Web-GIS based user interface system

```
layers: [
  new ol.layer.Group({
    title: 'Base maps',
    layers: [
      new ol.layer.Group({
        title: 'Bing Maps',
        type: 'base',
        combine: true,
        visible: true,
        layers: [
          new ol.layer.Tile({
            source: new ol.source.BingMaps({
              key: "AvcmFjEs4wUeEgcoyiNcImmFiKaHQA6-yWGPH5cEV4Sru8tQwjyOutXchQ_QLyX-",
              imagerySet: "AerialWithLabels",
            })
          }),
        ]
      }),
```

Figure 3.6 OpenLayers script to import data to Web-GIS based user interface system

GeoServer is an open-source server written in Java that allows users to share, process and edit geospatial data. Designed for interoperability, it publishes data from any major spatial data source using open standards. GeoServer has evolved to become an easy method of connecting existing information to virtual globes such as Google Earth as well as to web-based maps such as OpenLayers, Google Maps and Bing Maps. GeoServer functions as the reference implementation of the Open Geospatial Consortium Web Feature Service standard, and also implements the Web Map Service, Web Coverage Service and Web Processing Service specifications. GeoServer reads a variety of data formats, including PostGIS, Oracle Spatial, ArcSDE, MySQL, Shapefiles, and GeoTIFF etc. Through standard protocols it produces KML, GML, Shapefile, GeoRSS, PDF, GeoJSON, JPEG, GIF, SVG, PNG and more. In addition, one can edit data via the WFS transactional profile (WFS-T). GeoServer includes an integrated OpenLayers client for previewing data layers. In the present research work, GeoServer is used to publish flood inundation maps on a web interface. GeoServer interface with various layers used in the present research work is shown in Figure 3.7.

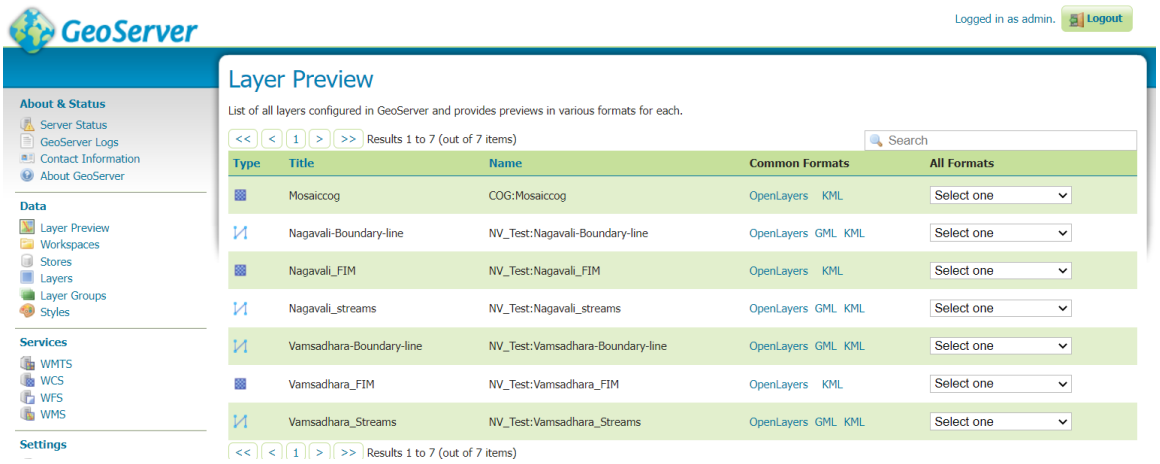

Figure 3.7 GeoServer interface with various layers used in the present research work

3.9 Procedure for Automation of the Research Work

The overall methodology includes downloading GFS forecasts, extraction of rainfall forecasts over the study area, bias correction of GFS rainfall forecasts, feeding rainfall data into SWAT model to obtain discharge hydrograph, assimilating simulated discharge hydrograph as upstream boundary condition in 2D HEC-RAS model to get flood inundation extent and depth, and finally uploading flood inundation maps into Web-GIS based user interface system automated using R and Python languages. The flowchart for the automation of research work is shown in Figure 3.8.

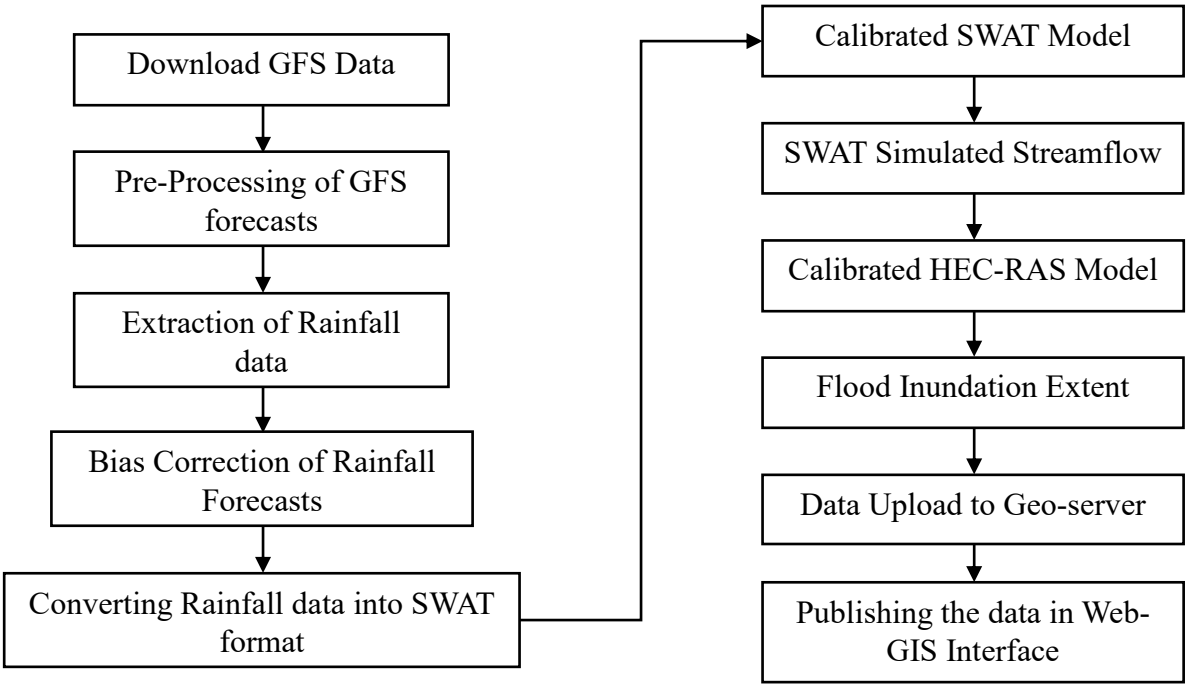

Figure 3.8 Methodology for the automation of the proposed research work

3.10 Closure

This chapter describes the overall methodology for developing an integrated hydrologic and hydraulic model based on SWAT and HEC-RAS for preparing flood inundation maps for the study river basins. The flowchart for the prediction of weather parameters using WRF model is given. The procedure for calculating rainfall extremes from daily time series data, trend analysis in rainfall and rainfall extremes, evaluation of NWP model forecasts, description of SWAT and HEC-RAS models to simulate floods and flood inundation extent, and flood frequency analysis for the calculation return periods, has been explained. Programming languages, mapping libraries, and web servers required to develop Web-GIS based user interface system have been explained. The flowchart for the automation of overall methodology is given.

Chapter - 4 Study Area and Database Preparation

4.1 Study Area

The selection of the study area is important for evaluating the efficient performance of the proposed methodology. The Nagavali and Vamsadhara river basins are selected in the present study. Location map of the study area is shown in Figure 4.1. These two river basins plays an important role in meeting irrigation and water supply demands in south Odisha and north Andhra Pradesh. The Nagavali and Vamsadhara rivers are two independent, adjacent and interstate eastern flowing rivers located between latitudes of 18° 10' to 19° 45' N and longitudes of 82° 54' to 84° 20' E. Both the rivers originate at Thuamul Rampur block of Kalahandi district of south Odisha, flow through nine districts and drain into the Bay of Bengal (BoB) at Bontala Koduru and Kalingapatnam in northeast Andhra Pradesh, respectively. The total length of Nagavali river from headwaters to its mouth in the Bay of Bengal is approximately 256 km, with a catchment area of 9510 square kilometers (sq.km), and Vamsadhara river is about 254 km, with a catchment area of 10830 sq.km. Annual rainfall ranges between 1200 and 1400 mm in both basins, with average minimum and maximum temperatures of 8 °C and 43 °C, respectively.

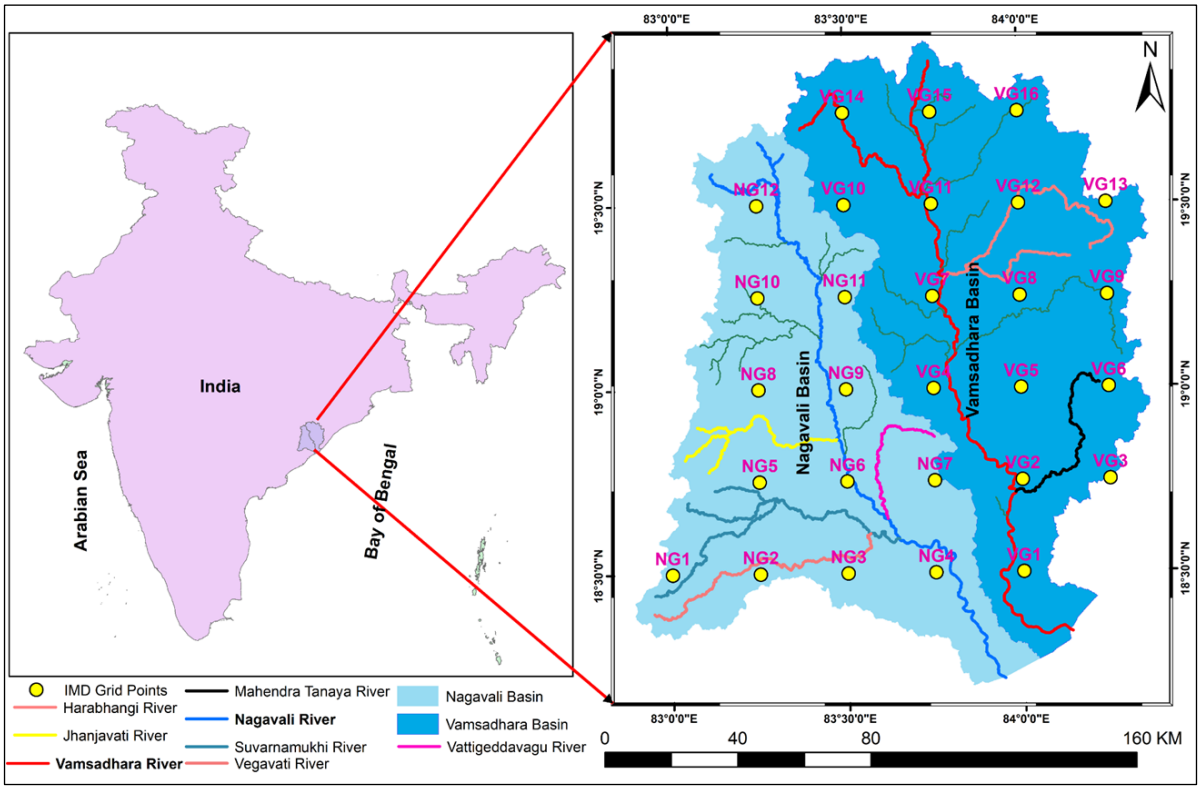

Figure 4.1 Geographical Location of the Nagavali and Vamsadhara River Basins, India

The Nagavali basin has elevations ranging from 0 to 1634 m, while the Vamsadhara basin has elevations ranging from 0 to 1505 m. The people in the catchment area rely primarily on agriculture. Paddy, cotton, red gram, sugarcane, groundnut, and sesame are among the crops grown in the basins during both Kharif and Rabi seasons. The field visit photos which shows the LULC, dam site, water depth measuring device are shown in Figure 4.2.

4.2 Data Used

The input data used in the present study includes hydrometeorological data and geospatial data. Details about the data which includes spatial resolution, organization name, and web source are given Table 4.1. The majority of the spatial, rainfall and temperature data used in the present research are freely available to the public. The observed streamflow and water levels are obtained from the Mahanadi & Eastern Rivers Organization (M&ERO), Bhubaneswar, India. The detailed explanation of the data used in the present research is described in the following sections.

Figure 4.2 Field observation photos of Nagavali and Vamsadhara basins

Table 4.1 Details of the datasets used in the present research study

Dataset	Spatial Resolution	Organization Name	Web Source
Rainfall	0.25° × 0.25°	IMD	https://www.imdpune.gov.in/Clim_Pred_LRF_New/Grided_Data_Download.html
Temperature	1° × 1°		
Stream Gauge Data	------	CWC, India	Mahanadi & Eastern Rivers Organization (M&ERO), Bhubaneswar.
FNL Data	1° × 1°	NCEP - FNL	https://rda.ucar.edu/datasets/ds083.2/
GFS Rainfall and Temperature Forecasts	0.25° × 0.25°	NCEP – GFS	https://rda.ucar.edu/datasets/ds084.1/
SRTM DEM	30 m × 30 m	SRTM	https://earthexplorer.usgs.gov/
Land Use Land Cover (LULC)	1:250k	NRSC	https://bhuvan-app1.nrsc.gov.in/thematic/thematic/index.php
Soil Data	1 km × 1 km	ISRIC	https://www.isric.org/explore/soil-geographic-databases

4.2.1 HydroMeteorological Data

Hydrometeorological data include rainfall, temperature, and streamflow. IMD provides daily rainfall (0.25° x 0.25°) records for a period of 120 years (i.e., 1901-2020) and temperature (1° x 1°) records for a period of 70 years (i.e., 1951-2020) in the gridded format. The average annual rainfall over Nagavali and Vamsadhara basins are 1230 mm and 1260 mm, respectively for 120 years. In both basins, the maximum temperature ranged between 20 °C to 43 °C and the minimum temperature ranged between 8 °C to 30 °C for 70 years. There are no missing records in the daily rainfall and temperature records. Rainfall data has been

verified with the rain gauge data provided by M&ERO and a good correlation of 0.79 is found between them. The details of the gauge data are given in Table 4.2.

The gauge data over a period of more than 25 years for both basins is obtained from M&ERO. Observed streamflow and water level data are provided by gauge stations at Srikakulam in the Nagavali basin and Gunupur, Kashinagar in the Vamsadhara basin. SWAT model is calibrated and validated using observed streamflow at Srikakulam and Kashinagar in the Nagavali and Vamsadhara basins, respectively. Water levels at Srikakulam are used to calibrate the HEC-RAS model in the Nagavali basin, while water levels at Kashinagar are used to calibrate in the Vamsadhara basin.

Table 4.2 Details of the gauge data in Nagavali and Vamsadhara basins

Name of the Station	Latitude	Longitude	River Name	Data Availability	Data Type
Gunupur	19° 05' 00" N	83° 48' 20"E	Vamsadhara	01.05.1978 - 31.05.2019	GDSQ
Kasinagar	18° 50' 54" N	83° 52' 23"E	Vamsadhara	01.07.1980 - 31.05.2019	GDSQ
Gudari	19° 23' 00" N	83° 47' 32"E	Vamsadhara	01.05.1978 - 31.05.2019	G
Kutragada	19° 36' 40" N	83° 33' 52"E	Vamsadhara	01.07.1987 - 31.05.2019	G
Mahendragarh	19° 13' 24" N	84° 15' 45"E	Vamsadhara	01.07.1987 - 31.05.2019	G
Mohana	19° 26' 41"N	84° 15' 41"E	Vamsadhara	01.07.1987 - 31.05.2019	G
Gottabarrage	18° 42' 00"N	83° 58' 00"E	Vamsadhara	01.07.1987 - 31.05.2019	G
Srikakulam	18°18' 48"N	85°53' 03"E	Nagavali	01.03.1988 - 31.05.2019	GDSQ

4.2.2 Geospatial Data

The geospatial data used in this study include DEM, LULC, and a soil map. The Shuttle Radar Topography Mission (SRTM) 30 m DEM is obtained from the US Geological Survey (USGS) earth explorer. The maximum elevations of the Nagavali and Vamsadhara basins are 1634 m and 1505 m, respectively. LULC data for both basins is obtained from Bhuvan, National Remote Sensing Center, at a scale of 1:250 km (Bhuvan-NRSC). There are 10 land cover patterns identified in both basins, such as built-up land, current fallow, deciduous forest, scrub forest, agricultural land, evergreen forest, plantation, shifting cultivation, wasteland, and waterbodies. The spatial plots of DEM and LULC maps of both basins are shown in Figure 4.2. The percentage of LULC in each basin is given in Table 4.3. Soil classification map is obtained from the International Soil Reference and Information Centre (ISRIC) soil data site. The soil map of the study area is shown in Figure 4.3. Loam, sandy loam, sandy clayey loam, and clayey loam soils are the important soil types found in both basins.

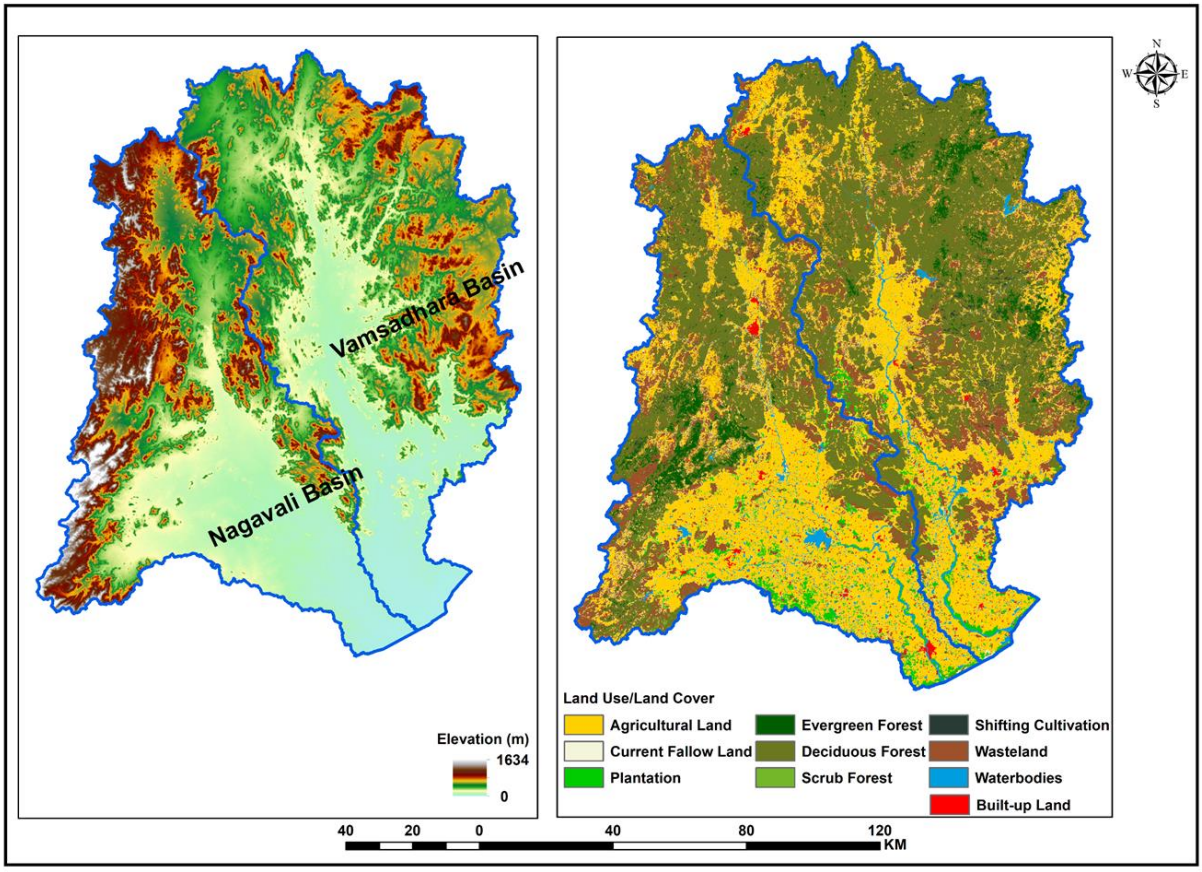

Figure 4.3 DEM and LULC of Nagavali and Vamsadhara basins

Table 4.3 Percentage area of each LULC in Nagavali and Vamsadhara Baisns

LULC	Nagavali Basin (%)	Vamsadhara Basin (%)
Built-up Land	1.14	1.03
Current Fallow	12.21	6.34
Deciduous Forest	29.34	51.45
Scrub forest	1.53	0.68
Agricultural land	26.19	16.38
Evergreen Forest	3.06	2.81
Plantation	2.94	0.75
Shifting Cultivation	1.62	1.2
Wasteland	19.05	17.79
Waterbodies	2.91	1.57

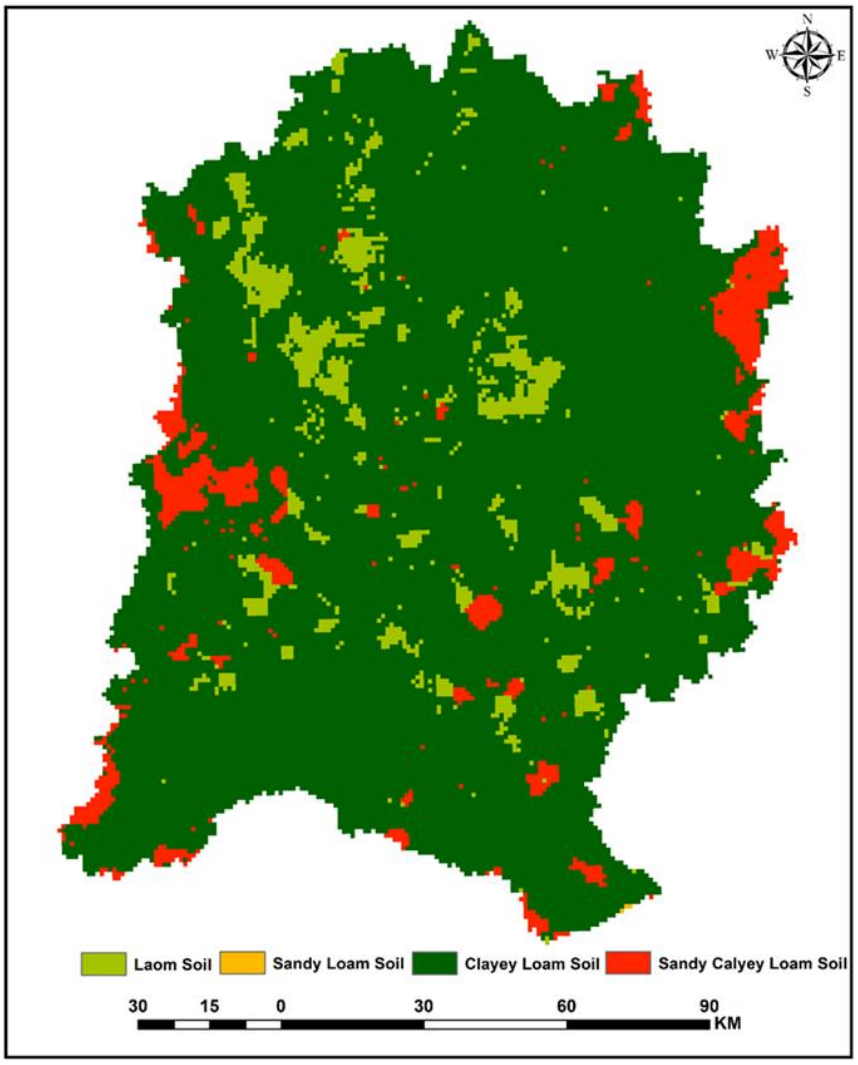

Figure 4.4 Soil Map of Nagavali and Vamsadhara Basin

4.2.3 GFS Forecast Data

In the present analysis, daily rainfall forecast data from GFS model are extracted for an area bounded between 18° - 20° N and 82.75° - 84.50° E at 0.25° × 0.25° grid resolution for a period of 2041 days i.e., from June 1, 2015 to December 31, 2020. A total of 28 grids falling over Nagavali and Vamsadhara basins. Out of these, 12 grids are over Nagavali basin and the remaining over Vamsadhara basin. Typical rainfall patterns for a day over Nagavali and Vamsadhara basins are shown in Figure 4.5.

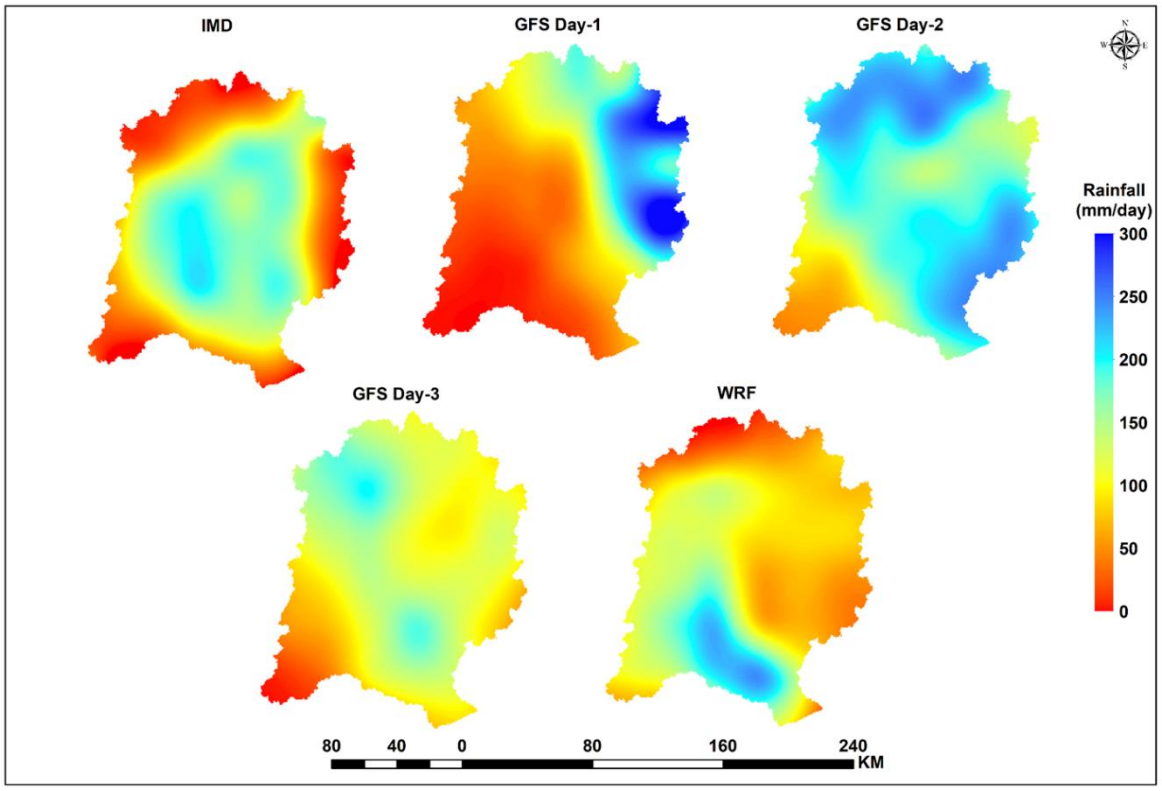

Figure 4.5 Rainfall map of various products on 11 - October - 2018 over study basins

4.2.4 Final Analysis Data

The NCEP Final (FNL) data has a horizontal resolution of 1° × 1° and available at six hour intervals. The FNL data is produced by Global Data Assimilation System (GDAS) through assimilating the observations from Global Telecommunications System (GTS). The meteorological variables in FNL data include, but are not limited to, cloud top pressure, surface winds, perceptible water, humidity, air temperature, and so on.

4.3 Details about the Tropical Cyclone

Regional Specialized Meteorological Centre (RMSC) issues national bulletins to public on cyclone formation from the stage of depression (D) onwards. During the stages of depression or deep depression, RMSC issues bulletins based on 00, 03, 06, 12, and 18 UTC observations. When the system intensifies into a cyclonic storm over the NIO, these bulletins are issued at 3-hour intervals based on previous observations. These bulletins contain present status of the system, expected damage and action suggested. These bulletins are completely made for national users and disseminated through various modes of communication (i.e. All India Radio, National TV, Telephone, SMS, print electronic media).

A set of 8 TCs formed over NIO during 2014 to 2018 are considered in the present study in order to assess the impact of microphysical schemes on their track and intensity predictions. Among the TCs, two had formed over AS and the remaining were in BoB. The details about the cyclones are given in Table 4.3. The best tracks provided by the study cyclones are shown in Figure 4.6 and the brief summery is given below.

Table 4.4 Details about the tropical cyclones

S.No	Period	Cyclone Name	Landfall	Category
1	7 – 17 Oct 2014	Hudhud	Visakhapatnam	Very Severe Cyclonic Storm
2	25 – 31 Oct 2014	Nilofar	No Landfall	Very Severe Cyclonic Storm
3	21 – 28 Oct 2016	Kyant	No Landfall	Cyclonic Storm
4	29 Nov – 05 Dec 2017	Ockhi	South Gujarat Coast	Very Severe Cyclonic Storm
5	19 – 22 Sept 2018	Daye	Gopalpur	Cyclonic Storm
6	8 – 13 Oct 2018	Titli	Palasa	Very Severe Cyclonic Storm
7	10 – 19 Nov 2018	Gaja	Puducherry	Very Severe Cyclonic Storm
8	13 – 18 Dec 2018	Phethai	Yanam	Severe Cyclonic Storm

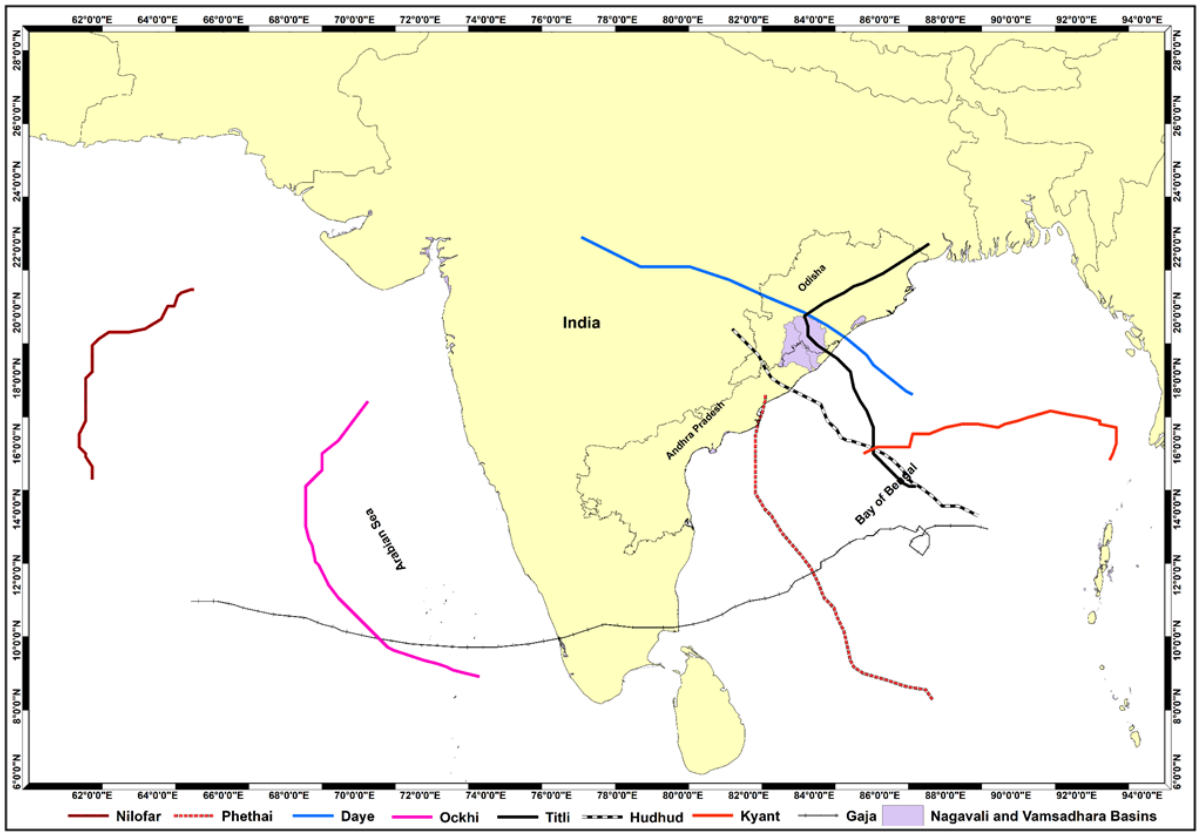

Figure 4.6 Best tracks of the TCs provided by RMSC.

Hudhud

In the morning of 6th Oct 2014, cyclone Hudhud formed as a low-pressure area (LPA) over BoB. It gradually intensified into Very Severe Cyclonic Storm (VSCS) in the afternoon of 10th Oct 2014. It made landfall near Visakhapatnam with northwestward movement on the morning of 12th Oct 2014 as VSCS and moved in the same direction. It then gradually weakened into a Well-Marked Low-Pressure Area (WMLA) on the evening of 14th Oct 2014 over eastern Utter Pradesh.

Nilofar

A VSCS Nilofar formed as an LPA over the southeast Arabian Sea (AS) on the morning of 21st Oct 2014. The cyclone initially moved northwestward on the day of formation and then recurved to northeastwards. It exhibited rapid intensification as well as rapid weakening and weakened into a WMLA near the North Gujarat coast on the morning of 31st Oct 2014.

Kyant

Cyclone Kyant formed as a depression (D) over east central BoB on 21st Oct 2016. The track followed by this system is rare in nature as it experienced two re-curvatures during its life

period. The rate of intensification was very slow and steady, taking about 4 days to become a cyclonic storm (CS) from the stage of D and the rate of weakening was rapid as it reduced to a WMLA from the CS stage within 30 hours on the morning of 28th Oct 2016.

Ockhi

Cyclone Ockhi formed as an LPA over Andaman Sea on 22nd Nov 2017. There was a rapid intensification during its genesis, as it intensified into CS within 6 hours from the stage of deep depression (DD). While moving west-northwestwards, Ockhi further intensified into Severe Cyclonic Storm (SCS) over Lakshadweep area early in the morning of 01st Dec 2017 and VSCS over southeast AS on the afternoon of the same day. It then moved northwestwards and attained the maximum intensity on afternoon of 2nd Dec 2017. It moved north-northwestwards and then northeastwards, crossed the south coast of Gujarat between Surat and Dahanu as a WMLA early in the morning of 06th Dec 2017.

Daye

Daye is the first cyclonic storm formed over NIO in the month of September after 2005. It formed as a D over east central parts of BoB on the afternoon of 19th Sept 2018. Moving nearly west-northwestwards, it intensified into DD on the morning of 20th Sept 2018 and into CS on the same day/night. It made landfall close to Gopalpur as a CS during 1900-2000 UTC of 20th Sept 2018. It continued to move west-northwestwards, and weakened into an LPA over south Haryana on the morning of 24th Sept 2018.

Titli

Titli cyclone formed as an LPA over the southeast BoB on the morning of 7th Oct 2018. Moving nearly west-northwestwards, it intensified into DD on the morning of 8th Oct 2018 and further into a CS around noon of 9th Oct 2018. It then moved northwestwards and on the early morning of 10th Oct 2018, it intensified into SCS. It then moved north-northwestwards and further intensified into VSCS around noon of 10th Oct 2018 and crossed the northern Andhra Pradesh and south Odisha coasts near Palasa during 2300 to 0000 UTC as a VSCS. Moving further west-northwestwards, it weakened into an SCS around the noon of 11th Oct 2018 and CS in the same evening. Under the influence of southwesterly winds, the system recurved northeastwards from 11th evening and gradually weakened into an LPA over Gangetic West Bengal and adjoining Bangladesh on the morning of 13th Oct 2018.

Gaja

VSCS Gaja originated from an LPA which formed over the Gulf of Thailand and adjoining Malay Peninsula on the morning of 8th Nov 2018. Under favorable conditions it concentrated into a D over southeast BoB n the morning of 10th Nov. Moving west-northwestwards, it intensified into DD in the same evening and further intensified into CS early in the morning of 11th Nov 2018. It then moved nearly westwards till early hours of 12th Nov 2018. Thereafter, it recurved south-southwestwards and followed an anticlockwise looping track till 13th Nov 2018. It then moved west-southwestwards and intensified into an SCS southwest BoB on the morning of 15th Nov 2018 and into VSCS on the same night. Moving further west-southwestwards it crossed Tamil Nadu and Puducherry coast between Nagapattinam and Vedaranniyam during 1900 to 2100 UTC of 16th Nov 2018. Thereafter, it moved nearly westwards, and weakened rapidly into an SCS, CS, and DD over interior Tamil Nadu on 16th Nov 2018. It then moved west-southwestwards and weakened into a D on the same evening over central Kerala. Moving nearly westwards, it emerged into southeast AS in the same mid night. Moving nearly westwards, it intensified into a DD over southeast AS in the early morning of 17th Nov 2018. Thereafter, it moved nearly west-northwestwards and crossed Lakshadweep Islands on 17th Nov 2018 afternoon as DD. It continued to move west-northwestwards and weakened into a D over the same region around the noon of 19th Nov 2018, WMLA in the same mid night and LPA on 21st Nov 2018.

Phethai

An SCS Phethai formed as an LPA over Equatorial Indian Ocean and adjoining central parts of south BoB on the evening of 9th December 2018. It laid as a WMLA over the same area on the morning of 11th December 2018. It continued to be WMLA till the morning of 13th and under favorable conditions it concentrated into a D over southeast BOB. Moving north-northwestwards, it intensified into DD over the same area on the same day at midnight. Continuing to move in the same direction, it intensified into a CS on the evening of 15th and into SCS on the afternoon of 16th. It maintained its intensity of SCS till the early morning of 17th and weakened into CS in the same morning. Continuing to move north-northwestwards and then northwards, it crossed Andhra Pradesh (close to south of Yanam and 40 km south to Kakinada) coast during the 17th afternoon as a CS. After landfall, the cyclone moved north-northeastwards and weakened rapidly into a DD near Kakinada coast in the same evening. Continuing to move in the same direction, it again crossed Andhra Pradesh coast near Tuni and weakened into a D over coastal Andhra Pradesh during the same day midnight.

It further weakened into WMLA over northwest and adjoining west central BoB and coastal Odisha in the early morning of 18th and into LPA northwest BoB and adjoining Odisha in the same morning.

4.4 Software's and Programming Languages used

Various GIS software's, modelling software, and programming languages are used in this research. These include ArcGIS, QGIS, WRF, SWAT, HEC-RAS, R-program, Python, HTML, CSS, JavaScript, OpenLayers, and GeoServer. ArcGIS and QGIS software are used for analyzing vector data and generating spatial maps from interpolation techniques. The WRF model is used for predicting the track, intensity, and rainfall of tropical cyclones in the BoB. SWAT model is used for streamflow simulation in QGIS environment. HEC-RAS model is used for the generation of flood inundation extent and inundation depth. Programming language R is used for the preparation of hydrometeorological data in SWAT and HEC-RAS format and for the SWAT simulations using SWATPlusR package. Programming language Python is used to automate HEC-RAS model by connecting it to HECRASController module. Other programming languages such as HTML, CSS, JavaScript, OpenLayers, and GeoServer are used develop a Web-GIS based interface for the timely dissemination of flood related information.

4.5 Initialization, Calibration, and Validation of Models

Based on the methodology framework proposed, different models are used in the study. Each of those model set-ups is explained in the following sections.

4.5.1 WRF Model

WRF (version 4.0) model is used to forecast rainfall during extreme weather events like TCs along with its track and intensity. The initial and boundary conditions for the prediction of TCs are considered from the 1° × 1° resolutions of NCEP-FNL model forecasts with 6-hour interval. The model is designed with two-way nested domains with 27 km horizontal resolution for the outer domain and 9 km horizontal resolution for the inner domain. The WRF domain configuration is presented in Figure 4.7. The terrain data of 10m resolution from the USGS has been used for both domains. The model utilized a total of seven microphysical schemes, namely, Lin, Thompson, Ferrier, Morrison, WSM3, WSM5, and

WSM6 for both domains. The KF CPS is used for the outer domain. YSU PBL scheme, Rapid Radiative Transfer Model (RRTM) for long-wave radiation, and Dudhia scheme for short-wave radiation have been used for both the inner and outer domains.

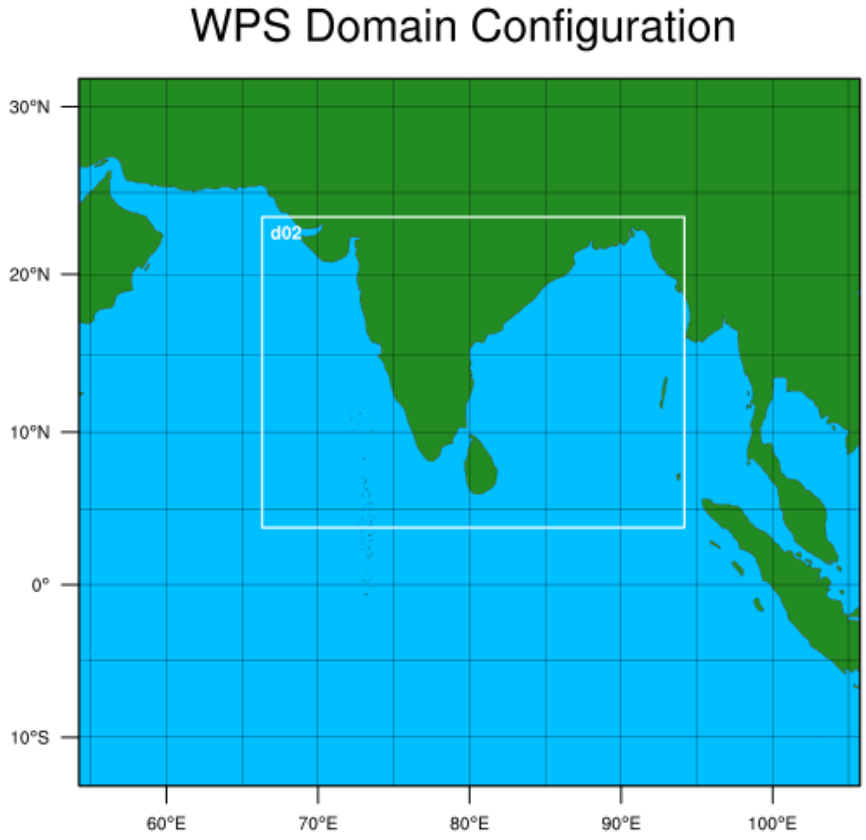

Figure 4.7 WRF Model Domain Configuration

The various microphysics schemes deal with the mixing ratios of the prognostic variables with different approaches under different assumptions. The mixing ratios of the prognostic variables in all the microphysical schemes considered in the study are presented in Table 4.5. Lin scheme includes all the prognostic variables. It is a most sophisticated scheme of WRF model and suitable for research studies (Lin et al. 1983). The new Eta Ferrier scheme has an ability to predict the changes in water vapor and estimates the precipitation ice density along with mixing ratios (Rogers et al. 2001). Thompson scheme used in the present study is a double-moment scheme which includes the prediction of ice concentration (Thompson et al. 2004). The scheme assumes that the snow size distribution depends on both water and ice content and temperature (Castro et al. 2019). Morrison's scheme is also a double-moment scheme which predicts the mixing ratios and concentrations of all prognostic variables. The scheme uses Kohler's theory to calculate the homogeneity and heterogeneity in the nucleation process and quasi-stationary saturation adjustment algorithm for droplet concentration

(Morrison et al. 2009). WSM3 is a simple ice scheme, which predicts only the liquid hydrometers (i.e., Q_v, Q_c, *and* Q_r). The expressions considered by WSM3 to predict liquid hydrometers are assumed to be above freezing point. Further, the scheme considers Q_c as Q_i and Q_r as Q_s when the temperature is less than or equal to freezing point. The WSM5 scheme predicts the mixing ratios of all prognostic variables except graupel (Hong et al. 2004). The WSM6 scheme is similar to that of WSM3, but includes a more complex process for predicting the mixing ratios of all the prognostic variables (Hong and Lim 2006). Compared to the double-moment schemes, single-moment schemes have the capability to simulate the TCs with smaller eye, stronger tangential wind, high positive temperature and closer latent heating area to cyclone center, and smaller radius of maximum wind (Li et al. 2020).

For sensitivity experiments, a total of 8 TCs are selected to study the sensitivity of microphysical schemes for the prediction of track and intensity of TCs over the NIO region that occurred from 2014 to 2018. The model initiation time and simulation period for the TCs are presented in Table 4.6. The detailed description about WRF model configuration is presented in Table 4.7. The simulated results of the TCs are validated against the best track given by IMD.

Table 4.5 The mixing ratios of the prognostic variables in the Microphysical Schemes

Microphysical Schemes	Mixed Phase Variable Processes
Ferrier	Water Vapor (Q_v), Cloud Water (Q_c), Rain (Q_r), Ice (Q_i)
Lin	Water Vapor, Cloud Water, Rain, Ice, Snow (Q_s), and Graupel (Q_g)
Morrison	Water Vapor, Cloud Water, Rain, Ice, Snow, and Graupel
Thompson	Water Vapor, Cloud Water, Rain, Ice, Snow, and Graupel
WSM3	Water Vapor, Cloud Water/Ice and rain/snow
WSM5	Water Vapor, Cloud Water, Rain, Ice, and Snow
WSM6	Water Vapor, Cloud Water, Rain, Ice, Snow, and Graupel

Table 4.6 Model initiation dates and simulation time considered for the study

Tropical Cyclone	Initial Date: Time	End Date: Time	Simulation Period (h)	Intensity Stages of TCs for Model Initialization
Hudhud	09-10-2014: 00	13-10-2014: 00	96	Severe Cyclonic Storm (SCS)
Nilofar	27-10 -2014: 00	31-10-2014: 00	96	Severe Cyclonic Storm (SCS)
Kyant	23-10-2016: 00	27-10-2016: 00	96	Depression (D)
Ockhi	01-12-2017: 00	05-12-2017: 00	96	Severe Cyclonic Storm (SCS)
Daye	20-09-2018: 00	22-09-2018: 00	48	Depression (D)
Titli	09-10-2018: 00	13-10-2018: 00	96	Deep Depression (DD)
Gaja	12-11-2018: 00	16-11-2018: 00	96	Cyclonic Storm (CS)
Phethai	14-12-2018: 00	18-12-2018: 00	96	Deep Depression (DD)

Table 4.7 Details of WRF Model Configuration

Model	WRF 4.0
Domain Center	10° N and 80° E
Number of Domains	2 (d01 = 27 km, d02 = 9 km)
Initial and Boundary Conditions	GFS ANL data (0.5° × 0.5°)
Cumulus Physics	Kain – Fritsch (Kain 2004)
Short-wave Radiation	Dudhia (Dudhia 1989)
Long-wave Radiation	RRTM (Mlawer et al. 1997)
Planetary Boundary Layer	Yonsei University (Hong et al. 2006)
Microphysics	Ferrier, Lin, Morrison, Thompson, WRF Single Moment 3 – Class (WSM3), WRF Single Moment 5 – Class (WSM5), WRF Single Moment 6 – Class (WSM6).

4.5.2 SWAT Model-Set-up

Initially, to set-up the SWAT model, DEM, LULC and soil data are projected into common projection as WGS 1984 UTM 44N. The Nagavali river basin is delineated into 34 sub-basins and 2153 hydrological response units (HRUs) and the Vamsadhara river basin is delineated into 30 sub-basins and 2183 HRUs based on the homogeneity of soil, land use, slope and 100 hectares (Ha) of threshold area (Figure 4.8). The Natural Resources Conservation Service (NRCS) method is used to simulate daily runoff by SWAT model. Observed daily streamflow is used to calibrate and validate the simulated streamflow. The SWAT model performance is evaluated using the coefficient of determination (R^2), Nash Sutcliff Efficiency (NSE), and percent bias (PBIAS). The values of R^2 ranged between 0 and 1. The values of NSE ranged between -∞ to 1 and they provide a measure of how well the simulated output matches the observed data along a 1:1 line. The optimal value for PBIAS is 0, a positive value represents model underestimation, while a negative value represents model overestimation. The model performance is considered satisfactory if the NSE is greater than 0.6 and PBIAS is within +/- 25% (Moriasi et al. 2007).

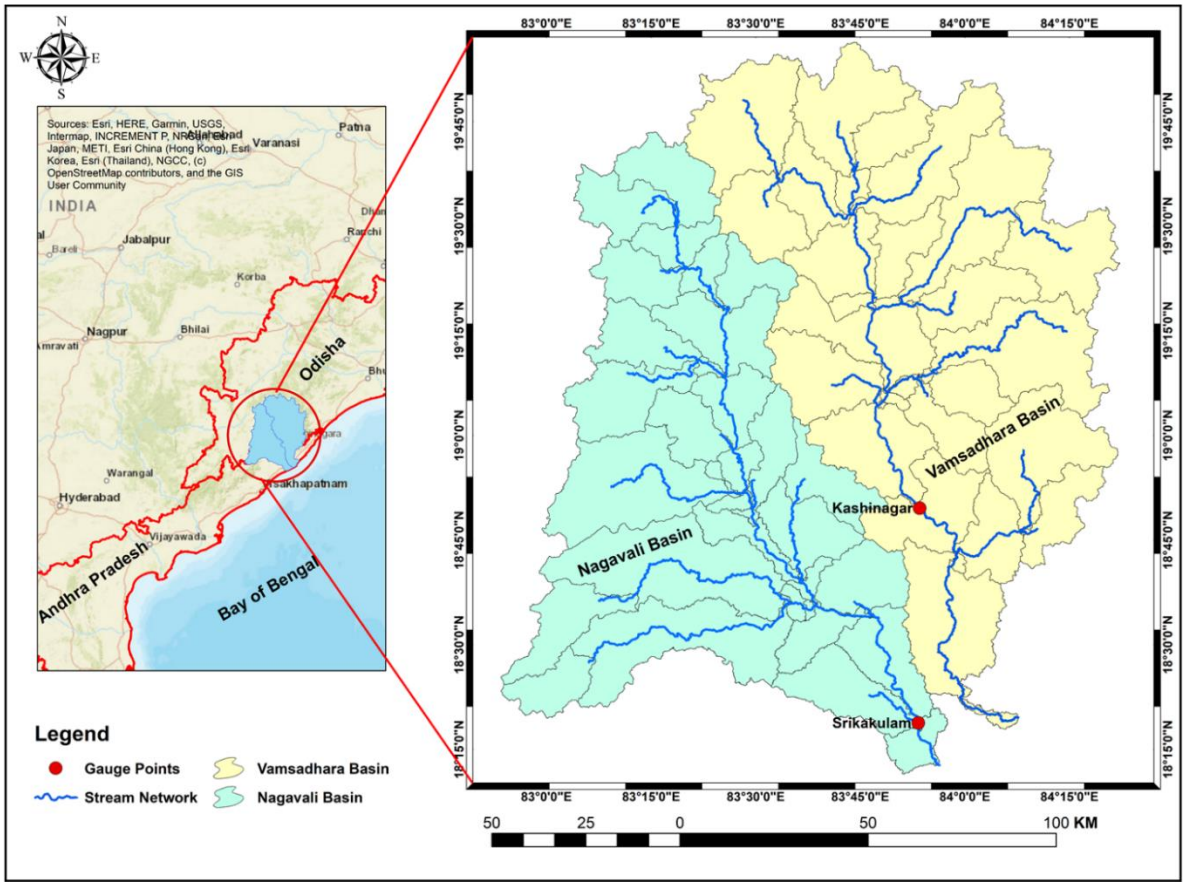

Figure 4.8 SWAT simulated sub-basins and observed gauge locations in Nagavali and Vamsadhara basins

The mathematical expressions for R^2 and PBIAS are given in equations 3.30 and 3.32. The expression for NSE is given below:

$$NSE = 1 - \frac{\sum_{i=1}^{n}\left(O_i^{obs} - O_i^{sim}\right)^2}{\sum_{i=1}^{n}\left(O_i^{obs} - O_{mean}^{obs}\right)^2} \quad (4.1)$$

Where, O_i^{obs} is the ith observed data, O_i^{sim} is the ith simulated data, O_{mean}^{obs} is the mean of observed data and n is the number of observations.

4.5.3 SWAT Model Calibration, Validation, and Sensitivity Analysis

SUFI-2 algorithm in the SWAT-CUP is used for calibration, validation, and sensitivity analysis. The observed streamflow at Srikakulam and Kashinagar stations is used to calibrate and validate the SWAT model on daily basis over Nagavali and Vamsadhara basins, respectively. The model is run for a total of 29 years, from 1986 to 2014. Of the 29 years, the first 5 years (1986-1990) are considered as warm-up period, the next 15 years (1991-2005) are considered for calibration, and the last 9 years (2006-2014) are considered for validation. The calibrated parameters and their fitted values for Nagavali and Vamsadhara basins are shown in Table 4.8. During the calibration and validation periods, the NSE values for daily streamflow at Srikakulam gauge station in Nagavali basin are 0.59 and 0.57, respectively, and 0.64 and 0.59 at Kashinagar gauge station in Vamsadhara basin. The PBIAS values during the calibration period is 0.8% in Nagavali basin and 6.5% in Vamsadhara basin. The PBIAS values during the validation period is 7% and 11% over Nagavali and Vamsadhara basins, respectively. From the PBIAS values, it is observed that the SWAT model underestimated the streamflow during the calibration and validation period in both basins.

Table 4.8 Statistics for the calibration and validation of daily streamflow over Nagavali and Vamsadhara basins

River Basin	Gauging Station	Calibration				Validation			
		Period	R^2	NSE	PBIAS	Period	R^2	NSE	PBIAS
Nagavali	Srikakulam	1991-005	0.59	0.59	0.8	2006-014	0.58	0.57	7
Vamsadhara	Kashinagar	1991-005	0.66	0.64	6.5	2006-014	0.60	0.59	11

A total of 17 parameters are considered during the calibration. Sensitivity analysis is conducted to identify the most sensitive parameters using P-value. Among the parameters, manning's n value for the main channel (CH_N2), curve number (CN2), groundwater revap coefficient (GW_REVAP), effective hydraulic conductivity in main channel alluvium (CH_K2), deep aquifer percolation fraction (RCHRG_DP), effective hydraulic conductivity in tributary channel alluvium (CH_K1), threshold depth of water in the shallow aquifer required for return flow to occur (GWQMN), and manning's "n" value for the tributary channels (CH_N1) are the most sensitive parameters for streamflow simulations in the Nagavali basin. In Vamsadhara basin, CN2, CH_K1, CH_N1, CH_N2, and GW_Delay are the most sensitive parameters for streamflow simulations. The calibrated parameters and their fitted values for Nagavali and Vamsadhara basins are shown in Table 4.9.

Table 4.9 Calibrated parameters and fitted values of the sensitive parameters over Nagavali and Vamsadhara basins

S.No	Parameter_Name	Minimum value	Maximum value	Fitted Value	
				Nagavali Basin	Vamsadhara Basin
1	R_CN2.mgt	-0.1	0.1	-0.04	-0.088
2	V__ALPHA_BF.gw	0.3	1	0.99	0.479
3	A__GW_DELAY.gw	-30	90	45.60	-23.2
4	A__GWQMN.gw	-1000	1000	-873.33	713.33
5	V__GW_REVAP.gw	0.02	0.2	0.05	0.093
6	A__REVAPMN.gw	-750	750	-77.50	-375.50
7	V__ALPHA_BF_D.gw	0	1	0.64	0.723
8	A__RCHRG_DP.gw	-0.05	0.05	0.04	0.035
9	R__SOL_AWC.sol	-0.05	0.05	-0.01	-0.029
10	V__ESCO.hru	0.3	0.6	0.41	0.439
11	V__LAT_TTIME.hru	0	120	94.00	12.4
12	V__SLSOIL.hru	0	120	14.80	27.6
13	V__CANMX.hru	0	20	1.27	2.20
14	V__CH_N2.rte	0.01	0.15	0.07	0.055
15	V__CH_K2.rte	0	100	69.67	53.00
16	V__CH_K1.sub	0	100	43.00	84.33
17	V__CH_N1.sub	0.01	15	0.10	0.143

4.5.4 HEC-RAS Model Set-up

Flood inundation extent and depth are predicted for Nagavali and Vamsadhara basins using two dimensional 2D HEC-RAS model developed by the U.S. Army Corps of Engineers, with unsteady flow and the diffusive wave equations (Brunner, 2016). The user can perform one-dimensional (1D), 2D, as well as coupled 1D and 2D hydraulic calculations with the model. Using 2D unsteady modeling, the river and its floodplain can be discretized into a group of individual cells, which are also known as computational cells. The computational cells store information about the elevation as well as roughness values at that specific location. The model calculates the Water Surface Elevation (WSE) at the center of the cell at each time step using a finite volume approach.

The terrain for 2D HEC-RAS model in both Nagavali and Vamsadhara basins is developed using SRTM DEM with a resolution of 30 m. The 2D flow area is marked by a polygon, which specifies the extent of the area in which 2D flow calculation can be performed in lateral and longitudinal directions, assuming velocity in z-direction is negligible. Based on the 2D flow area, a 2D computational mesh is defined with cell spacing of 100 m × 100 m, yielding 95735 and 77322 computational cells in Nagavali and Vamsadhara basins, respectively. During the generation of 2D computational mesh, the cell size is selected based on the computational time step and model stability. A time step of one minute is chosen for both basins to accurately predict the hydrograph and fulfill the courant condition. The courant number is a dimensionless value representing the time step taken by a water particle to travel from one cell to another in a computational mesh. SWAT simulated discharge is applied to the upstream boundary conditions at three different locations in Nagavali basin and two different locations in Vamsadhara basin, with a calculated energy slope of 0.001816 and 0.001327, respectively. The downstream boundary condition in both basins is set to normal depth. The roughness values are assigned to 2D computational mesh in both basins using NRSC LULC map. Banklines are established at every 10 km interval in both basins to extract depth information. Figure 4.9 illustrates a schematic representation of 2D HEC-RAS model setup for Nagavali and Vamsadhara basins.

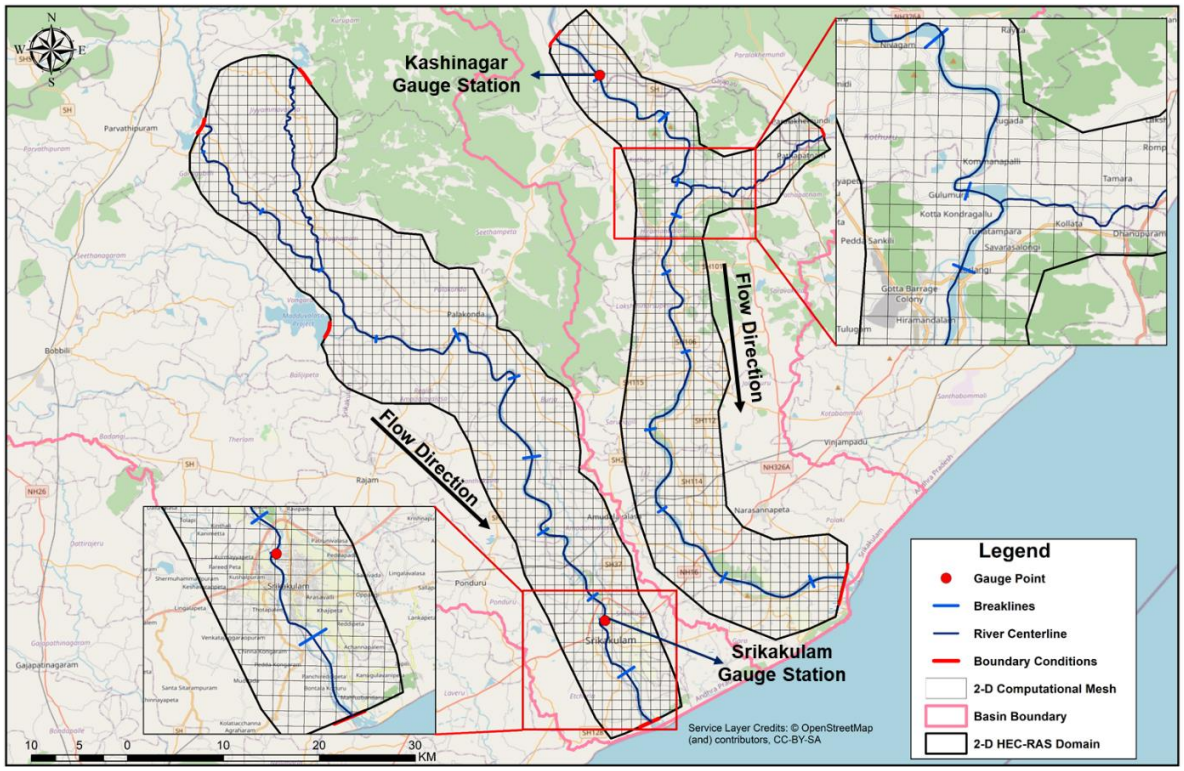

Figure 4.9 2D HEC-RAS model setup for Nagavali and Vamsadhara basins.

4.5.5 Validation of HEC-RAS Model

Two approaches are used to validate the flood inundation maps generated by the HEC-RAS model. In the first approach, the simulated depths for historical events are compared with observed water levels at the Srikakulam and Kashinagar gauge stations in Nagavali and Vamsadhara basins, respectively. In the second approach, the inundation maps generated by HEC-RAS model for Titli cyclone over Vamsadhara basin using SWAT simulated discharge from IMD rainfall and GFS forecasts are validated against the flood inundation map provided by Bhuvan-NRSC. Based on overlapping areas between the inundation map generated by the model and the inundation map provided by NRSC, the performance of HEC-RAS model is assessed (Tamiru and Dinka 2021). The intersection tool is used to get the percentage of overlapping area between NRSC flood inundation maps and the HEC-RAS model.

4.5.6 Integration of SWAT and HEC-RAS Model

The calibrated and validated SWAT model is used to generate the discharge hydrograph, which is then linked with 2D HEC-RAS model to generate flood inundation extent and depth. The SWAT model simulates discharge when it receives input parameters such as rainfall and

temperature. The HEC-RAS model subsequently assimilated the simulated discharge as upstream boundary conditions in both basins to generate flood inundation extent and depth.

4.5.7 Setting-up the GeoServer

To display the flood inundation extent on the web interface, the spatial data must be fed into GeoServer and OpenLayers. To achieve this, a workspace needs to be created in the GeoServer and services such as Web Map Service (WMS) and Web Feature Service (WFS) should be enabled. Once the workspace has been created, a new data store needs to be created, which will become the data source. The vector data store is created with Shapefile, and the raster data store with GeoTIFF. Once the vector and raster data stores have been created, all the layers need to be published with proper coordinate system and styles. The publishing process can be automated using GeoServer's REST API. Once the layers are published and available, OpenLayers can access them to display on the web interface. To access the layers from GeoServer, a WMS or WFS request has to be generated which will need to be sent to the GeoServer requesting data. The code used by OpenLayers to access the layers with WMS request is presented in Figure 4.10.

The Uniform Resource Locator (URL) given in Figure 4.10 contains information about the name of the workspace in which the layers are stored. This code generates and sends a WMS request to the GeoServer whenever a particular layer is to be accessed and retrieves the data in the form of tiles. OpenLayers then displays these tiles on the web interface. Using layer switcher, these tiles can be turned on or off. Code has been written to access all the required layers as they are updated in the database and GeoServer.

```
new ol.layer.Tile({
  title: 'Nagavali Boundary',
  visible: false,
  source: new ol.source.TileWMS({
    url: 'http://localhost:8080/geoserver/SPARC/wms',
    params: {'LAYERS': 'SPARC:Nagavali-Boundary-line', 'TILED': true},
    serverType: 'geoserver',
    transition: 0,
  })
}),
```

Figure 4.10 Code used by OpenLayers to publish layers from GeoServer

4.5.8 Automation of SWAT and HEC-RAS Models

SWAT and HEC-RAS models are automated using R and Python programming languages to forecast floods and flood inundation extent at regular intervals on a daily time scale. To run the SWAT model in a programming environment, SWATPlusR package needs to be installed. After installing SWATPlusR package, SWAT executable has to be copied into the folder where the SWAT project is stored. SWATPlusR package offers support for SWAT 2012 version and SWAT+ version. If the SWAT project is created using SWAT 2012, "run_swat2012" command has to be selected to run SWAT model in R environment. The script for running SWAT model in R environment is given in Figure 4.11.

The HECRASController module in python is required to run HEC-RAS model in a programming environment. It will be installed during HEC-RAS model installation and does not require any further installation. The script for running HEC-RAS model is python environment when is given in Figure 4.12.

```
q_sim_nag <- run_swat2012(project_path = 'F:\\SPARC\\N_RSWAT\\TxtInOut',
                          output = define_output(file = "rch",
                                                 variable = "FLOW_OUT",
                                                 unit = 1:34),
                          start_date = "2021-01-01",
                          end_date = "2021-01-10")
```

Figure 4.11 Script for running SWAT model in R environment

```
import win32com.client
from osgeo import gdal
RC = win32com.client.Dispatch("RAS610.HECRASController")
RC.ShowRAS()
#Nagavali HEC-RAS File
RC.Project_Open(r"F:\SPARC\Inundation_Maps\Nagavali_2d_1d -
Copy\Nagavali_2d_1d.prj")
Simulation=RC.Compute_CurrentPlan(None,None,True)
RC.Project_Save()
RC.QuitRAS()
src = gdal.Open(r"F:\SPARC\Inundation_Maps\Nagavali_2d_1d -
Copy\N_1d_2d\Depth (Max).Nagavali_SRTM_DEM.tif")
src1 = r"F:\SPARC\Inundation_Maps\data_dir\Inundation_Maps
\Nagavali_FIM.tif"
ds = gdal.Translate(src1,src)
ds = None
```

Figure 4.12 Script for running HEC-RAS model is python environment

4.6 Closure

Two medium sized east flowing river systems, namely, Nagavali and Vamsadhara basins are chosen as study areas in the present research work. Geospatial database in the required format for the hydrologic and hydraulic models is prepared using ArcGIS software. The hydrometeorological data in the required format for hydrologic and hydraulic models are prepared using R and python programming language. Initialization, calibration, and validation of various models (WRF, SWAT, and HEC-RAS) have been explained. Explanation about the GeoServer to publish flood inundation maps via web-interface with OpenLayers and automation of SWAT and HEC-RAS models in programming environment is given in this chapter.

Chapter - 5 Results and Discussions (Part-I)

5.1 General

For the selected study area, trends and patterns in rainfall characteristics are analyzed using various trend analysis methods explained in chapter 3. Based on the trends and patterns in rainfall characteristics over the study area, the predictions of track and intensity of tropical cyclones are analyzed using WRF model. A detailed explanation about the trends and patterns in rainfall characteristics, and track and intensity prediction of tropical cyclones using WRF model are given in the following sections.

5.2 Trends in Rainfall and Rainfall Extremes

Monthly, seasonal, and annual trends in rainfall and rainfall extremes are analyzed using four different MK tests (i.e., MK1/MK2/MK3/MK4) for 28 grids covering Nagavali and Vamsadhara basins (Figure 4.1) at a confidence level of 90% or higher. If any grid is showing either positive or negative trends in at least 3 tests, then it is considered as threshold value and the trends of those grids are analyzed. The total number of grids showing significant trends (positive/negative) at a 90% confidence level are presented in Table 5.1. The spatial patterns of trends in rainfall and rainfall extremes are mapped using kriging interpolation method. Detailed analysis of the annual and seasonal results are presented in the following sections and the monthly results are presented in Appendix-A.

5.2.1 Trends in Seasonal and Annual Rainfall

The Z statistics of the trends in seasonal and annual rainfall are evaluated and presented in Table A1 (Appendix-A). As illustrated, 4 out of 12 grids in Nagavali basin and 3 out of 16 grids in Vamsadhara basin showed negative trends in winter. In the pre-monsoon and monsoon seasons, positive trends are observed in both the basins. The anecdotal evidence for positive trends in pre-monsoon can be tied to the landfall of cyclones in this region that are formed in BoB (Uddin et al. 2019). It is observed that the grids that are showing significant trends (positive/negative) in the pre-monsoon and monsoon seasons have also shown some similar trends at the annual scale. In the post-monsoon season, however a negative trend is observed in Nagavali basin and no significant trend is observed in Vamsadhara basin. The spatial patterns of trends in seasonal and annual rainfall using four MK tests are presented in Figure 5.1.

Table 5.1 Total number of IMD grids showing significant trends (≥ 90% confidence level) for rainfall and rainfall extremes in both Nagavali and Vamsadhara Basin

		Rainfall		CDD		CWD		PRCPTOT		R10MM		R20MM		R40MM		R95PTOT		RX1DAY		RX5DAY	
		N+/N-	V+/V-	N+/N-	V+/V-	N+/N-	V+/V-	N+/N-	V+/V-	N+/N-	V+/V-	N+/N-	V+/V-	N+/N-	V+/V-	N+/N-	V+/V-	N+/N-	V+/V-	N+/N-	V+/V-
Long-Term	Annual	2/1	7/0	2/0	2/0	2/1	6/0	2/1	7/0	2/1	7/0	4/1	6/1	4/0	0/0	5/0	1/0	4/0	0/0	1/0	2/0
	Winter	0/4	0/3	0/3	0/1	0/4	0/3	0/2	0/1	0/8	0/1	0/1	0/0	0/0	0/2	0/0	0/2	0/6	0/1	0/2	0/6
	Pre-Monsoon	2/0	9/0	0/4	0/7	0/1	2/0	5/0	6/0	3/0	5/0	2/0	4/0	1/0	7/0	2/0	3/0	3/0	8/0	0/0	9/0
	Monsoon	5/1	9/1	2/0	2/4	2/1	5/0	6/1	8/0	2/2	9/2	5/1	8/0	6/1	6/0	4/1	6/0	3/1	2/0	1/1	7/0
	Post-Monsoon	0/1	0/0	3/0	1/0	0/0	1/0	0/0	0/1	0/1	0/0	0/1	0/0	0/0	0/0	0/0	0/0	0/0	0/0	0/0	0/0
Pre-1950	Annual	0/0	0/0	0/0	0/0	0/0	0/2	0/0	0/0	2/0	1/0	0/0	0/0	0/1	0/0	0/1	0/0	0/1	0/0	0/0	0/0
	Winter	0/0	0/0	0/0	0/0	0/0	0/0	0/0	0/0	0/1	0/0	1/0	1/1	1/0	1/1	0/0	0/4	0/0	1/0	0/0	0/1
	Pre-Monsoon	2/0	0/0	0//0	0/0	9/0	2/0	3/0	0/0	4/0	4/0	2/0	3/0	0/0	0/0	0/0	0/0	2/0	3/0	5/0	0/0
	Monsoon	0/0	0/3	0/0	0/0	2/0	0/2	0/0	0/3	0/0	0/0	0/0	0/1	0/0	0/1	0/0	0/1	0/7	0/5	0/0	0/2
	Post-Monsoon	2/0	0/0	0/0	0/0	10/0	0/1	0/0	0/0	4/0	4/0	2/0	3/0	2/0	2/0	0/0	0/0	2/0	3/0	5/0	0/0
Post-1950	Annual	0/2	2/0	1/0	0/0	1/10	0/2	0/2	2/0	1/5	3/2	0/1	1/0	2/1	1/0	2/1	1/0	1/2	2/0	0/2	0/0
	Winter	0/0	0/0	0/0	0/0	0/0	0/0	0/0	0/0	0/0	0/0	0/0	0/0	0/0	0/0	0/0	0/0	0/0	0/0	0/0	0/0
	Pre-Monsoon	0/4	0/1	0/0	0/0	0/6	0/6	0/4	0/1	0/4	0/6	0/1	0/4	5/0	12/0	0/0	1/0	0/0	0/0	0/0	0/0
	Monsoon	0/3	6/0	2/1	2/1	0/10	0/2	0/3	6/0	1/5	6/1	0/1	3/0	0/1	3/0	1/2	1/0	2/2	3/0	0/2	4/0
	Post-Monsoon	0/3	0/1	0/0	0/0	0/7	0/5	0/4	0/1	0/4	0/5	0/1	0/0	0/1	0/0	0/0	1/0	3/0	0/0	0/0	0/1
Total		13/19	33/9	10/8	7/13	26/40	16/23	16/17	29/7	19/31	39/17	16/8	29/7	21/5	32/4	17/5	14/7	20/19	22/6	12/7	22/10

Note: N indicates Nagavali Basin, V indicates Vamsadhara Basin, + sign indicates number of grids showing increasing trend, - sign indicates number of grids showing decreasing trend.

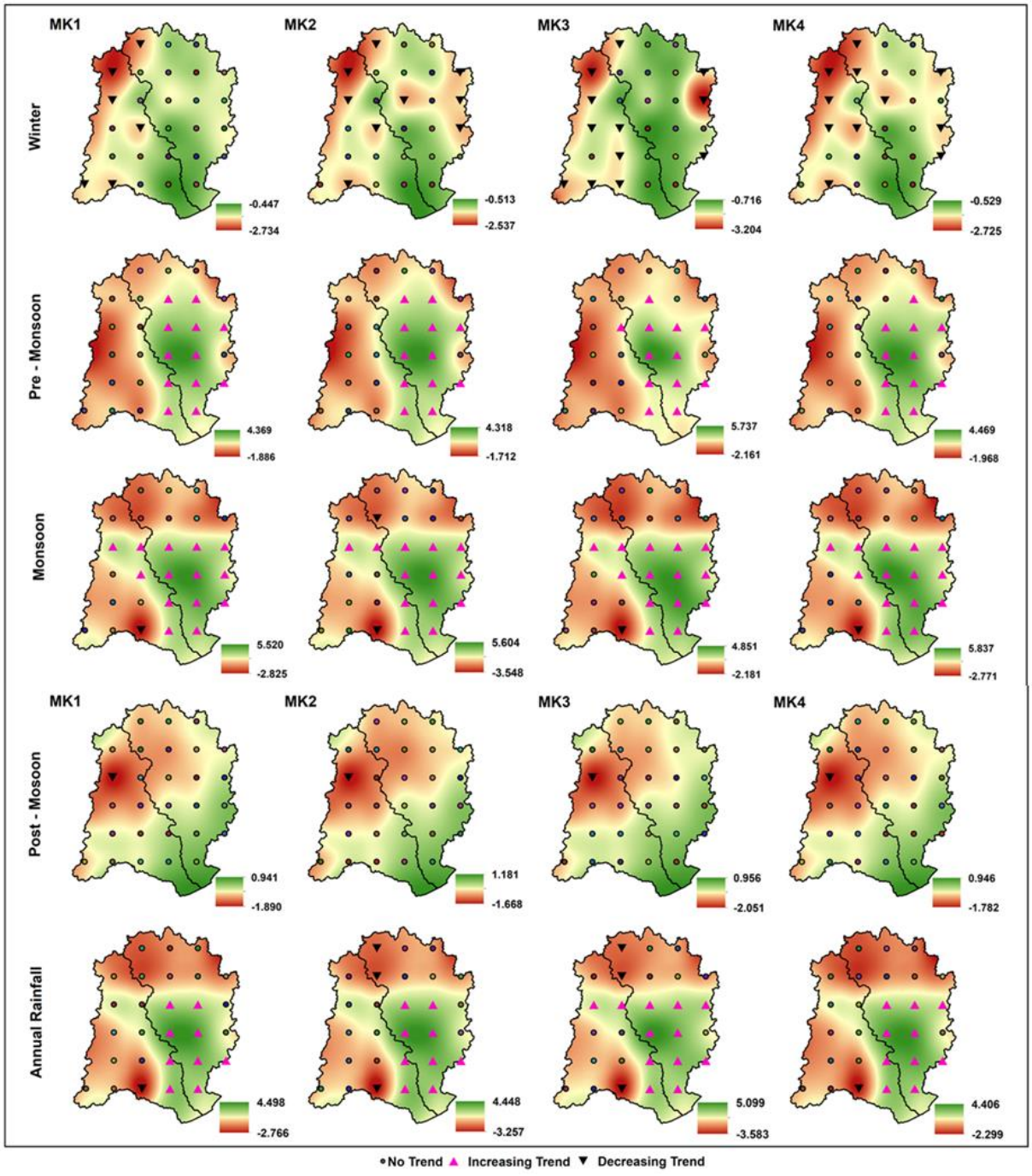

Figure 5.1Trends in seasonal and annual rainfall

From these figures, it is evident that the grids with decreasing trends in winter are present in both basins except at the lower portion of Vamsadhara basin. However, no significant trend is found in the northern parts of Vamsadhara basin. The grids with increasing trends in the pre-monsoon are present in the lower portion of Nagavali basin and at all locations in Vamsadhara basin. Due to barotropic and baroclinic instabilities caused by tropical depressions formed in BoB and their interactions with mean monsoonal flow (Krishnamurthy et al. 2009), the grids showing increasing trends in monsoon and annual rainfall are present in the lower and middle portions of both the basins. Whereas, in the post-monsoon season decreasing trends are present in the middle of Nagavali basin.

The Z statistics of trends in the seasonal and annual rainfall for pre-1950 are evaluated and presented in Table A2 (Appendix-A). In Nagavali basin, an increasing trend is observed at grids NG6 and NG11 in the pre-monsoon season and no obvious trends are found for rest of the seasons and in annual scale. In Vamsadhara basin, a decreasing trend is observed in the monsoon season and no significant trend is observed in other seasons and in annual scale. From the spatial patterns it is observed that, the grids show an increasing trend in the pre-monsoon season at the middle and upper portions of the Nagavali basin. In Vamsadhara basin, the grids with decreasing trend are present in the middle portion of the basin. The Z statistics of trends in seasonal and annual rainfall for post-1950 period are evaluated and presented in Table A2 (Appendix-A). In winter season, no significant trends are observed in both the basins. Except winter season, a decreasing trend is observed in Nagavali basins in all other seasons and in annual scale. In Vamsadhara basin, a decreasing trend is observed at grid VG13 in both the pre- and post-monsoon seasons. Whereas, an increasing trend is observed in the monsoon season and in annual scale.

The spatial patterns trends in seasonal and annual rainfall for the period of post-1950 are presented in Figure A1 and A2 (Appendix-A). From these figures, it is evident that the grids showing decreasing trend in the pre-monsoon are present in the lower and middle portions of the Nagavali basin and at the upper portion of the Vamsadhara basin. Whereas, in the post-monsoon, the grids with decreasing trend are presented in all portions of the Nagavali basin and upper portion of the Vamsadhara basin. In the monsoon season, the grids showing decreasing trends in Nagavali basin are present at lower and middle portions of the basin whereas, in Vamsadhara the grids with increasing trend are present all over the basin. The grids showing decreasing trends at annual scales in Nagavali basin are present at middle and lower portions of the basins and the grids with increasing trend in Vamsadhara basin are present in

the middle portion of the basin. The girds which showed significant trends in post-1950 in both the basins showed similar trends in the overall period (i.e., 1901-2018) trend analysis.

5.2.2 Trends in Rainfall Extremes

The Z statistics of annual rainfall extremes at three time periods (i.e., long-term, pre-1950, and post-1950) have been computed. However, only the Z statistics of long-term annual rainfall extremes are presented in Table A3 (Appendix-A). In pre-1950, no obvious trends are observed for all the extremes in both basins. Whereas, post-1950, an increasing trend for CDD and decreasing trend for all other rainfall extremes is observed in Nagavali basin. However, an increasing trend is observed for the extremes CWD, R10MM, R40MM, R95PTOT, and RX1DAY at very few grid points (i.e., ≤ 2). The results of R95PTOT for these basins are in good agreement with results by Bisht at al., (2018a). In Vamsadhara basin, no significant trend observed for extremes CDD and RX5DAY. An increasing trend is observed for extremes PRCPTOT, R20MM, R40MM, R95PTOT, and RX1DAY. However, CWD has shown decreasing trend and both the trends are observed for R10MM. In the long-term, an increasing trend is observed for all rainfall extremes in Nagavali basin. However, a decreasing trend is observed at grid NG12 for CWD and at grid NG3 for PRCPTOT, R10MM, and R20MM in Nagavali basin. In Vamsadhara basin, no significant trend is observed for R40MM and RX1DAY. Whereas, an increasing trend is observed for other rainfall extremes. The trends in R95PTOT and RX5DAY are found to be in good agreement with Bisht et a., (2018a).

The spatial patterns of the trends in long-term annual rainfall extremes are presented in Figures 5.2 and 5.3. Increasing trends in CDD at a rate of 2 days per decade are present in the upper portion of both basins and as expected the same grids showed a decreasing trend for CWD. Interestingly, the rate of decrease in CWD is also found to be the same. For extremes, PRCPTOT, R10MM, and R20MM a decreasing trend is observed in the lower portion of Nagavali basin and the upper portion of Vamsadhara basin. For CWD, the grids showing increasing trends are observed in both the basins except at the upper portion of the Nagavali basin. The grids showing increasing trends for PRCPTOT, R10MM, and R20MM are observed in the lower and middle portions of both the basins. For extremes, R95PTOT, RX1DAY, and RX5DAY increasing trends are seen in the middle and upper portions of Nagavali basin. In Vamsadhara basin, the grids showing increasing trends for R95PTOT are observed in the lower portion of the basin and for RX5DAY at the middle and upper portions of the basin because of cyclonic storms as they produce rainfall for more than 5 days (Dash et al. 2009).

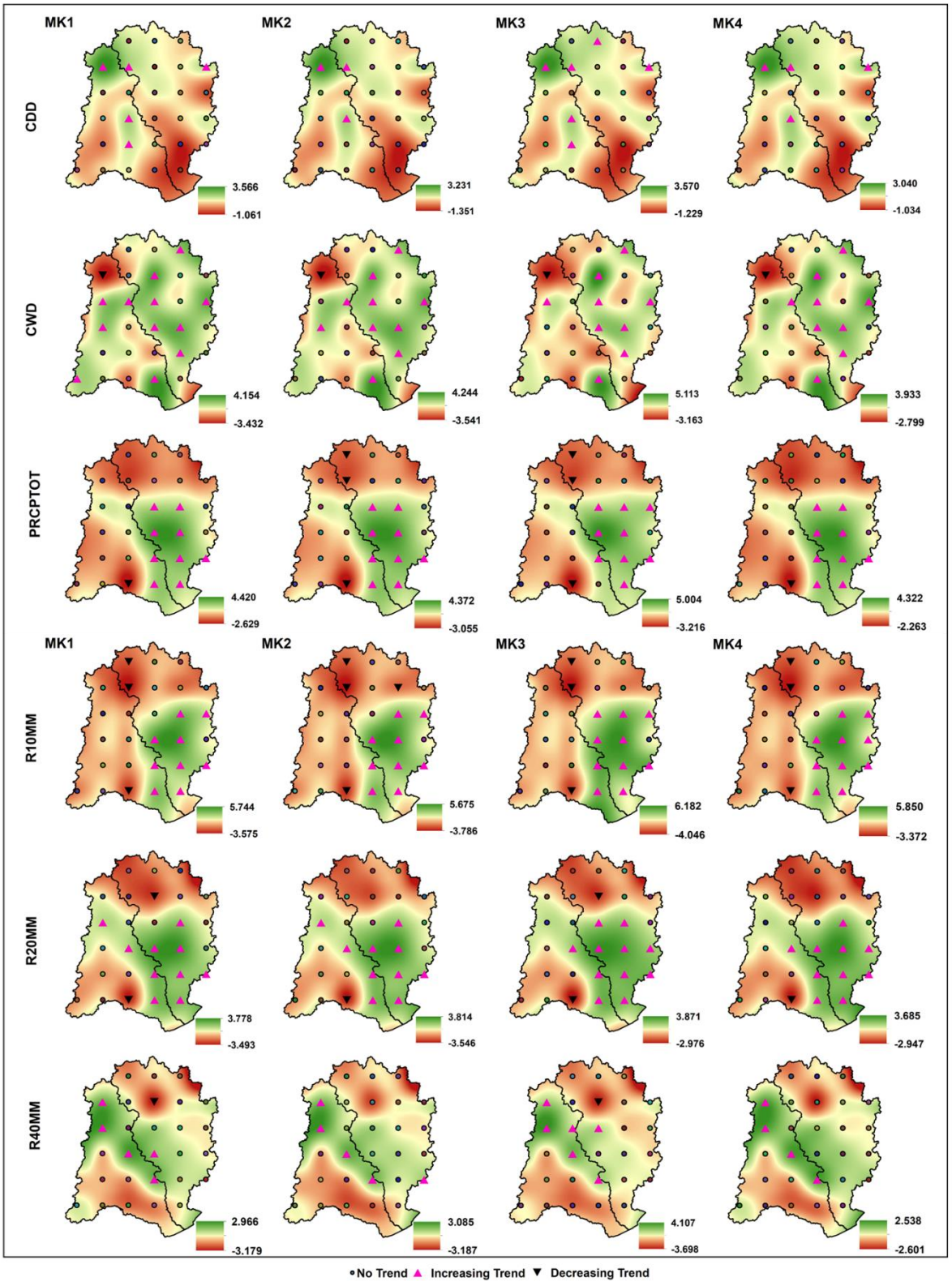

Figure 5.2 Annual trends in rainfall extremes for CDD, CWD, PRCPTOT, R10MM, R20MM, and R40MM

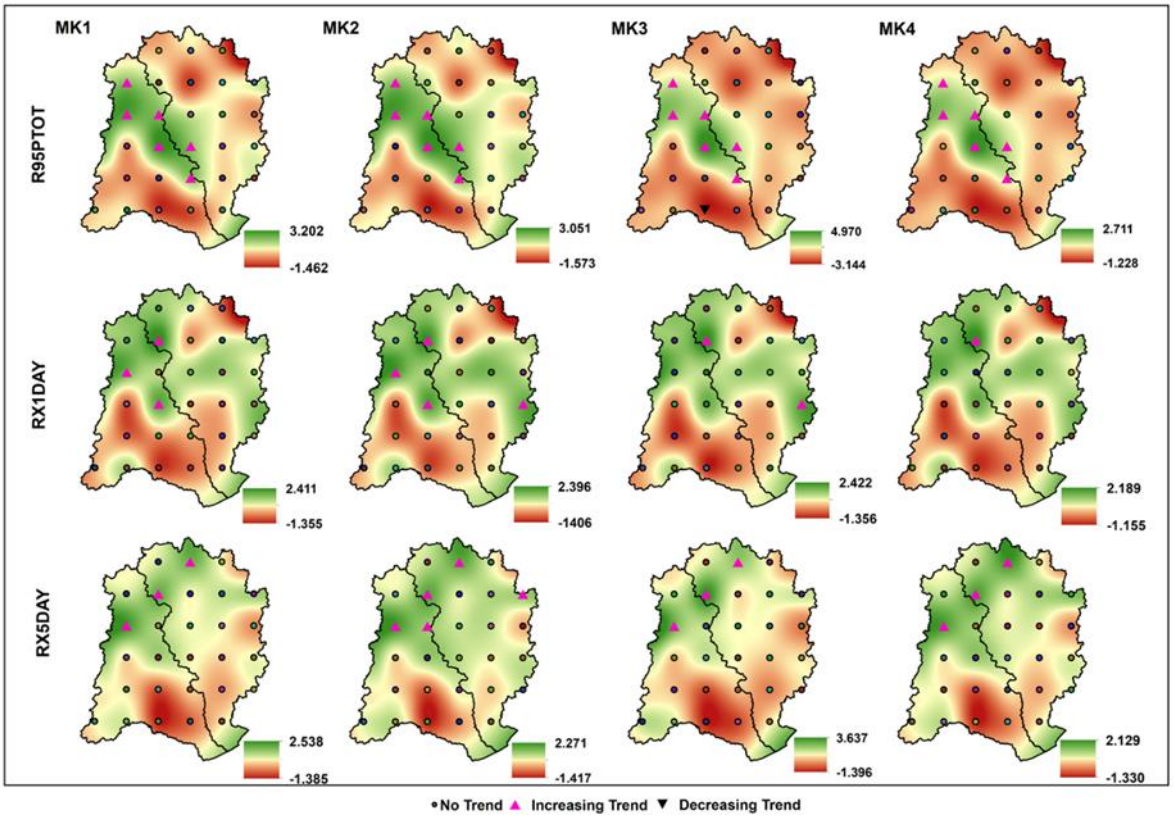

Figure 5.3 Annual trends in rainfall extremes for R95PTOT, RX1DAY, and RX5DAY

The Z statistics of rainfall extremes in monsoon are presented in Table A4 (Appendix-A). In winter season, no trend is evident for R40MM and R95PTOT in Nagavali basin and R20MM in Vamsadhara basin. Except CDD, a decreasing trend is observed for all rainfall extremes in winter season. In both pre-monsoon and monsoon seasons, a positive trend is observed for all rainfall extremes except CDD and R10MM in Vamsadhara basin and CWD in Nagavali basin at one grind in the monsoon season. In Vamsadhara basin, a clear negative trend is observed for CDD in the pre-monsoon season. In the monsoon season a negative trend is observed over three grids and a positive trend for two grids in the basin. For CWD in Nagavali basin, a negative trend is observed at NG8 in pre-monsoon season and at NG12 in monsoon. A positive trend is observed at NG4 and NG11 in monsoon season. At grid NG3, a negative trend is observed for all rainfall extremes except for CDD and CWD. For R10MM in Vamsadhara basin, a clear positive trend is observed during pre-monsoon season. In the monsoon season a positive trend is observed at nine grids and a negative trend at three grids. No significant trend is observed for rainfall extremes in post-monsoon season except for CDD where it showed a positive trend for a few grids in both basins. The spatial patterns of rainfall extremes in all seasons are computed. However, only the spatial patterns of rainfall extremes for the monsoon

season are presented in Figures 5.4 and 5.5 and the spatial patterns of winter season are presented in Figures A6 to A8 (Appendix-A). Increasing trends for CDD in winter season are seen in all parts of Nagavali basin. For the extremes, CWD, R10MM, and RX1DAY decreasing trends are present in most of Nagavali basin. For R95PTOT and RX5DAY, decreasing trend is present in the middle and upper portions of Nagavali basin and in the middle for R20MM. In Vamsadhara basin, decreasing trends for CWD, R10MM, and PRCPTOT are present in the middle portion of the basin. For extremes, R95PTOT and RX1DAY decreasing trends are seen in the upper portion of the basin and for R40MM and RX5DAY decreasing trends are seen in the middle and upper portions of the basin.

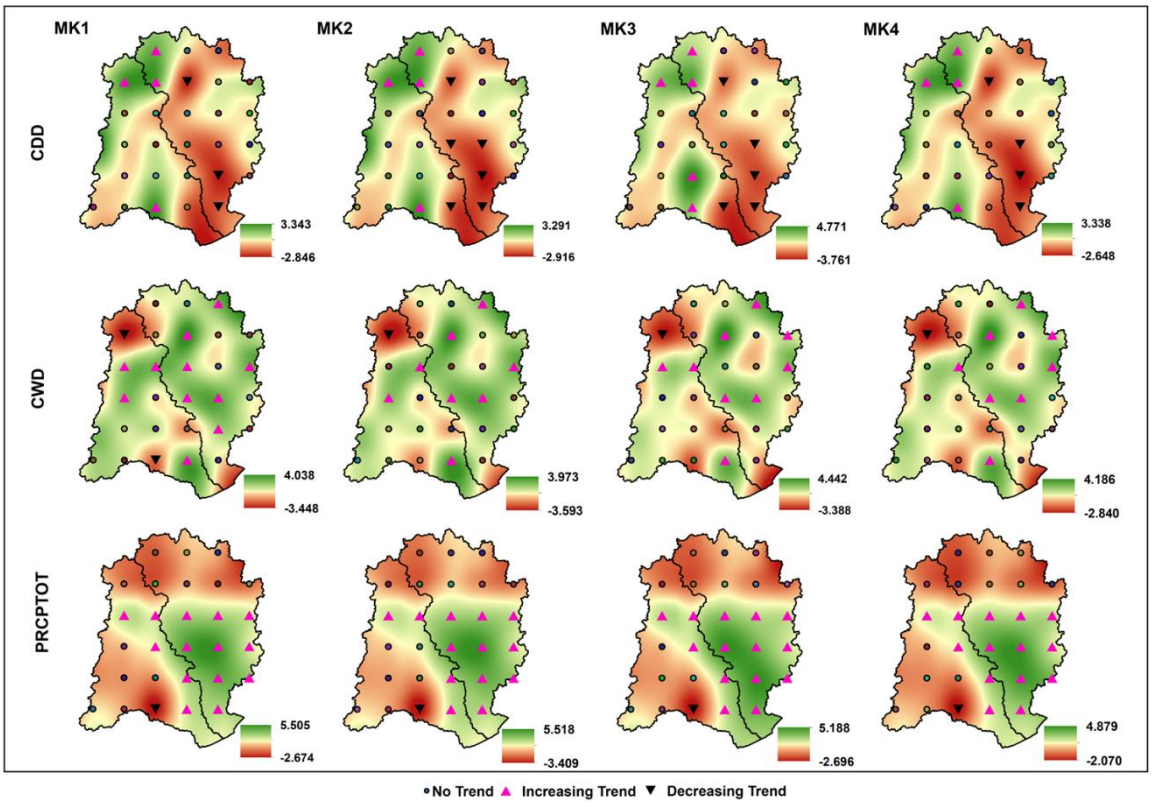

Figure 5.4 Monsoon trends in rainfall extremes for CDD, CWD, and PRCPTOT

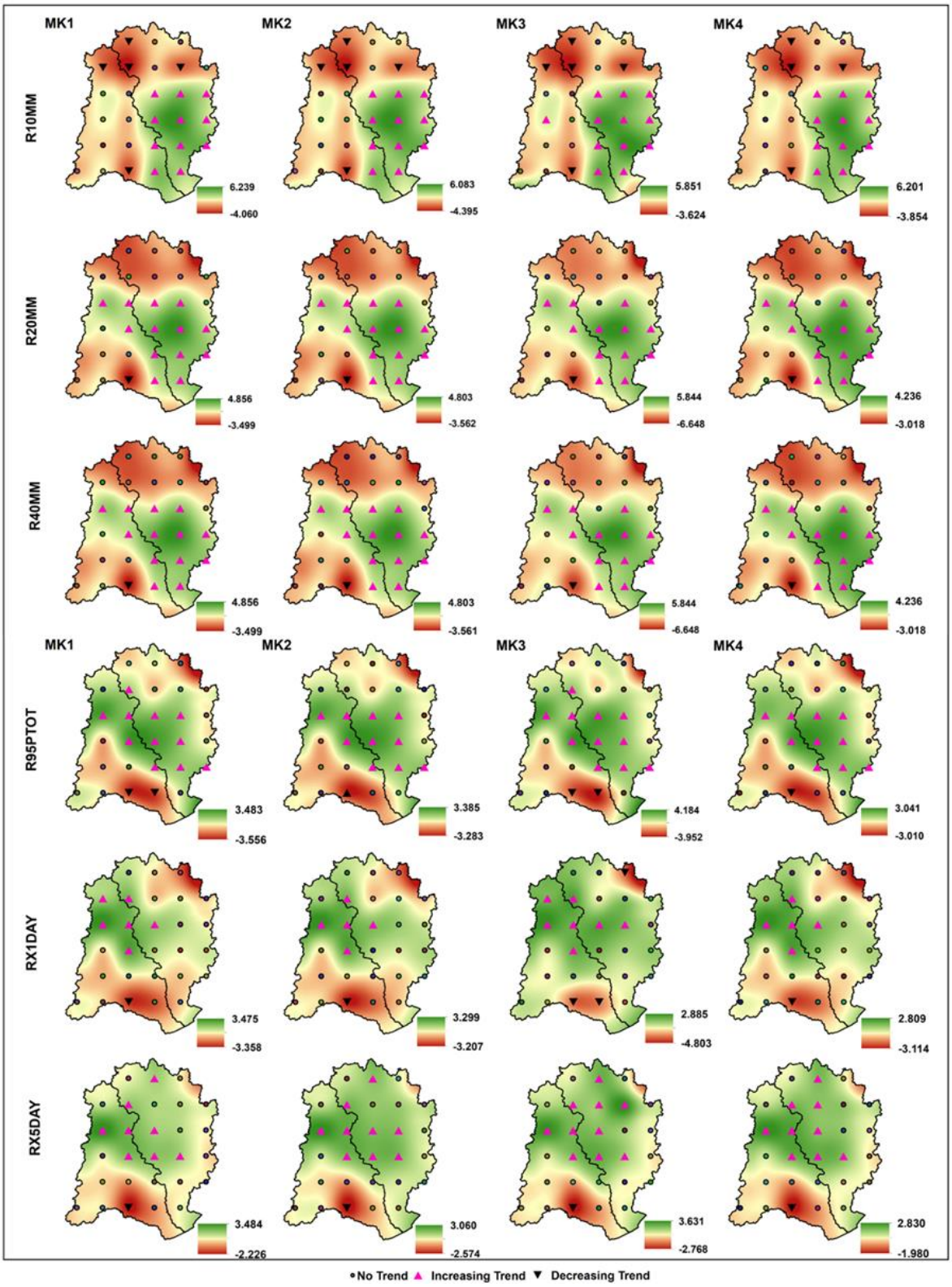

Figure 5.5 Monsoon trends in rainfall extremes R10MM, R20MM, R40MM R95PTOT, RX1DAY, and RX5DAY.

In pre-monsoon season, the decreasing trend for CDD is seen in both the basins except at the lower portion of Vamsadhara basin. In Nagavali basin, the grids with decreasing trends for CWD and increasing trends for PRCPTOT are observed in the lower and middle portions. The increasing trends for R20MM, R95PTOT, and RX1DAY are seen in the middle and upper portions of Nagavali basin. For R40MM, increasing trend is seen in the upper portion of the basin. In Vamsadhara basin, increasing trend is seen in the entire basin except for CDD and CWD. For CWD, an increasing trend is seen in the upper portion of the basin.

In monsoon season, increasing trends with all rainfall extremes for all portions of the Nagavali basin are evident except at grid point NG12 in the upper portion of the basin for CWD. Interestingly, grid NG3 in the lower portion of Nagavali basin has shown a decreasing trend for all rainfall extremes except CDD. In Vamsadhara basin, the increasing trend for all the rainfall extremes are seen in the lower and middle portions of the basin except for CDD, CWD, and RX5DAY. CDD has shown a decreasing trend at a few grids in all portions of the basin and an increasing trend at a few grids in the upper portion of the basin. For CWD and RX5DAY, the grids shown increasing trends are present in the entire basin. In the upper portion of Vamsadhara basin, a decreasing trend for R10MM is seen. In post-monsoon season, an increasing trend for CDD is seen in the middle and upper portions of Nagavali basin and in the middle portion of Vamsadhara basin. In post-monsoon season, no significant trend is observed in rainfall extremes except for CDD where it showed increasing trend in all parts of Nagavali basin and upper portion of Vamsadhara basin.

In winter, no significant trend is evident in pre- and post-1950 period for all the rainfall extremes in both basins. In the pre-1950 period, an increasing trend is observed for most of the extremes in both Nagavali and Vamsadhara basins in pre- and post-monsoon seasons. In post-1950 period, a decreasing trend is observed in pre- and post-monsoon seasons. In monsoon season, in post-1950 period, a decreasing trend is observed in all extremes in Nagavali basin compared to pre-1950 period. In Vamsadhara basin an increasing trend is observed in all extremes in post-1950 period and decreasing trend in pre-1950 period. The spatial patterns of rainfall extremes for the post-1950 period are presented in Figures A9 to A11 (Appendix-A).

5.3 Magnitude of the Trends

The magnitudes of rainfall and rainfall extremes are calculated using the Sen's slope method. It is observed that the annual rainfall in Nagavali basin increased at the rate of 2 mm/decade and in Vamsadhara basin it increased at the rate of 8.5 mm/decade in the last 118 years. The maximum rate of increase in seasonal rainfall is observed in the monsoon season. Rainfall in the monsoon season also increased at the rate of 4 mm/decade in Nagavali basin and 9 mm/decade in Vamsadhara basin.

5.4 Drivers of Rainfall Variability

Both Nagavali and Vamsadhara basins have shown significant trends in rainfall and rainfall extremes in the past 118 years at various temporal scales. The trend analysis has been carried out using high resolution daily gridded data. According to Tank et al. (2006), changes in data observation practices and irregular spatial distribution of rainfall stations, inhomogeneities are introduced in the time series data which could impact the computation of extreme indices. Due to this, there might be uncertainties in trend analysis carried out using gridded products. In the present study, regions with higher density of rainfall stations has shown significant trends in both Nagavali and Vamsadhara basins. It is also known that BoB is one of the hot spots for the genesis of tropical cyclones which propagates either westwards or northwards, playing a major role in rainfall extremes (Krishnamurthy et al. 2009). Both Nagavali and Vamsadhara basins are coastal basins with coastal plains adjoining BoB and receive high rainfall in pre- and post-monsoon seasons due to cyclonic storms. Hence, the results exhibited significant increasing trend in the pre-monsoon season. Another possible reason for increasing trends in rainfall and rainfall extremes in both basins is because of changes in LULC. In the last three decades, the forest cover in Nagavali basin has decreased rapidly because of urbanization (Rao et al. 2019). The increasing trend in Nagavali basin may be attributed to the effect of urbanization, as Bisht et al. (2018a) suggested that the basin showed a decreasing trend in pre-urbanization era (1901-1970), an increasing trend in post-urbanization era (1971-2015) and an increasing trend over the long term for both annual and monsoon rainfall. In Vamsadhara basin no significant changes in land use and land cover are found. Hence, the results from trend analysis results in Vamsadhara basin for rainfall and rainfall extremes at various temporal scales are in good agreement with data from existing literature.

With regard to spatial patterns in rainfall and rainfall extremes, Vamsadhara basin showed significant increasing trends in lower and middle portion of the basin when compared with Nagavali basin. These increasing trends may be attributed to local convective processes as well as extreme topography of the region, as the Eastern Ghats are densely located in the middle and upper portions of Vamsadhara basin.

5.5 Simulation of Tropical Cyclones over BoB for the Prediction of Track and Intensity

From the trend analysis, it is observed that the rainfall extremes are increasing in the lower and middle portions of Nagavali and Vamsadhara basins. The increasing trends in rainfall extremes in the lower and middle portions of both basins may be attributed to TCs that are formed in BoB. Hence, in this research work, WRF model is used to capture rainfall and movement of previous tropical cyclones over Nagavali and Vamsadhara basins. From the literature mentioned in section 2.3.1, it is observed that numerous studies have been conducted for the prediction of TCs using WRF model. However, it is difficult to identify a suitable microphysical scheme (CMP) for the prediction of TCs. Therefore, numerical experiments are conducted using WRF model to find a suitable microphysical scheme for the prediction of TCs.

In the present research work, a total of seven CMP schemes, Lin, Ferrier, Morrison, Thompson, WRF Single Moment 3-Class (WSM3), WSM5, and WSM6 are studied. The sensitivity of the seven CMP schemes is analyzed by studying eight TCs (Daye, Kyant, Gaja, Hudhud, Nilofar, Ockhi, Phethai, and Titli) over NIO that occurred between 2014 and 2018 to determine the optimum combination physical parameterization schemes for the prediction of TC. Except Daye cyclone, the simulation period for the selected TCs is 96 h. However, for Daye cyclone the simulation period is 48 h as the lifespan of the cyclone itself is only 48 h. The model errors for MSW, MSLP, and track position are calculated with respect to the observed values.

5.5.1 Track and Intensity of Errors

The predicted tracks of the selected cyclones for all the combinations of CMP schemes and the best track provided by IMD are shown in Figures 5.6 and 5.7. The direct positional errors (DPE) for the selected TCs are shown in Figure 5.8 and 5.9. From the results, it is observed that, the intensity stages (Depression, Deep Depression, Cyclonic Storm, Severe Cyclonic Storm, and Very Severe Cyclonic Storm) of TCs during the model initialization have a significant impact

on track prediction. The cyclones initiated at deep depression or higher stages showed an increasing trend in average track error from the model initiation to the end of the simulation. Whereas, the cyclones initiated at the depression stage showed a decreasing trend in average track error till the 48 h of model simulation and then gradually increased to the end of the simulation. Except for cyclones Daye and Kyant, the predicted track is close to the observed track during the initial stages of the model simulation with an average error of 64 km for all the schemes. The results are in good agreement with previous studies (Osuri et al. 2012; Kanase and Salvekar 2015). Subsequently, as the time of simulation increased the predicted track also started moving away from the best track. At the end of the simulation period, the average track error is found to be 247 km. For cyclone Kyant, an average track error of 88 km is found during the initial stages which gradually reduced to 67 km up to the 48 h of the model simulation and then gradually increased to 347 km at the end. Similarly, for cyclone Daye, the average track error is gradually reduced from 162 km to 78 km from the model initiation to the end of the simulation.

The model performance is evaluated by calculating MAE, MSE, and average track errors at every 24h interval (i.e., 24h, 48h, 72h, and 96h). The 24 hourly average track error for TCs are presented in Figure 5.10 and 5.11. The WSM3 scheme simulated cyclones Nilofar, Kyant, Ockhi, Daye, and Phethai with an average track error ranging from 83 to 190 km, 45 to 195 km, 42 to 75 km, 102 to 47 km, and 113 to 115 km, respectively at 24h to end of the simulation time. Hudhud cyclone is well simulated by all CMP schemes with a maximum average track error of 63 km at 24 h simulation time. From then, the average track error gradually increased to 555 km at the end of the simulation with a least error of 219 km by WSM6 scheme. Cyclone Gaja is well simulated by Ferrier with least average track errors of 110, 264, 231, and 139 km at 24, 48, 72, and 96h of the model simulation time. In case of Titli the average track has been considered for the overall simulation period because, Morrison scheme provided the least average track error of 64 km and 39 km during the initial stages of model simulation while WSM6 scheme produced the least error of 111 km and 37 km at the end of the simulation. Hence, WSM6 scheme is considered to provide superior results for Titli cyclone. The single moment or double moment schemes did not show any significant variations in TCs track prediction. The deviations in the predicted tracks may be attributed to the variations in the intensification process during the model simulation. The schemes which showed rapid intensification process during the model simulation showed minimum deviation from the observed track and vice-versa (Park et al. 2020).

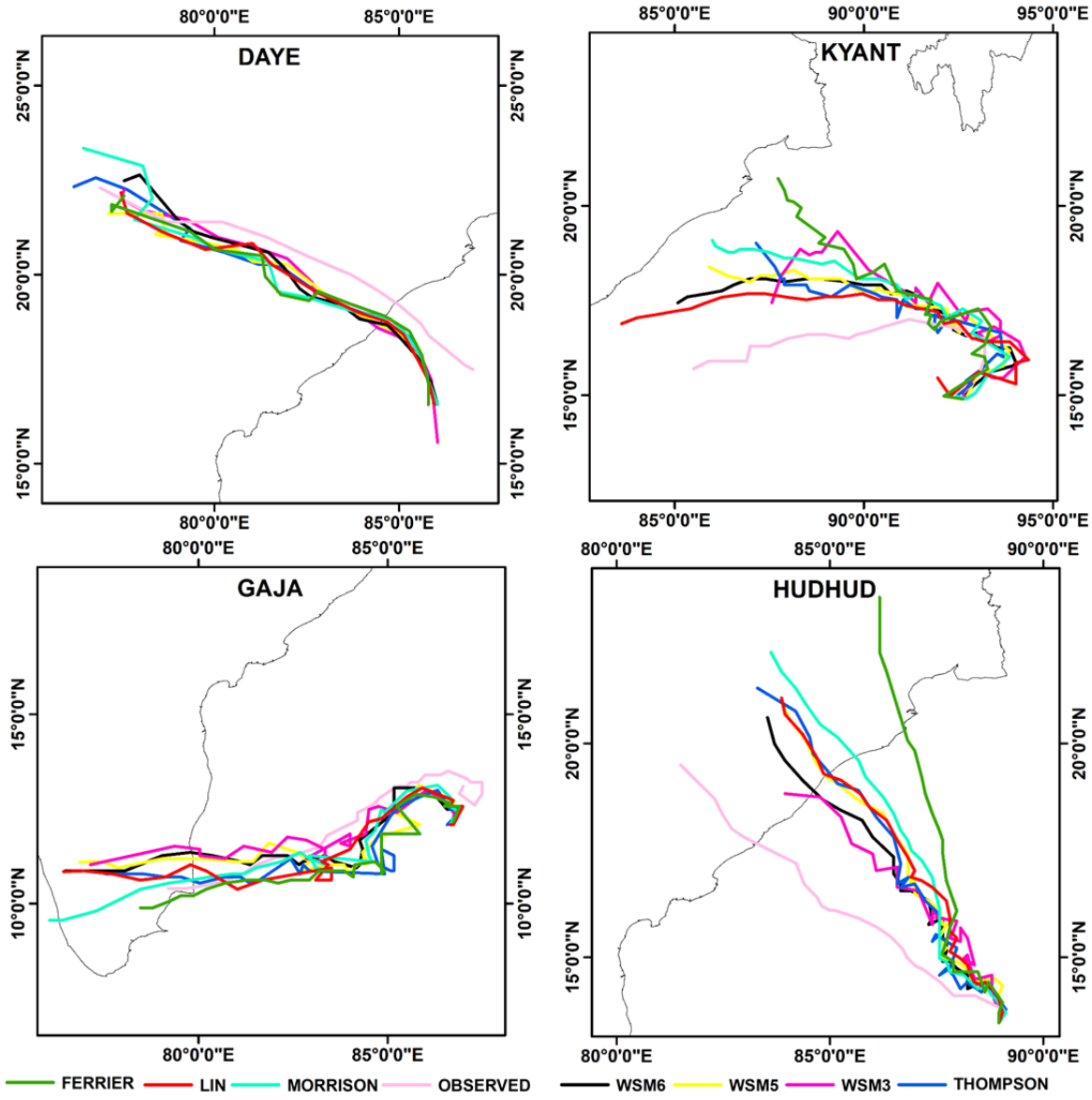

Figure 5.6 Observed and predicted tracks of TCs Daye, Kyant, Gaja, and Hudhud

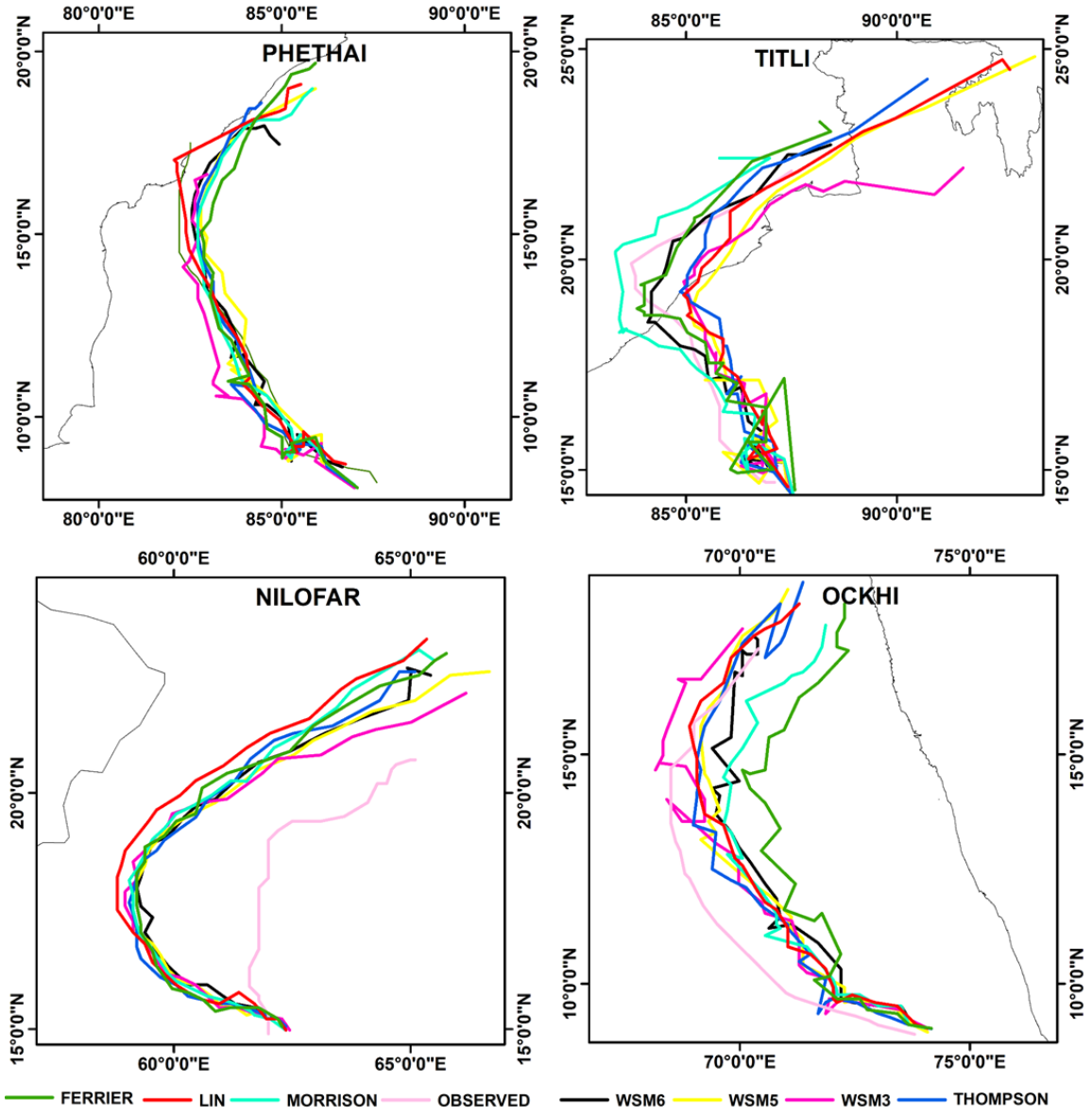

Figure 5.7 Observed and predicted tracks of TCs Phethai, Titli, Nilofar, and Ockhi

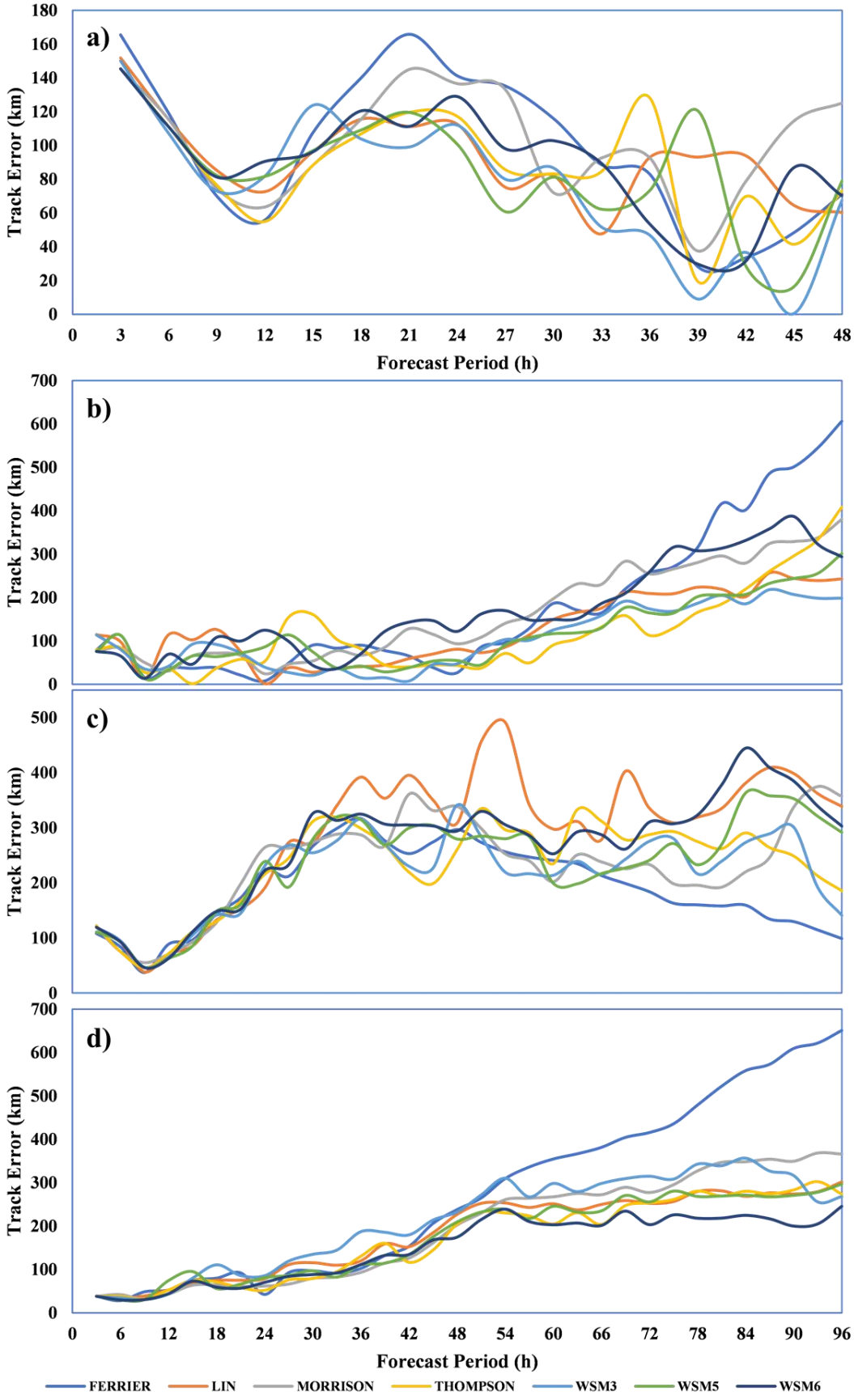

Figure 5.8 Direct Positional Errors for TCs a) Daye, b) Kyant, c) Gaja, and d) Hudhud

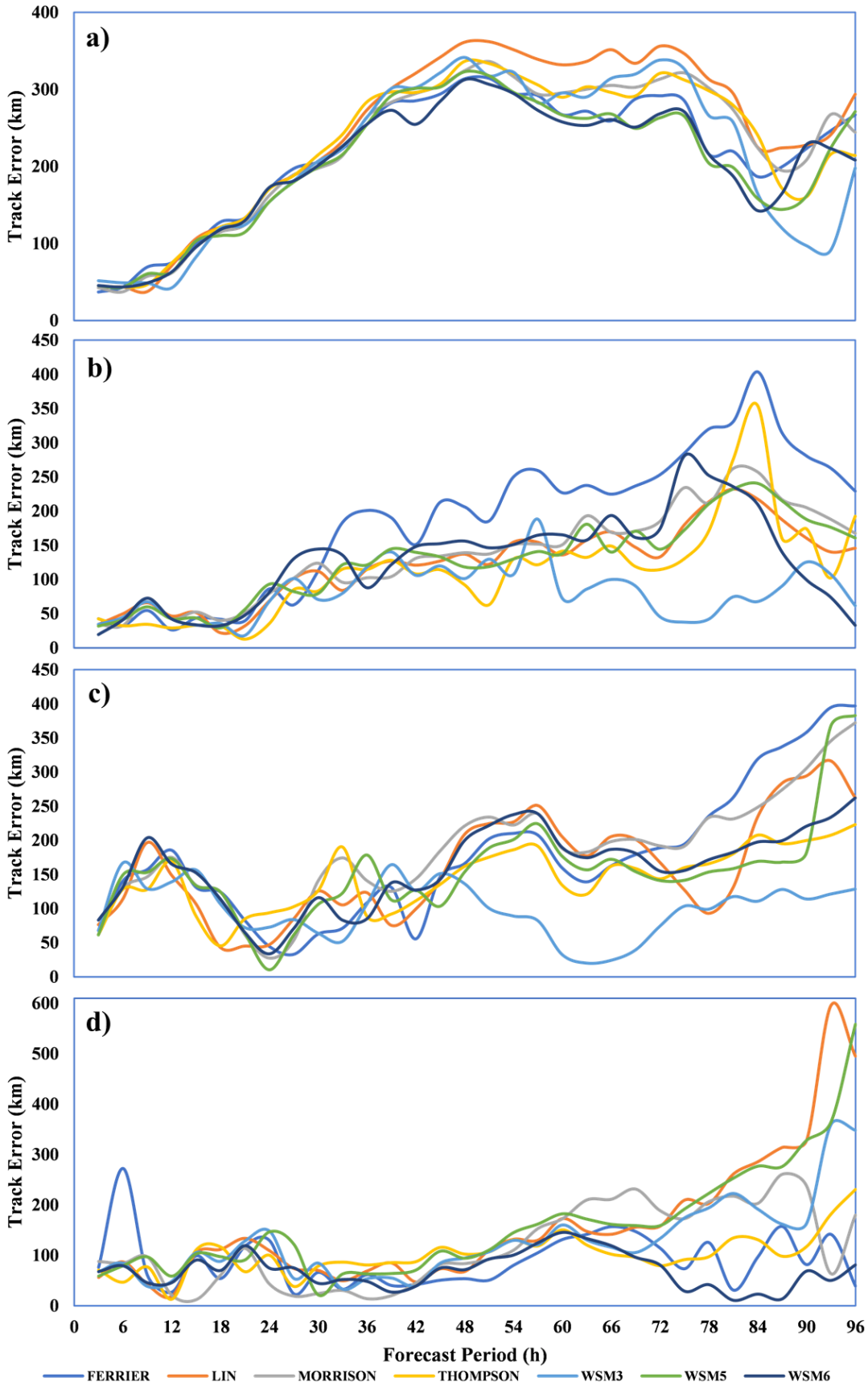

Figure 5.9 Direct Positional Errors for TCs a) Nilofar, b) Ockhi, c) Phetahi, and d) Titli

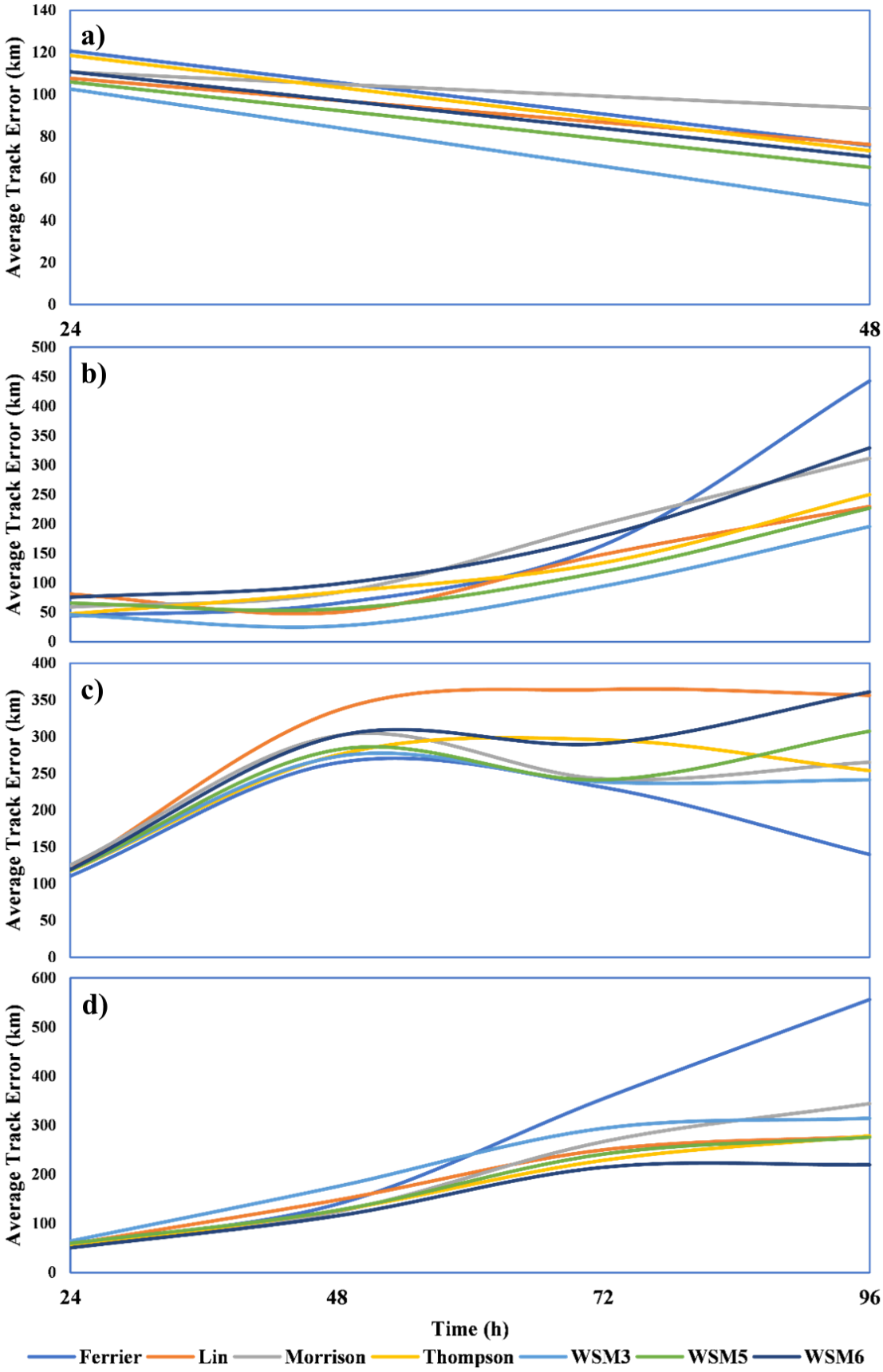

Figure 5.10 Average track error at every 24 – hour interval for TCs a) Daye, b) Kyant, c) Gaja, and d) Hudhud

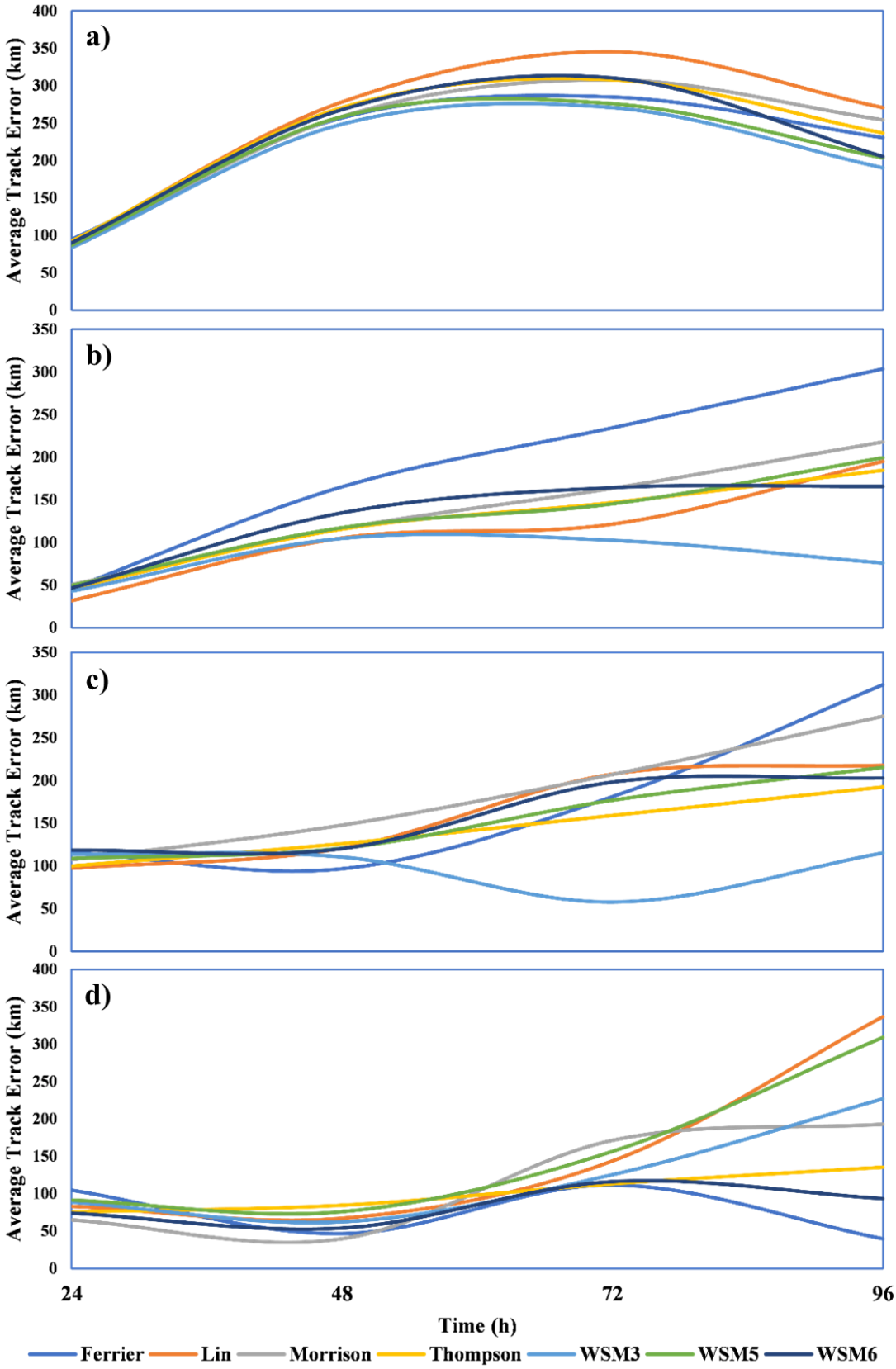

Figure 5.11 Average track error at every 24 – hour interval for TCs a) Nilofar, b) Ockhi, c) Phetahi, and d) Titli

The MAE and MSE of MSW for all CMP are calculated and the results of TC Hudhud are shown in Figure 5.12. In the case of Nilofar, Kyant, Daye, and Phethai cyclones WSM3 indicates the lowest MAE and MSE. The lowest MAE for the TCs ranged from 4.73 to 17.08 m/s, 6.84 to 4.63 m/s, 8.60 to 1.45 m/s, and 7.16 to 3.66 m/s for MSW at 24h to the end of the simulation. The lowest MSE for the TCs ranged from 10.14 to 11.31 m^2/s^2, 2.89 to 4.97 m^2/s^2, 6.56 to 0.88 m^2/s^2, and 2.29 to 6.29 m^2/s^2. The lowest MAE and MSE for Gaja cyclone is obtained from the Ferrier scheme and ranged from 4.19 to 9.94 m/s and 5.77 to 13.46 m^2/s^2 respectively. For Hudhud, Titli and Ockhi cyclones, WSM6 and Lin scheme provided the lowest MAE ranging from 2.44 to 9.49 m/s, 5.08 to 3.91 m/s and 4.85 to 3.85 m/s respectively and MSE ranged from 1.60 to 1.48 m^2/s^2, 5.39 to 8.63 m^2/s^2 and 6.44 to 12.45 m^2/s^2, respectively. The schemes which predicted MSW well also predicted MSLP for the respective TCs.

The intensity of TC is influenced by the auto conversion process between the hydrometers and the amount of latent heat released during the conversion process (Kanase et al. 2014). To assess the impact of various microphysical schemes on the intensity of TCs, the vertical profile of the area averaged mixing ratios is calculated at every 3-hour interval. An average value of the prognostic variables over all the time steps has been taken for the analysis. The averaged values of the prognostic variables for cyclone Hudhud are presented in Figure 5.13 and for other cyclones presented in Figures B1 to B7 (Appendix-B). From the results, it is observed that WSM3 scheme predicted only liquid hydrometers for all the cyclones. It indicates that WSM3 scheme assumed that the temperature of the clouds is above freezing point. Compared to other microphysical schemes, WSM3 scheme produced significant amounts of cloud water and rain in the lower troposphere for cyclones Nilofar, Kyant, Daye, and Phethai. For cyclones Kyant, Daye, and Phethai, all the microphysical schemes showed significant decrease in frozen hydrometers in middle troposphere. This results in slowing down the vertical acceleration of intense updrafts in the eye wall of the storm, which might be the reason for inhibiting storm intensification (Maw and Min 2017). For the cyclone Nilofar, the frozen hydrometers predicted by all microphysical schemes in middle troposphere are in negligible quantity and the liquid hydrometers predicted by Lin, WSM5 and WSM6 in the lower troposphere are also in negligible quantity. Compared to Ferrier, Morrison, and Thompson schemes which produced cloud water and rain in the lower troposphere WSM3 scheme produced more amount. The presence of cloud water and rain in the lower troposphere helps in its intensification. Therefore, the WSM3 scheme produced more intensity for the cyclones Nilofar, Daye, Kyant, and Phethai.

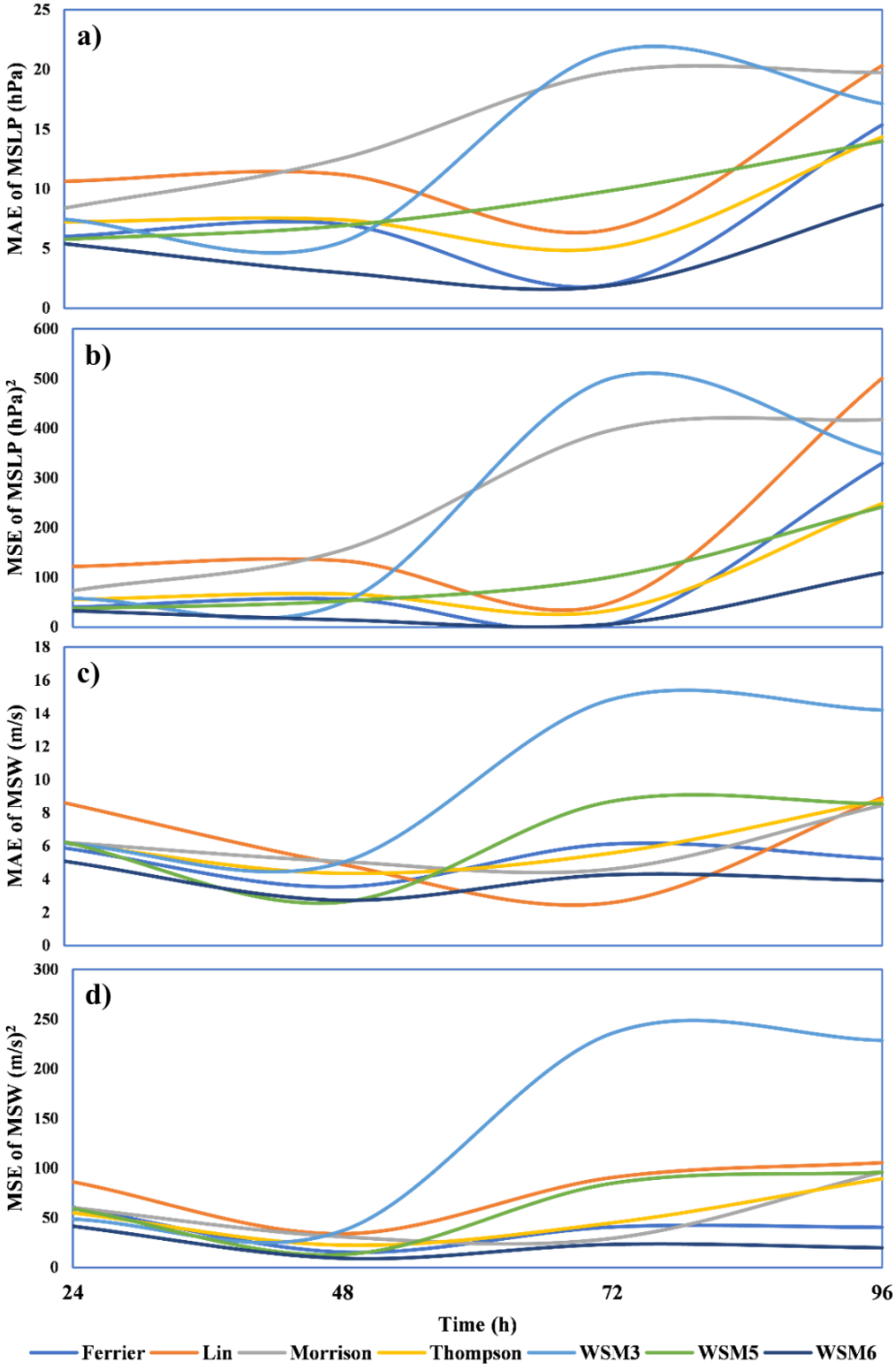

Figure 5.12 MAE and MSE of MSLP and MSW of cyclone Hudhud

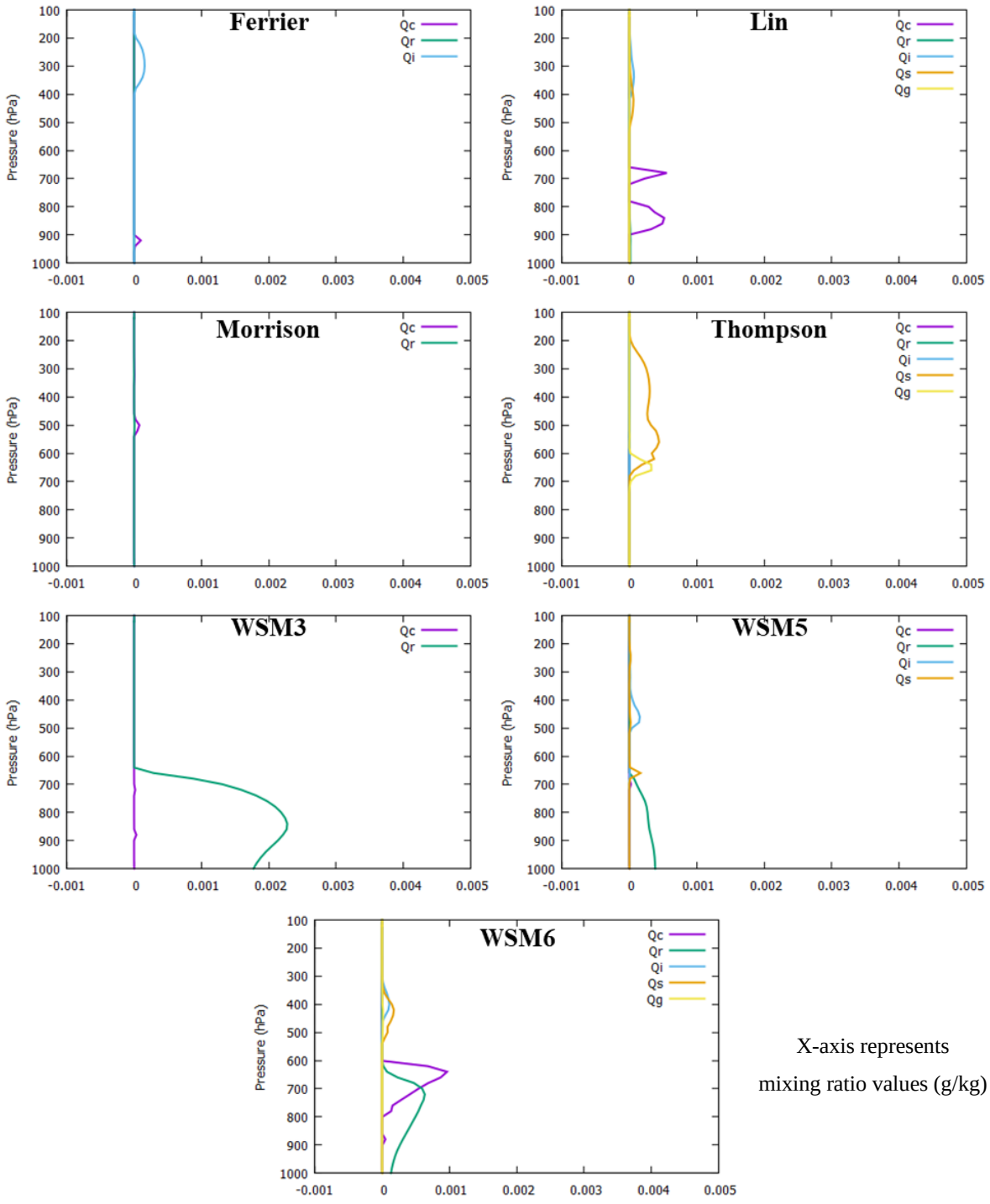

Figure 5.13 Time evolution of area averaged mixing ratios (g/kg) of cyclone Hudhud

The WSM6 scheme has produced a significantly large amount of cloud water and rain in lower troposphere compared to WSM3 for cyclone Hudhud, Ockhi, and Titli. The presence of cloud water and rain in the lower troposphere which helps in the release of latent heat and cyclone intensification, WSM6 scheme provided high intensity for cyclones Hudhud, Ockhi and Titli. Other microphysical schemes showed significant decrease in the frozen hydrometers in the middle troposphere which prevents the intensification of cyclones. In the case of Gaja cyclone, Ferrier, Lin, Thompson, and WSM6 schemes have produced cloud water in the lower troposphere and all the schemes have produced negligible quantities of all the other prognostic variables. Compared to other schemes, due to the presence of a large amount of cloud water in the lower troposphere, Ferrier scheme has predicted Gaja cyclone with more intensity.

5.5.2 Skill Score

SS is calculated to obtain information about the improvement in the model forecast over reference forecast. It is easy to identify any improvement in the model performance as SS provides a single value. In the present study, sensitivity experiments with Lin scheme are considered as a reference forecast and the skill score for all other microphysical schemes is calculated. The skill scores for the DPE, MSW and MSLP at the end of the simulation are provided in Table 5.2 to 5.4.

The WSM3 scheme showed an improvement of 18%, 17%, 19% and 41% in DPE for cyclones Nilofar, Kyant, Daye, and Phethai respectively. The WSM6 scheme showed an improvement of 17%, 35% and 58% in DPE for the cyclones Hudhud, Ockhi, and Titli. For Gaja cyclone, Ferrier scheme showed an improvement of 35% over the reference forecast. Similar results are obtained for MSW and MLSP.

Table 5.2 Skill score for Direct Positional Error

Cyclone/CMP	Ferrier	Morrison	Thompson	WSM3	WSM5
Hudhud	-0.52	-0.07	0.07	-0.16	0.04
Nilofar	0.13	0.08	0.08	**0.18**	0.17
Kyant	-0.44	-0.31	0.06	**0.17**	0.08
Ockhi	-0.54	-0.12	0.07	-0.04	-0.04
Daye	-0.09	-0.16	0.04	**0.19**	0.08
Titli	0.49	0.28	0.37	0.21	0.01
Gaja	**0.35**	0.20	0.21	0.26	0.19
Phethai	-0.11	-0.17	0.10	**0.41**	0.03

Table 5.3 Skill score for Maximum Sustained Wind

Cyclone/CMP	Ferrier	Morrison	Thompson	WSM3	WSM5	WSM6
Hudhud	0.33	0.18	0.10	-1.33	0.00	**0.43**
Nilofar	0.22	0.01	0.23	**0.47**	0.21	0.11
Kyant	0.15	0.26	0.66	**0.70**	0.61	0.53
Ockhi	-0.24	-0.56	-0.38	-0.90	-0.33	**0.01**
Daye	0.01	-0.08	-0.02	**0.17**	-0.10	-0.07
Titli	0.13	0.15	0.05	0.09	-0.17	**0.26**
Gaja	**0.62**	0.61	0.33	-0.16	0.18	0.14
Phethai	0.27	0.12	0.20	**0.47**	0.33	0.26

Table 5.4 Skill score for Mean Sea Level Pressure

Cyclone/CMP	Ferrier	Morrison	Thompson	WSM3	WSM5	WSM6
Hudhud	0.45	-0.30	0.50	-0.16	0.51	**0.74**
Nilofar	0.41	0.05	0.30	**0.70**	0.44	0.25
Kyant	0.24	0.37	0.38	**0.68**	0.62	0.07
Ockhi	-0.85	-0.25	-0.94	-1.68	-0.92	**0.15**
Daye	-0.02	0.21	0.18	**0.29**	0.11	0.10
Titli	0.11	0.22	0.03	0.35	-0.15	**0.35**
Gaja	**0.47**	0.41	0.43	-0.23	0.03	0.33
Phethai	0.23	0.10	0.31	**0.40**	0.28	0.20

5.6 Rainfall Prediction by WRF Model

Rainfall intensity and distribution of TCs are influenced mainly by the interaction of storm with the Earth's surface as well as humidity, and intensity of TC. In recent years, most of these parameters have been incorporated into WRF model for predicting the track, intensity, and rainfall of TCs. In this study, rainfall produced by Titli cyclone is predicted using WRF model with seven CMP schemes. The time series plot of rainfall predicted by WRF model along with IMD observed rainfall for cyclone Titli is shown in Figure 5.14. From the results, it is observed that the pattern of rainfall predicted by WRF model is in good agreement with observed data, but rainfall is overestimated byWRF model. WSM6 scheme predicted a maximum rainfall of 220 mm for TC Titli that predicted the track and intensity as well.

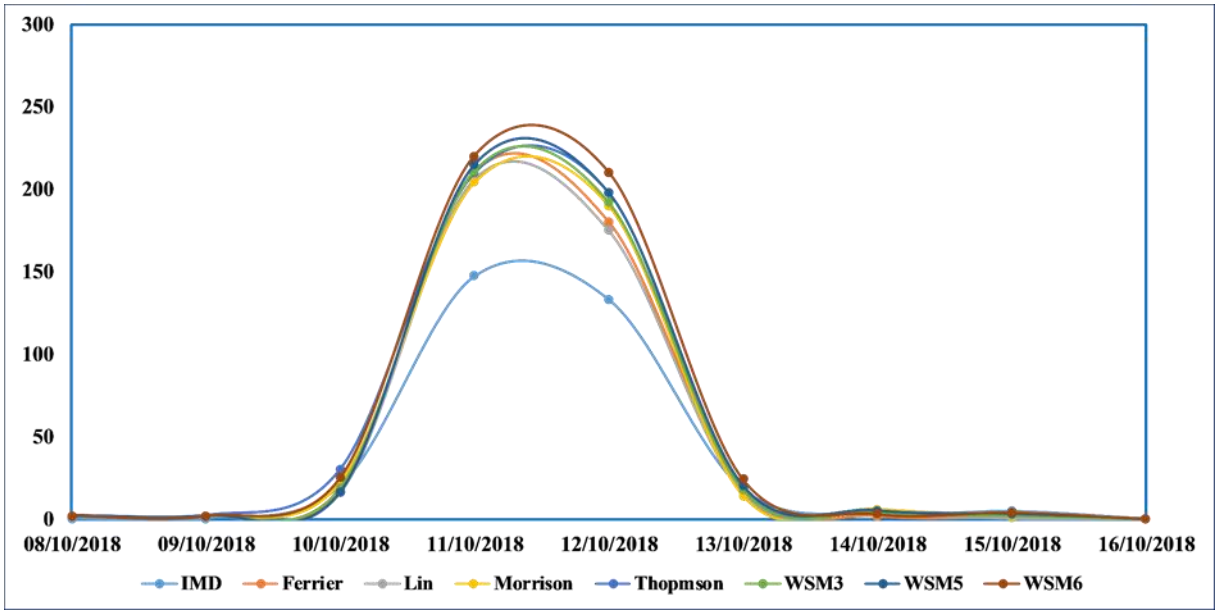

Figure 5.14 Rainfall predicted by WRF model for TC Titli

5.7 Closure

In this chapter, the spatio-temporal variations of trends in rainfall characteristics over Nagavali and Vamsadhara basins are analyzed to identify areas that are vulnerable to floods. Using WRF model, the performance of various microphysical schemes on the track and intensity prediction of tropical cyclones over NIO are assessed.

Chapter - 6 Results and Discussions (Part-II)

6.1 General

For the selected study area, based on the trends and patterns in rainfall characteristics and prediction of TCs using WRF model, the skill of GFS based rainfall forecasts have been evaluated and bias correction applied. After evaluating the skill of GFS based rainfall forecasts, an integrated hydrologic and hydraulic model based on SWAT and HEC-RAS is developed which simulates floods using GFS rainfall forecasts with a lead time of 48 hours. A Web-GIS based user interface system is developed for the visualization and timely dissemination of flood related information. Finally, the overall methodology is automated using R and Python programming languages. A detailed explanation about the evaluation of GFS rainfall forecasts, development of integrated hydrologic and hydraulic model, development of Web-GIS based user interface system, and the automation of the overall methodology is given in the following sections.

6.2 Evaluation of GFS based Rainfall Forecasts

From the section 5.6, it is clear that WRF model is able to predict rainfall for an extreme event. Although WRF model is able to predict rainfall for an extreme event, the model is sensitive to initial and boundary conditions, grid resolution, representation of physical parameterization schemes, and geographical location. For the prediction of rainfall in real-time, the initial and boundary conditions of the model need to be updated at regular intervals. A small error in initial conditions during the initialization of the model causes a large error in the forecast with an increase in simulation time. To avoid these kind of problems, rainfall predicted by WRF model for TC Titli is compared with GFS based rainfall forecasts. The time series plot of the WRF predicted rainfall, GFS based rainfall forecast, and observed data for TC Titli is shown in Figure 6.1. From the results, it observed that rainfall predicted by WRF model and GFS based rainfall forecast are in good agreement with the observed rainfall provided by IMD.

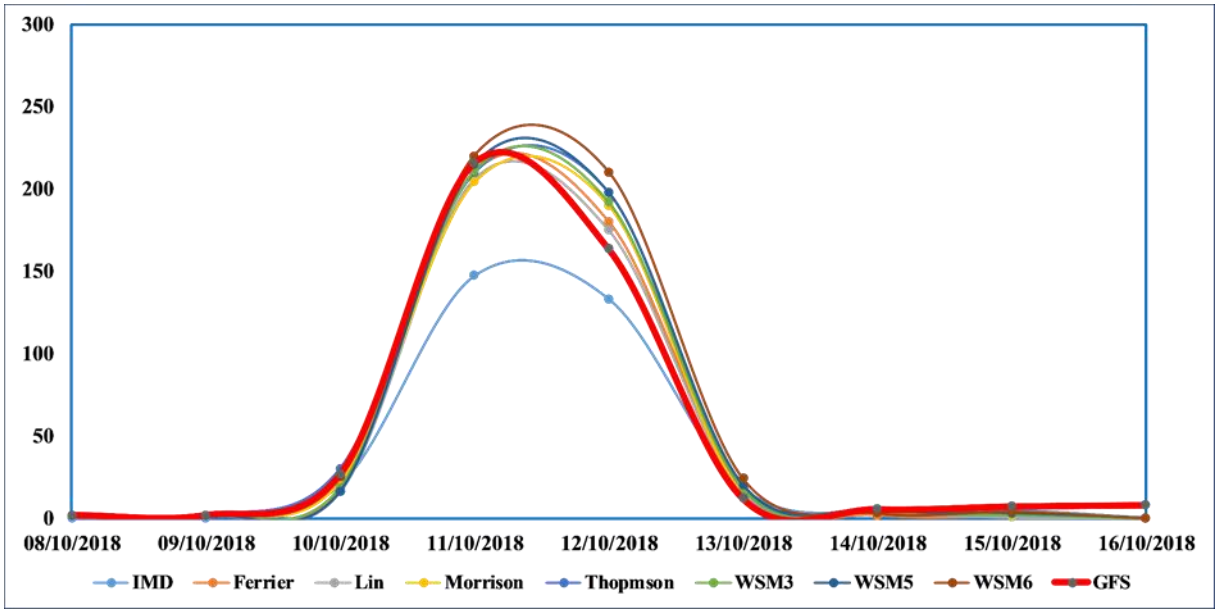

Figure 6.1 Rainfall predicted by WRF model along with GFS based rainfall forecast and observed data for Titli cyclone

Although GFS model is able to forecast rainfall, it is suffering from three types of errors (i) location, (ii) magnitude, and (iii) timing. This may limit the usefulness of GFS rainfall forecasts to simulate the streamflow. Hence, the skill of GFS based rainfall forecasts needs be verified before using them for any hydrometeorological applications.

6.2.1 Spatial Characteristics of Statistical Indices

The box plots of statistical indices (CC, BIAS, RMSE, and ME) of GFS rainfall forecasts from day-1 to day-5 against IMD rainfall over the Nagavali and Vamsadhara basins are presented in Figures 6.2 and 6.3, respectively. From the box plots of CC, it is observed that day-1 forecasts have shown the highest correlation in both basins and gradually decreased with an increase in lead time. The decrease in CC with the increase in lead time may be attributed to the variations in the SST and rainfall relationship. As the lead time increases, the relationship between SST and rainfall shifts from positive to negative because of the periodic forcing imposed by the northward propagating monsoon intra seasonal oscillations (Sahai et al. 2013). Durai and Das, (2019) suggested that rainfall forecasts from NWP models with a CC greater than 0.3 are considered good. In both basins, the magnitude of CC for day-2 and day-3 forecasts is within the acceptable range. From the magnitude of CC, it is observed that, GFS model is able to capture rainfall forecasts in both basins with a lead time of 3 days. The BIAS values indicated that, on average, the GFS model overestimated the rainfall in both the basins. The average overestimation for day-1 forecast is more than 38% in Nagavali basin and 40% percent in

Vamsadhara basin. In both basins, the overestimation of rainfall is gradually reduced from day-1 to day-3 and then increased on day-4 and day-5. Similar results are obtained for ME in both basins. The random component of the forecast error is measured using RMSE. It showed an average value of approximately 12 mm/day in Nagavali basin and 14 mm/day in Vamsadhara basin and no significant changes are found with increase in lead time.

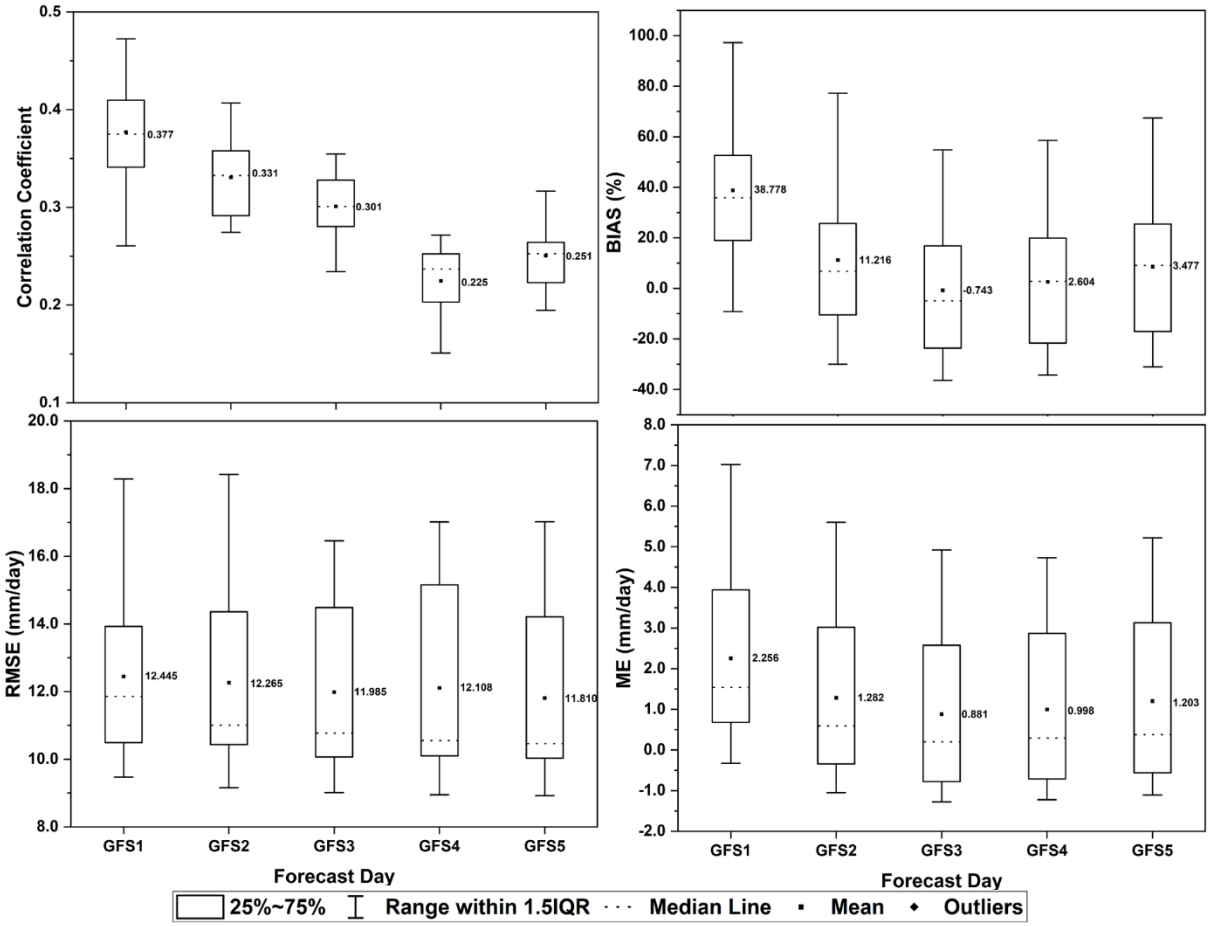

Figure 6.2 CC, BIAS, RMSE, and ME for Nagavali basin

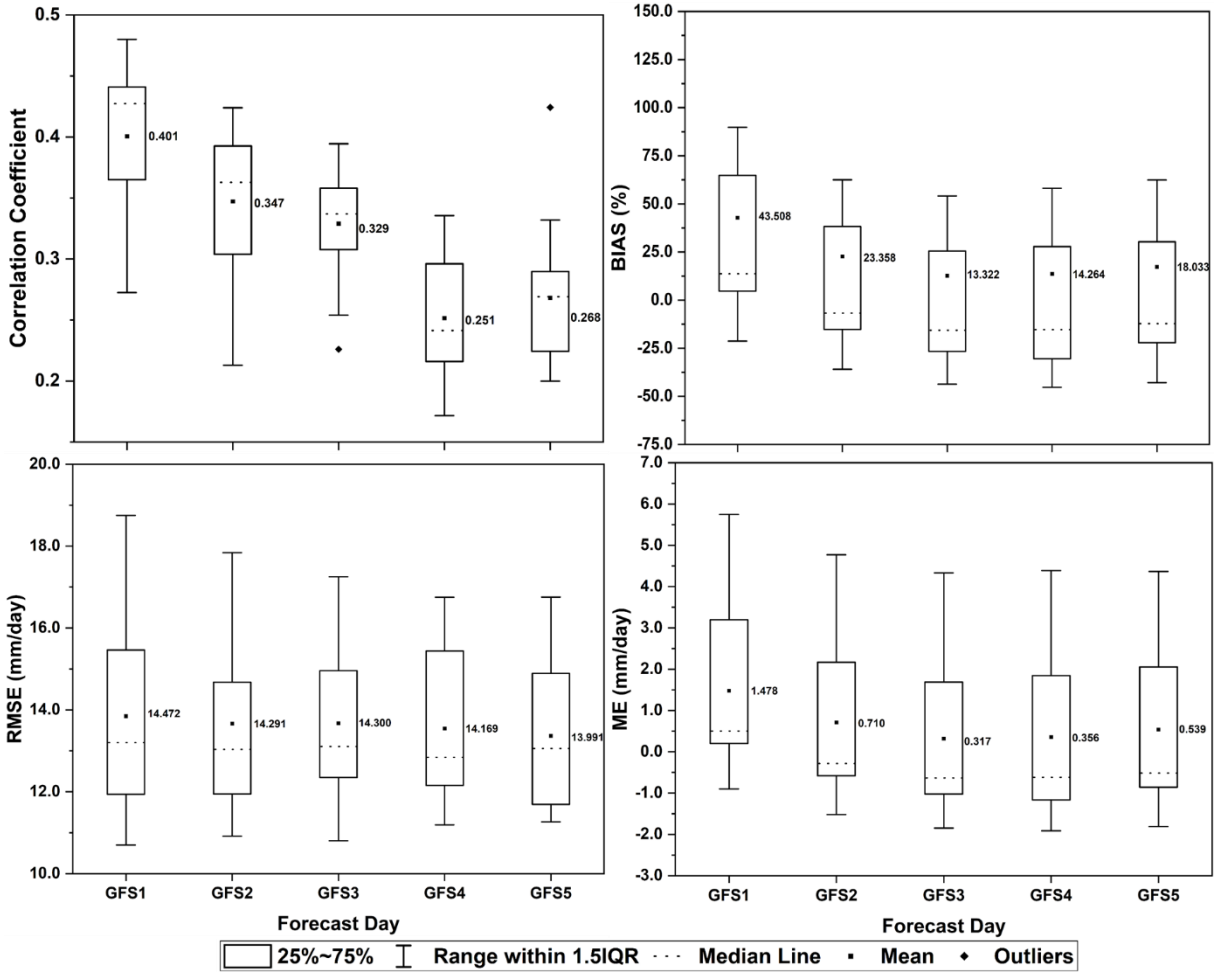

Figure 6.3 CC, BIAS, RMSE, and ME for Vamsadhara basin

The spatial distribution of statistical indices (CC, BIAS, RMSE, and ME) of GFS rainfall forecasts from day-1 to day-5 are presented in Figure 6.4. The magnitude of day-1 CC ranged between 0.3 to 0.5 in both Nagavali and Vamsadhara basins, with maximum values in middle and upper portions. Rainfall forecasts from NWP models with a CC greater than 0.3 are considered good (Durai and Das 2019). In both basins, the magnitude of CC decreased with a decrease in forecast lead time. The magnitude of CC decreased to less than 0.3 for day-2 to day-5 forecasts in all parts of Nagavali basin. The magnitude of CC for day-2 and day-3 forecasts is within the acceptable range (greater than 0.3) in all parts of Vamsadhara basin. In contrast, the magnitude of CC is less than 0.3 in all parts of the basin for day-4 and day-5 forecasts. The CC values showed that the trend in rainfall forecasts is in good agreement with observed data in both basins from day-1 to day-3.

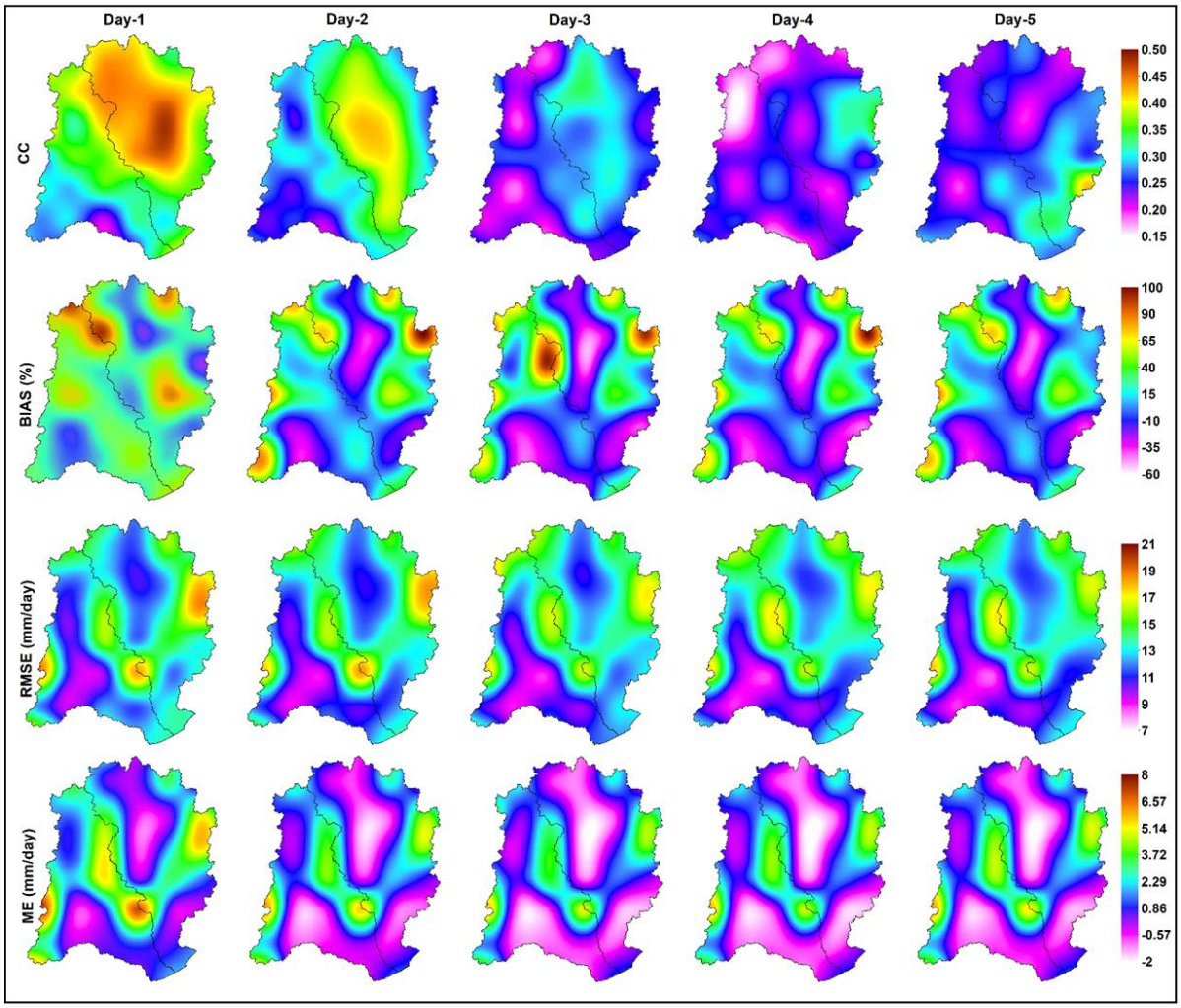

Figure 6.4 CC, BIAS, RMSE, and ME for GFS five-day rainfall forecasts

From the spatial patterns of BIAS (Figure 6.4), the model overestimated the rainfall in day-1 forecast in most parts of both Nagavali and Vamsadhara basins. The overestimation for day-1 forecast is ranged between 20% to 80%. Rainfall forecasts shifted from overestimation to underestimation as forecast length increased. In Vamsadhara basin, shift from overestimation to underestimation occurred in almost all parts of the basin. In Nagavali basin, however, the shift occurred mainly in the lower portion of the basin. The magnitude of RMSE ranged from 9 to 27 mm/day for day-1 to day-5 forecasts. The RMSE displayed similar spatial patterns from day-1 to day-5. In almost all parts of Vamsadhara basin, RMSE values greater than 12 mm/d are observed. The spatial distribution of RMSE values from day-1 to day-5 did not differ significantly in Nagavali basin. However, a decrease in the magnitude of RMSE values is observed throughout the basin. For day-1 to day-5 forecasts, the magnitude of ME ranged between -2 to 12 mm/day. The spatial patterns of ME shows that the highest values (greater than 4 mm/day) of ME are found along the boundary of Nagavali basin (adjacent to

Vamsadhara basin). Lower ME values (-2 to 4 mm/day) are found in all parts of both basins except along Nagavali basin boundary. The magnitude of ME changed from positive to negative as the forecast lead time increased, but no significant difference is observed in spatial plots of ME from day-1 to day-5. From the results of BIAS and ME, it is observed that GFS model overestimated rainfall forecasts on day-1. GFS model underestimated the rainfall from day-2 forecast onwards due to the forecast lead time. The findings are consistent with those of Durai and Das (2019).

6.2.2 Analysis of Contingency Statistics

The contingency statistics (POD, FAR, CSI, and TSS) of GFS rainfall forecasts from day-1 to day-5 are calculated for yes/no rainfall condition at a threshold of 1 mm/day for both basins (Figures 6.5 and 6.6).

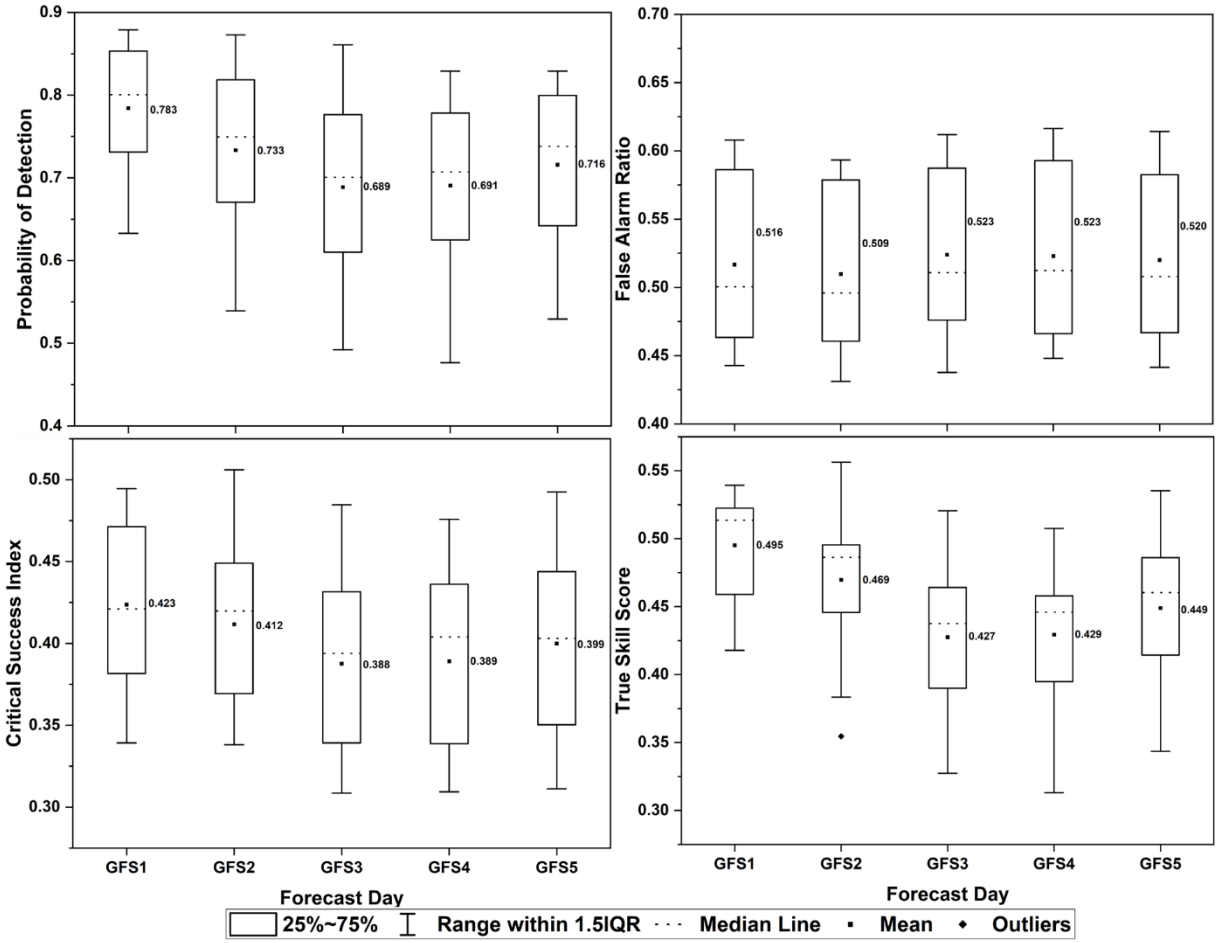

Figure 6.5 POD, FAR, CSI, and TSS for Nagavali basin for GFS five-day rainfall forecasts

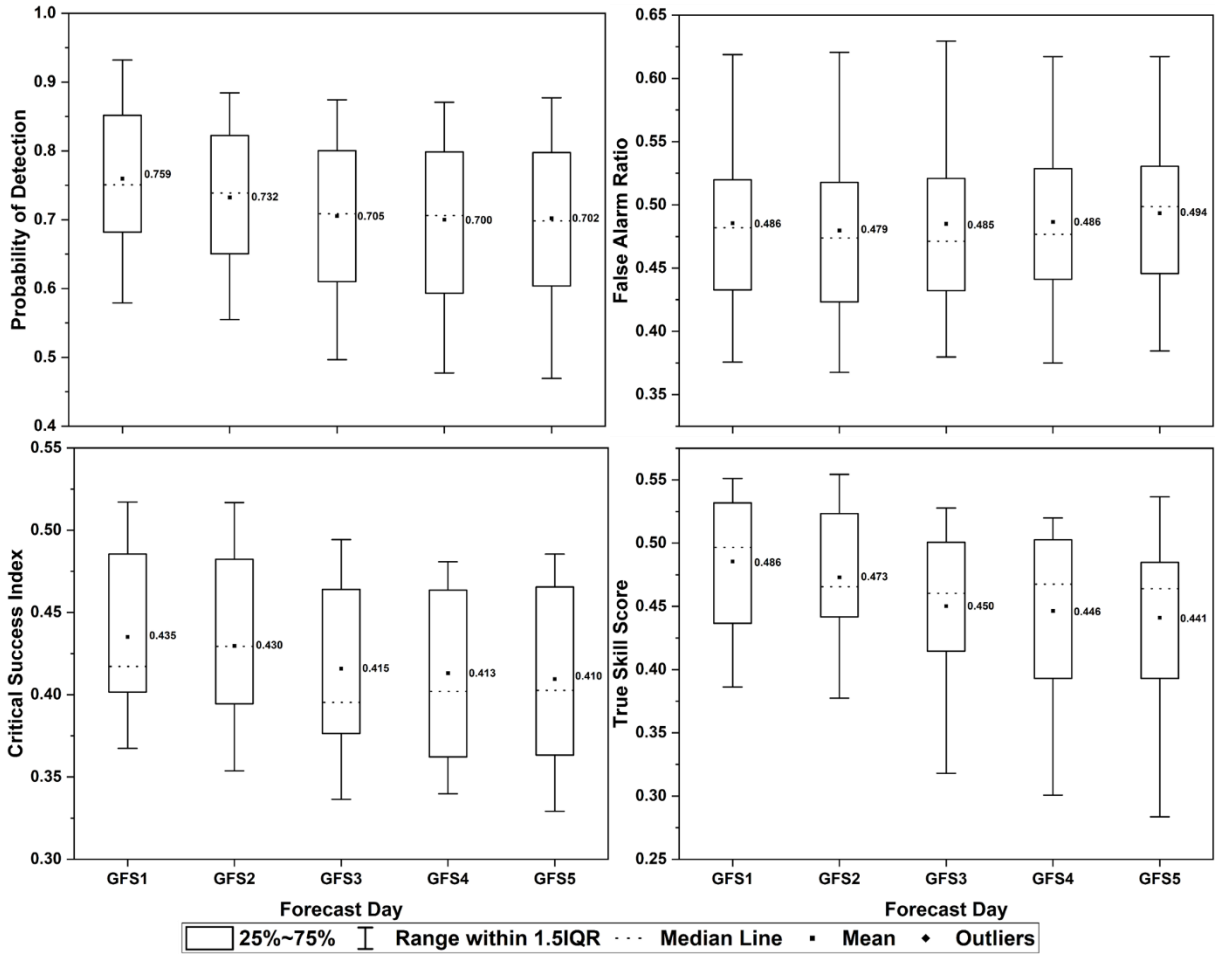

Figure 6.6 POD, FAR, CSI, and TSS for Vamsadhara basin for GFS five-day rainfall forecasts

From Figures 6.5 and 6.6, it is observed that the POD values of GFS forecasts are good and the highest value of 0.783 is found in Nagavali basin and 0.759 in Vamsadhara basin. A slight decrease in POD values is observed with an increase in lead time. Although there is a decrease in POD values with an increase in lead time, the GFS model is able to capture at least 68% of the rainfall events over the Nagavali basin and 70% of rainfall events in Vamsadhara basin. The FAR values indicate that, from day-1 to day-5 forecasts, the GFS model is unable to capture approximately 50% of rainfall events over Nagavali basin and 48% of rainfall events over Vamsadhara basin. The fraction of rainfall events correctly detected by the model is measured by CSI. CSI has highest value of 0.423 and 0.435 on day-1 forecast in Nagavali and Vamsadhara basins, respectively. The values of CSI indicated that the GFS model is able to forecast nearly 40% of rainfall events. TSS assessed the model's ability to distinguish between the occurrence and non-occurrence of events. From the values of TSS, the ability of GFS model to distinguish between the occurrence and non-occurrence of events is more than 40%.

The spatial distribution of contingency statistics (POD, FAR, CSI, and TSS) is presented in Figure 6.7. The results show that POD is greater than 0.6 for a threshold of 1 mm/day in all parts of Nagavali and Vamsadhara basins for day-1 and day-2 forecast. With the forecast lead time, POD is decreasing in lower Nagavali basin and upper middle and upper portion of Vamsadhara basin. Despite the forecast lead time, the minimum POD values in Nagavali and Vamsadhara basins are 0.55 and 0.5, respectively. POD values indicated that the GFS model is able to detect more than 50% of rainfall events with a five-day lead time. Higher FAR values of FAR are evident in all parts of Nagavali basin, except for the upper middle portion. Higher FAR values are found in the lower middle and lower portions of Vamsadhara basin. Lower FAR values are found in the upper middle and upper portion of the basin. With an increase in forecast lead time, FAR increased in almost all parts of the basin. CSI score over most parts of the basin is in between 0.4 and 0.5 for day-1 to day-5 forecast. The results shown by CSI are consistent with Durai and Das (2019).

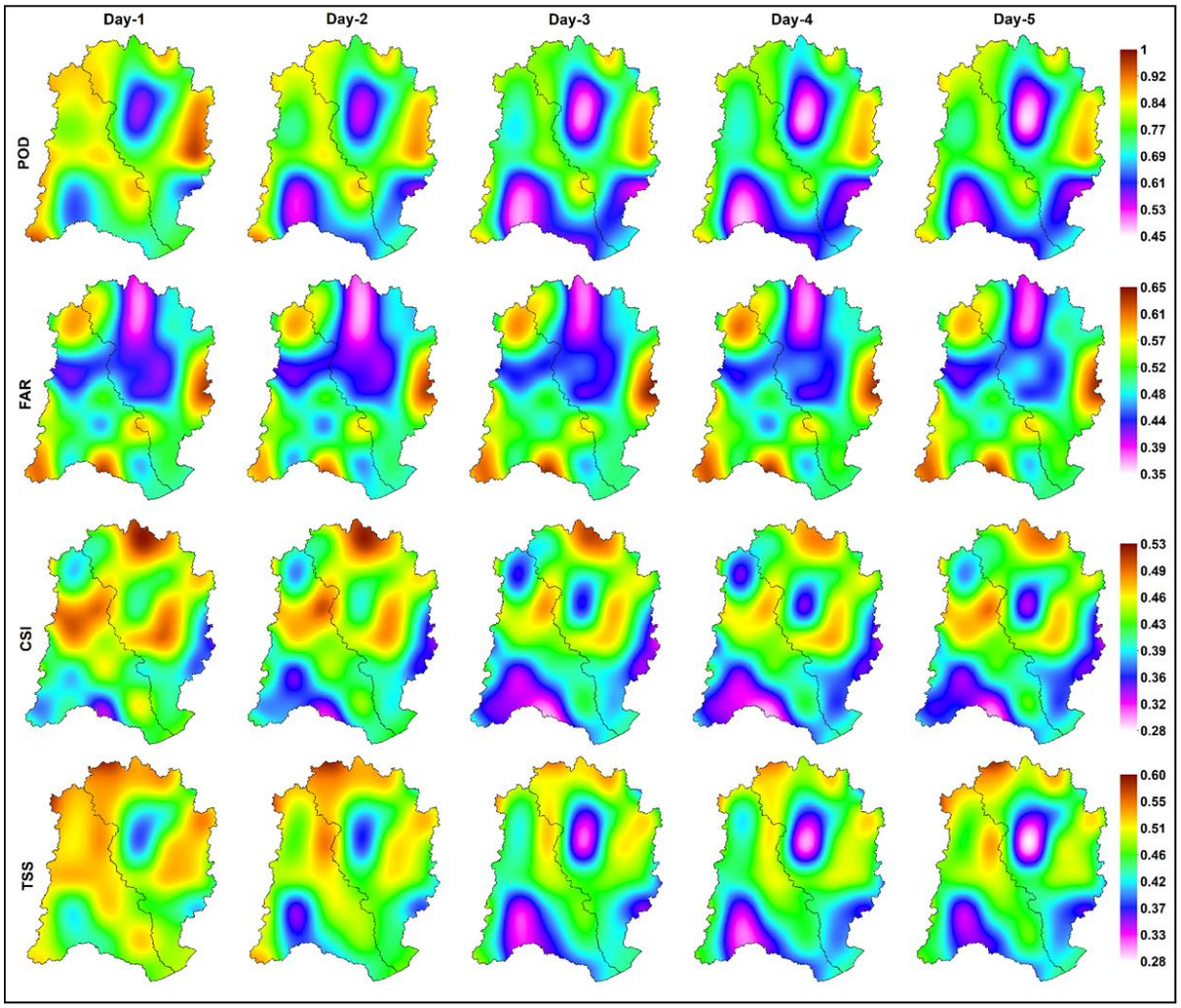

Figure 6.7 POD, FAR, CSI, and TSS for GFS five-day rainfall forecast

TSS score is more than 0.4 in all parts of both basins for day-1. The value of TSS decreased as forecast lead time increased. The lower portion of Nagavali basin and upper most middle portion of Vamsadhara basin had the greatest reduction in TSS value. Even with increased lead time, the GFS model distinguished more than 30% of rainfall events on day-5 forecast.

Error Decomposition

The total bias of GFS day-1 to day-5 forecast are decomposed into three independent components such as HB, MB, and FB. Box plots are an easy method to express the characteristics of a data set, such as symmetry, outliers, and variance. The box plots for HB, MB, FB and TB are shown in Figure 6.8. These biases are calculated for both Nagavali and Vamsadhara basins using total daily dataset. From the results, HB and FB are more dominant than MB in GFS rainfall forecasts. The magnitude of HB gradually decreased from day-1 to day-3 forecast and a small increase is observed on day-4 and day-5 forecast. The results obtained by MB and FB are comparable to those obtained by HB.

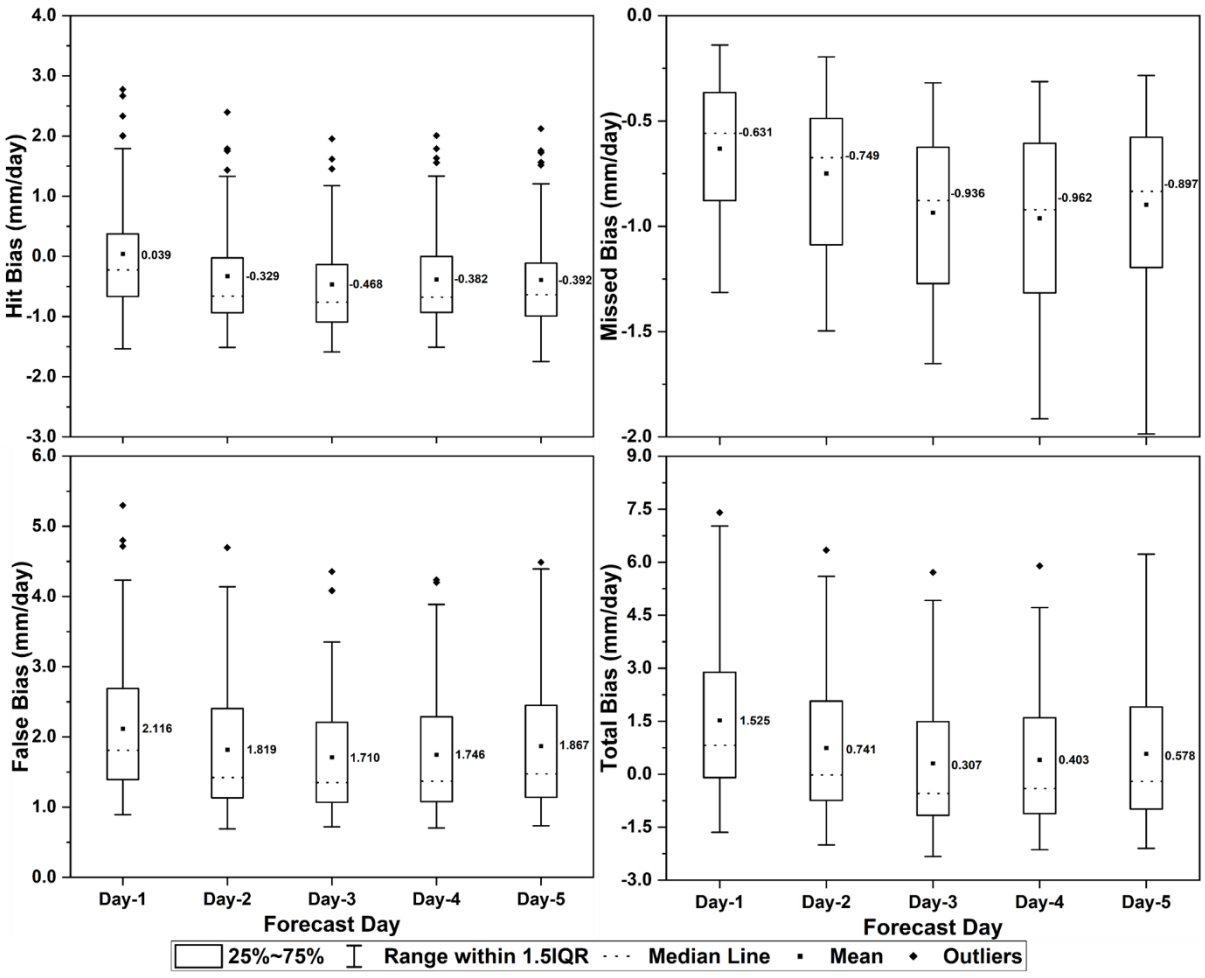

Figure 6.8 Decomposed error components of GFS rainfall forecasts

To further investigate the influence of HB, FB, and MB on total bias, the spatial distribution of the decomposed error components is presented in Figure 6.9. From the spatial patterns, it is evident that the spatial distribution of ME is mainly influenced by HB and FB. All of the error decomposed components displayed similar spatial patterns, with a change in magnitude. For day 1 to day 5, the magnitude of HB ranged from -1.6 to 2.8 mm/day, MB ranged from 0.06 to -2 mm/day, and FB ranged from 0.6 to 5.3 mm/day. The higher values of HB (greater than 2 mm/day) are located in the lower middle portion of Vamsadhara basin and the middle portion of Nagavali basin along the boundary adjacent to Vamsadhara for day-1 forecast. The magnitude of HB changed from positive to negative as forecast lead time increased, following the same spatial patterns as day-1 forecast. The change in HB from positive to negative suggested that the GFS model forecasts overestimated the rainfall on day-1 and gradually underestimated as lead time increased.

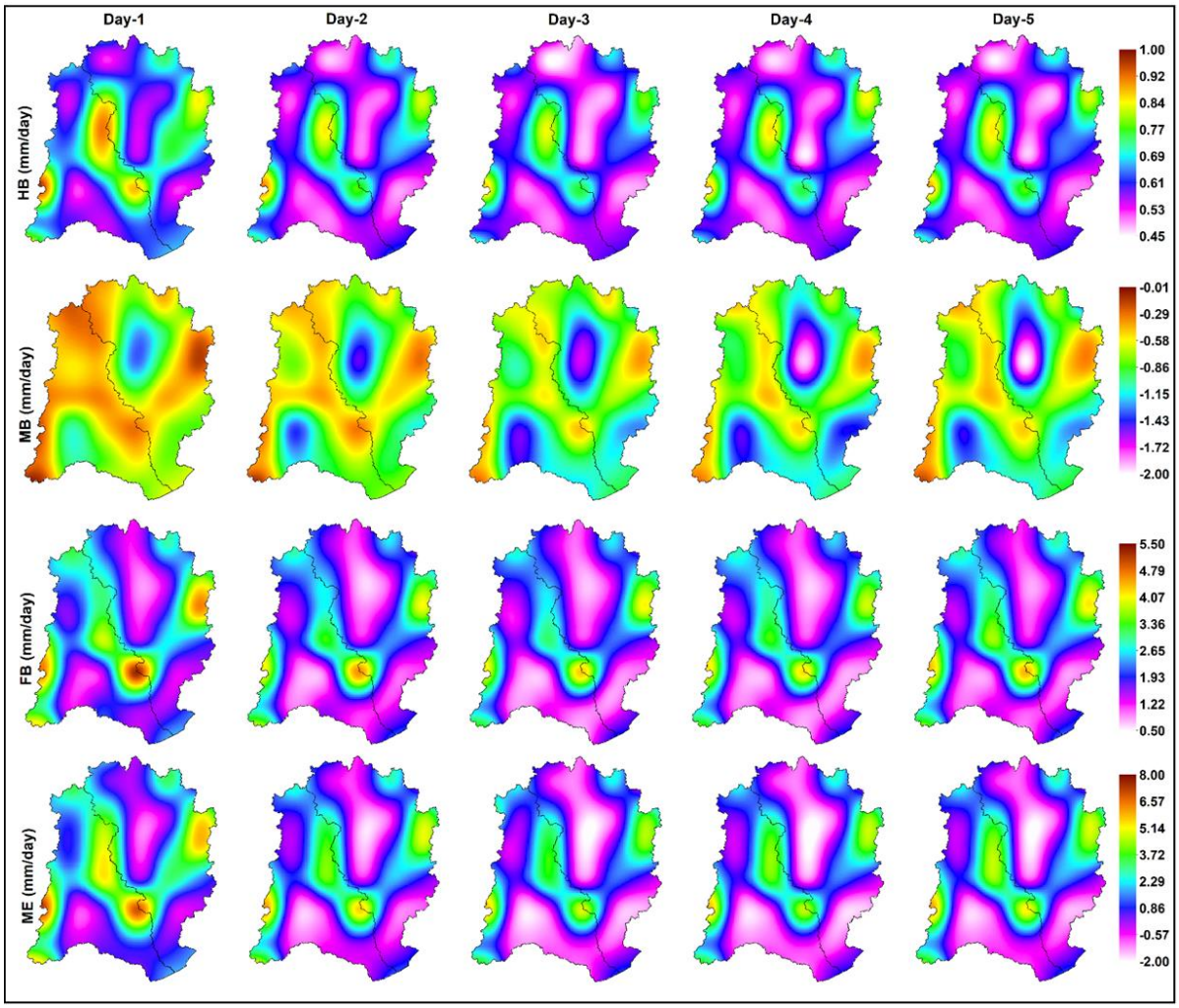

Figure 6.9 Decomposed error components for GFS rainfall forecasts

Higher MB values are found in the upper middle portion of Vamsadhara basin along Nagavali boundary and in the lower portion of Nagavali basin. With increasing lead time, the magnitude of MB gradually increased. The increase in magnitude of MB indicates that the number of missing events in GFS model forecast increased as lead time increased. The spatial distribution of FB is comparable to that of HB. The magnitude range of FB gradually decreased from 0.8 to 5.3 mm/day to 0.6 to 4.2 mm/day as forecast lead time increased. The decrease in magnitude of FB with forecast lead time indicated a reduction in false events. From the results, HB is always contributing to ME. Compared to MB, FB is the major influencing component of ME at the beginning of the GFS forecast; on the other hand, MB influenced ME with forecast lead time.

6.2.3 Intensity Distribution Plots

The intensity distribution of rainfall amount provided unique insights into error dependence on rain rate as well as the potential impact of errors on hydrological applications. This is due to the fact that most hydrological processes, such as surface runoff, are highly sensitive to both intensity distribution and total rainfall amounts. The intensity distribution is calculated as the ratio of the total amount of rainfall in each bin to the total amount of rainfall observed over the entire study period. Figure 6.10 depicts the intensity distribution plots of total, hit, missed, and false rainfall. From the intensity distribution of total rainfall, the GFS model forecasts underestimated the rainfall with rain rate less than 12 mm/day and greater than 64 mm/day. The model, on the other hand, overestimated the rainfall, with rain rates ranging from 12 mm/day to 64 mm/day. The intensity distribution of hit events followed a similar pattern to the intensity distribution of total rainfall, indicating that hit bias is a significant contributor to total bias. Missed rainfall forecasts ranged from 1 mm/day to 32 mm/day for day-1 to day-5 forecast. The number of missing rainfall events in the forecast gradually increased as the forecast lead time increased. The model forecasted false rainfall is greater than the missed rainfall, with rain rates ranging from 2 mm/day to 64 mm/day. The number of false rainfall events in the forecast gradually decreased as lead time increased.

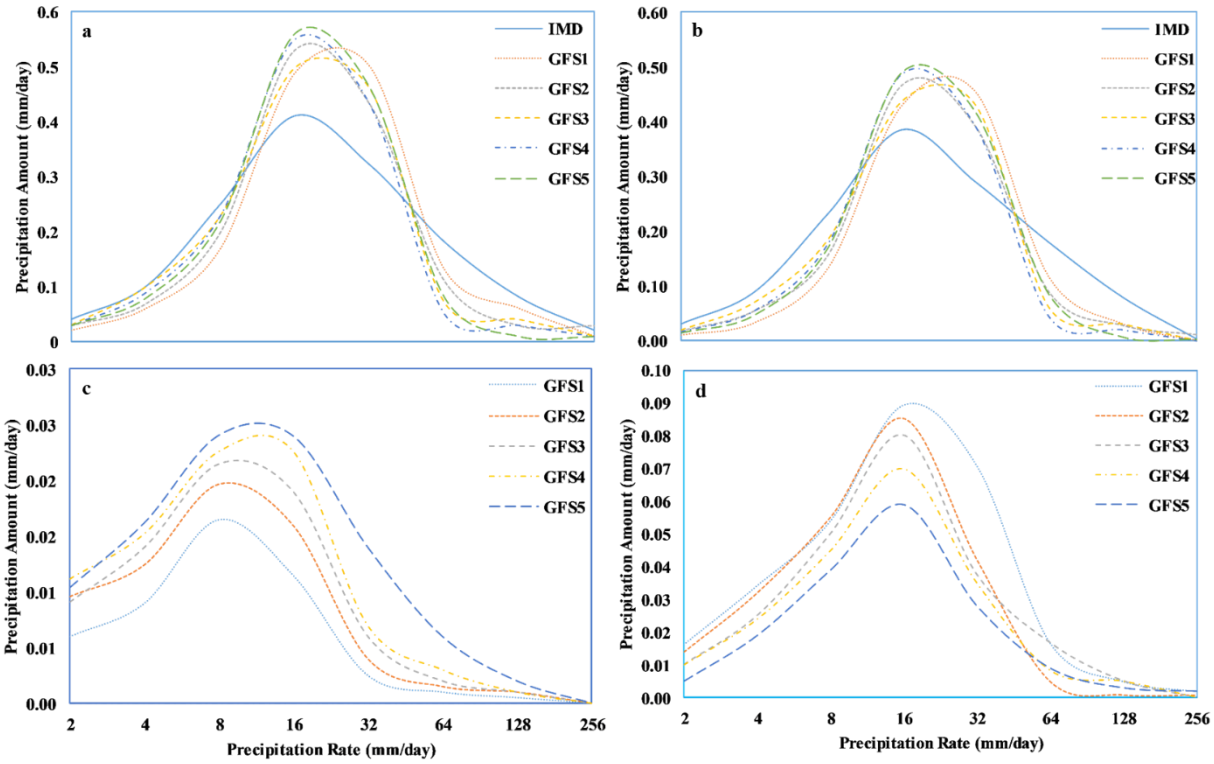

Figure 6.10 Intensity distribution plots of GFS rainfall forecast over Nagavali and Vamsadhara basins: a) Total Rainfall, b) Hit Rainfall, c) Missed Rainfall, and d) False Rainfall.

6.2.4 Bias Correction of Rainfall

The GFS rainfall forecasts are corrected for bias using the simple multiplication scheme mentioned in chapter III. Bias factors are calculated and verified by dividing the entire dataset into two parts: dataset-1 (from June 2015 to December 2018) and dataset-2 (from January 2019 to December 2020). The bias factors are calculated with dataset1 and validated with dataset2. The intensity distribution plots (Fig. 6(a) and 6(b)) show that the GFS model overestimated the rainfall events with intensities greater than 12mm/day, resulting in false alarms. The categorical rainfall thresholds chosen for calculating the bias factors are 8mm, 12mm, 16mm, and 20mm. The dataset-1 is divided into two groups for each threshold. For instance, to calculate the bias factor at a threshold of 8mm, dataset-1 is divided into two groups as rainfall less than or equal to 8 mm/day and greater than 8 mm/day. The bias factors for rainfall forecasts from day-1 to day-5 for both Nagavali and Vamsadhara basins at different thresholds are presented in Table 6.1. To avoid underestimation of rainfall, the bias factors are applied to dataset-2 for rainfall events with intensity greater than the threshold value.

Table 6.1 Calculated bias factors for the GFS five-day (i.e., day-1 to day-5) rainfall forecasts using IMD gridded observed data from June 2015 to December 2018 over Nagavali and Vamsadhara basins

Forecast day	RI ≤ 8	RI > 8	RI ≤ 12	RI > 12	RI ≤ 16	RI > 16	RI ≤ 20	RI > 20
GFS1	1.059	0.612	0.888	0.648	0.727	0.655	1.059	0.612
GFS2	0.987	0.717	0.888	0.787	0.762	0.801	0.987	0.717
GFS3	0.936	0.831	0.891	0.891	0.779	1.004	0.936	0.831
GFS4	0.681	0.933	0.854	0.877	0.698	1.203	0.681	0.933
GFS5	0.940	0.765	0.853	0.833	0.754	0.899	0.940	0.765

Note: RI indicates rainfall intensity in mm/day.

After recalculating the statistical indices for bias corrected GFS rainfall forecasts, skill scores are calculated to see if there is any improvement in forecast after bias correction. The skill scores for statistical indices at different threshold values are presented in Table 6.2. The magnitude of CC over both Nagavali and Vamsadhara basins improved slightly at all threshold values after bias correction as per Table 6.2. Based on the skill score values of BIAS, RMSE, and ME in both basins, a significant improvement is observed after bias correction at all threshold values. Over the Nagavali basin, the improvement in BIAS and ME ranged between 38 to 64%, 44 to 65%, 22 to 53%, and 3 to 53% at thresholds of 8, 12, 16, and 20 mm/day, respectively with a maximum improvement on day-1 forecast. The RMSE improved by a maximum of 23%, 23%, 21% and 17% for day-1 forecast at thresholds of 8, 12, 16, and 20 mm/day, respectively. From day-2 to day-5, the improvement in RMSE ranged from 4 to 8%, 5 to 9%, 3 to 7%, and 0 to 5% at thresholds of 8, 12, 16, and 20 mm/day, respectively. Over Vamsadhara basin, the improvement in BIAS and ME ranged from 14 to 57%, 65 to 93%, 31 to 68%, and 4 to 42% at thresholds of 8, 12, 16, and 20 mm/day, respectively. The improvement in RMSE ranged from 2 to 18%, 3 to 18%, 2 to 16%, and 0 to 14% at the respective threshold values. From the skill score values, it is observed that the bias correction for rainfall with intensity greater than 12 mm/day in both basins showed maximum improvement when compared with other thresholds.

Table 6.2 Percentage improvement in statistical indices of GFS rainfall forecast for the study basins over a two-year period (i.e., from January 2019 to December 2020)

Forecast Day	Nagavali Basin			Vamsadhara Basin		
	BIAS	RMSE	ME	BIAS	RMSE	ME
	8/12/16/20	8/12/16/20	8/12/16/20	8/12/16/20	8/12/16/20	8/12/16/20
Day-1	64/65/57/53	23/23/21/17	64/65/57/53	57/7758/42	18/18/16/14	57/77/58/42
Day-2	59/62/38/22	8/9/7/5	59/62/38/22	24/93/58/34	5/5/4/3	24/93/58/34
Day-3	38/44/22/3	4/5/1/0	38/44/22/3	16/76/68/5	2/3/2/0	16/76/68/5
Day-4	43/49/23/3	5/5/3/0	43/49/23/3	14/65/31/4	3/3/2/0	14/65/31/4
Day-5	52/53/29/11	7/7/5/2	52/53/29/11	15/85/46/18	3/3/2/1	15/85/46/18

Note: 8/12/16/20 indicates the threshold values considered for the calculation of bias factors and 64/65/57/53 indicates the improvement in the model forecast after the bias correction at respective threshold values.

To further investigate the influence of bias correction of GFS rainfall forecasts over both basins, the spatial distribution of statistical indices before and after the bias correction are presented in Figure 6.11 and 6.12. From the spatial patterns of spatial indices, it is evident that the magnitude of CC improved from day-1 to day-5 in all parts of both basins after bias correction. For day-1 and day-2 forecasts, the maximum improvement in CC is observed in the lower parts of both basins. Whereas, from day-3 to day-5 an improvement in CC is observed in all parts of both basins. From the spatial patterns of BIAS, it is observed that the overestimation of rainfall decreased significantly from day-1 to day-5 in all parts of both basins. For day-1 forecasts, before bias correction, the overestimation ranged from 55 % to 90% in the middle and upper portions of Nagavali basin and in the middle portion of Vamsadhara basin. After bias correction, the overestimation in the middle and upper portions of Nagavali basin and in the middle portion of Vamsadhara basin decreased to 21 – 38%. Similarly, from day-2 to day-5 the overestimation of rainfall decreased significantly in all parts of both basins. The spatial patterns of ME followed similar patterns of BIAS in both Nagavali and Vamsadhara basins. Spatial patterns of RMSE showed that its magnitude decreased significantly from day-1 to day-5 in all parts of both basins after bias corrections. The spatial patterns of ME followed a pattern similar to BIAS in both basins.

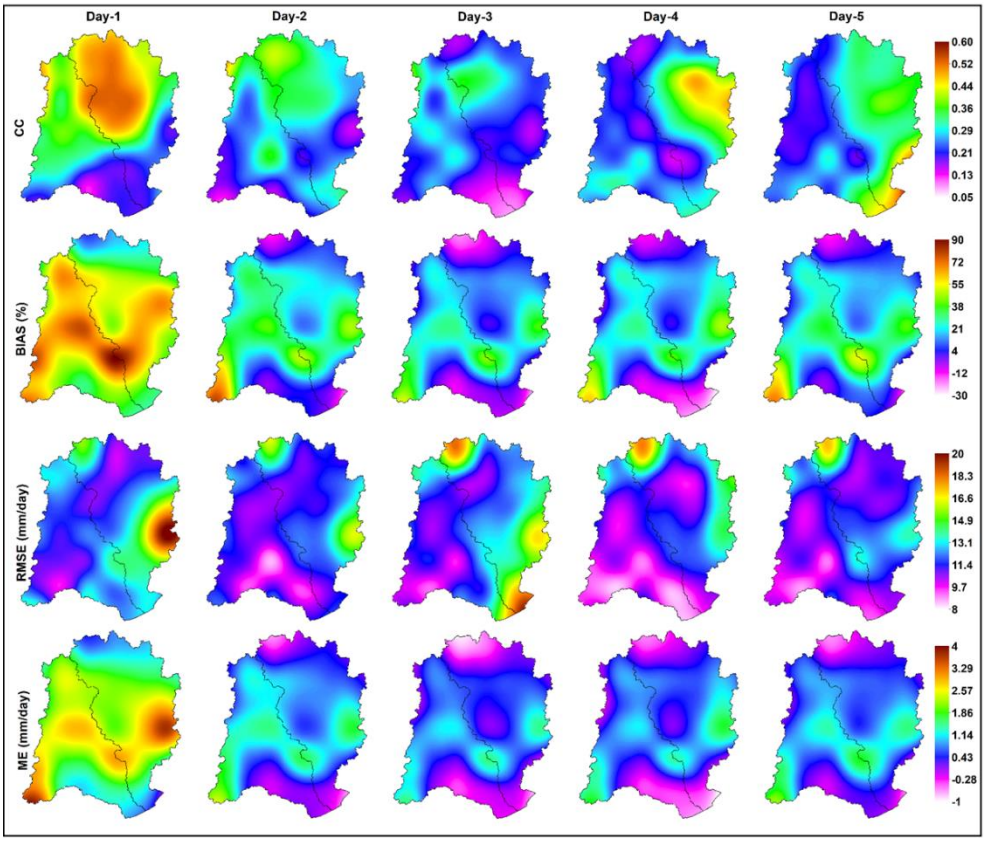

Figure 6.11 CC, BIAS, RMSE, and ME for the dataset-2 before the bias corrections

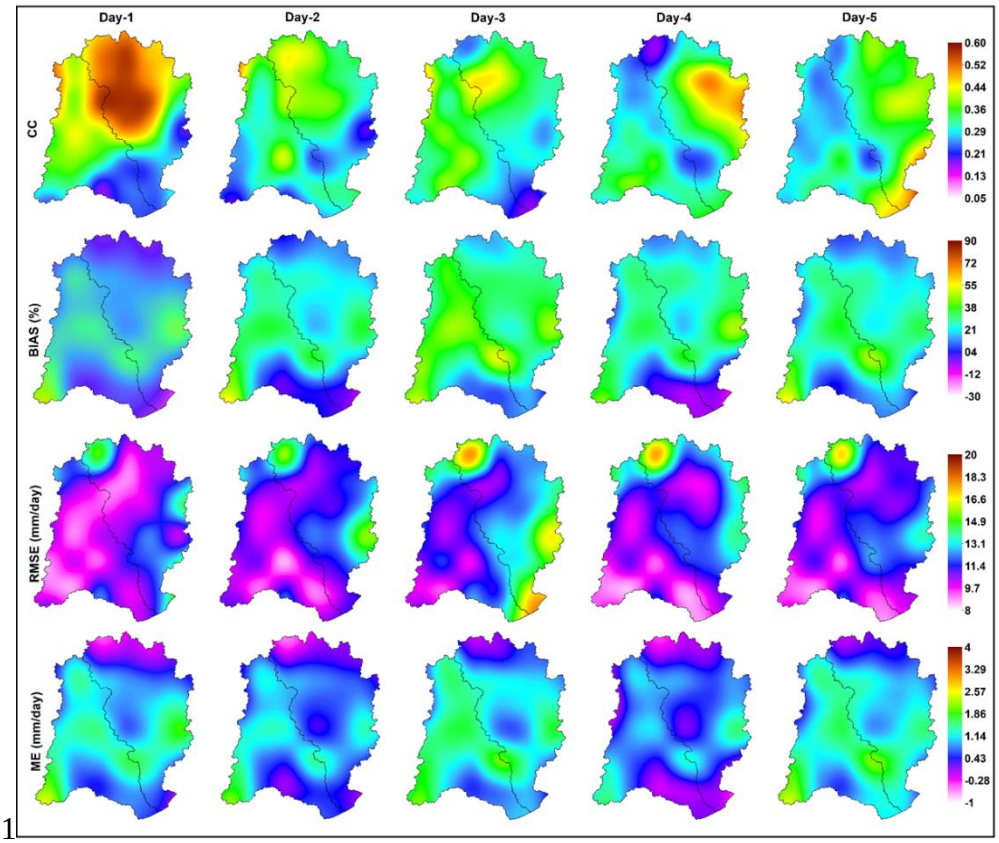

1

Figure 6.12 CC, BIAS, RMSE, and ME for the dataset-2 after bias correction

6.3 Forecasting of Floods using Integrated Model

From the analysis of trends and patterns in rainfall characteristics, it is observed that the lower and middle portions of Nagavali and Vamsadhara basins are vulnerable to frequent floods due to heavy rainfall in the monsoon season and TCs that are formed over BoB during the pre- and post-monsoon seasons. Due to lack of flood forecasting and warning system, authorities frequently struggle to evacuate villagers during floods. Hence, there is a need for an integrated modelling framework to forecast floods and flood inundation extent. In the present study, an integrated hydrologic and hydraulic model is developed based on SWAT and 2D HEC-RAS models for simulation of floods using GFS based rainfall forecasts.

The SWAT model is used in this study to estimate streamflow in both Nagavali and Vamsadhara basins. The estimated streamflow is calibrated and validated using SUFI-2 algorithm in SWAT-CUP. SWAT model evaluation includes a sensitivity analysis to identify the parameters for streamflow simulations. The simulated streamflow from SWAT model is given as input to HEC-RAS model to predict flood inundation extent and flood depth. The following sections provide a detailed explanation of the results.

6.3.1 Flood Frequency Analysis

The National Disaster Management Authority (NDMA) recommended a discharge threshold of 1500 m^3/s for modeling flood events in Nagavali and Vamsadhara basins in its hazard assessment report for Andhra Pradesh and Odisha states (RMSI 2015). A study by Hajaj et al. (2019) found that the Nagavali basin has been flooded more than nine times since 1990. It suggests that flood events with discharges of less than 1500 m^3/s caused floods in the basin. As a result, in the present analysis, a flood frequency analysis has been performed instead of considering NDMA's recommended threshold for modelling of floods. Flood frequency analysis uses annual maximum discharge collected at gauge stations to provide information on both the magnitude and frequency of floods. In the present study, stationary and nonstationary flood frequency analysis is conducted to estimate flood peaks for different return periods of 2, 5, 10, 25, 50, and 100 years in Nagavali and Vamsadhara basins. In both stationary and nonstationary analyses, four distributions, namely, Log-Pearson Type-III, Log-Normal, Weibull, and Gumbel are used to estimate the peak discharges (Yang et al. 2019). The parameters of the distributions are estimated by maximum likelihood estimation method. Two open source R programming based packages, namely, “extremes” (Gilleland 2020; Gilleland

and Katz 2016) and "gamlss" (Rigby et al. 2005) are used to perform stationary and nonstationary analysis. Under the stationary assumption, best fit distribution is selected based on Akaike Information Criterion (AIC) value.

Compared to other distributions, Log-Pearson Type-III provided the minimum AIC of 459 in Nagavali basin and 741 in Vamsadhara basin. Under the nonstationary assumption, six different cases are set for each distribution, where the scale and location parameters vary with time (Table 6.3). Log-Pearson Type-III distribution performed best for the nonstationary analysis. The residuals for Log-Pearson Type-III distribution are presented in Table 6.4 and 6.5 for Nagavali and Vamsadhara basins, respectively.

Table 6.3 Location and Scale parameters with time t in nonstationary analysis

Models	Location	Scale
M1	$\mu = \mu_0 + \mu_1 * t$	σ = Constant
M2	$\mu = \mu_0 + \mu_1 * t$	$\sigma = \sigma_0 + \sigma_1 * t$
M3	$\mu = \mu_0 + \mu_1 * t + \mu_2 * t^2$	σ = Constant
M4	$\mu = \mu_0 + \mu_1 * t + \mu_2 * t^2$	$\sigma = \sigma_0 + \sigma_1 * t$
M5	$\mu = \mu_0 + \mu_1 * t + \mu_2 * t^2 + \mu_3 * t^3$	$\sigma = \sigma_0 + \sigma_1 * t$
M6	$\mu = \mu_0 + \mu_1 * t + \mu_2 * t^2 + \mu_3 * t^3$	$\sigma = \sigma_0 + \sigma_1 * t + \sigma_2 * t^2$

Table 6.4 Residuals of Log-Pearson Type-III distribution over Nagavali basin

Model	AIC	Mean	Variance	Coefficient of Skewness	Coefficient of Kurtosis
M1	459.357	0	1.03	0.975	0.897
M2	457.801	0	1.03	0.815	0.625
M3	453.050	0	1.03	0.739	0.912
M4	453.050	0	1.03	0.739	0.912
M5	459.357	0	1.03	0.975	0.897
M6	456.668	0	1.03	0.604	0.274

All the six models have the same mean and variance in the both basins. The M3 and M4 models have the smallest AIC values, while M3 has the smallest Kurtosis value in the Vamsadhara basin compared to M4. Therefore, M3 model has been selected for the calculation of peak discharges under nonstationary conditions. The estimated peak discharges for basins under stationary and nonstationary analysis are shown in Table 6.6. From the statistics, it is found that peak discharges estimated by the non-stationary method at various return periods are less than the peak discharges estimated by stationary method. The difference in peak discharge estimates from stationary and non-stationary techniques is relatively small during short return periods and increased with the length of return period. The smaller difference between peak discharges calculated by stationary and non-stationary methods may be attributed to the fact that only time is considered as a covariate in calculating return periods. This may be because only time is considered as covariate in the calculation of design floods. Flood events with discharges greater than or equal to 2-year return period discharge calculated using the nonstationary method are considered for flood simulation in this study.

Table 6.5 Residuals of Log-Pearson Type-III distribution over Vamsadhara basin

Model	AIC	Mean	Variance	Coefficient of Skewness	Coefficient of Kurtosis
M1	741.090	0	1.02	0.081	-0.886
M2	742.419	0	1.02	0.171	-1.148
M3	741.005	0	1.02	0.080	-0.765
M4	741.005	0	1.02	0.080	-1.148
M5	741.090	0	1.02	0.082	-0.886
M6	742.646	0	1.02	0.270	-1.272

Table 6.6 Estimated peak discharges of the study basins with different return periods using Log-Pearson Type-III distribution

Return Period (T years)	Peak Discharge (m^3/s)			
	Nagavali River		Vamsadhara River	
	Stationary Analysis	Nonstationary Analysis	Stationary Analysis	Nonstationary Analysis
2	1223	1200	1365	1360
5	1948	1877	2634	2596
10	2650	2490	3841	3774
25	3750	3443	5960	5837
50	4770	4252	8110	7916
100	5989	5195	10900	10605

6.3.2 SWAT Simulated Streamflow

SWAT model underestimated the streamflow during the calibration and validation period in both basins. The observed versus simulated streamflow during the calibration and validation period at Srikakulam and Kashinagar stations in Nagavali and Vamsadhara basins, respectively are presented in Figure 6.13 and 6.14. During the calibration and validation period, the time series plot of simulated streamflow reflected rainfall patterns over Nagavali and Vamsadhara basins and matched with observed streamflow. In Nagavali and Vamsadhara basins, the monsoon season produced the most streamflow (i.e., from June to September). In Nagavali basin, SWAT model overestimated the streamflow flow from 2004 to 2009. The overestimation of streamflow in Nagavali basin may be attributed to uncertainty in gridded products caused by inhomogeneity in observation practices and irregular distribution of observation stations.

Streamflow in both basins has been increasing since 1991. The annual average streamflow has increased at a rate of 14 m^3/s in Nagavali basin and 16 m^3/s in Vamsadhara basin. According to the observed flow data, the average annual flow in Nagavali basin is 83.52 m^3/s and in Vamsadhara basin it is 88.72 m^3/s. The highest peak flow of 5624.74 m^3/s is recorded in Nagavali basin on August 04, 2006, while 7321.54 m^3/s is recorded in Vamsadhara basin on October 07, 2007. The peak flow recorded in Vamsadhara basin on October 07, 2007, could have been caused by measurement error or spurious data, as there is no scientific evidence of heavy rainfall or a cyclone passing over the basin at that time. The Vamsadhara basin received secondary peak of 4250 m^3/s on September 07, 2014. According to SWAT simulated streamflow, the average annual flow in Nagavali basin is 79.71 m^3/s and 72.50 m^3/s in Vamsadhara basin. The highest peak flow evidenced in the simulated streamflow is 6753 m^3/s on August 04, 2006 in Nagavali basin and 3884 m^3/s on September 07, 2014 in Vamsadhara basin. The SWAT simulated peak flows that are in good agreement with observed flow. The maximum annual discharge in Nagavali basin is 2070 Billion Cubic Meters (BCM) in 2010, while the maximum annual discharge in Vamsadhara basin is 2295 BCM in 2006. Minimal annual discharges of 212 and 252 BCM in 2002 are observed in Nagavali and Vamsadhara basins.

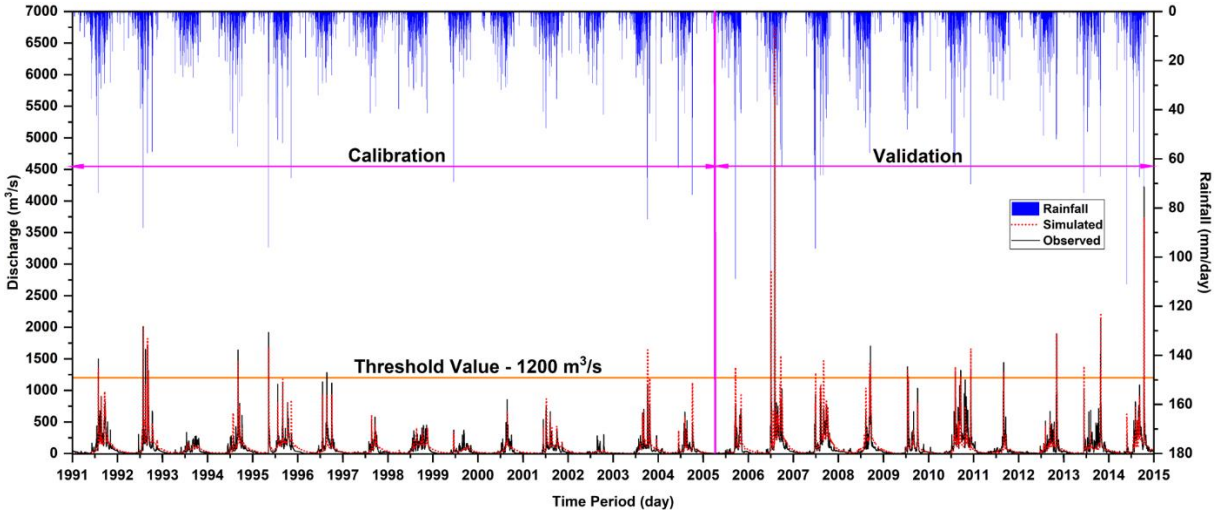

Figure 6.13 Observed and simulated streamflow in Nagavali basin

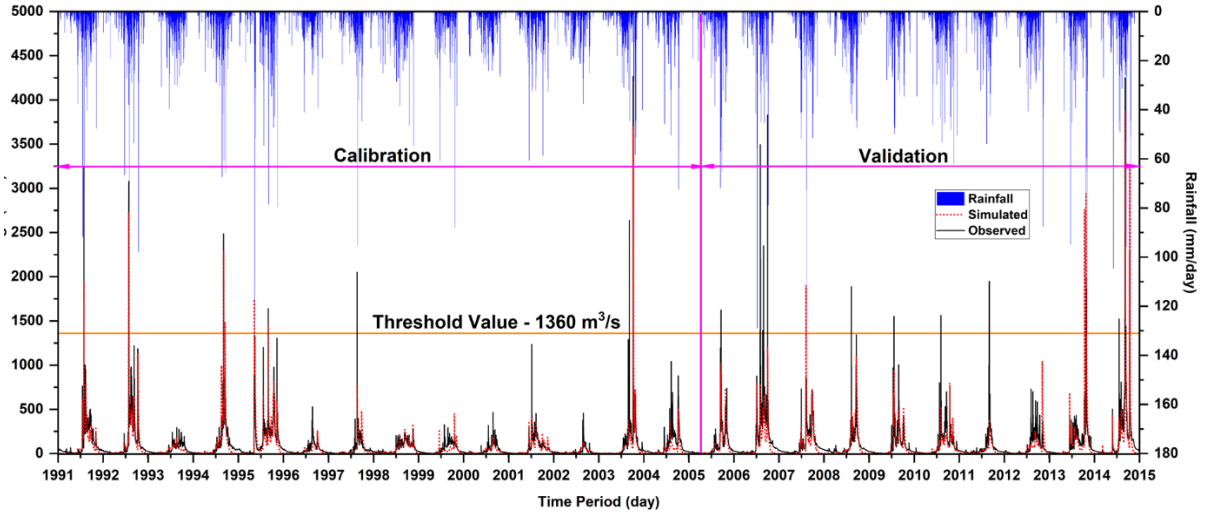

Figure 6.14 Observed and simulated streamflow in Vamsadhara basin

6.3.3 Flood Inundation Maps of the Historical Flood Events

The Nagavali and Vamsadhara basins are frequently flooded as a result of heavy rainfall during the monsoon season and tropical cyclones during the pre- and post-monsoon seasons. Based on a 2-year return period peak discharge (1200 m^3/s in Nagavali basin and 1360 m^3/s in the Vamsadhara basin), Nagavali basin is flooded 16 times, while Vamsadhara basin is flooded 9 times between 1991 and 2014. In Nagavali basin, 11 flood events occurred during the monsoon season, four during the post-monsoon season, and the rest during the pre-monsoon season. In Vamsadhara basin, six events occurred during the monsoon season and the rest during the post-monsoon season. The flood inundation maps for historical events from 1991 to 2014 are generated using HEC-RAS model with discharge hydrographs as inputs from SWAT model.

Flood inundation maps for historical events in Nagavali basin are shown in Figures 6.15 and 6.16. Figure 6.17 shows flood inundation maps of Vamsadhara basin.

Based on historical flood events, the flood inundation area in the Nagavali basin varied from 182 to 229 sq.km, with a minimum inundation area in 1992 and a maximum inundation area in 2006. The flood inundation area predicted by integrated hydrologic and hydraulic model over Nagavali basin for different flood events are in good agreement with Iqbal and Yarrakula, (2020). Over 115 villages across 10 mandals namely, Vangara, Veeragattam, Regidi, Palakonda, Burja, Santhakaviti, Ponduru, Amudalavalasa, Etcherla and Srikakulam rural in Srikakulam district, Andhra Pradesh are affected due to floods in Nagavali Basin. In Vamsadhara basin, the flood inundation area is varied from 245 to 309 sq.km, with a minimum inundation area in 1995 and a maximum inundation area in 2003. In the years 1994 and 2013, Vamsadhara basin received streamflow over 1000 m^3/s for more than three consecutive days, resulting in an increase in the inundation area despite a lower peak discharge when compared to previous flood events. More than 139 villages across 11 mandals namely, Bhamini, Kotturu, Hiramandal, Jalumuru, L N Peta, Sarubujjili, Narasannapeta, Polaki, Amudalavalasa, Srikakulam rural and Gara have been affected in Vamsadhara basin by floods. Average area of 220 sq. km and at least 1 lakh people in115 villages in Nagavali basin, and an area of 272 sq.km and 1.25 lakh people in 135 villages in Vamsadhara basin are vulnerable to floods. Geographical locations of the villages in both basins that are prone to floods are shown in Figure 6.18.

6.3.4 Validation of Flood Inundation Depth

The flood inundation depth predicted by 2D HEC-RAS model is compared with observed data from gauge stations in Nagavali and Vamsadhara basins at Srikakulam and Kashinagar, respectively. Graphical representation of observed vs simulated flood depths is shown in Figure 6.19. The inundation depths provided by 2D HEC-RAS model in both basins are clearly in good agreement with observed depths. Flood inundation depths predicted by the model ranged from 2.70 to 4.51 m and 2.28 to 3.77 m for Nagavali and Vamsadhara basins, respectively. In contrast, the observed inundation depths in the respective basins varied from 2.55 to 6.05 m and 2.16 to 3.65 m, respectively.

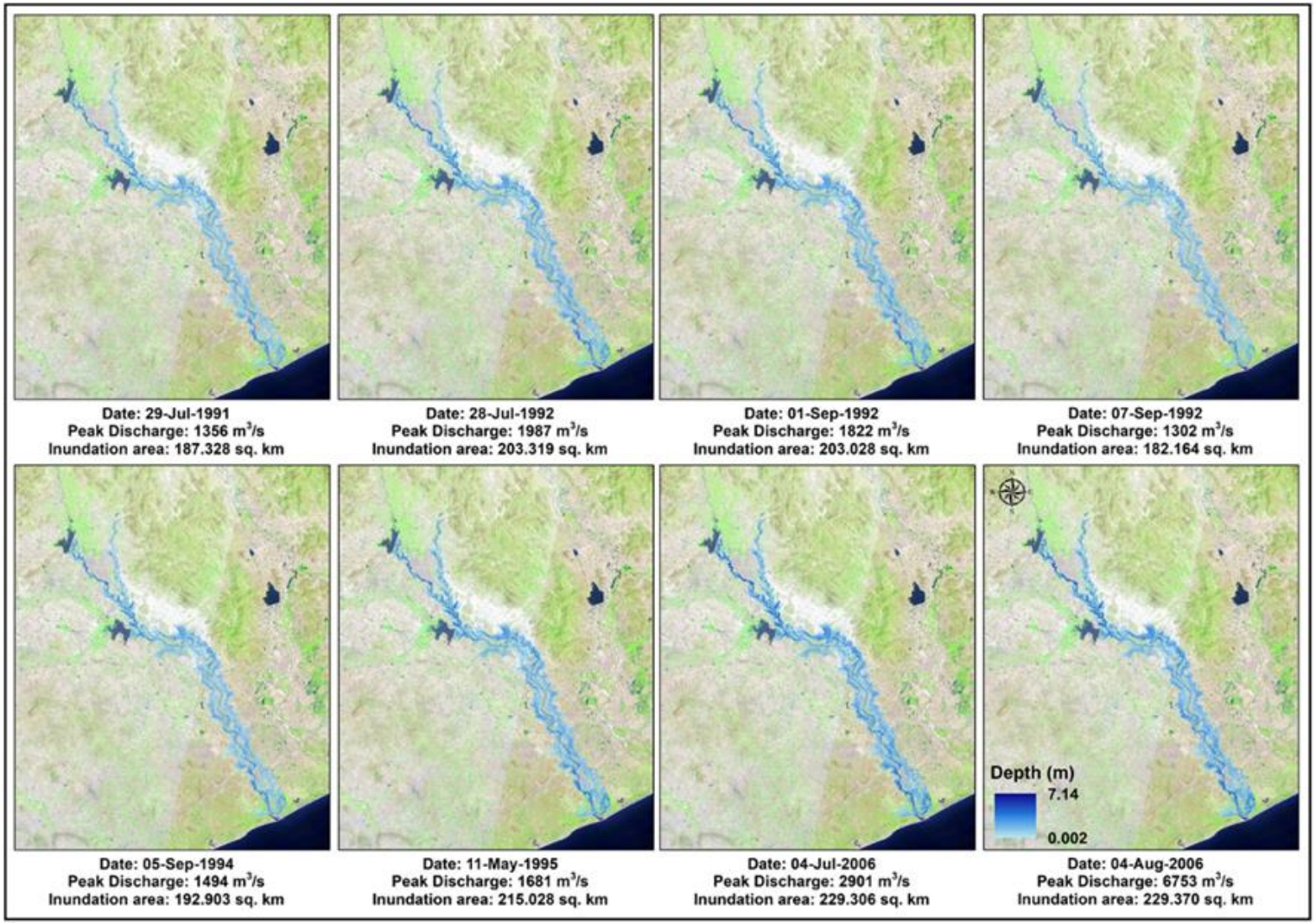

Figure 6.15 Flood inundation maps generated by HEC-RAS model using SWAT simulated discharge as upstream boundary from 1991 – 2006 over the Nagavali basin

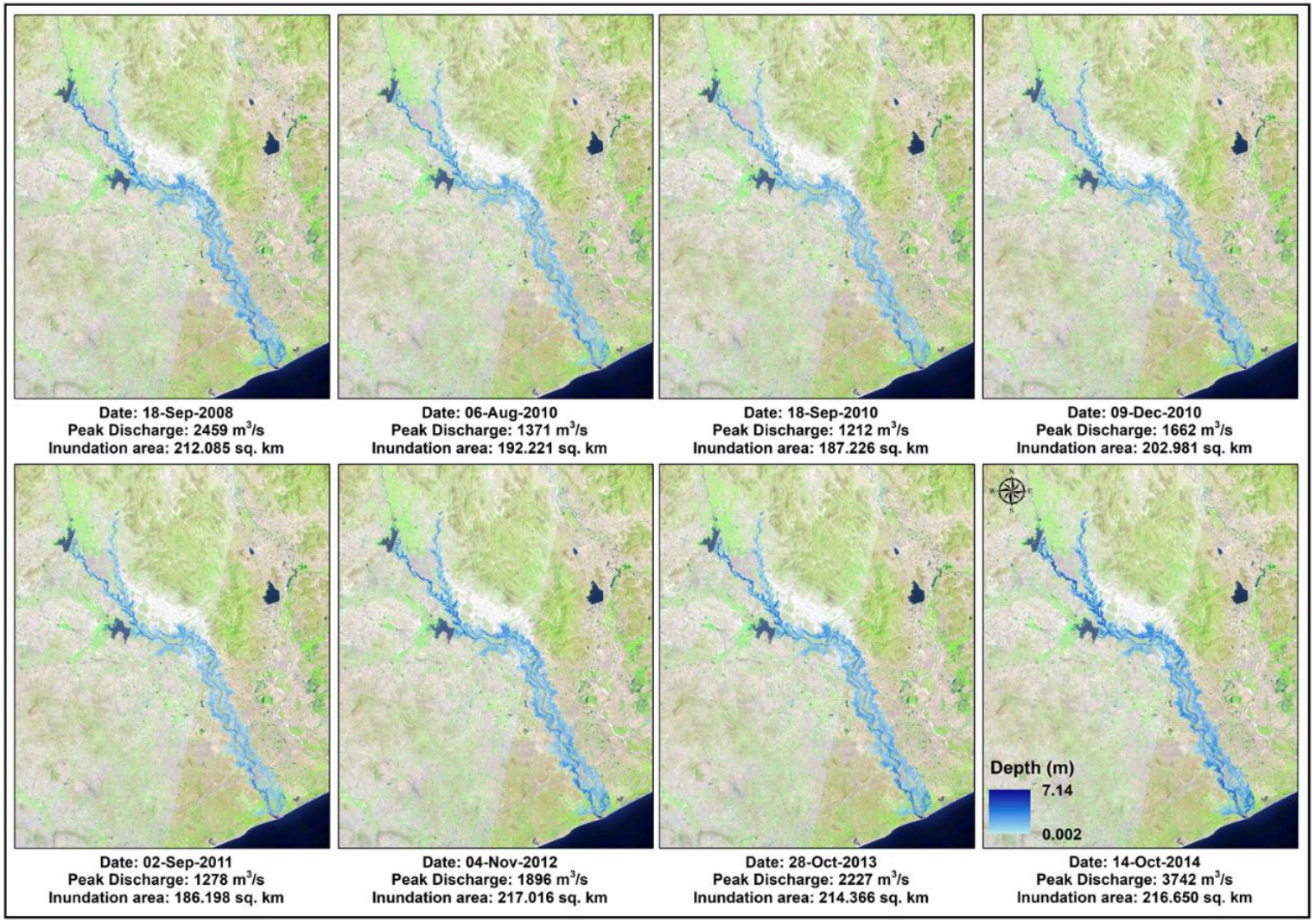

Figure 6.16 Flood inundation maps generated by HEC-RAS model using SWAT simulated discharge as upstream boundary from 2008 - 2014 over Nagavali basin

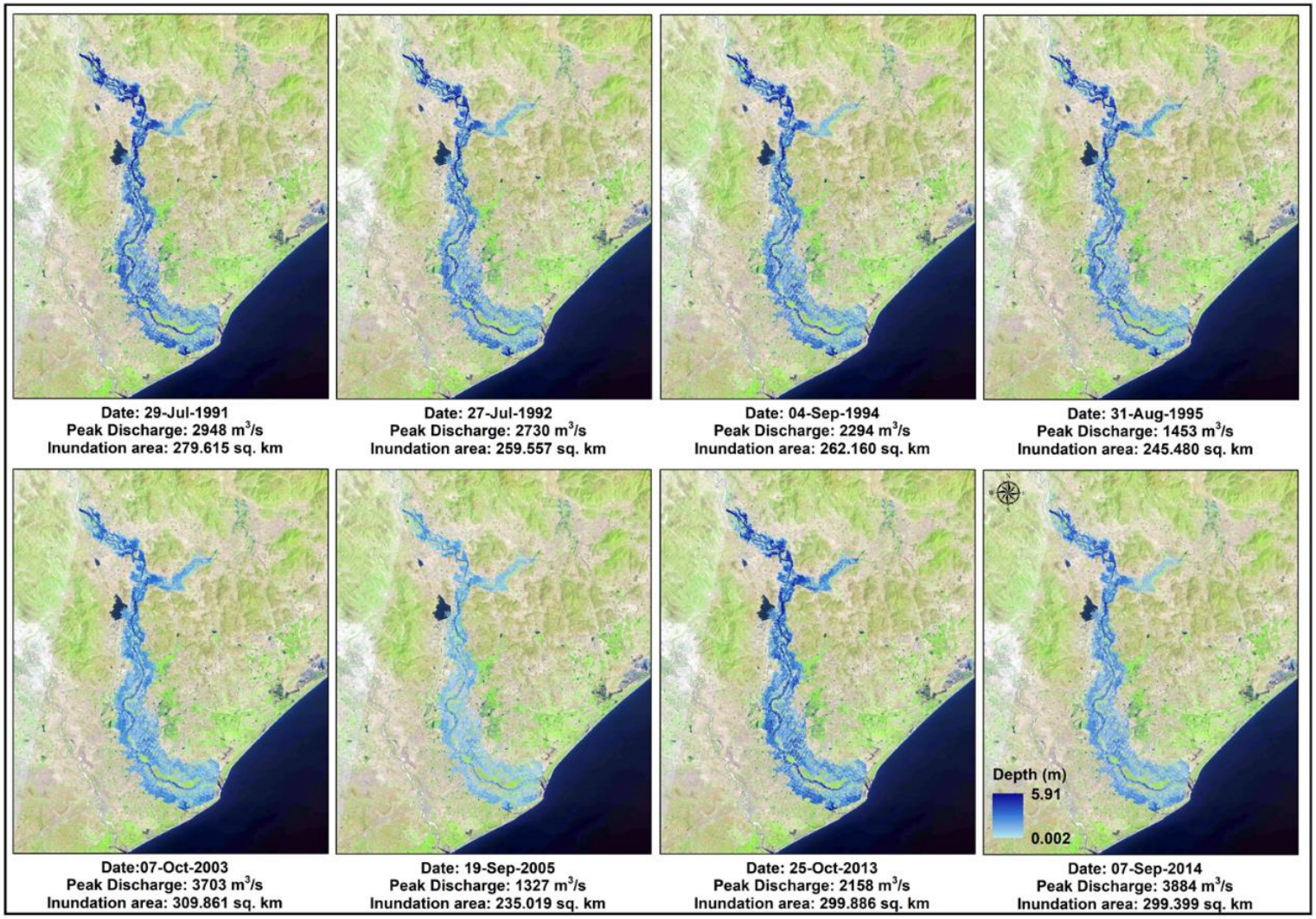

Figure 6.17 Flood inundation maps generated by HEC-RAS model using SWAT simulated discharge as upstream boundary from 1991 - 2014 over Vamsadhara basin

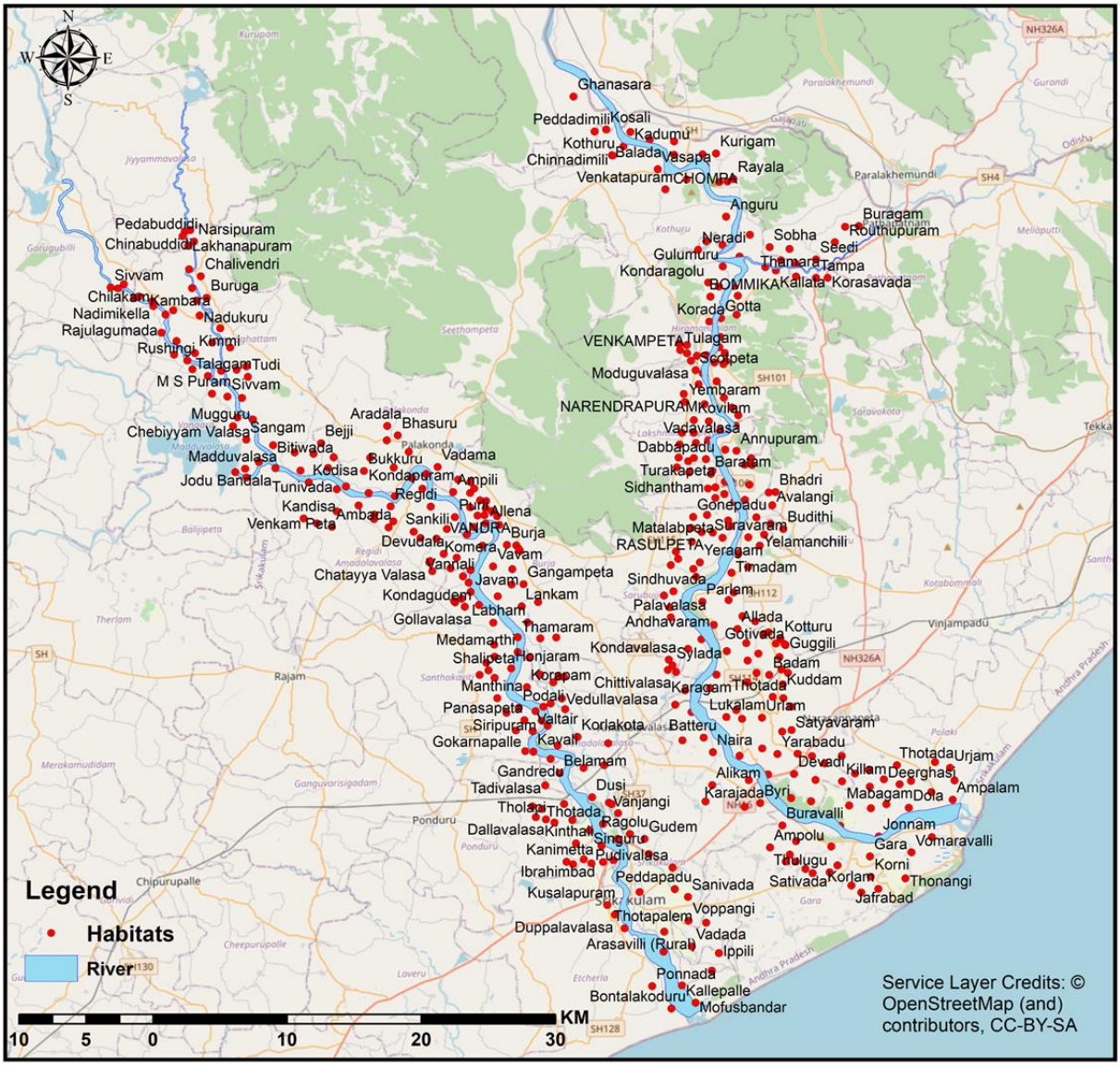

Figure 6.18 Habitats vulnerable to floods in Nagavali and Vamsadhara basins

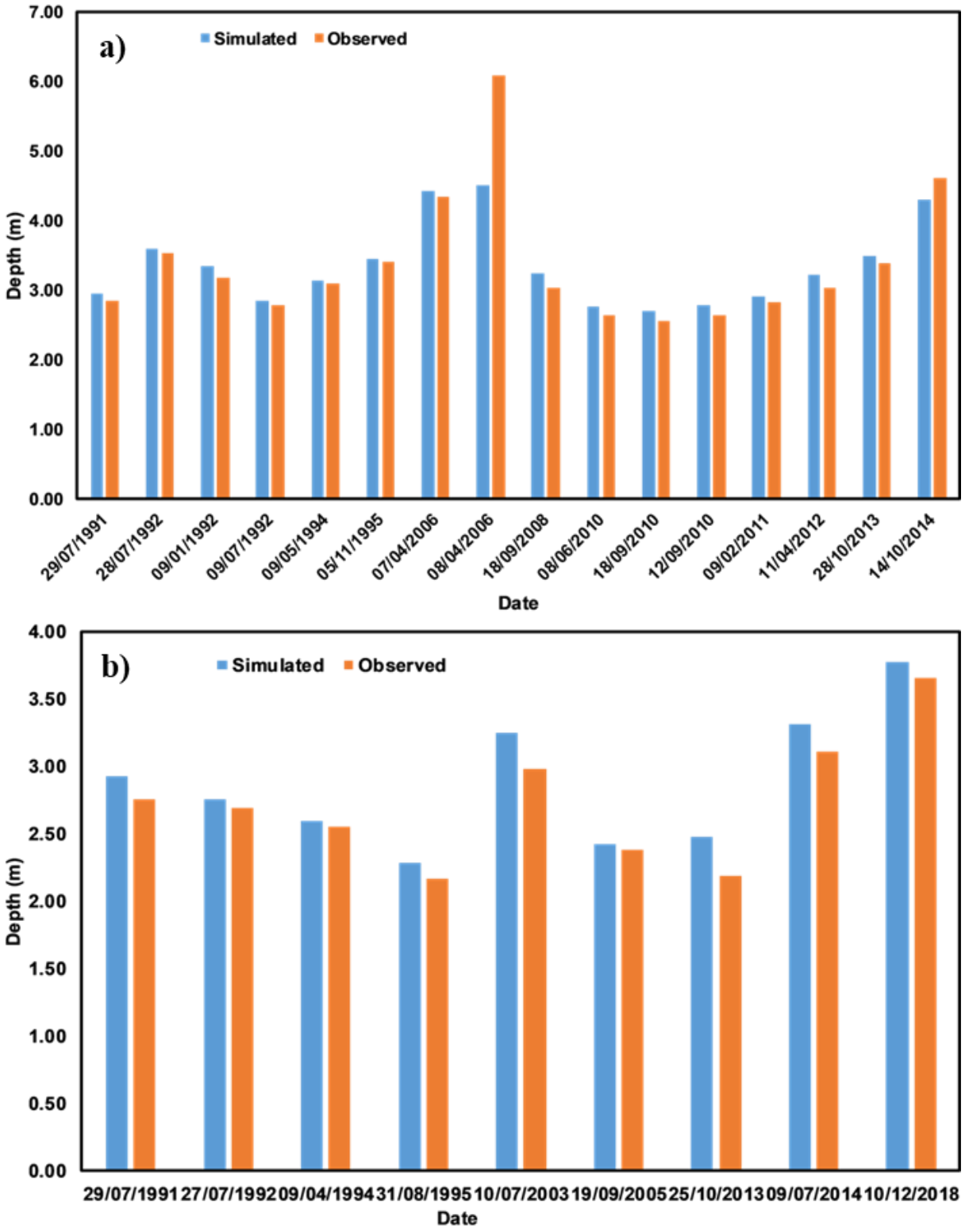

Figure 6.19 Observed versus simulated flood inundation depths a) Srikakulam gauge station in Nagavali basin and b) Kashinagar gauge station in Vamsadhara basin

Except for two floods in Nagavali basin in August 2006 and October 2014, the 2D HEC-RAS model overestimated inundation depths in both basins. Except for those two flood events, the difference in observed and simulated depths in Nagavali basin ranged from 0.04 to 0.20 m, and in Vamsadhara basin it ranged from 0.04 to 0.29 m. The flood inundation depth is underestimated by 1.58 m and 0.32 m in Nagavali basin for the flood events in August 2006 and October 2014.

6.3.5 Flood Inundation Modeling of Tropical Cyclone Titli

Tropical Cyclone Titli is a powerful cyclonic storm that hit Vamsadhara basin in October 2018. According to state government records, the basin received 426 mm and 352 mm of rainfall on 11th October at the Booravilli and Kanchili_ARG gauge stations, respectively and 153 mm at Sarubujji and Levidi gauge stations on 12th October 2018, resulting in an increase in water levels and floods in the basin on 13th October 2018. Flooding from cyclone Titli affected nearly 25,000 families in over 200 villages in Vamsadhara basin. A total of 1, 39,844 hectares of agricultural crops as well as 14,378 hectares of horticultural crops were damaged, with a combined loss of ₹ 3600 crores (TNIE 2018; GOI-UNDP 2018).

The SWAT model, which had been calibrated and validated, is used to estimate streamflow for Titli cyclone, which hit Vamsadhara basin from October 8th to October 12th, 2018. The basin experienced heavy rainfall on 11th and 12th October. According to IMD gridded data, the basin received 148 mm of rainfall on October 11th and 133 mm on October 12th. On October 11th, the GFS model forecasted rainfall of 186 mm, 131 mm, 107 mm, 70 mm, and 50 mm from day-1 to day-5. The WRF model predicted a rainfall of 215 mm on 11th October 2018 for TC Titli. The streamflow for Titli cyclone is simulated using observed rainfall, WRF predicted rainfall, and bias corrected GFS rainfall forecasts. Peak discharges simulated by the SWAT model are 4332 m^3/s for observed rainfall, 2924 m^3/s for WRF predicted rainfall, and 2281, 2661, 1536, 1090, and 700 m^3/s for GFS 1-day to 5-day forecasts, respectively. SWAT simulated streamflow revealed that GFS 1-day and 2-day streamflow's are in good agreement with the observed streamflow. The streamflow simulated by the SWAT model using 3-day to 5-day GFS forecasts are less than half of the observed streamflow. The underestimation of streamflow using 3-day to 5-day forecasts are mainly due to variations in rainfall intensity. For further analysis, GFS 1-day and 2-day forecasts are considered. The hydrograph for the observed and

simulated discharge based on IMD rainfall, WRF predicted rainfall, and GFS day-1 and day-2 forecasts are shown in Figure 6.20.

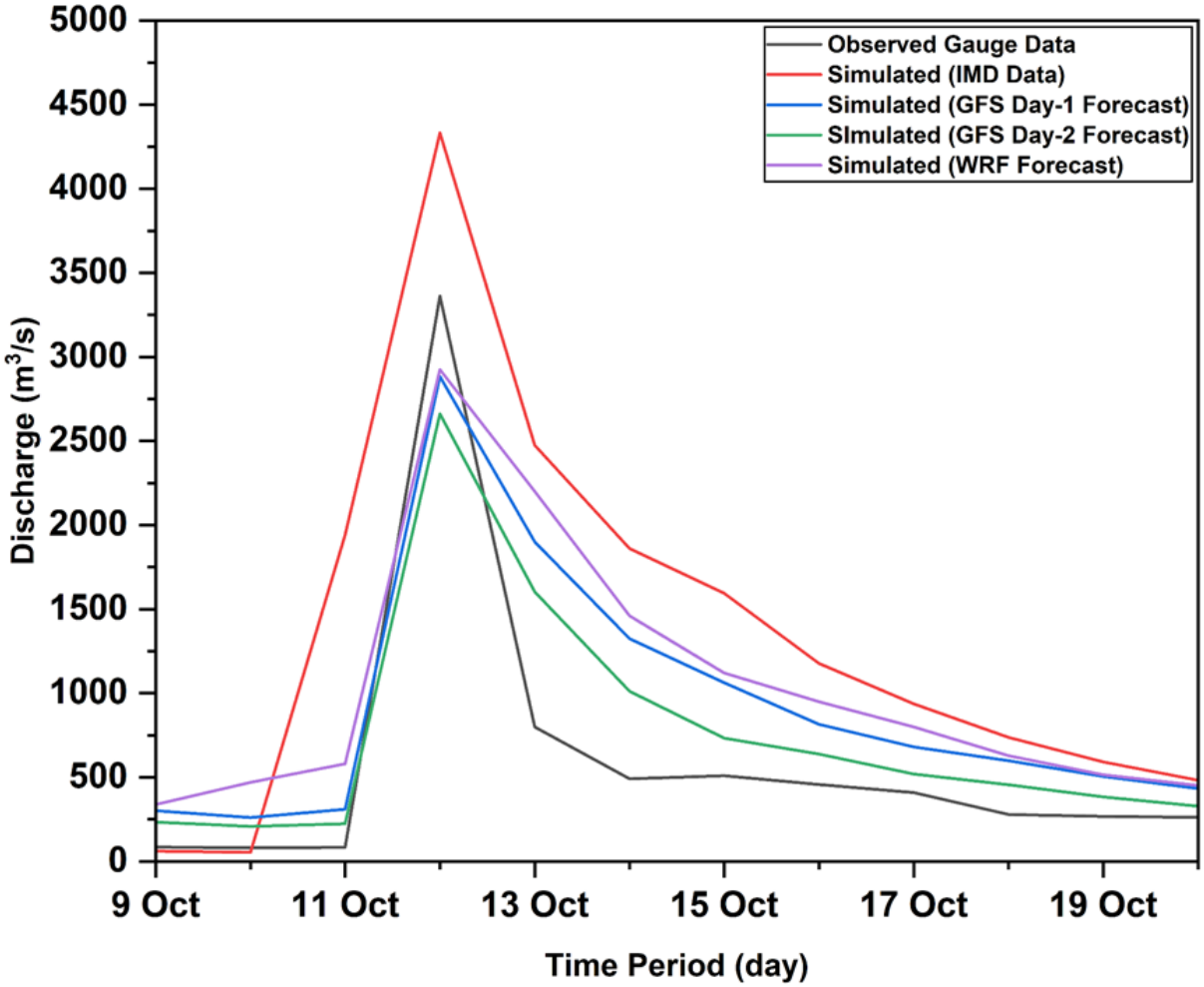

Figure 6.20 Hydrograph for observed and simulated discharge based on IMD rainfall, WRF predicted rainfall, and GFS day-1 and day-2 forecasts of Titli cyclone in Vamsadhara basin

The simulated discharges from SWAT model are used as an upstream boundary condition in the 2D HEC-RAS model to generate inundation maps during Titli Cyclone (Figure 6.21). The inundation area for Titli cyclone has varied from 290.674 to 311.601 sq.km for streamflow hydrographs from various sources (IMD, WRF, GFS, and observed gauge data). The flood inundation maps generated by 2D HEC-RAS model are validated with Bhuvan-NRSC flood inundation map and are evaluated based on overlapping area. Intersection tool is used to calculate the area that overlapped between the observed and simulated inundation maps (Tamiru and Dinka 2021). From the calculated overlapping areas, it is observed that 2D HEC-RAS model is able to predict at least 75% of the inundation area when compared to Bhuvan-NRSC data. From the simulated flood inundation maps, it is observed that more than 150

villages are affected, and an area of 177 sq.km of crops (agriculture and horticulture) are damaged in Vamsadhara basin. The areas of crops affected by the cyclone are in good agreement with observed statistics (Sphere-India 2018).

The inundation depth from 2D HEC-RAS model is further compared with the observed depth. When SWAT model simulated discharge using IMD rainfall is given as the upstream boundary condition, 2D HEC-RAS model overestimated the inundation depth by 0.12 m. For other simulations, using observed gauge data and SWAT simulated discharge with WRF predicted rainfall and GFS day-1 and d-2ay rainfall forecasts, the 2D HEC-RAS model underestimated inundation depth by 0.38, 0.41, 0.46, and 0.53 m, respectively. The overestimation and underestimation of flood inundation depths for the tropical cyclone Titli may be attributed to variations in peak discharges. The results showed that the developed integrated hydrologic and hydraulic model is able to predict runoff, flood inundation extent and inundation depth with a lead time of 48 hours.

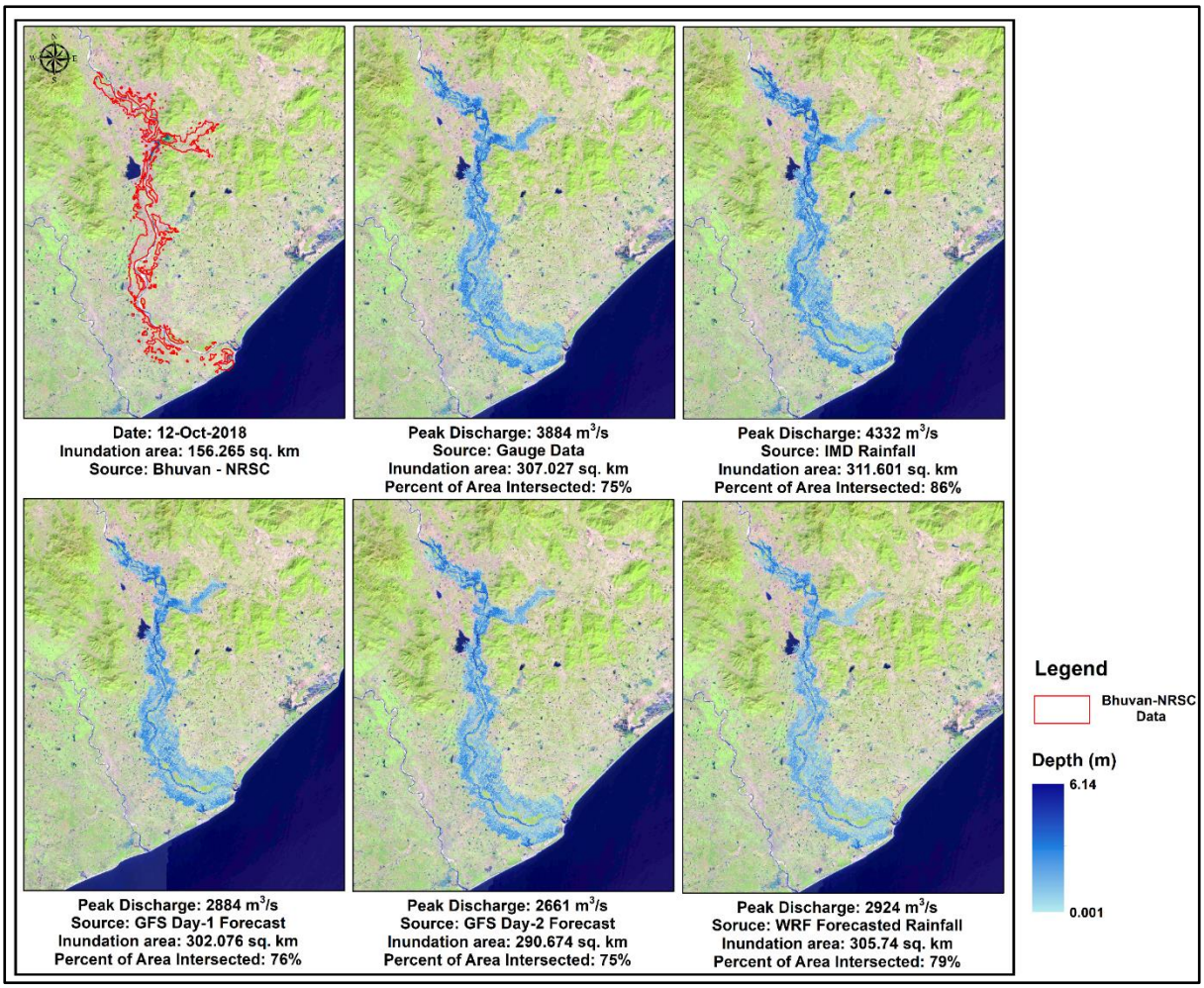

Figure 6.21 Flood inundation maps for the tropical cyclone Titli from various sources

6.4 Web-GIS based User Interface System for Flood Visualization and Dissemination

A Web-GIS based user interface system for flood visualization and dissemination is developed using HTML, CSS, and JavaScript. The pictorial representation of the interface is shown in Figure 6.22. The base maps for satellite view and terrain view are taken from Bing maps OpenStreetMap (OSM), respectively. Using GeoServer, a database is prepared to store the information about flood inundation extent, stream network, and boundary in the form of raster and vector layers for both Nagavali and Vamsadhara basins. All the layers from the GeoServer are imported into the user interface system. By default, the interface loads with the flood inundation maps for both basins along with satellite image in the background. The legend is provided in the interface, which gives information about flood inundation depth. Layer

switcher is added in the interface for users to enable or disable layers. Complete script for the development of Web-GIS based user interface system is given in Appendix-C.

6.5 Automation of Integrated Model

In order to provide information about the floods and flood inundation extent in real-time, the overall methodology presented in this research is automated by using both R and python programming languages. A script is written in R-program to download and pre-process the GFS forecasts. The pre-processing of GFS forecasts involves extracting rainfall and temperature data for both Nagavali and Vamsadhara basins and applying for bias correction to rainfall with intensity greater than 12 mm/day. After bias correction, rainfall and temperature data are converted into SWAT format. SWATplusR package in R program is used to run the calibrated and validated SWAT model for both basins in order to generate discharge hydrographs. The generated discharge hydrograph at various locations in Nagavali and Vamsadhara basins are then used as upstream boundary conditions in the respective basins in 2D HEC-RAS model using R script. HECRASController module in python program is used to run 2D HEC-RAS model to forecast floods and flood inundation extent. Flood inundation maps are further updated into GeoServer data and then exported into Web-GIS base user interface system for visualization and dissemination. Public and government agencies can access the data through web browser in real-time to issue early warnings and plan rescue operations. The script for the automation of the model is given in Appendix-D.

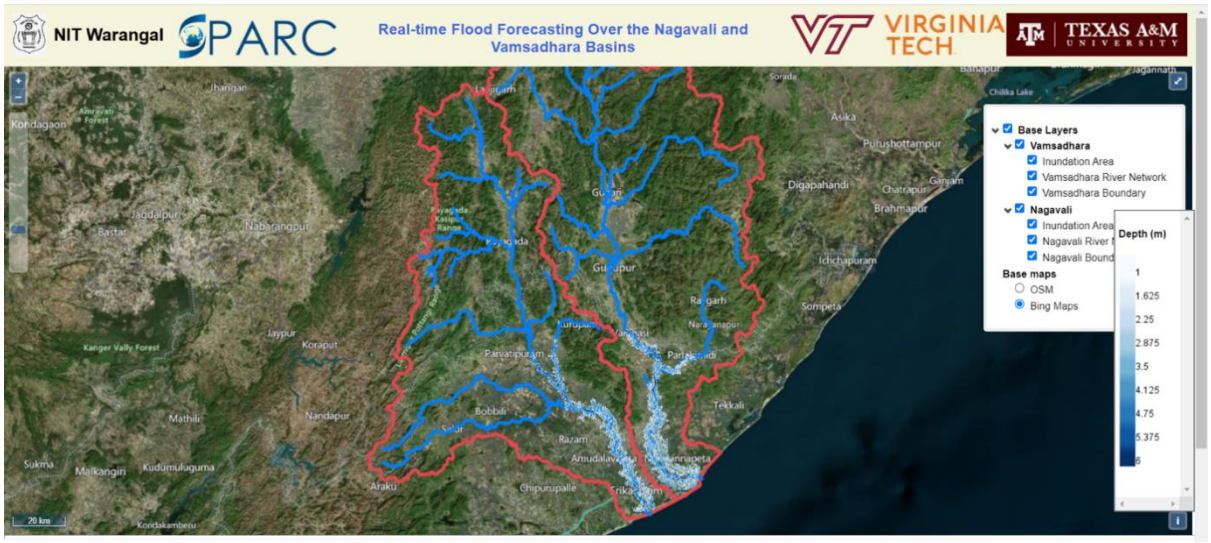

Figure 6.22 Web-GIS based platform for flood visualization and dissemination system

6.6 Closure

In this chapter, the skill of GFS model in forecasting rainfall over the study area is analyzed and a bias in GFS rainfall forecast is identified. An integrated hydrological and hydraulic model based on SWAT and 2D HEC-RAS is developed to forecast flood and flood inundation extent based on bias corrected GFS rainfall with a lead-time of 48 hours. A Web-GIS based user interface system is developed for visualization and dissemination of flood related information and the whole procedure is automated using R and python programming languages.

Chapter - 7 Summary and Conclusions

7.1 Summary

The purpose of the present research work is to develop an integrated hydrologic and hydraulic model that forecasts streamflow and generates flood inundation extent based on rainfall forecasts which will be published in Web-GIS based user interface system for the public use. To achieve this, the spatial and temporal variations of trend in rainfall and rainfall extremes over the Nagavali and Vamsadhara basins are examined using the long-term rainfall time series at three time periods (i.e., long-term (1901-2018), pre-1950, and post-1950) which provides extensive information about variations in rainfall patterns over the basins. From the trend analysis, it is observed that rainfall extremes are increasing in the lower and middle portions of the Nagavali and Vamsadhara basins. The increasing trends in rainfall extremes in the lower and middle portions of both basins may be attributed to TCs that are formed in BoB. Hence, WRF model is used to assess the impact of microphysical schemes prediction of previous tropical cyclones over the Nagavali and Vamsadhara basins. WRF model performance is assessed using direct positional error, mean absolute error, mean square error, and skill score calculated based on the observations provided by IMD to find a suitable microphysical scheme for the prediction of tropical cyclones.

Further, the skill of GFS model to forecast rainfall is examined using statistical metrics (CC, RMSE, ME, and BIAS), as well as contingency statistics (POD, FAR, CSI, and TSS) and it is found that the model performed well in forecasting rainfall over study basins. A simple bias correction is applied to GFS rainfall forecasts to improve rainfall accuracy. After that, an integrated hydrologic and hydraulic model based on SWAT and 2D HEC-RAS model is developed which is capable of providing flood forecasts using bias corrected GFS rainfall with a lead time of 48 hours. To visualize and disseminate flood related information in real-time, Web-GIS based user interface system has been developed. Finally, the overall methodology is automated using R and python programming languages.

7.2 Conclusions

The following are the important conclusions from the present research work:

- In the long-term trend analysis, an increasing trend in rainfall and rainfall extremes is observed in pre-monsoon and monsoon seasons.
- The increasing trends in rainfall and rainfall extremes are located in the lower and middle portions of both basins resulting in flood in this region, causing significant damage to human lives, agriculture, and infrastructure.
- WSM3 scheme can be used as a suitable microphysical scheme for the prediction of track and intensity of tropical cyclones over NIO.
- The rainfall forecasts from NCEP GFS model are in good agreement with observed data for day-1 to day-3 forecasts.
- Bias correction needs to be applied to GFS rainfall forecasts with an intensity greater than 12 mm/day before utilizing them for hydrometeorological applications.
- The integrated model based on SWAT and HEC-RAS is able to predict at least 75% of the flood inundation area.
- The integrated model is able to provide flood forecasts with a lead time of 48 h, which is crucial for government agencies in issuing early warnings to the public during flood events and evacuating people from vulnerable areas.
- Web-GIS based user interface system enables users to access information about flood inundation extent and depth in real-time to take necessary action during the floods.

7.3 Research Contributions

The following are the important research contributions of the present research work:

- Detailed basin level trends in rainfall and rainfall extremes are found out for the study basins.
- Suitable microphysical scheme for the prediction of tropical cyclones over the study area is found out.
- Bias in GFS rainfall forecasts over Nagavali and Vamsadhara basins are evaluated.
- An integrated model based on SWAT and HEC-RAS is developed to forecast streamflow and flood inundation extent with lead time.

- Web-GIS based user interface is developed for visualization and dissemination of flood inundation and depth maps
- A robust and simple approach is developed for automating the process from data download to flood forecasting using an integrated model based on SWAT and HEC-RAS, and to publish layers through a Web-GIS based user interface system.

7.4 Limitations

The limitations of the present research work are as follows:

- Very high resolution spatial and temporal rainfall data is not used in the present study.
- Due to requirement of high computational resources, WRF model is not used further to forecast rainfall.
- Flood forecasts are only available on daily timescale.
- The archival information about past flood events are not available to the users in the current version of Web-GIS based user interface system.

7.5 Scope for Further Research

The scope of the further research related to this work is as follows:

- ❖ Localized rainfall forecasts from the WRF model can be used to forecast floods.
- ❖ Dynamic changes in LULC and soil moisture information can be incorporated in the integrated model.
- ❖ The integrated model can be updated to sub-daily time scale for the simulation of floods.
- ❖ Web-GIS based user-interface system can be improved further to make it more user friendly and more rich in information.

References

Adarsh, S., and M. Janga Reddy, 2015: Trend analysis of rainfall in four meteorological subdivisions of southern India using nonparametric methods and discrete wavelet transforms. *Int. J. Climatol.*, **35**, 1107–1124, https://doi.org/10.1002/joc.4042.

Ali, H., P. Modi, and V. Mishra, 2019: Increased flood risk in Indian sub-continent under the warming climate. *Weather Clim. Extrem.*, **25**, 100212, https://doi.org/10.1016/j.wace.2019.100212.

Ashrit, R., and Coauthors, 2020: Prediction of the August 2018 heavy rainfall events over Kerala with high-resolution NWP models . *Meteorol. Appl.*, **27**, 1–14, https://doi.org/10.1002/met.1906.

Auynirundronkool, K., N. Chen, C. Peng, C. Yang, J. Gong, and C. Silapathong, 2012: Flood detection and mapping of the Thailand Central plain using RADARSAT and MODIS under a sensor web environment. *Int. J. Appl. Earth Obs. Geoinf.*, **14**, 245–255, https://doi.org/10.1016/j.jag.2011.09.017.

Bhanduri, A., 2019: Bihar floods: Dinesh Kumar Mishra on the flawed strategies that have turned state into watery grave. *Firstpost*.

Bhatt, C. M., G. S. Rao, P. G. Diwakar, and V. K. Dadhwal, 2017: Development of flood inundation extent libraries over a range of potential flood levels: a practical framework for quick flood response. *Geomatics, Nat. Hazards Risk*, **8**, 384–401, https://doi.org/10.1080/19475705.2016.1220025.

Bhowmik, S. K. R., D. Joardar, and H. R. Hatwar, 2007: Evaluation of precipitation prediction skill of IMD operational NWP system over Indian monsoon region. *Meteorol. Atmos. Phys.*, **95**, 205–221, https://doi.org/10.1007/s00703-006-0198-3.

Biancamaria, S., P. D. Bates, A. Boone, and N. M. Mognard, 2009: Large-scale coupled hydrologic and hydraulic modelling of the Ob river in Siberia. *J. Hydrol.*, **379**, 136–150, https://doi.org/10.1016/j.jhydrol.2009.09.054.

Bisht, D. S., C. Chatterjee, N. S. Raghuwanshi, and V. Sridhar, 2018a: Spatio-temporal trends of rainfall across Indian river basins. *Theor. Appl. Climatol.*, **132**, 419–436, https://doi.org/10.1007/s00704-017-2095-8.

——, ——, ——, and ——, 2018b: An analysis of precipitation climatology over Indian urban

agglomeration. *Theor. Appl. Climatol.*, **133**, 421–436, https://doi.org/10.1007/s00704-017-2200-z.

Bonnifait, L., G. Delrieu, M. Le Lay, B. Boudevillain, A. Masson, P. Belleudy, E. Gaume, and G. M. Saulnier, 2009: Distributed hydrologic and hydraulic modelling with radar rainfall input: Reconstruction of the 8-9 September 2002 catastrophic flood event in the Gard region, France. *Adv. Water Resour.*, **32**, 1077–1089, https://doi.org/10.1016/j.advwatres.2009.03.007.

Bronaugh, D., 2019: PCIC Implementation of Climdex Routines. https://cran.r-project.org/web/packages/climdex.pcic/climdex.pcic.pdf.

Broorks, H., B. Brown, B. Ebert, C. Ferro, I. Jolliffe, T.-Y. Koh, P. Roebber, and D. Stephenson, 2017: Forecast Verification methods Across Time and Space Scales. https://www.cawcr.gov.au/projects/verification/.

Brunner., G. W., 2016: *HEC-RAS River Analysis System User's Manual Version 5.0.7*.

Castro, D. M., S. Kumar, J. L. F. Rojas, A. M. Alvarez, J. M. V. Prado, E. V. Puma, C. D. C. Velarde, and Y. S. Vidal, 2019: The Impact of Microphysics Parameterization in the Simulation of Two Convective Rainfall Events over the Central Andes of Peru Using WRF-ARW. *Atmosphere (Basel).*, **10**, 1–29, https://doi.org/10.3390/atmos10080442.

Chandrasekar, R., and C. Balaji, 2012: Sensitivity of tropical cyclone Jal simulations to physics parameterizations. *J. Earth Syst. Sci.*, **121**, 923–946, https://doi.org/10.1007/s12040-012-0212-8.

Chang, L. C., F. J. Chang, S. N. Yang, I. F. Kao, Y. Y. Ku, C. L. Kuo, and I. M. Z. bin M. Amin, 2018: Building an intelligent hydroinformatics integration platform for regional flood inundation warning systems. *Water (Switzerland)*, **11**, https://doi.org/10.3390/w11010009.

Choudhury, D., and S. Das, 2017: The sensitivity to the microphysical schemes on the skill of forecasting the track and intensity of tropical cyclones using WRF-ARW model. *J. Earth Syst. Sci.*, **126**, 1–10, https://doi.org/10.1007/s12040-017-0830-2.

Chowdhuri, I., S. C. Pal, and R. Chakrabortty, 2020: Flood susceptibility mapping by ensemble evidential belief function and binomial logistic regression model on river basin of eastern India. *Adv. Sp. Res.*, **65**, 1466–1489, https://doi.org/10.1016/j.asr.2019.12.003.

CWC-FRMD, 2020: *Flood Forecasting and Warning Network Performance Appraisal Report 2018*.

CWC, 2020: Standard Operating Procedure For Flood Forecasting. *Cent. Water Comm.*,. http://www.cwc.gov.in/standard-operating-procedure-flood-forecasting-april-2020 (Accessed February 10, 2022).

Damrath, U., G. Doms, D. Frühwald, E. Heise, B. Richter, and J. Steppeler, 2000: Operational quantitative precipitation forecasting at the German Weather Service. *J. Hydrol.*, **239**, 260–285, https://doi.org/10.1016/S0022-1694(00)00353-X.

Dash, S. K., M. A. Kulkarni, U. C. Mohanty, and K. Prasad, 2009: Changes in the characteristics of rain events in India. *J. Geophys. Res. Atmos.*, **114**, https://doi.org/10.1029/2008JD010572.

Demir, I., E. Yildirim, Y. Sermet, and M. A. Sit, 2018: FLOODSS: Iowa flood information system as a generalized flood cyberinfrastructure. *Int. J. River Basin Manag.*, **16**, 393–400, https://doi.org/10.1080/15715124.2017.1411927.

Deng, P., M. Zhang, H. Guo, C. Xu, J. Bing, and J. Jia, 2018: Error analysis and correction of the daily GSMaP products over Hanjiang River Basin of China. *Atmos. Res.*, **214**, 121–134, https://doi.org/10.1016/j.atmosres.2018.07.022.

Deshpande, M. S., S. Pattnaik, and P. S. Salvekar, 2012: Impact of cloud parameterization on the numerical simulation of a super cyclone. *Ann. Geophys.*, **30**, 775–795, https://doi.org/10.5194/angeo-30-775-2012.

Deshpande, N. R., D. R. Kothawale, and A. Kulkarni, 2016: Changes in climate extremes over major river basins of India. *Int. J. Climatol.*, **36**, 4548–4559, https://doi.org/10.1002/joc.4651.

Di, Z., and Coauthors, 2015: Assessing WRF model parameter sensitivity: A case study with 5 day summer precipitation forecasting in the Greater Beijing Area. *Geophys. Res. Lett.*, **42**, 579–587, https://doi.org/10.1002/2014GL061623.

Dube, A., R. Ashrit, A. Ashish, K. Sharma, G. R. Iyengar, E. N. Rajagopal, and S. Basu, 2014: Forecasting the heavy rainfall during Himalayan flooding-June 2013. *Weather Clim. Extrem.*, **4**, 22–34, https://doi.org/10.1016/j.wace.2014.03.004.

Dubey, S. K., and D. Sharma, 2018: Spatio-Temporal Trends and Projections of Climate

Indices in the Banas River Basin, India. *Environ. Process.*, **5**, 743–768, https://doi.org/10.1007/s40710-018-0332-5.

Dudhia, J., 1989: Numerical Study of Convection Observed during the Winter Monsoon Experiment Using a Mesoscale Two-Dimensional Model. *J. Atmos. Sci.*, **46**, 3077–3107, https://doi.org/10.1175/1520-0469(1989)046<3077:NSOCOD>2.0.CO;2.

Durai, V. R., and S. K. R. Bhowmik, 2014: Prediction of Indian summer monsoon in short to medium range time scale with high resolution global forecast system (GFS) T574 and T382. *Clim. Dyn.*, **42**, 1527–1551, https://doi.org/10.1007/s00382-013-1895-5.

——, and R. Bhradwaj, 2014: Evaluation of statistical bias correction methods for numerical weather prediction model forecasts of maximum and minimum temperatures. *Nat. Hazards*, **73**, 1229–1254, https://doi.org/10.1007/s11069-014-1136-1.

Durai, V. R., and A. K. Das, 2019: NWP products for monsoon weather monitoring and prediction at various temporal / spatial scales. *Monsoon: A Report 2019*, Vol. 01 of, 134–162.

Durai, V. R., S. K. Roy Bhowmik, and B. Mukhopadhyay, 2010: Performance evaluation of precipitation prediction skill of NCEP global Forecasting System (GFS) over Indian region during summer monsoon 2008. *Mausam*, **61**, 139–154.

——, R. Bhardwaj, S. K. Roy Bhowmik, and Y. V. Rama Rao, 2015: Verification of quantitative precipitation forecasts from operational ensemble prediction systems over India. *Mausam*, **66**, 479–496.

Duvvuri, S., 2019: GIS Based Management System for Flood Forecast Applications. *Proceedings of International Conference on Remote Sensing for Disaster Management*, 1–12.

Ebert, E. E., 2001: Ability of a poor man's ensemble to predict the probability and distribution of precipitation. *Mon. Weather Rev.*, **129**, 2461–2480, https://doi.org/10.1175/1520-0493(2001)129<2461:AOAPMS>2.0.CO;2.

Eckstein, D., V. Künzel, and L. Schäfer, 2021: Global climate risk index 2021. *Ger. e.V.*, 28.

ESCAP, 2017: Flood Forecasting and Early Warning in Transboundary River Basins: A Toolkit. *United Nations Econ. Soc. Comm. Asia Pacific*, 83.

Fan, Y., and H. van den Dool, 2011: Bias Correction and Forecast Skill of NCEP GFS Ensemble Week-1 and Week-2 Precipitation, 2-m Surface Air Temperature, and Soil Moisture Forecasts. *Weather Forecast.*, **26**, 355–370, https://doi.org/10.1175/WAF-D-10-05028.1.

FMISC, 2007: *Flood Report 2007: Flood Managment Information System Cell*. 1–59 pp.

Ganai, M., S. Tirkey, R. P. M. Krishna, and P. Mukhopadhyay, 2021: The impact of modified rate of precipitation conversion parameter in the convective parameterization scheme of operational weather forecast model (GFS T1534) over Indian summer monsoon region. *Atmos. Res.*, **248**, 105185, https://doi.org/10.1016/j.atmosres.2020.105185.

Ghosh, S., D. Das, S. C. Kao, and A. R. Ganguly, 2012: Lack of uniform trends but increasing spatial variability in observed Indian rainfall extremes. *Nat. Clim. Chang.*, **2**, 86–91, https://doi.org/10.1038/nclimate1327.

Gilleland, E., 2020: Bootstrap methods for statistical inference. Part ii: Extreme-value analysis. *J. Atmos. Ocean. Technol.*, **37**, 2135–2144, https://doi.org/10.1175/JTECH-D-20-0070.1.

——, and R. W. Katz, 2016: ExtRemes 2.0: An extreme value analysis package in R. *J. Stat. Softw.*, **72**, https://doi.org/10.18637/jss.v072.i08.

Godara, N., and O. Bruland, 2019: Choosing an Appropriate Hydrologic Model. *Roorkee Water Conclave*, 1–18.

GOI-UNDP, 2018: *Note on Severe Cyclone Storm Titli's Impact on the State of Andhra Pradesh & Strengthening Local Governance System for Mainstreaming DRR and CCA [GOI-UNDP Rehabilitation Initiatives]*.

Goswami, B. N., V. Venugopal, D. Sengupta, M. S. Madhusoodanan, and P. K. Xavier, 2006: Increasing Trend of Extreme Rain Events Over India in a Warming Environment. *Science (80-.).*, **314**, 1442–1445, https://doi.org/10.1126/science.1132027.

Grimaldi, S., A. Petroselli, E. Arcangeletti, and F. Nardi, 2013: Flood mapping in ungauged basins using fully continuous hydrologic-hydraulic modeling. *J. Hydrol.*, **487**, 39–47, https://doi.org/10.1016/j.jhydrol.2013.02.023.

Guhathakurta, P., and M. Rajeevan, 2008: Trends in the rainfall pattern over India. *Int. J. Climatol.*, **28**, 1453–1469, https://doi.org/10.1002/joc.1640.

——, O. P. Sreejith, and P. A. Menon, 2011: Impact of climate change on extreme rainfall events and flood risk in India. *J. Earth Syst. Sci.*, **120**, 359–373, https://doi.org/10.1007/s12040-011-0082-5.

——, M. Rajeevan, D. R. Sikka, and A. Tyagi, 2015: Observed changes in southwest monsoon rainfall over India during 1901-2011. *Int. J. Climatol.*, **35**, 1881–1898, https://doi.org/10.1002/joc.4095.

——, P. Menon, P. M. Inkane, U. Krishnan, and S. T. Sable, 2017: Trends and variability of meteorological drought over the districts of India using standardized precipitation index. *J. Earth Syst. Sci.*, **126**, 1–18, https://doi.org/10.1007/s12040-017-0896-x.

Guo, R., H. Yu, Z. Yu, J. Tang, and L. Bai, 2021: Application of the frequency-matching method in the probability forecast of landfalling typhoon rainfall. *Front. Earth Sci.*, https://doi.org/10.1007/s11707-021-0880-2.

Gupta, K., 2007: Urban flood resilience planning and management and lessons for the future: A case study of Mumbai, India. *Urban Water J.*, **4**, 183–194, https://doi.org/10.1080/15730620701464141.

Hamed, K. H., 2008: Trend detection in hydrologic data: The Mann-Kendall trend test under the scaling hypothesis. *J. Hydrol.*, **349**, 350–363, https://doi.org/10.1016/j.jhydrol.2007.11.009.

——, and R. A. Rao, 1998: A modified Mann-Kendall trend test for autocorrelated data. *J. Hydrol.*, **204**, 182–196, https://doi.org/10.1016/S0022-1694(97)00125-X.

Han, S., and P. Coulibaly, 2017: Bayesian flood forecasting methods: A review. *J. Hydrol.*, **551**, 340–351, https://doi.org/10.1016/j.jhydrol.2017.06.004.

Harsha, 2020: Playing catch up in flood forecasting technology - The Hindu. *The Hindu*,. https://www.thehindu.com/opinion/lead/playing-catch-up-in-flood-forecasting-technology/article32797281.ece (Accessed February 11, 2022).

Hong, S.-Y., and J.-O. J. Lim, 2006: The WRF single–moment 6–class microphysics scheme (WSM6). *J. Korean Meteorol. Soc.*, **42**, 129–151.

——, J. Dudhia, and S.-H. Chen, 2004: A Revised Approach to Ice Microphysical Processes for the Bulk Parameterization of Clouds and Precipitation. *Mon. Weather Rev.*, **132**, 103–120, https://doi.org/10.1175/1520-0493(2004)132<0103:ARATIM>2.0.CO;2.

——, Y. Noh, and J. Dudhia, 2006: A New Vertical Diffusion Package with an Explicit Treatment of Entrainment Processes. *Mon. Weather Rev.*, **134**, 2318–2341, https://doi.org/10.1175/MWR3199.1.

Horita, F. E. A., J. P. de Albuquerque, L. C. Degrossi, E. M. Mendiondo, and J. Ueyama, 2015: Development of a spatial decision support system for flood risk management in Brazil that combines volunteered geographic information with wireless sensor networks. *Comput. Geosci.*, **80**, 84–94, https://doi.org/10.1016/j.cageo.2015.04.001.

IFRC, 2020: *IFRC Annual Report 2020*. http://media.corporate-ir.net/media_files/irol/10/100529/nike2011ar/nike2011ar/docs/Nike_2011_10-K.pdf.

Iqbal, T. H. P. K. M., and K. Yarrakula, 2020: Probabilistic flood inundation mapping for sparsely gauged tropical river. *Arab. J. Geosci.*, **13**, https://doi.org/10.1007/s12517-020-05980-w.

Jain, S. K., P. C. Nayak, Y. Singh, and S. K. Chandniha, 2017: Trends in rainfall and peak flows for some river basins in India. *Curr. Sci.*, **112**, 1712–1726, https://doi.org/10.18520/cs/v112/i08/1712-1726.

Jain, S. K., and Coauthors, 2018: A Brief review of flood forecasting techniques and their applications. *Int. J. River Basin Manag.*, **16**, 329–344, https://doi.org/10.1080/15715124.2017.1411920.

Jandaghian, Z., A. G. Touchaei, and H. Akbari, 2018: Sensitivity analysis of physical parameterizations in WRF for urban climate simulations and heat island mitigation in Montreal. *Urban Clim.*, **24**, 577–599, https://doi.org/10.1016/j.uclim.2017.10.004.

Joshi, H., 2020: Floods across the country highlight need for a robust flood management structure. *Mongabay*,. https://india.mongabay.com/2020/08/floods-across-the-country-highlight-need-for-a-robust-flood-management-structure/ (Accessed December 10, 2021).

Kain, J. S., 2004: The Kain–Fritsch Convective Parameterization: An Update. *J. Appl. Meteorol.*, **43**, 170–181, https://doi.org/10.1175/1520-0450(2004)043<0170:TKCPAU>2.0.CO;2.

Kanase, R. D., and P. S. Salvekar, 2015: Impact of physical parameterization schemes on track and intensity of severe cyclonic storms in Bay of Bengal. *Meteorol. Atmos. Phys.*, **127**,

537–559, https://doi.org/10.1007/s00703-015-0381-5.

——, P. Mukhopadhyay, and P. S. Salvekar, 2014: Understanding the Role of Cloud and Convective Processes in Simulating the Weaker Tropical Cyclones over Indian Seas. *Pure Appl. Geophys.*, **172**, 1751–1779, https://doi.org/10.1007/s00024-014-0996-3.

Knight, P. J., T. Prime, J. M. Brown, K. Morrissey, and A. J. Plater, 2015: Application of flood risk modelling in a web-based geospatial decision support tool for coastal adaptation to climate change. *Nat. Hazards Earth Syst. Sci.*, **15**, 1457–1471, https://doi.org/10.5194/nhess-15-1457-2015.

Krishnamurthy, C. K. B., U. Lall, and H. H. Kwon, 2009: Changing frequency and intensity of rainfall extremes over India from 1951 to 2003. *J. Clim.*, **22**, 4737–4746, https://doi.org/10.1175/2009JCLI2896.1.

Krishnan, R., and Coauthors, 2020: Introduction to Climate Change Over the Indian Region. *Assessment of Climate Change over the Indian Region*, R. Krishnan, J. Sanjay, C. Gnanaseelan, M. Mujumdar, A. Kulkarni, and S. Chakraborty, Eds., Springer Singapore, 1–20.

Kumar, S., V. Merwade, J. Kam, and K. Thurner, 2009: Streamflow trends in Indiana: Effects of long term persistence, precipitation and subsurface drains. *J. Hydrol.*, **374**, 171–183, https://doi.org/10.1016/j.jhydrol.2009.06.012.

Kumar, S., S. K. Jain, and S. Gurrapu, 2020: Challenges and Recent Developments in Flood Forecasting in India. *Roorkee Water Conclave*.

Lagmay, A. M. F. A., B. A. Racoma, K. A. Aracan, J. Alconis-Ayco, and I. L. Saddi, 2017: Disseminating near-real-time hazards information and flood maps in the Philippines through Web-GIS. *J. Environ. Sci.*, **59**, 13–23, https://doi.org/10.1016/j.jes.2017.03.014.

Lekula, M., M. W. Lubczynski, E. M. Shemang, and W. Verhoef, 2018: Validation of satellite-based rainfall in Kalahari. *Phys. Chem. Earth*, **105**, 84–97, https://doi.org/10.1016/j.pce.2018.02.010.

Li, J., C. Ding, F. Li, and Y. Chen, 2020: Effects of single- and double-moment microphysics schemes on the intensity of super typhoon Sarika (2016). *Atmos. Res.*, **238**, 104894, https://doi.org/10.1016/j.atmosres.2020.104894.

Lin, Y.-L., R. D. Farley, and H. D. Orville, 1983: Bulk Parameterization of the Snow Field in

a Cloud Model. *J. Clim. Appl. Meteorol.*, **22**, 1065–1092, https://doi.org/10.1175/1520-0450(1983)022<1065:BPOTSF>2.0.CO;2.

Loi, N. K., and Coauthors, 2019: Automated procedure of real-time flood forecasting in vu gia – thu bon river basin, vietnam by integrating swat and hec-ras models. *J. Water Clim. Chang.*, **10**, 535–545, https://doi.org/10.2166/wcc.2018.015.

Mai, D. T., and F. De Smedt, 2017: A combined hydrological and hydraulic model for flood prediction in Vietnam applied to the Huong river basin as a test case study. *Water (Switzerland)*, **9**, https://doi.org/10.3390/w9110879.

Mandal, V., U. K. De, and B. K. Basu, 2007: Precipitation forecast verification of the Indian Summer Monsoon with Intercomparison of Three Diverse Regions. *Weather Forecast.*, **22**, 428–443, https://doi.org/10.1175/WAF1010.1.

Maw, K. W., and J. Min, 2017: Impacts of Microphysics Schemes and Topography on the Prediction of the Heavy Rainfall in Western Myanmar Associated with Tropical Cyclone ROANU (2016). *Adv. Meteorol.*, **2017**, 1–22, https://doi.org/10.1155/2017/3252503.

Mccorkle, T. A., J. D. Horel, A. A. Jacques, and T. Alcott, 2018: Evaluating the experimental High-Resolution Rapid Refresh-Alaska modeling system using US array pressure observations. *Weather Forecast.*, **33**, 933–953, https://doi.org/10.1175/WAF-D-17-0155.1.

Mishra, S., C. Sharad, P. Rohit, and A. K. Dubey, 2020: WebGIS for water level monitoring and flood forecasting using Open Source Technology. *J. Geomatics*, **14**, 49–54.

Mishra, V., S. Aaadhar, H. Shah, R. Kumar, D. R. Pattanaik, and A. D. Tiwari, 2018: The Kerala flood of 2018: combined impact of extreme rainfall and reservoir storage. *Hydrol. Earth Syst. Sci. Discuss.*, 1–13, https://doi.org/10.5194/hess-2018-480.

Mlawer, E. J., S. J. Taubman, P. D. Brown, M. J. Iacono, and S. A. Clough, 1997: Radiative transfer for inhomogeneous atmospheres: RRTM, a validated correlated-k model for the longwave. *J. Geophys. Res. Atmos.*, **102**, 16663–16682, https://doi.org/10.1029/97JD00237.

Mohanty, A., 2020: *Preparing India for Extreme Climate Events: Mapping Hotspots and Response Mechanisms*. https://www.hindustantimes.com/ht-insight/climate-change/preparing-india-for-extreme-climate-events-101625127345593.html.

Mohanty, M. P., and S. Karmakar, 2021: WebFRIS: An efficient web-based decision support tool to disseminate end-to-end risk information for flood management. *J. Environ. Manage.*, **288**, 112456, https://doi.org/10.1016/j.jenvman.2021.112456.

——, S. Mudgil, and S. Karmakar, 2020: Flood management in India: A focussed review on the current status and future challenges. *Int. J. Disaster Risk Reduct.*, **49**, 101660, https://doi.org/10.1016/j.ijdrr.2020.101660.

Mohanty, U. C., K. K. Osuri, S. Pattanayak, and P. Sinha, 2012: An observational perspective on tropical cyclone activity over Indian seas in a warming environment. *Nat. Hazards*, **63**, 1319–1335, https://doi.org/10.1007/s11069-011-9810-z.

MOI, 2022: India Natural Hazards Map - Maps of India. http://www.maps-of-india.com/india-climatic-map/india-natural-hazards-map/attachment/india-natural-hazards-map/ (Accessed April 21, 2022).

Moriasi, D. N., J. G. Arnold, M. W. Van Liew, R. L. Bingner, R. D. Harmel, and T. L. Veith, 2007: Model evaluation guidelines for systematic quantification of accuracy in watershed simulations. *Trans. ASABE*, **50**, 885–900.

Morrison, H., G. Thompson, and V. Tatarskii, 2009: Impact of Cloud Microphysics on the Development of Trailing Stratiform Precipitation in a Simulated Squall Line: Comparison of One- and Two-Moment Schemes. *Mon. Weather Rev.*, **137**, 991–1007, https://doi.org/10.1175/2008MWR2556.1.

Moya-Álvarez, A. S., D. Martínez-Castro, S. Kumar, R. Estevan, and Y. Silva, 2019: Response of the WRF model to different resolutions in the rainfall forecast over the complex Peruvian orography. *Theor. Appl. Climatol.*, **137**, 2993–3007, https://doi.org/10.1007/s00704-019-02782-3.

Mukhopadhyay, P., S. Taraphdar, and B. N. Goswami, 2011: Influence of moist processes on track and intensity forecast of cyclones over the north Indian Ocean. *J. Geophys. Res. Atmos.*, **116**, 1–21, https://doi.org/10.1029/2010JD014700.

——, and Coauthors, 2019: Performance of a very high-resolution global forecast system model (GFS T1534) at 12.5 km over the Indian region during the 2016–2017 monsoon seasons. *J. Earth Syst. Sci.*, **128**, 1–18, https://doi.org/10.1007/s12040-019-1186-6.

Nam, D. H., D. T. Mai, K. Udo, and A. Mano, 2014: Short-term flood inundation prediction

using hydrologic-hydraulic models forced with downscaled rainfall from global NWP. *Hydrol. Process.*, **28**, 5844–5859, https://doi.org/10.1002/hyp.10084.

Nandargi, S., A. Gaur, and S. S. Mulye, 2016: Hydrological analysis of extreme rainfall events and severe rainstorms over Uttarakhand, India. *Hydrol. Sci. J.*, **61**, 2145–2163, https://doi.org/10.1080/02626667.2015.1085990.

Nanditha, J. S., and V. Mishra, 2021: On the need of ensemble flood forecast in India. *Water Secur.*, **12**, 100086, https://doi.org/10.1016/j.wasec.2021.100086.

Narasimhan, B., S. M. Bhallamudi, A. Mondal, S. Ghosh, and P. Mujumdar, 2016: *Chennai Floods 2015: A Rapid Assessment*.

Natarajan, S., and N. Radhakrishnan, 2020: An Integrated Hydrologic and Hydraulic Flood Modeling Study for a Medium-Sized Ungauged Urban Catchment Area: A Case Study of Tiruchirappalli City Using HEC-HMS and HEC-RAS. *J. Inst. Eng. Ser. A*, **101**, 381–398, https://doi.org/10.1007/s40030-019-00427-2.

NDMA, National Disaster Managmemnt Authority of Foods. *2022*,. https://ndma.gov.in/Natural-Hazards/Floods (Accessed April 22, 2022).

Nguyen, P., A. Thorstensen, S. Sorooshian, K. Hsu, and A. Aghakouchak, 2015: Flood forecasting and inundation mapping using HiResFlood-UCI and near-real-time satellite precipitation data: The 2008 Iowa flood. *J. Hydrometeorol.*, **16**, 1171–1183, https://doi.org/10.1175/JHM-D-14-0212.1.

——, and Coauthors, 2016: A high resolution coupled hydrologic–hydraulic model (HiResFlood-UCI) for flash flood modeling. *J. Hydrol.*, **541**, 401–420, https://doi.org/10.1016/j.jhydrol.2015.10.047.

Ning, S., F. Song, P. Udmale, J. Jin, B. R. Thapa, and H. Ishidaira, 2017: Error Analysis and Evaluation of the Latest GSMap and IMERG Precipitation Products over Eastern China. *Adv. Meteorol.*, **2017**, https://doi.org/10.1155/2017/1803492.

Olaya, V., 2018: *Introduction to GIS*. 138 pp.

Osuri, K. K., U. C. Mohanty, A. Routray, M. A. Kulkarni, and M. Mohapatra, 2012: Customization of WRF-ARW model with physical parameterization schemes for the simulation of tropical cyclones over North Indian Ocean. *Nat. Hazards*, **63**, 1337–1359, https://doi.org/10.1007/s11069-011-9862-0.

Park, J., D. Cha, M. K. Lee, J. Moon, S. Hahm, K. Noh, J. C. L. Chan, and M. Bell, 2020: Impact of Cloud Microphysics Schemes on Tropical Cyclone Forecast Over the Western North Pacific. *J. Geophys. Res. Atmos.*, **125**, https://doi.org/10.1029/2019JD032288.

Patakamuri, S. K., and N. O'Brien, 2019: Modified Versions of Mann Kendall and Spearman's Rho Trend Tests. https://cran.r-project.org/web/packages/modifiedmk/modifiedmk.pdf.

Patankar, A., 2020: Impacts of Natural Disasters on Households and Small Businesses in India. *SSRN Electron. J.*, https://doi.org/10.2139/ssrn.3590902.

Pattanaik, D. R., and Y. V. Rama Rao, 2009: Track prediction of very severe cyclone "Nargis" using high resolution weather research forecasting (WRF) model. *J. Earth Syst. Sci.*, **118**, 309–329, https://doi.org/10.1007/s12040-009-0031-8.

Pattanayak, S., U. C. Mohanty, and K. K. Osuri, 2012: Impact of Parameterization of Physical Processes on Simulation of Track and Intensity of Tropical Cyclone Nargis (2008) with WRF-NMM Model. *Sci. World J.*, **2012**, 1–18, https://doi.org/10.1100/2012/671437.

Perumal, M., T. Moramarco, S. Barbetta, F. Melone, and B. Sahoo, 2011: Real-time flood stage forecasting by Variable Parameter Muskingum Stage hydrograph routing method. *Hydrol. Res.*, **42**, 150–161, https://doi.org/10.2166/nh.2011.063.

Prakash, S., A. K. Mitra, I. M. Momin, E. N. Rajagopal, S. F. Milton, and G. M. Martin, 2016a: Skill of short- to medium-range monsoon rainfall forecasts from two global models over India for hydro-meteorological applications. *Meteorol. Appl.*, **23**, 574–586, https://doi.org/10.1002/met.1579.

——, I. M. Momin, A. K. Mitra, P. S. Bhattacharjee, F. Yang, and V. Tallapragada, 2016b: An Early Assessment of Medium Range Monsoon Precipitation Forecasts from the Latest High-Resolution NCEP-GFS (T1534) Model over South Asia. *Pure Appl. Geophys.*, **173**, 2215–2225, https://doi.org/10.1007/s00024-016-1248-5.

——, A. K. Mitra, A. AghaKouchak, Z. Liu, H. Norouzi, and D. S. Pai, 2018: A preliminary assessment of GPM-based multi-satellite precipitation estimates over a monsoon dominated region. *J. Hydrol.*, **556**, 865–876, https://doi.org/10.1016/j.jhydrol.2016.01.029.

Rajeevan, M., J. Bhate, and A. K. Jaswal, 2008: Analysis of variability and trends of extreme rainfall events over India using 104 years of gridded daily rainfall data. *Geophys. Res.*

Lett., **35**, 1–6, https://doi.org/10.1029/2008GL035143.

Raju, P. V. S., J. Potty, and U. C. Mohanty, 2011: Sensitivity of physical parameterizations on prediction of tropical cyclone Nargis over the Bay of Bengal using WRF model. *Meteorol. Atmos. Phys.*, **113**, 125–137, https://doi.org/10.1007/s00703-011-0151-y.

——, ——, and ——, 2012: Prediction of severe tropical cyclones over the Bay of Bengal during 2007-2010 using high-resolution mesoscale model. *Nat. Hazards*, **63**, 1361–1374, https://doi.org/10.1007/s11069-011-9918-1.

Ramachandraiah, C., 2011: Coping with urban flooding: A study of the 2009 kurnool floods, India. *Environ. Urban.*, **23**, 431–446, https://doi.org/10.1177/0956247811418733.

Rao, G. V., K. V. Reddy, and V. Sridhar, 2020: Sensitivity of microphysical schemes on the simulation of post-monsoon tropical cyclones over the north Indian Ocean. *Atmosphere (Basel).*, **11**, 1–17, https://doi.org/10.3390/atmos11121297.

Rigby, R. A., D. M. Stasinopoulos, and P. W. Lane, 2005: Generalized additive models for location, scale and shape. *J. R. Stat. Soc. Ser. C Appl. Stat.*, **54**, 507–554, https://doi.org/10.1111/j.1467-9876.2005.00510.x.

Rogers, E., T. Black, B. Ferrier, Y. Lin, D. Parrish, and G. DiMego, 2001: NCEP Meso Eta Analysis and Forecast System: Increase in resolution, new cloud microphysics, modified precipitation assimilation, modified 3DVAR analysis. *NWS Tech. Proced. Bull.*, **488**, 1–15.

Roy, S. Sen, and R. C. Balling, 2004: Trends in extreme daily precipitation indices in India. *Int. J. Climatol.*, **24**, 457–466, https://doi.org/10.1002/joc.995.

Sahai, A. K., and Coauthors, 2013: Simulation and extended range prediction of monsoon intraseasonal oscillations in NCEP CFS/GFS version 2 framework. *Curr. Sci.*, **104**, 1394–1408.

Saksena, S., V. Merwade, and P. J. Singhofen, 2021: An Alternative Approach for Improving Prediction of Integrated Hydrologic-Hydraulic Models by Assessing the Impact of Intrinsic Spatial Scales. *Water Resour. Res.*, **57**, 1–31, https://doi.org/10.1029/2020wr027702.

Sandeep, C. P. R., C. Krishnamoorthy, and C. Balaji, 2018: Impact of Cloud Parameterization Schemes on The Simulation of Cyclone *Vardah* using the WRF Model. *Curr. Sci.*, **115**,

1143, https://doi.org/10.18520/cs/v115/i6/1143-1153.

Santillan, J. R., E. M. O. Morales, M. Makinano-Santillan, A. M. Amora, J. T. Marqueso, and A. L. Gingo, 2020: A web GIS-based visualization and analytical platform for near-real time flood characterization, forecasting and impact assessment. *40th Asian Conf. Remote Sensing, ACRS 2019 Prog. Remote Sens. Technol. Smart Futur.*, 1–10.

Satyanarayana, G. C., and S. C. Kar, 2016: Medium-range forecasts of extreme rainfall events during the Indian summer monsoon. *Meteorol. Appl.*, **23**, 282–293, https://doi.org/10.1002/met.1553.

Šaur, D., 2017: Forecasting of Convective Precipitation Through NWP Models and Algorithm of Storms Prediction. *Advances in Intelligent Systems and Computing*, Vol. 573 of, 125–136.

Schumann, G. J.-P., J. C. Neal, N. Voisin, K. M. Andreadis, F. Pappenberger, N. Phanthuwongpakdee, A. C. Hall, and P. D. Bates, 2013: A first large-scale flood inundation forecasting model. *Water Resour. Res.*, **49**, 6248–6257, https://doi.org/10.1002/wrcr.20521.

Shahrban, M., J. P. Walker, Q. J. Wang, A. Seed, and P. Steinle, 2016: An evaluation of numerical weather prediction based rainfall forecasts. *Hydrol. Sci. J.*, **61**, 2704–2717, https://doi.org/10.1080/02626667.2016.1170131.

Sharma, K., R. Ashrit, E. Ebert, G. Iyengar, and A. Mitra, 2015: NGFS rainfall forecast verification over India using the contiguous rain area (CRA) method. *Mausam*, **66**, 415–422.

——, ——, R. Bhatla, A. K. Mitra, G. R. Iyengar, and E. N. Rajagopal, 2017: Skill of Predicting Heavy Rainfall Over India: Improvement in Recent Years Using UKMO Global Model. *Pure Appl. Geophys.*, **174**, 4241–4250, https://doi.org/10.1007/s00024-017-1640-9.

——, ——, S. Kumar, S. Milton, E. N. Rajagopal, and A. K. Mitra, 2021: Unified model rainfall forecasts over India during 2007–2018: Evaluating extreme rains over hilly regions. *J. Earth Syst. Sci.*, **130**, https://doi.org/10.1007/s12040-021-01595-1.

Sholichin, M., and W. Qadri, 2020: Predicting flood hazards area using swat and hec-ras simulation in Bila river, South Sulawesi. *IOP Conf. Ser. Earth Environ. Sci.*, **437**,

https://doi.org/10.1088/1755-1315/437/1/012055.

Shrestha, D. L., D. Robertson, T. Pagano, P. Hapuarachchi, and Q. J. Wang, 2012: Evaluation of numerical weather prediction model rainfall forecasts for streamflow forecasting. *Proc. 34th Hydrol. Water Resour. Symp. HWRS 2012*, 856–863, https://doi.org/10.5194/hessd-9-12563-2012.

Singh, D., M. R. Bhutiyani, and T. Ram, 2014: Station-based verification of qualitative and quantitative MM5 precipitation forecasts over Northwest Himalaya (NWH). *Meteorol. Atmos. Phys.*, **125**, 107–118, https://doi.org/10.1007/s00703-014-0321-9.

Somasekhar, M., 2020: Hyderabad floods: Hyderabad needs a plan for disaster mitigation. *Mongabay*.

Sphere-India, 2018: *HUMANITARIAN SNAPSHOT REPORT IN INDIA: Cyclone "TITLI" and Flood Status*.

Sravani, D., 2018: GIS Based Management System for Flood Forecast Applications. *Proceedings of International Conference on Remote Sensing for Disaster Management Issues and Challenges in Disaster Management*, 1–12.

Sridevi, C., K. K. Singh, P. Suneetha, V. R. Durai, and A. Kumar, 2018: Rainfall forecast skill of Global Forecasting System (GFS) model over India during summer monsoon 2015. *Geofizika*, **35**, 39–52, https://doi.org/10.15233/gfz.2018.35.4.

Sridevi, C., K. K. Singh, P. Suneetha, V. R. Durai, and A. Kumar, 2020: Rainfall forecasting skill of GFS model at T1534 and T574 resolution over India during the monsoon season. *Meteorol. Atmos. Phys.*, **132**, 35–52, https://doi.org/10.1007/s00703-019-00672-x.

Sridhar, V., and P. Valayamkunnath, 2018: Land–Atmosphere Interactions in South Asia: A Regional Earth Systems Perspective. 699–712, https://doi.org/10.1007/978-3-319-67474-2_30.

——, X. Jin, and W. T. A. Jaksa, 2013: Explaining the hydroclimatic variability and change in the Salmon River basin. *Clim. Dyn.*, **40**, 1921–1937, https://doi.org/10.1007/s00382-012-1467-0.

Su, L., C. Miao, D. Kong, Q. Duan, X. Lei, Q. Hou, and H. Li, 2018: *Long-term trends in global river flow and the causal relationships between river flow and ocean signals*. 818–833 pp.

Sudheer, K. P., S. Murty Bhallamudi, B. Narasimhan, J. Thomas, V. M. Bindhu, V. Vema, and C. Kurian, 2019: Role of dams on the floods of August 2018 in Periyar River Basin, Kerala. *Curr. Sci.*, **116**, 780–794, https://doi.org/10.18520/cs/v116/i5/780-794.

Sujatha, E. R., and V. Sridhar, 2017: Mapping debris flow susceptibility using analytical network process in Kodaikkanal Hills, Tamil Nadu (India). *J. Earth Syst. Sci.*, **126**, 1–18, https://doi.org/10.1007/s12040-017-0899-7.

Sun, Q., C. Miao, Q. Duan, H. Ashouri, S. Sorooshian, and K.-L. Hsu, 2017: A review of global precipitation datasets: data sources, estimation, and intercomparisons. *Rev. Geophys.*, 1–29, https://doi.org/10.1002/2017RG000574.

Tamiru, H., and M. O. Dinka, 2021: Application of ANN and HEC-RAS model for flood inundation mapping in lower Baro Akobo River Basin, Ethiopia. *J. Hydrol. Reg. Stud.*, **36**, 100855, https://doi.org/10.1016/j.ejrh.2021.100855.

Thameemul Hajaj, P. M., K. Yarrakula, K. H. V. Durga Rao, and A. Singh, 2019: A Semi-distributed Flood Forecasting Model for the Nagavali River Using Space Inputs. *J. Indian Soc. Remote Sens.*, **47**, 1683–1692, https://doi.org/10.1007/s12524-019-01019-0.

Thompson, G., R. M. Rasmussen, and K. Manning, 2004: Explicit Forecasts of Winter Precipitation Using an Improved Bulk Microphysics Scheme. Part I: Description and Sensitivity Analysis. *Mon. Weather Rev.*, **132**, 519–542, https://doi.org/10.1175/1520-0493(2004)132<0519:EFOWPU>2.0.CO;2.

Tian, Y., and Coauthors, 2009: Component analysis of errors in Satellite-based precipitation estimates. *J. Geophys. Res. Atmos.*, **114**, 1–15, https://doi.org/10.1029/2009JD011949.

TNIE, 2018: After Titli, floods make lives of Srikakulam people miserable- The New Indian Express. *The New Indian Express*.

Tyralis, H., 2016: *Hurst-Kolmogorov Process Version*. https://cran.r-project.org/web/packages/HKprocess/HKprocess.pdf.

Uddin, M. J., Y. Li, K. K. Cheung, Z. M. Nasrin, H. Wang, L. Wang, and Z. Gao, 2019: Rainfall contribution of Tropical Cyclones in the Bay of Bengal between 1998 and 2016 using TRMM satellite data. *Atmosphere (Basel).*, **10**, https://doi.org/10.3390/atmos10110699.

Venkata Rao, G., K. Venkata Reddy, R. Srinivasan, V. Sridhar, N. V. Umamahesh, and D. Pratap, 2020: Spatio-temporal analysis of rainfall extremes in the flood-prone Nagavali

and Vamsadhara Basins in eastern India. *Weather Clim. Extrem.*, **29**, 100265, https://doi.org/10.1016/j.wace.2020.100265.

Vittal, H., S. Karmakar, and S. Ghosh, 2013: Diametric changes in trends and patterns of extreme rainfall over India from pre-1950 to post-1950. *Geophys. Res. Lett.*, **40**, 3253–3258, https://doi.org/10.1002/grl.50631.

Wan, Z., Y. Hong, S. Khan, J. Gourley, Z. Flamig, D. Kirschbaum, and G. Tang, 2014: A cloud-based global flood disaster community cyber-infrastructure: Development and demonstration. *Environ. Model. Softw.*, **58**, 86–94, https://doi.org/10.1016/j.envsoft.2014.04.007.

Wang, S., L. Yu, and S. Zhu, 2020: Precipitation forecast on the township scale using the frequency matching method. *IOP Conf. Ser. Earth Environ. Sci.*, **467**, https://doi.org/10.1088/1755-1315/467/1/012050.

Wang, W., and N. L. Seaman, 1997: A comparison study of convective parameterization schemes in a mesoscale model. *Mon. Weather Rev.*, **125**, 252–278, https://doi.org/10.1175/1520-0493(1997)125<0252:ACSOCP>2.0.CO;2.

——, and Coauthors, 2018: *Advanced Research WRF (ARW) Version 4.0 Modeling System User's Guide*. 464 pp.

World Meteorological Organization, 1977: *Manual on the Global Data-Processing System: Global Aspects*.

Yadav, R., S. K. Tripathi, G. Pranuthi, and S. K. Dubey, 2014: Trend analysis by Mann-Kendall test for precipitation and temperature for thirteen districts of Uttarakhand. *J. Agrometeorol.*, **16**, 164–171.

Yang, C., H. Yuan, and X. Su, 2020: Bias correction of ensemble precipitation forecasts in the improvement of summer streamflow prediction skill. *J. Hydrol.*, **588**, 124955, https://doi.org/10.1016/j.jhydrol.2020.124955.

Yang, L., J. Li, H. Sun, Y. Guo, and B. A. Engel, 2019: Calculation of nonstationary flood return period considering historical extraordinary flood events. *J. Flood Risk Manag.*, **12**, 1–10, https://doi.org/10.1111/jfr3.12463.

Yang, M., X. Chen, and C. S. Cheng, 2016: Hydrological impacts of precipitation extremes in the Huaihe River Basin, China. *Springerplus*, **5**, 1–13, https://doi.org/10.1186/s40064-

016-3429-1.

Yue, S., P. Pilon, and B. Phinney, 2003: Canadian streamflow trend detection: Impacts of serial and cross-correlation. *Hydrol. Sci. J.*, **48**, 51–64, https://doi.org/10.1623/hysj.48.1.51.43478.

Zarei, M., M. Najarchi, and R. Mastouri, 2021: Bias correction of global ensemble precipitation forecasts by Random Forest method. *Earth Sci. Informatics*, **14**, 677–689, https://doi.org/10.1007/s12145-021-00577-7.

Zhu., Y., and Z. Toth, 2004: Implementation of bias-corrected QPF and PQPF forecasts. NOAA/NWS/Environmental Modeling Center. http://wwwt.emc.ncep.noaa.gov/gmb/ens/index.html.

Zhu, Y., and Y. Luo, 2015: Precipitation calibration based on the frequency-matching method. *Weather Forecast.*, **30**, 1109–1124, https://doi.org/10.1175/WAF-D-13-00049.1.

List of Publications

Journals

Rao, G V, Reddy, K.V., Sridhar, V., 2020. Sensitivity of microphysical schemes on the simulation of post-monsoon tropical cyclones over the north Indian Ocean. Atmosphere (Basel). 11, 1–17. https://doi.org/10.3390/atmos11121297.

Rao, G V, Venkata Reddy, K., Srinivasan, R., Sridhar, V., Umamahesh, N. V., Pratap, D., 2020. Spatio-temporal analysis of rainfall extremes in the flood-prone Nagavali and Vamsadhara Basins in eastern India. Weather Clim. Extrem. 29, 100265. https://doi.org/10.1016/j.wace.2020.100265.

Rao, G V, Venkata Reddy, K., Sridhar, V., Srinivasan, R., Umamahesh, N. V., Pratap, D., 2022. Evaluation of GFS based Rainfall Forecasts over the Nagavali and Vamsadhara Basins, India. Atmospheric Research (2nd review completed).

Rao, G V, Nageswara Reddy N, Venkata Reddy, K., Sridhar, V., Srinivasan, R., Umamahesh, N. V., Pratap, D., 2022. Real-Time Flood Forecasting Using an Integrated Hydrologic and Hydraulic model for the Vamsadhara and Nagavali basins, Eastern India. Journal of River Basin Managament (Under Review).

Book Chapters

Rao, G V., Venkata Reddy, K., Navatha, Y., 2020. Assessment of Microphysical Parameterization Schemes on the Track and Intensity of Titli Cyclone Using ARW Model. Adv. Intell. Syst. Comput. 979, 35–42. https://doi.org/10.1007/978-981-15-3215-3_4

Rao, G V., Venkata Reddy, K. (2022). Validation and Correction of GSMaP_Gauge Product Over the Nagavali Basin in Eastern India. In: Dikshit, A.K., Narasimhan, B., Kumar, B., Patel, A.K. (eds) Innovative Trends in Hydrological and Environmental Systems. Lecture Notes in Civil Engineering, vol 234. Springer, Singapore. https://doi.org/10.1007/978-981-19-0304-5_34

Conferences

Rao, G V., Venkata Reddy, K., Navatha, Y., 2019. "Assessment of Microphysical Parameterization Schemes on the Track and Intensity of Titli Cyclone Using ARW Model" in the International Conference on Numerical Optimization in Engineering and Sciences (NOIEAS-2019) during 19-21 June, 2019, at NIT Warangal, India.

Rao, G V., K Venkata Reddy., And Y Navatha., 2019. "Impact of Grid Resolution on the Prediction of Tropical Cyclone FANI Using ARW Model" in the ISH - Hydro 2019 International Conference- Osmania University during December 17-19, 2019, at

Hyderabad, India.

Rao, G V., and Venkata Reddy, K. 2021. “Verification of GSMaP_Gauge rainfall product over the Nagavali basin in Eastern India” in the International Conference on 'Innovative Trends in Hydrological and Environmental Systems (ITHES-2021)' during 28th to 30th April, 2021 at NIT Warangal, India

Rao, G V., Venkata Reddy, K., Srinivasan, R., Sridhar, V., Umamahesh, NV, Pratap, D., 2021. "Real-time Flood Forecasting Using an Integrated Hydrologic and Hydraulic Model on the Vamsadhara River in Eastern India" in the AGU Fall Meeting, New Orleans, LA USA. Online Everywhere, 13-17 Dec 2021.

Appendix-A

The main aim of this research is to target water resource management and agricultural usage. The of monthly analysis are presented in Appendix-A.

Trends in Monthly Rainfall

The Z statistics for the monthly rainfall for 28 grids, 12 of which are over Nagavali and 16 over Vamsadhara is studied using four different Mann-Kendall (MK) tests and are presented in Appendix-A Table A9.

In the Nagavali basin, no long-term trend is observed in January, October, and November. A negative trend is observed at less than 3 out of 12 grids in February, May, August, September, and December. A positive trend is observed over a very few grids (i.e., ≤ 2) during March, April, May, and June. However, a positive trend is observed for 9 grids in July.

In the Vamsadhara basin, no long-term trend is observed between September and February. A negative trend is observed at VG14 in June. However, a positive trend is observed from March to August. Over the Vamsadhara basin, out of 16 grids, a positive trend is observed over 4 grids in March, 2 in April, 8 in both May and July, 6 in June and 3 in August, respectively. This implies the temporal and spatial variability of rainfall trends even in a relatively small watersheds in this region.

The spatial patterns of trends in the monthly rainfall using four MK tests are presented in Appendix-A Figures A12 – A15. From the figures, it is observed that most of the grids in the lower and upper portion of the Nagavali basin shown decreasing trends except in May and September. In the Vamsadhara basin, the grids showing the decreasing trends are seen in the upper portion of the basin. The grids showing the increasing trends are present in the lower and middle portions of both the basins.

Trends in Monthly Rainfall Extremes

The trends in monthly rainfall extremes are evaluated and presented in this section. The Z statistics of the rainfall extremes in July are provided in Appendix-A Table A10 as it is the peak month of monsoon season. The spatial patterns of the rainfall extremes for July are presented in Appendix-A Figures A16 – A18. The detailed analysis of rainfall extremes in each month are presented in the following sections.

Consecutive Dry Days

No significant trend is observed for CDD in January, April and December in the Nagavali basin. In the Vamsadhara basin no significant trend is observed between October and February. Negative trend is observed in March, May, July, and August in both the basins except at one or two grids in the Nagavali basin. A positive trend is observed in February, June and September.

From the spatial patterns, it is observed that the grids showing the trends (positive/negative) are present in the lower portions of both the basins except for March and September. In March, the grids showed a decreasing trend for both the basins. In September, positive trend is present in all portions of the Nagavali basin. The grids showing a decreasing trend in the Vamsadhara basin are present in the lower and middle portions of the basin and a positive trend in the upper portion.

Consecutive Wet Days

A very few grids in both the basins have shown significant trends for CWD. No significant trend is observed between October and January. In both the basins, a negative trend is observed for a few grids in February and June. A positive trend is observed in both the basins except at grid NG12 in the Nagavali basin from March to August. In September, a negative trend in the Nagavali basin and a positive trend in the Vamsadhara basin are observed.

In the Nagavali basin, the grids showing positive trends are present in the lower and middle portions except at grid NG12 in July and August, whereas a decreasing trend is seen in the upper portion of the basin. In the Vamsadhara basin, the grids showing decreasing trends are present in the middle and upper portions of the basin except at VG2 in April, where it showed an increasing trend in the lower portion of the basin.

Actual Total Wet Day Precipitation (PRCPTOT)

A clear positive trend is observed for PRCPTOT from March to August except at NG8 and NG10 in April, VG14 in June and NG3 in August where a negative trend is observed in both the basins. A negative trend is observed in February and September. No significant trend is observed between October and January.

The grids with decreasing trends are present in the middle and upper portions of the Nagavali basin except at NG3 in August and September where it showed decreasing trend in the lower

portion of the basin. In March, an increasing trend is present in the upper portion of the basin whereas from April to June it is in the lower portion of the basin. In July, an increasing trend is present in all parts of the Nagavali basin. In the Vamsadhara basin, the grids with decreasing trends are present in the upper portion of the basin and increasing trends are present in the lower and middle portions of the basin.

Heavy Rainfall Days (R10MM)

A negative trend is observed in February, September, and November and positive trend from May to July in both the basins. No significant trend is observed in March and April over the Nagavali basin whereas a positive trend is observed in the Vamsadhara basin. In August, a negative trend in the Nagavali basin and a positive trend in the Vamsadhara basin is observed except at grid VG10. No significant trend is observed in January and from October to December.

The grids with decreasing trends are present in the upper portions of both the basins except at grid NG2 in February, grid NG3 in August and September where they showed decreasing trends in the lower portion of the Nagavali basin. The grids with increasing trends are present in both the basins except over the upper portion of the Vamsadhara basin.

Very Heavy Rainfall Days (R20MM)

A positive trend is observed for R20MM in both the basins in March and from May to August and a negative trend in February and September. In April and November, a negative trend is observed only in the Vamsadhara basin and no significant trend is observed in the Nagavali basin. No significant trend is observed during January and December.

In the Nagavali basin, the grids with decreasing trends in August are present in the lower portion of the basin and in the middle portion of the basin in November. Whereas, the grids showing a decreasing trend in February and increasing trends in June and July are present in the entire basin. The grids with increasing trend are seen in March and May in the upper portion of the basin and in August in the middle portion of the basin. In the Vamsadhara basin, the grids with decreasing trend are present in the middle and upper portions of the basin and increasing trend are seen in the lower sections of the basin.

Number of Days with Rainfall greater than 40 mm (R40MM)

No significant trend is observed for the grids having rainfall greater than 40 mm in January, February, and from September to December. A positive trend is observed in all the months except in April at grids VG11 and VG13 in the Vamsadhara basin. The grids showing increasing trend are present in the upper portion of the Nagavali basin. In the Vamsadhara basin, the grids showing decreasing trend are present in the upper portion of the basin and the opposite in the lower portion. Whereas, an increasing trend is present in May over the upper portion.

Very Wet Days (R95PTOT)

A positive trend is observed for very wet days in March, June, and July in both the basins. No significant trend is observed in January and from August to December. A negative trend is observed in February in both the basins. In April, a positive trend is observed in the Nagavali basin and a negative trend in the Vamsadhara basin. Whereas in May, a positive trend is observed in the Vamsadhara basin and a negative trend in the Nagavali basin.

The grids showing both increasing or decreasing trends are present in the middle and upper portions of the Nagavali basin. In the Vamsadhara basin, the grids showing a decreasing trend are present in the upper portion and increasing trend in the lower portion of the basin. Whereas in May, the grids showing increasing trend are present in the middle and upper portions of the basin.

Monthly Maximum One-Day and Five-Day Precipitation (RX1DAY and RX5DAY)

A positive trend is observed from April to July in both the basins. In the Nagavali basin, a negative trend is observed in August, November, and December. No significant trend is observed in January, February, September, and October for both RX1DAY and RX5DAY. In the Vamsadhara basin, no significant trend is observed in January, February, and from August to December except at VG14 grid in November where it showed a negative trend for RX1DAY.

The grids showing increasing trend are present in the middle and upper portions of the Nagavali basin and at the lower and middle portions of the Vamsadhara basin. The grids showing decreasing trends are present in the upper portion of both the basins except at one grid in the lower portion of the Nagavali basin.

Table A1. Z statics of seasonal and annual rainfall trend analysis (**Note:** Bold number indicates significant trends confidence level at 90% or above ($Z \geq 1.65$); NG represents Gird point over Nagavali Bain, VG represent Grid point over Vamsadhara Basin.)

Grid Id	DJF	MAM	JJAS	ON	Annual
	MK1/MK2/MK3/MK4	**MK1/MK2/MK3/MK4**	**MK1/MK2/MK3/MK4**	**MK1/MK2/MK3/MK4**	**MK1/MK2/MK3/MK4**
NG1	**-1.67**/-1.50/-2.30/-1.63	0.23/0.56/0.25/0.26	1.19/0.60/0.76/0.99	-0.80/-0.73/-0.80/-0.76	0.33/-0.03/0.47/0.25
NG2	**-1.82/-1.84/-2.04/-2.01**	0.92/1.25/0.91/1.03	0.31/0.04/0.24/0.31	-0.25/0.03/-0.23/-0.25	0.30/0.19/0.58/0.27
NG3	-1.41/-1.47/**-2.00**/-1.53	-0.17/0.00/-0.18/-0.18	**-2.77/-3.49/-2.12/-2.60**	-0.36/-0.16/-0.36/-0.35	**-2.67/-3.16/-3.52/-2.18**
NG4	-0.49/-0.59/-0.86/-0.57	**2.18/2.37/1.96/2.29**	**2.42/2.32/1.99/3.24**	0.25/0.48/0.23/0.26	**2.54/2.51/2.40/2.54**
NG5	-1.45/-1.43/-1.64/-1.48	-0.23/0.00/-0.23/-0.27	-0.10/-0.37/-0.10/-0.09	-0.38/-0.27/-0.41/-0.39	-0.25/-0.40/-0.22/-0.27
NG6	-1.37/-1.43/**-2.06**/-1.47	0.23/0.51/0.22/0.27	-0.21/-0.60/-0.19/-0.21	-0.41/-0.22/-0.41/-0.41	-0.72/-0.96/-0.77/-0.72
NG7	-0.95/-0.97/-1.04/-1.03	**2.54/2.53/2.54/2.96**	**3.05/2.84/2.96/3.05**	0.02/0.22/0.02/0.02	**2.60/2.43/2.60/2.93**
NG8	-1.52/-1.37/**-1.71/-1.70**	-0.58/-0.42/-0.68/-0.66	0.69/0.53/0.61/0.58	-1.10/-0.92/-1.19/-1.10	-0.08/-0.14/-0.08/-0.08
NG9	**-1.82/-1.72/-1.82/-2.04**	1.26/1.29/1.26/1.40	**1.78**/1.51/**1.70/2.11**	-1.05/-0.85/-1.13/-1.06	1.17/0.99/1.38/1.19
NG10	**-1.82/-1.75/-2.04/-2.07**	-0.74/-0.55/-0.74/-0.76	**2.64/2.21/1.95/2.64**	**-1.88/-1.66/-2.04/-1.77**	1.60/1.44/**1.76**/1.29
NG11	-1.01/-0.85/-1.01/-1.16	1.50/1.60/**1.71**/1.60	**2.00/1.75/1.76/2.13**	-1.23/-0.99/-1.33/-1.23	1.52/1.31/**1.83**/1.48
NG12	**-2.68/-2.49/-3.11/-2.68**	0.74/1.01/0.64/0.70	-0.69/-0.94/-0.65/-0.67	-0.82/-0.58/-0.82/-0.80	-0.66/-0.91/-0.66/-0.65
VG1	-0.77/-0.76/-1.09/-0.86	**1.91/2.00/1.91/2.21**	**3.08/2.88/3.05/4.37**	0.48/0.65/0.49/0.47	**2.22/2.27/2.22/2.41**
VG2	-0.84/-0.94/-1.09/-0.93	**2.96/2.86/2.96/3.47**	**4.47/4.29/4.56/4.99**	0.10/0.29/0.12/0.10	**3.25/3.22/3.25/3.62**
VG3	-1.48/-1.49/**-1.85/-1.67**	**2.02/2.03/2.02/2.33**	**3.44/3.31/3.54/3.44**	0.37/0.57/0.38/0.37	**2.04/2.29/2.78/2.37**
VG4	-0.76/-0.85/-0.76/-0.79	**4.05/3.96/5.62/4.23**	**4.81/4.78/4.10/5.72**	-0.27/0.01/-0.27/-0.25	**4.22/4.15/5.03/3.87**
VG5	-1.10/-1.16/-1.10/-1.23	**3.87/3.86/4.36/3.87**	**5.14/5.26/4.48/4.77**	-0.32/-0.12/-0.35/-0.32	**3.89/3.91/3.68/4.00**
VG6	-1.57/**-1.79/-1.64/-1.79**	0.77/0.82/0.68/0.92	**2.13/2.08/2.18/2.20**	0.30/0.48/0.27/0.32	0.96/1.20/1.39/1.19
VG7	-1.55/**-1.84**/-1.57/**-1.88**	**2.98/3.05/3.58/2.84**	**2.98/2.95/2.67/3.42**	-0.85/-0.70/-0.91/-0.80	**2.25/2.27/2.05/2.21**
VG8	-1.39/-1.61/-1.36/-1.61	**2.77/3.00/2.23/2.60**	**2.84/2.96/2.46/2.49**	-0.65/-0.52/-0.60/-0.65	**2.13/2.24/2.39/2.17**
VG9	-1.43/**-1.65/-3.19**/-1.60	2.04/2.11/2.25/2.42	**2.42/2.42/2.50/2.40**	-0.08/0.04/-0.08/-0.09	1.40/1.48/**2.25/1.77**
VG10	-1.61/-1.47/-1.63/**-1.89**	0.79/0.96/0.95/0.73	-1.36/-1.66/-1.25/-1.53	-1.06/-0.94/-1.13/-1.05	-1.60/**-1.83/-1.97**/-1.57
VG11	-1.32/-1.38/-1.34/-1.61	**1.66/1.84/1.87**/1.57	0.48/0.40/0.42/0.53	-1.04/-0.98/-1.04/-0.99	-0.46/-0.41/-0.42/-0.44
VG12	-1.11/-1.18/-1.11/-1.36	**1.89/1.98**/1.38/**1.74**	-0.71/-0.79/-0.65/-0.73	-0.56/-0.52/-0.45/-0.55	-0.34/-0.30/-0.33/-0.32
VG13	-1.46/**-1.77/-2.09/-1.86**	0.34/0.20/0.40/0.35	-1.07/-1.17/-0.89/-1.04	-0.41/-0.37/-0.41/-0.40	-0.92/-0.94/-0.96/-0.87
VG14	**-2.03/-1.86/-2.03/-2.26**	0.11/0.15/0.12/0.10	-1.22/-1.46/-1.15/-1.22	-0.88/-0.70/-0.88/-0.90	-1.47/**-1.67/-1.68**/-1.43
VG15	-1.11/-1.16/-1.12/-1.32	1.01/1.12/1.38/0.96	0.39/0.30/0.36/0.43	-0.70/-0.60/-0.78/-0.69	-0.67/-0.78/-1.07/-0.69
VG16	-1.23/-1.38/-1.24/-1.48	0.84/0.96/0.98/0.80	0.22/0.19/0.20/0.27	-0.39/-0.40/-0.44/-0.38	-0.65/-0.66/-0.59/-0.64

Table A2. Z statics of seasonal and annual rainfall of pre- and post-1950

Grid Id	Pre-1950					Post-1950				
	DJF	MAM	JJAS	ON	Annual	DJF	MAM	JJAS	ON	Annual
	MK1/MK2/MK3/MK4	MK1/MK2/MK3/MK4	MK1/MK2/MK3/MK4	MK1/MK2/MK3/MK4	MK1/MK2/MK3/MK4	MK1/MK2/MK3/MK4	MK1/MK2/MK3/MK4	MK1/MK2/MK3/MK4	MK1/MK2/MK3/MK4	MK1/MK2/MK3/MK4
NG1	0.38/0.49/0.46/0.38	1.39/**1.70/1.67**/1.42	-0.02/-0.65/-0.02/-0.02	1.39/**1.70/1.67**/1.42	1.19/1.06/1.19/1.47	0.37/0.15/0.40/0.36	**-1.66/-1.62/-1.66/-1.63**	0.05/0.07/0.03/0.03	**-1.66**/-1.62/**-1.66**/-1.63	-0.36/0.17/-0.27/-0.25
NG2	-0.06/0.35/-0.09/-0.07	1.47/**1.94/1.78**/1.40	-0.82/-1.44/-1.10/-0.97	1.47/**1.94/1.78**/1.40	0.97/1.09/0.97/1.17	-0.36/-0.81/-0.36/-0.37	-1.33/-1.46/-1.33/-1.45	-0.91/-1.03/-0.91/-0.65	-1.33/-1.46/-1.33/-1.45	-0.42/-0.11/-0.49/-0.37
NG3	-0.16/-0.15/-0.15/-0.18	1.52/**1.90**/1.52/1.51	-0.30/-0.70/-0.30/-0.33	1.52/**1.90**/1.52/1.51	0.33/0.09/0.33/0.36	-0.62/-1.10/-0.62/-0.65	**-1.80/-2.04/-2.50/-1.87**	**-3.40/-3.96/-3.26/-2.18**	**-1.80/-2.04/-2.50/-1.87**	**-3.28/-3.52/-2.90/-2.50**
NG4	0.38/0.68/0.39/0.45	1.25/**1.68**/1.25/1.21	-0.73/-1.06/-0.73/-0.80	1.25/**1.68**/1.25/1.21	-0.18/-0.06/-0.16/-0.21	0.34/0.18/0.34/0.39	-0.89/-0.89/-0.89/-0.98	1.08/1.55/1.08/0.77	-0.89/-0.89/-0.89/-0.98	1.45/1.47/1.45/1.42
NG5	-0.60/0.01/-0.50/-0.71	1.51/**1.75**/1.51/1.48	-0.03/-0.47/-0.03/-0.04	1.51/**1.75**/1.51/1.48	0.95/0.58/0.79/1.16	0.78/0.57/0.78/0.70	-0.61/-0.65/-0.61/-0.69	-1.20/-1.30/-0.87/-1.10	-0.61/-0.65/-0.61/-0.69	-0.64/-0.39/-0.64/-0.66
NG6	-0.36/-0.25/-0.53/-0.41	**1.67/2.03/1.67/1.69**	-0.13/-0.42/-0.13/-0.16	**1.67/2.03/1.67/1.69**	0.50/0.25/0.50/0.59	0.13/-0.31/0.13/0.13	-1.57/**-1.68**/-1.57/**-1.71**	**-2.68/-2.58/-2.68/-2.26**	-1.57/**-1.68**/-1.57/**-1.71**	**-2.24/-2.24/-2.24/-2.27**
NG7	0.01/0.03/0.01/0.01	1.27/1.58/1.27/1.21	-0.33/-0.65/-0.33/-0.39	1.27/1.58/1.27/1.21	0.14/0.04/0.14/0.16	1.16/1.10/1.16/1.27	-0.12/-0.35/-0.12/-0.13	0.11/-0.10/0.14/0.10	-0.12/-0.35/-0.12/-0.13	0.85/0.24/0.85/1.01
NG8	-0.65/-0.01/-0.68/-0.78	1.49/**1.73**/1.49/1.45	0.00/-0.30/0.00/0.00	1.49/**1.73**/1.49/1.45	0.92/0.66/0.81/1.16	0.51/0.25/0.51/0.54	-1.48/-1.49/-1.48/-1.65	-1.65/-1.58/-1.37/-1.32	-1.48/-1.49/-1.48/-1.65	-1.59/-1.29/-1.46/-1.47
NG9	-0.54/-0.13/-0.56/-0.65	1.29/1.59/1.29/1.26	0.12/-0.16/0.17/0.15	1.29/1.59/1.29/1.26	0.80/0.56/0.72/0.99	0.45/0.20/0.45/0.49	-1.01/-1.18/-1.01/-1.11	**-1.76/-2.00/-1.76/-1.66**	-1.01/-1.18/-1.01/-1.11	-1.17/-1.28/-1.28/-1.21
NG10	-0.62/-0.15/-0.64/-0.75	1.54/**1.89**/1.54/1.50	-0.57/-0.66/-0.57/-0.69	1.54/**1.89**/1.54/1.50	1.12/0.58/1.00/1.43	0.30/0.12/0.30/0.34	**-1.93/-1.91/-1.93/-1.99**	-0.34/-0.48/-0.35/-0.23	**-1.93/-1.91/-1.93/-1.99**	-0.69/-0.38/-0.69/-0.50
NG11	-0.63/-0.20/-0.65/-0.75	**1.67/1.80/1.67/1.89**	0.05/-0.20/0.07/0.06	1.19/1.54/1.19/1.16	0.89/0.58/0.89/1.11	0.97/0.79/0.97/1.11	**-2.31/-2.10/-3.17/-2.30**	-1.08/-1.25/-1.09/-0.85	-1.11/-1.25/-1.11/-1.22	-0.68/-0.74/-0.68/-0.64
NG12	-1.31/-0.97/-1.04/-1.42	1.04/1.37/1.04/0.94	0.33/-0.37/0.38/0.26	**1.67/1.80/1.67/1.89**	0.65/0.15/0.65/0.54	-1.39/-1.80/-1.39/-1.39	-0.45/-0.78/-0.45/-0.48	-0.23/-0.38/-0.23/-0.23	**-2.31/-2.10/-3.17/-2.30**	-0.86/-0.75/-0.86/-0.90
VG1	0.22/0.34/0.60/0.25	1.19/**1.65**/1.19/1.07	-0.39/-0.85/-0.37/-0.51	1.04/1.37/1.04/0.94	0.02/-0.04/0.02/0.02	0.56/0.52/0.56/0.63	-0.54/-0.81/-0.54/-0.55	0.93/0.84/1.14/0.81	-0.45/-0.78/-0.45/-0.48	1.35/1.18/1.35/1.48
VG2	0.12/0.13/0.15/0.13	1.20/**1.66**/1.20/1.08	-0.33/-0.47/-0.36/-0.42	1.19/1.65/1.19/1.07	0.23/0.32/0.23/0.25	0.32/0.31/0.33/0.36	-0.87/-0.80/-0.87/-0.96	1.34/1.00/1.45/1.30	-0.54/-0.81/-0.54/-0.55	1.30/0.99/1.30/1.51
VG3	-0.59/-0.22/-0.79/-0.68	1.40/**1.80**/1.40/1.29	-0.59/-0.82/-0.65/-0.68	1.20/**1.66**/1.20/1.08	0.17/0.28/0.17/0.18	-0.57/-0.76/-0.57/-0.65	-0.47/-0.74/-0.66/-0.47	**1.70/1.48/1.70/1.71**	-0.87/-0.80/-0.87/-0.96	1.01/0.96/1.01/1.23
VG4	0.07/0.09/0.07/0.07	1.04/1.41/1.21/0.94	-0.02/-0.32/-0.02/-0.02	1.40/**1.80**/1.40/1.29	0.79/0.63/0.79/0.88	0.84/0.54/0.84/0.85	-0.58/-0.75/-0.55/-0.64	1.29/1.12/1.20/0.98	-0.47/-0.74/-0.66/-0.47	1.29/1.26/1.45/1.13
VG5	-0.49/-0.32/-0.87/-0.58	1.09/1.46/1.31/1.00	-0.75/-1.13/-0.81/-0.92	1.04/1.41/1.21/0.94	-0.24/-0.08/-0.26/-0.27	-0.01/-0.19/-0.01/-0.01	-0.96/-0.93/-0.96/-1.14	**2.17/1.81/2.42/1.72**	-0.58/-0.75/-0.55/-0.64	**1.77**/1.46/1.59/**1.83**
VG6	-1.46/-1.20/**-1.83/-1.79**	1.19/1.54/1.19/1.16	**-1.96/-1.92/-1.96/-2.15**	1.09/1.46/1.31/1.00	-0.43/-0.15/-0.46/-0.49	-1.10/-1.31/-1.32/-1.20	-1.11/-1.25/-1.11/-1.22	**1.78/1.74/2.36/1.88**	-0.96/-0.93/-0.96/-1.14	0.57/0.52/1.06/0.75
VG7	-0.85/-1.03/**-1.66**/-1.15	1.27/1.27/1.48/1.06	0.27/-0.09/0.27/0.30	1.27/1.27/1.48/1.06	0.74/0.75/0.74/0.70	0.75/0.49/0.75/0.85	-0.59/-0.76/-0.59/-0.64	1.52/1.16/1.70/1.20	-0.59/-0.76/-0.59/-0.64	**1.79/1.53/1.66/1.80**
VG8	-1.24/-1.27/-1.10/-1.57	1.14/1.35/1.35/1.02	**-1.69/-1.75/-1.69/-2.14**	1.14/1.35/1.35/1.02	0.03/0.01/0.03/0.04	0.01/-0.22/0.01/0.01	-1.02/-1.02/-1.02/-1.14	**2.54/2.45/2.54/2.03**	-1.02/-1.02/-1.02/-1.14	**2.10/1.87/1.90/2.08**
VG9	-1.05/-0.92/-0.98/-1.28	1.27/1.35/1.49/1.15	**-1.81/-1.72/-1.93/-2.20**	1.27/1.35/1.49/1.15	-0.07/0.18/-0.07/-0.08	-0.97/-1.17/-1.00/-1.05	-1.40/-1.42/-1.33/-1.67	**2.08/1.97/2.08/2.12**	-1.40/-1.42/-1.33/-1.67	0.78/0.68/1.41/1.02
VG10	-1.33/-0.94/-1.62/-1.64	1.34/1.63/1.34/1.35	0.22/-0.20/0.22/0.22	1.34/1.63/1.34/1.35	0.79/0.44/0.79/0.78	0.75/0.65/0.75/0.90	-1.44/-1.53/-**1.97**/-1.55	0.36/0.21/0.46/0.32	-1.44/-1.53/-1.97/-1.55	-0.10/-0.17/-0.10/-0.10
VG11	-1.07/-1.18/-1.13/-1.49	1.62/1.44/1.62/1.40	-0.07/-0.30/-0.07/-0.07	1.62/1.44/1.62/1.40	0.62/0.54/0.62/0.58	0.99/0.95/0.99/1.08	-1.18/-1.23/-1.18/-1.29	1.41/1.34/1.19/1.06	-1.18/-1.23/-1.18/-1.29	1.56/1.29/1.70/1.66
VG12	-1.22/-1.25/-1.19/**-1.71**	1.56/1.46/1.56/1.36	-0.01/-0.30/-0.01/-0.01	1.56/1.46/1.56/1.36	0.64/0.58/0.64/0.59	0.57/0.26/0.57/0.59	-1.32/-1.32/-1.11/-1.47	**1.81/1.66/1.81/1.61**	-1.32/-1.32/-1.11/-1.47	1.92/1.67/2.55/1.99
VG13	-1.15/-1.32/**-1.88/-1.66**	1.52/1.46/1.52/1.36	-0.05/-0.37/-0.05/-0.05	1.52/1.46/1.52/1.36	0.99/0.75/0.99/0.96	-0.06/-0.46/-0.06/-0.07	**-1.93/-1.99/-1.93/-2.15**	1.46/1.23/1.46/1.12	**-1.93/-1.99/-1.93/-2.15**	1.09/0.91/1.09/1.07
VG14	-1.48/-1.15/-1.23/**-1.81**	1.53/**1.85**/1.53/1.63	0.84/0.39/1.10/0.75	1.53/**1.85**/1.53/1.63	0.90/0.58/1.26/0.83	-0.53/-0.69/-0.53/-0.56	-0.39/-0.35/-0.39/-0.42	-1.52/-1.36/-1.52/-1.48	-0.39/-0.35/-0.39/-0.42	-0.93/-0.77/-0.93/-0.94
VG15	-1.29/-1.27/**-2.94/-1.79**	1.51/1.37/1.51/1.41	0.40/0.03/0.67/0.42	1.51/1.37/1.51/1.41	0.62/0.61/0.67/0.58	0.51/0.27/0.51/0.52	0.31/0.38/0.31/0.32	-0.43/-0.12/-0.43/-0.37	0.31/0.38/0.31/0.32	0.87/0.78/0.96/0.99
VG16	-1.24/-1.34/**-2.89/-1.71**	**1.71**/1.51/**1.71**/1.48	0.05/-0.01/0.05/0.05	1.71/1.51/**1.71**/1.48	0.53/0.41/0.48/0.43	0.65/0.43/0.65/0.68	-0.43/-0.21/-0.43/-0.47	0.73/0.43/1.03/0.70	-0.43/-0.21/-0.43/-0.47	1.54/1.18/1.25/2.04

Table A3. Z statics of long-term annual rainfall extremes

Grid Id	CDD	CWD	PRCPTOT	R10MM	R20MM	R40MM	R95PTOT	RX1DAY	RX5DAY
	MK1/MK2/MK3/MK4	**MK1/MK2/MK3/MK4**	**MK1/MK2/MK3/MK4**	**MK1/MK2/MK3/MK4**	**MK1/MK2/MK3/MK4**	**MK1/MK2/MK3/MK4**	**MK1/MK2/MK3/MK4**	**MK1/MK2/MK3/MK4**	**MK1/MK2/MK3/MK4**
NG1	0.49/0.22/0.62/0.40	**1.73**/1.48/1.54/1.56	0.14/-0.09/0.13/0.11	0.14/-0.09/0.13/0.11	-0.49/-0.68/-0.32/-0.38	1.00/0.79/0.92/0.91	0.16/0.12/0.20/0.14	1.00/0.79/0.92/0.91	0.51/0.56/1.35/0.45
NG2	0.87/0.65/1.36/0.82	1.08/0.48/0.92/0.87	0.11/0.04/0.11/0.11	0.11/0.04/0.11/0.11	0.67/0.82/0.59/0.71	-0.16/-0.11/-0.13/-0.15	0.50/0.53/0.59/0.47	-0.16/-0.11/-0.13/-0.15	0.85/0.91/1.04/0.86
NG3	1.27/1.00/1.27/1.20	-1.64/-1.31/-1.30/-1.25	**-2.54/-2.97/-3.17/-2.10**	**-2.54/-2.97/-3.17/-2.10**	**-1.98/-2.28/-2.42/-1.70**	-1.01/-1.00/-0.90/-0.79	-1.40/-1.58/**-1.77**/-1.30	-1.01/-1.00/-0.90/-0.79	-1.25/-1.27/-1.25/-1.20
NG4	-0.36/-0.56/-0.51/-0.34	**3.44/3.60/4.14/3.11**	**2.35/2.31/1.62/2.43**	**2.35/2.31**/1.62/**2.43**	**2.47/2.35/2.61/2.32**	-0.66/-0.80/-0.55/-0.78	-1.12/-1.01/-1.44/-1.09	-0.66/-0.80/-0.55/-0.78	-0.67/-0.33/-0.86/-0.57
NG5	-0.02/-0.25/-0.02/-0.02	0.73/0.38/0.56/0.63	-0.39/-0.51/-0.31/-0.42	-0.39/-0.51/-0.31/-0.42	-0.43/-0.55/-0.66/-0.47	-0.14/-0.41/-0.14/-0.15	-0.42/-0.52/-0.50/-0.42	-0.14/-0.41/-0.14/-0.15	0.33/0.20/0.28/0.32
NG6	**1.66**/1.39/**1.66**/1.61	0.96/0.45/0.64/0.70	-0.70/-0.91/-0.80/-0.71	-0.70/-0.91/-0.80/-0.71	-0.03/-0.19/-0.03/-0.02	-0.27/-0.32/-0.29/-0.23	-0.25/-0.44/-0.25/-0.23	-0.27/-0.32/-0.29/-0.23	-0.82/-0.85/-0.79/-0.80
NG7	0.78/0.45/0.78/0.75	-1.08/-0.85/-1.26/-0.95	**2.55/2.35/2.55/2.91**	**2.55/2.35/2.55/2.91**	**2.74/2.58/2.74/2.73**	**2.16/2.14/2.16/2.17**	**1.90/1.89/1.90/1.88**	**2.16/2.14/2.16/2.17**	0.27/0.63/0.31/0.30
NG8	0.49/0.30/0.44/0.42	**2.23/1.91**/1.44/1.58	-0.23/-0.41/-0.22/-0.22	-0.23/-0.41/-0.22/-0.22	0.46/0.26/0.41/0.50	0.01/-0.06/0.02/0.01	-0.17/-0.17/-0.17/-0.14	0.01/-0.06/0.02/0.01	0.30/0.17/0.30/0.29
NG9	**1.99/1.74/1.99/1.73**	-0.30/-0.43/-0.24/-0.23	1.02/0.86/1.14/1.07	1.02/0.86/1.14/1.07	**1.83/1.66/2.04/1.83**	**2.65/2.37/2.97/2.18**	**3.04/2.85/4.84/2.54**	**2.65/2.37/2.97/2.18**	1.24/1.15/1.24/1.15
NG10	1.19/0.94/1.02/1.02	**1.75**/1.49/**1.66**/1.42	1.45/1.32/1.34/1.20	1.45/1.32/1.34/1.20	**1.72/1.67/1.63**/1.59	**2.71/2.83/3.94/2.17**	**2.71/2.56/3.05/1.92**	**2.71/2.83/3.94/2.17**	**2.24/2.00/2.24/1.82**
NG11	0.67/0.33/0.57/0.58	**2.22/1.78**/1.42/**1.70**	1.39/1.20/1.48/1.40	1.39/1.20/1.48/1.40	1.25/1.02/1.35/1.30	1.52/1.15/**1.81**/1.27	**2.14/2.12/2.85/1.84**	1.52/1.15/1.81/1.27	1.14/1.18/1.31/1.05
NG12	**3.53/3.19/3.53/3.00**	**-3.33/-3.40/-2.44/-2.70**	-0.51/-0.76/-0.51/-0.50	-0.51/-0.76/-0.51/-0.50	0.70/0.51/0.74/0.70	**2.25/2.18/2.25/2.18**	**2.00/1.89/2.00/1.81**	**2.25/2.18/2.25/2.18**	0.88/0.62/1.09/0.81
VG1	-0.84/-1.15/-0.77/-0.81	0.67/0.75/0.61/0.62	**2.10/2.22/2.10/2.31**	**2.10/2.22/2.10/2.31**	**2.46/2.49/2.55/2.89**	0.44/0.34/0.44/0.48	0.39/0.42/0.39/0.38	0.44/0.34/0.44/0.48	0.35/0.47/0.67/0.32
VG2	-0.89/-1.14/-1.06/-0.88	**2.05/2.17/1.70/1.77**	**3.15/3.17/3.15/3.52**	**3.15/3.17/3.15/3.52**	**2.34/2.30/2.85/2.59**	1.12/1.08/1.12/1.11	0.28/0.54/0.32/0.27	1.12/1.08/1.12/1.11	-0.19/0.05/-0.31/-0.18
VG3	0.60/0.40/0.71/0.58	0.53/0.78/0.52/0.54	**1.99/2.18/2.68/2.32**	**1.99/2.18/2.68/2.32**	**2.15/2.28/2.81/2.63**	1.29/1.72/1.36/1.40	1.21/1.38/1.16/1.19	1.29/**1.72**/1.36/1.40	0.59/0.84/0.64/0.54
VG4	0.11/-0.12/0.12/0.10	**2.25/2.14/2.65/2.28**	**4.18/4.12/4.94/3.86**	**4.18/4.12/4.94/3.86**	**3.45/3.38/3.80/2.96**	**1.75**/1.52/1.44/1.62	**1.95/2.02/2.34/1.81**	**1.75**/1.52/1.44/**1.65**	0.66/0.87/0.76/0.65
VG5	0.76/0.66/1.11/0.67	**2.89/2.98/2.89/2.53**	**3.78/3.80/3.58/3.91**	**3.78/3.80/3.58/3.91**	**3.52/3.57/3.33/3.59**	1.20/1.42/1.46/1.28	0.40/0.56/0.55/0.39	1.20/1.42/1.46/1.28	0.23/0.50/0.35/0.21
VG6	1.47/1.27/1.47/1.39	1.07/1.34/1.07/1.15	1.02/1.23/1.48/1.27	1.02/1.23/1.48/1.27	1.50/1.29/2.14/1.81	0.48/0.84/0.60/0.59	0.69/1.12/0.70/0.75	0.48/0.84/0.60/0.59	0.60/0.80/0.60/0.58
VG7	1.40/1.24/1.40/1.31	**1.84/1.80/1.84/1.74**	**2.13/2.20/2.17/2.08**	**2.13/2.20/2.17/2.08**	1.46/1.58/1.91/1.24	1.40/1.58/1.87/1.42	1.17/1.36/1.14/1.14	1.40/1.58/1.87/1.42	0.58/0.76/0.75/0.53
VG8	0.87/0.75/11.02/0.80	0.42/0.46/0.42/0.43	**2.09/2.16/2.35/2.13**	**2.09/2.16/2.35/2.13**	**2.30/2.21/2.30/2.51**	0.43/0.55/0.39/0.41	0.46/0.69/0.41/0.46	0.43/0.55/0.39/0.41	0.57/0.81/0.65/0.55
VG9	-0.50/-0.76/-0.50/-0.48	**3.05/3.03/2.76/3.33**	1.20/1.36/**2.33**/1.53	1.20/1.36/2.33/1.53	0.85/0.86/1.08/1.03	0.40/0.50/0.51/0.48	-0.39/-0.16/-0.33/-0.42	0.40/0.50/0.51/0.48	-0.36/-0.16/-0.42/-0.38
VG10	**1.97/1.71/1.97/1.83**	-0.87/-1.11/-0.84/-0.75	-1.62/**-1.80/-1.99**/-1.58	-1.62/**-1.80/-1.99**/-1.58	-1.04/-1.10/-0.90/-1.06	0.81/0.83/0.97/0.70	1.13/1.17/1.13/0.93	0.81/0.83/0.97/0.70	**1.86/1.76/2.88/1.79**
VG11	1.34/1.04/1.34/1.28	**3.45/3.13/5.08/3.61**	-0.54/-0.48/-0.55/-0.51	-0.54/-0.48/-0.55/-0.51	-1.66/-1.55/-1.91/-1.65	**-1.76**/-1.23/**-1.87**/-1.51	-1.33/-1.01/-1.41/-1.20	**-1.76**/-1.23/**-1.87**/-1.51	0.58/0.59/0.59/0.57
VG12	1.03/0.81/1.03/0.97	0.52/0.33/0.53/0.54	-0.39/-0.33/-0.38/-0.37	-0.39/-0.33/-0.38/-0.37	-0.03/0.04/-0.03/-0.02	0.60/0.66/0.50/0.54	0.50/0.68/0.50/0.44	0.60/0.66/0.50/0.54	1.03/1.00/1.01/1.03
VG13	**1.79**/1.54/**1.79/1.84**	1.25/1.24/1.25/1.36	-0.96/-1.00/-0.96/-0.90	-0.96/-1.00/-0.96/-0.90	-0.39/-0.42/-0.39/-0.38	0.81/0.80/0.96/0.71	0.93/0.84/1.00/0.85	0.81/0.80/0.96/0.71	1.28/1.17/1.28/1.30
VG14	1.64/1.41/1.64/1.57	0.24/-0.05/0.24/0.26	-1.51/**-1.66/-1.72**/-1.46	-1.51/**-1.66/-1.72**/-1.46	-1.50/-1.44/-1.64/-1.41	-0.57/-0.35/-0.57/-0.51	-0.04/-0.11/-0.04/-0.04	-0.57/-0.35/-0.57/-0.51	0.88/0.89/1.10/0.82
VG15	1.26/1.04/1.86/1.23	0.56/0.20/0.56/0.60	-0.66/-0.78/-1.08/-0.68	-0.66/-0.78/-1.08/-0.68	-0.79/-0.60/-0.66/-0.73	0.19/0.31/0.20/0.18	0.30/0.45/0.30/0.27	0.19/0.31/0.20/0.18	**1.78/1.70/1.78/1.90**
VG16	0.78/0.53/0.85/0.86	2.20/2.00/2.83/2.21	-0.65/-0.73/-0.59/-0.63	-0.65/-0.73/-0.59/-0.63	-0.75/-0.75/-0.59/-0.68	-0.64/-0.35/-0.55/-0.52	-0.88/-0.81/-1.01/-0.79	-0.64/-0.35/-0.55/-0.52	0.47/0.51/0.67/0.47

Table A4. Z statistics of annual rainfall extremes of pre-1950

Grid Id	CDD	CWD	PRCPTOT	R10	R20	R40	R95	1Day	5day
	MK1/MK2/MK3/MK4	MK1/MK2/MK3/MK4	MK1/MK2/MK3/MK4	MK1/MK2/MK3/MK4	MK1/MK2/MK3/MK4	MK1/MK2/MK3/MK4	MK1/MK2/MK3/MK4	MK1/MK2/MK3/MK4	MK1/MK2/MK3/MK4
NG1	0.52/-0.04/0.74/0.41	2.25/1.96/2.25/2.1	1.14/0.94/1.14/1.41	0.41/0.45/0.41/0.45	1.35/1.06/1.87/1.52	0.14/0.38/0.22/0.19	-0.14/0.27/-0.22/-0.19	-0.8/-0.32/-0.8/-0.97	0.77/1.22/1.21/1
NG2	-0.08/-0.42/-0.08/-0.09	3.69/3.42/3.69/3.95	1.09/1.11/1.27/1.31	1.62/1.44/1.4/1.95	-0.29/-0.04/-0.45/-0.37	**-1.70/-1.59/-1.70/-1.67**	**-1.71/-1.78/-1.5/-1.82**	**-1.66/-0.85/-2.42/-1.94**	0.58/1.16/0.65/0.67
NG3	0.24/-0.2/0.24/0.24	-0.09/-0.06/-0.09/-0.09	0.35/0.09/0.35/0.39	0.68/0.25/0.59/0.67	0.28/0.09/0.28/0.3	0.93/0.40/0.93/0.82	0.23/0.01/0.23/0.23	-0.23/0.11/-0.74/-0.25	0.83/0.87/0.83/0.97
NG4	-0.28/-0.75/-0.35/-0.29	0/0.29/0/0	-0.17/-0.03/-0.15/-0.19	0.44/0.21/0.55/0.48	0/-0.08/0/0	0.05/0.16/0.05/0.06	-0.59/-0.44/-0.53/-0.62	-0.03/0.32/-0.02/-0.03	0.44/0.73/0.36/0.48
NG5	-0.38/-0.7/-0.53/-0.36	0.76/0.66/0.76/0.91	0.97/0.63/0.8/1.19	0.86/0.7/0.86/0.89	0.44/0.09/0.48/0.52	0.19/-0.22/0.19/0.22	-0.17/-0.13/-0.23/-0.18	-1.16/-1.2/-1.13/-1.1	0.44/0.15/0.43/0.43
NG6	0.33/-0.03/0.33/0.32	1.03/0.65/1.03/1.1	0.49/0.27/0.49/0.57	0.76/0.41/0.76/0.84	0.37/0.19/0.37/0.37	0.53/0.14/0.53/0.49	0.33/0.01/0.33/0.31	-0.72/-0.46/-3.51/-0.77	0.22/0.44/0.22/0.24
NG7	0.18/-0.25/0.18/0.17	1.06/1.14/1.55/1.01	0.18/0.09/0.18/0.21	0.65/0.3/0.65/0.77	0.9/0.7/0.96/1.04	0.42/0.41/0.53/0.40	0.15/0.18/0.18/0.14	-0.81/-0.32/-0.86/-1.02	0.55/1.13/0.59/0.62
NG8	0.28/-0.04/0.35/0.23	1.47/1.23/1.72/1.24	0.99/0.68/0.87/1.25	**1.79/1.53/2.34/1.88**	0.4/0.2/0.36/0.47	-0.39/-0.35/-0.39/-0.40	-0.69/-0.78/-0.69/-0.73	-1.21/-1.11/-1.56/-1.19	-0.01/-0.16/-0.01/-0.01
NG9	0.53/0.11/0.53/0.47	0.93/0.63/0.82/0.89	0.91/0.54/0.81/1.13	**1.89/1.54/1.89/2.16**	0.76/0.49/0.76/0.92	-0.36/-0.53/-0.36/-0.37	-0.67/-0.68/-0.65/-0.66	-1.3/-1.09/-1.67/-1.32	-0.16/-0.22/-0.21/-0.15
NG10	0.66/0.22/0.93/0.55	-0.4/-0.76/-0.58/-0.39	1.14/0.58/1.01/1.45	1.63/1.32/1.63/1.76	0.62/0.73/0.62/0.78	-0.26/-0.10/-0.26/-0.27	-0.36/-0.42/-0.36/-0.37	-1.46/-1.18/-1.46/-1.55	-0.13/-0.25/-0.13/-0.12
NG11	0.53/0.11/0.53/0.47	0.94/0.63/0.83/0.9	0.96/0.63/0.96/1.2	1.31/1.13/1.31/1.49	0.78/0.49/0.78/0.89	-0.64/-0.61/-0.64/-0.65	-0.49/-0.58/-0.49/-0.49	-1.38/-1.13/-1.81/-1.36	-0.28/-0.35/-0.36/-0.25
NG12	0.33/-0.06/0.33/0.36	0.73/0.36/0.73/0.76	0.64/0.13/0.64/0.52	0.95/0.77/0.95/1.01	0.27/-0.16/0.27/0.24	-0.29/-0.53/-0.34/-0.28	-0.49/-0.7/-0.49/-0.46	-0.72/-0.89/-1.31/-0.73	-0.31/-0.63/-0.31/-0.31
VG1	-0.38/-0.82/-0.38/-0.37	**-2.35/-1.92/-2.35/-2.5**	-0.02/-0.04/-0.02/-0.02	-0.23/-0.18/-0.33/-0.27	1.27/1.37/1.36/1.53	-0.14/-0.32/-0.14/-0.16	-0.35/-0.42/-0.35/-0.3	-1.15/-0.65/-1.43/-1.37	0.32/0.68/0.32/0.32
VG2	0.2/-0.13/0.27/0.22	**-2.39/-2.03/-2.39/-2.43**	0.27/0.3/0.27/0.28	-0.86/-0.85/-1.3/-0.99	1.33/1.44/1.44/1.54	0.26/0.30/0.24/0.23	-0.03/-0.01/-0.03/-0.03	0.03/0.47/0.03/0.03	0.83/1.18/0.83/0.84
VG3	1.27/0.82/1.73/1.37	-1.44/-1.34/-1.65/-1.54	0.22/0.28/0.22/0.23	0.01/-0.03/0.01/0.01	1.41/1.65/1.5/1.68	0.01/0.20/0.01/0.01	0.19/0.51/0.19/0.16	0.74/0.84/0.74/0.82	0.59/0.94/0.59/0.59
VG4	0/-0.32/0/0	1.02/1.28/1.19/1.21	0.79/0.56/0.79/0.88	1.04/0.66/1.11/1.15	1.51/1.65/1.62/1.73	-0.60/-0.71/-0.60/-0.54	-0.62/-0.46/-0.71/-0.56	0.03/0.47/0.03/0.04	1.19/1.44/1.52/1.32
VG5	1.26/0.84/1.79/1.39	-0.73/-0.44/-0.73/-0.7	-0.18/-0.06/-0.2/-0.2	0.36/0.23/0.39/0.45	0.73/1.2/1.03/0.89	0.31/0.26/0.31/0.30	-0.11/0.16/-0.11/-0.1	-0.08/0.03/-0.08/-0.1	0.13/0.49/0.13/0.13
VG6	2.09/1.56/2.97/2.38	-0.46/-0.25/-0.62/-0.5	-0.33/-0.23/-0.36/-0.38	0.09/0/0.09/0.09	0.34/0.08/0.54/0.36	-0.60/-0.27/-0.60/-0.64	-0.69/-0.39/-0.69/-0.74	-0.61/-0.2/-0.61/-0.6	-0.55/-0.3/-0.55/-0.52
VG7	0.48/0.09/0.51/0.54	1.37/1.44/1.37/1.5	0.75/0.8/0.75/0.72	**1.82/1.66/1.82/1.86**	-0.08/0/-0.07/-0.08	-0.36/-0.08/-0.36/-0.39	-0.8/-0.42/-0.8/-0.83	-1.46/-1.39/-1.46/-1.72	-0.64/-0.37/-0.64/-0.61
VG8	0.91/0.32/1.17/1.15	0.52/0.52/0.52/0.55	0.03/0.01/0.03/0.04	0.5/0.2/0.58/0.49	0.13/0.38/0.13/0.15	-0.53/-0.02/-0.53/-0.57	-0.17/0.01/-0.17/-0.19	-0.28/0.11/-0.28/-0.35	-0.34/-0.03/-0.34/-0.34
VG9	1.87/1.34/2/2.2	1.01/0.95/1.01/0.93	-0.07/0.16/-0.07/-0.08	0.55/0.37/0.55/0.64	-0.59/-0.75/-0.59/-0.72	-0.32/-0.09/-0.48/-0.42	-1.07/-0.68/-1.15/-1.16	-0.16/0.44/-0.13/-0.18	0.1/0.41/0.1/0.1
VG10	0.57/0.2/0.61/0.65	0.31/0.03/0.35/0.31	0.76/0.39/0.76/0.75	0.35/0.03/0.35/0.3	1.03/0.92/1.03/1.08	-0.25/-0.46/-0.20/-0.23	0.32/0.08/0.3/0.31	0.69/0.56/1.09/0.72	0.01/-0.11/0.01/0.01
VG11	0.49/0.01/0.67/0.54	1.23/0.7/1.17/1.5	0.64/0.61/0.64/0.6	1.34/1.08/1.48/1.45	0.38/0.51/0.38/0.37	-0.18/-0.22/-0.22/-0.16	0.18/0.13/0.24/0.17	1.39/1.47/1.83/1.76	0.62/0.68/0.62/0.61
VG12	0.87/0.32/0.94/0.97	1.33/0.82/1.33/1.61	0.64/0.61/0.64/0.59	1.02/0.65/1.02/1.1	0.47/0.5/0.52/0.46	-0.34/-0.17/-0.37/-0.30	0.07/-0.03/0.09/0.06	1.4/1.35/1.83/1.76	0.65/0.63/0.54/0.64
VG13	0.56/0.41/0.6/0.67	1.7/1.53/1.7/2.09	1/0.78/1/0.98	1.17/0.85/1.17/1.25	0.76/0.73/0.76/0.81	-0.15/-0.07/-0.15/-0.13	0.12/-0.11/0.12/0.1	1.3/1.28/1.3/1.48	1.25/1.09/1.25/1.16
VG14	-0.11/-0.52/-0.12/-0.13	0.03/-0.34/0.46/0.05	0.9/0.66/1.28/0.83	0.15/0.01/0.26/0.15	1.51/1.58/1.51/1.45	1.07/1.07/0.96/1.16	0.99/0.89/0.88/1.04	0.84/0.68/1.34/0.86	0.45/0.37/0.45/0.47
VG15	0.1/-0.18/0.11/0.11	-0.36/-1.11/-0.36/-0.41	0.64/0.58/0.64/0.6	1.32/1.04/1.32/1.43	0.02/0.13/0.01/0.02	0.51/0.47/0.55/0.47	0.62/0.54/0.57/0.58	1.59/1.73/1.59/1.84	0.66/0.66/0.72/0.67
VG16	0.1/-0.25/0.11/0.12	-0.12/-0.23/-0.12/-0.14	0.56/0.34/0.52/0.46	0.91/0.99/0.91/0.85	0.35/0.17/0.31/0.3	0.41/0.34/0.25/0.33	0.17/0.15/0.17/0.15	0.83/0.85/0.83/0.91	0.52/0.58/0.46/0.5

Table A5. Z statistics of annual rainfall extremes of post-1950

Grid Id	CDD MK1/MK2/MK3/MK4	CWD MK1/MK2/MK3/MK4	PRCPTOT MK1/MK2/MK3/MK4	R10 MK1/MK2/MK3/MK4	R20 MK1/MK2/MK3/MK4	R40 MK1/MK2/MK3/MK4	R95 MK1/MK2/MK3/MK4	1Day MK1/MK2/MK3/MK4	5day MK1/MK2/MK3/MK4
NG1	-1.07/-0.83/-1.09/-0.93	**-1.73/-1.8/-1.58/-1.69**	-0.35/0.15/-0.28/-0.25	-1.72/-1.57/-1.13/-1.19	-0.19/0.34/-0.09/-0.12	1.54/2.00/1.28/1.27	0.71/1.11/0.59/0.54	0.36/0.53/0.38/0.31	0.53/0.74/0.78/0.41
NG2	-0.02/0.34/-0.02/-0.02	**-2.16/-2.25/-2.16/-1.94**	-0.48/-0.16/-0.56/-0.43	-0.51/-0.54/-0.51/-0.47	0.54/0.73/0.54/0.53	1.46/1.50/1.46/1.38	1.07/1.33/1.07/1.02	0.35/0.21/0.35/0.3	-0.3/-0.23/-0.36/-0.29
NG3	0.28/0.61/0.23/0.25	**-2.83/-2.97/-3.48/-2.01**	**-3.24/-3.39/-2.87/-2.48**	**-2.65/-2.63/-2.19/-1.97**	**-2.06/-2.59/-2.41/-1.6**	**-2.24/-2.05/-1.81/-1.73**	**-1.75/-1.88/-1.75/-1.61**	**-2.01/-2.33/-3.28/-1.91**	**-2.32/-2.64/-2.54/-2.22**
NG4	-1.44/-1.11/-1.16/-1.36	**2.24/2/2.24/2.01**	1.39/1.46/1.39/1.36	**2.08/2.24/2.23/2.02**	1.42/1.94/1.57/1.2	-0.29/-0.42/-0.25/-0.34	-1.12/-1.07/-1.12/-1.07	-1.08/-1.1/-1.53/-0.79	-0.84/-1.19/-0.92/-0.6
NG5	-1.01/-0.68/-1.01/-0.87	**-2.09/-2.22/-2.32/-1.68**	-0.61/-0.29/-0.61/-0.63	-0.22/0.08/-0.26/-0.26	-0.1/0.08/-0.08/-0.11	0.30/0.17/0.35/0.29	-0.33/-0.52/-0.38/-0.3	**-1.66/-1.54/-2.14/-1.64**	-0.79/-0.95/-0.66/-0.78
NG6	0.01/0.27/0.01/0.01	**-4.15/-4.35/-4.43/-3.84**	**-2.24/-2.25/-2.24/-2.27**	-1.35/-1.43/-1.37/-1.52	-0.02/0/-0.02/-0.02	0.10/-0.12/0.11/0.08	0.09/-0.1/0.15/0.08	-0.28/-0.64/-0.27/-0.28	**-1.9/-2.26/-2.34/-1.89**
NG7	-0.82/-0.56/-0.82/-0.85	0.59/0.35/0.59/0.5	0.92/0.27/0.92/1.09	1.76/1.44/1.8/1.66	-0.85/-1.16/-0.85/-0.85	-0.88/-1.39/-0.88/-0.97	-0.87/-1.2/-0.87/-0.97	-1.45/-1.96/-1.46/-1.49	-0.53/-0.76/-0.45/-0.61
NG8	-0.42/-0.12/-0.42/-0.37	**-3.23/-3.5/-3.23/-2.78**	-1.59/-1.28/-1.45/-1.46	-1.2/-0.93/-1.19/-1.28	0.5/0.5/0.42/0.52	0.10/-0.06/0.13/0.07	0.08/0.24/0.1/0.06	-0.58/-0.74/-0.58/-0.61	-0.71/-1.03/-0.71/-0.71
NG9	-0.49/-0.28/-0.49/-0.44	**-2.59/-2.92/-1.67/-2.11**	-1.14/-1.28/-1.24/-1.18	**-2.19/-2.19/-1.88/-2.38**	0.34/0.12/0.34/0.3	0.41/-0.01/0.51/0.31	0.73/0.61/0.73/0.6	0.24/-0.01/0.24/0.2	-1.14/-1.53/-1.14/-1.13
NG10	-0.22/0.12/-0.22/-0.19	**-1.85/-2.19/-1.83/-1.6**	-0.7/-0.41/-0.7/-0.52	**-2.04/-1.81/-2.04/-1.78**	0.54/0.41/0.43/0.43	**1.84/2.02/2.35/1.39**	1.7/1.58/3.02/1.15	1.23/1.19/1.23/0.95	0.86/0.83/1.1/0.68
NG11	-1.14/-0.91/-1.14/-1.01	**-3.6/-3.69/-3.6/-3.46**	-0.67/-0.77/-0.67/-0.63	**-2.47/-2.28/-2.47/-2.45**	0.96/0.68/1.06/0.93	1.05/0.61/1.04/0.84	**1.92/1.85/1.96/1.57**	0.3/0.09/0.3/0.26	-0.34/-0.65/-0.34/-0.33
NG12	**2.1/2.34/2.1/1.65**	**-4.26/-4.28/-3.78/-3.63**	-0.76/-0.68/-0.76/-0.79	**-3.01/-2.91/-3.01/-2.8**	0.24/0.23/0.29/0.25	**2.87/2.50/4.39/2.96**	**2.94/2.77/4.1/2.87**	**2.11/1.73/2.11/1.97**	1.24/0.98/1.51/1.14
VG1	-1.35/-1.11/-1.12/-1.33	1.54/1.36/1.42/1.4	1.3/1.22/1.3/1.43	0.56/0.86/0.49/0.68	0.93/1/0.76/1.09	-0.11/-0.29/-0.11/-0.12	0.52/0.24/0.52/0.52	0.79/0.45/1.12/0.75	0.01/-0.31/0.01/0
VG2	-0.78/-0.37/-1.02/-0.72	1.61/**1.76**/1.61/1.45	1.27/1/1.27/1.48	0.74/0.61/0.74/0.92	0.93/0.69/0.93/1.01	0.97/0.74/0.97/1.04	0.59/0.23/0.51/0.61	0.35/0.01/0.35/0.35	-0.14/-0.5/-0.19/-0.13
VG3	0.31/0.62/0.31/0.29	0.58/0.65/0.69/0.58	0.98/0.93/0.98/1.19	1.16/1.35/1.96/1.62	0.73/1.04/0.73/0.91	0.50/0.60/0.50/0.60	0.95/0.69/0.95/1.01	1.31/1.07/1.24/1.07	0.02/-0.26/0.02/0.01
VG4	-0.71/-0.43/-0.71/-0.72	0.01/-0.03/0.01/0	1.32/1.24/1.49/1.15	1.25/1.21/1.38/1.05	0.66/0.57/0.64/0.51	0.16/-0.26/0.17/0.17	0.89/0.57/0.98/0.87	0.07/-0.31/0.09/0.07	0.17/-0.17/0.17/0.17
VG5	0.2/0.74/0.17/0.16	0.55/0.3/0.55/0.48	1.75/1.43/1.56/1.8	1.37/1.19/1.37/1.44	**2.09/1.89/1.77/1.98**	1.17/0.79/1.09/1.39	0.79/0.44/0.79/0.82	0.51/0.18/0.5/0.44	0.74/0.45/0.74/0.68
VG6	0.29/0.71/0.29/0.26	1.07/1.27/1.07/1.1	0.67/0.61/1.02/0.89	0.96/1.43/1.56/1.34	0.43/0.89/0.43/0.54	0.13/0.18/0.24/0.17	0.92/0.71/0.92/1.01	0.95/0.73/0.91/0.81	-0.13/-0.3/-0.13/-0.13
VG7	-0.19/0.22/-0.19/-0.16	0.09/-0.3/0.11/0.08	1.77/1.48/1.6/1.76	0.84/0.8/0.92/0.85	1.67/1.6/1.39/1.3	1.24/0.82/1.36/1.25	1.62/1.27/1.76/1.56	1.23/0.65/1.23/1.07	0.93/0.76/1.34/0.84
VG8	-0.64/-0.22/-0.45/-0.5	1.03/0.96/1.03/1.05	**2.08/1.82/2.71/2.06**	**2.4/2.15/3.32/2.55**	2.08/1.88/2.08/2.27	1.10/0.75/1.20/1.03	1.14/0.83/1.36/1.09	0.82/0.63/0.71/0.74	0.57/0.34/0.57/0.56
VG9	-0.35/0/-0.35/-0.32	1.03/1.08/1.03/1.21	0.78/0.63/1.41/1.02	**1.81/1.99/1.81/2.47**	0.58/0.58/0.58/0.71	0.91/0.93/0.91/1.07	0.25/0.01/0.25/0.28	0.12/-0.13/0.12/0.1	-1/-1.21/-1/-1.09
VG10	-0.65/-0.39/-0.65/-0.57	**-3.6/-3.87/-4.26/-3.02**	-0.15/-0.26/-0.15/-0.15	**-2.25/-2.12/-1.85/-2.3**	0.39/0.1/0.42/0.42	**1.66/1.73/1.66/1.49**	**2.63/2.46/3.37/2.17**	**2.97/2.67/2.97/2.6**	1.24/0.95/1.57/1.11
VG11	-0.02/0.26/-0.02/-0.01	1.07/0.87/1.07/1.06	1.58/1.22/**1.73/1.69**	1.43/1.26/1.43/1.7	0.62/0.44/0.69/0.67	0.81/0.43/1.08/0.77	1.4/1.13/1.79/1.32	1.17/0.91/1.17/1.24	1.42/1/1.42/1.52
VG12	-0.2/0.18/-0.17/-0.17	-0.82/-0.89/-0.75/-0.74	**1.91/1.61/2.54/1.99**	1.57/1.59/1.58/1.76	1.64/1.46/1.8/1.6	2.05/2.07/2.05/1.97	1.6/1.5/1.6/1.43	0.96/0.95/1.1/0.88	0.46/0.1/0.54/0.48
VG13	0.21/0.53/0.33/0.21	0.01/-0.06/0.01/0.01	1.02/0.87/1.02/1	1.28/1.33/1.47/1.37	0.73/0.68/0.92/0.69	1.42/1.46/1.42/1.33	1.46/1.34/1.46/1.39	0.46/0.64/0.58/0.4	0.54/0.21/0.63/0.58
VG14	0.77/1.1/0.77/0.69	**-2.25/-2.14/-2.25/-2.36**	-0.93/-0.77/-0.93/-0.93	**-2.51/-2.51/-2.84/-2.48**	-0.68/-0.58/-0.68/-0.68	0.41/0.65/0.41/0.33	0.89/1.23/0.89/0.71	**1.85/2.06/1.85/1.69**	0.89/0.97/0.89/0.78
VG15	0.12/0.47/0.13/0.12	-0.82/-0.92/-0.91/-0.86	0.92/0.77/1.16/1.04	1.18/1.34/1.18/1.45	0.57/0.56/0.53/0.52	0.99/0.90/1.11/0.92	1/1/1/0.9	0.77/0.9/0.77/0.84	1.11/0.9/1.15/1.29
VG16	0.4/0.53/0.36/0.43	-1.26/-1.49/-1.26/-1.3	1.6/1.2/**3.18/2.12**	**1.97/2.33/3.32/2.56**	1.05/0.83/1.03/1.06	1.33/1.26/1.40/1.34	1.23/1.01/1.28/1.31	1.12/1.26/1.17/1.19	0.5/0.26/0.53/0.56

Table A6. Z statistics of rainfall extremes for monsoon season

Grid Id	CDD	CWD	PRCPTOT	R10	R20	R40	R95	1Day	5Day
NG1	-0.18/-0.46/-0.18/-0.18	1.50/1.06/1.29/1.36	1.09/0.51/0.89/0.71	-0.53/-0.64/-0.39/-0.36	0.22/0.07/0.20/0.16	0.22/0.07/0.20/0.16	1.16/0.45/0.85/0.83	0.66/0.29/0.52/0.46	0.38/0.41/0.28/0.25
NG2	0.13/-0.23/0.13/0.14	0.93/0.28/0.81/0.76	0.18/-0.12/0.18/0.14	1.29/1.14/1.29/1.18	1.23/0.99/1.45/1.17	1.23/0.99/1.45/1.17	0.40/0.18/0.36/0.30	0.15/-0.01/0.11/0.11	0.43/0.45/0.46/0.34
NG3	**3.00/2.94/2.57/2.69**	**-1.98**/-1.63/-1.61/-1.56	**-2.63/-3.36/-2.50/-2.02**	**-2.59/-3.22/-2.01/-2.00**	**-2.22/-2.42/-2.69/-1.89**	**-2.22/-2.42/-2.69/-1.89**	**-1.92/-2.17/-1.92/-1.71**	**-1.95/-2.39/-2.44/-1.71**	**-2.17/-2.50/-2.71/-1.93**
NG4	-1.58/**-1.91/-2.65**/-1.36	**2.98/3.24/2.98/2.69**	**2.21/2.15/2.23/1.88**	**3.86/3.63/4.53/3.77**	**1.94/1.73/1.66/1.81**	**1.94/1.73/1.66/1.81**	**-1.84**/-1.63/**-2.90**/-1.56	-1.63/-1.56/**-2.16**/-1.37	-0.60/-0.62/-0.80/-0.55
NG5	-0.12/-0.24/-0.12/-0.12	0.95/0.45/0.85/0.78	**2.92/2.70/4.11/2.93**	0.38/0.22/0.45/0.41	0.46/0.19/0.46/0.51	**2.78/2.57/3.20/3.13**	-0.40/-0.64/-0.41/-0.42	-0.39/-0.48/-0.37/-0.38	0.72/0.78/0.66/0.70
NG6	1.31/1.18/1.60/1.15	1.19/0.78/0.82/0.88	-0.22/-0.45/-0.19/-0.23	-0.47/-0.76/-0.54/-0.48	0.17/-0.14/0.17/0.15	0.46/0.19/0.46/0.51	0.20/0.17/0.19/0.17	0.41/0.14/0.72/0.39	0.19/-0.08/0.18/0.19
NG7	-0.26/-0.41/-0.31/-0.24	-1.47/-1.15/-1.35/-1.42	-0.23/-0.59/-0.23/-0.22	**2.62/2.41/2.91/2.57**	**3.12/2.89/2.97/2.77**	0.17/-0.14/0.17/0.15	**1.86/1.72/2.20/1.66**	0.33/0.13/0.30/0.30	-0.47/-0.78/-0.62/-0.44
NG8	0.00/-0.08//0.00	**2.35/2.05**/1.47/1.62	**2.98/2.73/2.98/2.93**	1.37/1.20/**1.84**/1.37	1.28/0.99/1.19/1.32	**3.12/2.89/2.97/2.77**	-0.33/-0.26/-0.33/-0.26	0.12/0.07/0.12/0.12	1.02/0.93/1.57/1.00
NG9	0.72/0.52/0.84/0.65	-0.06/-0.37/-0.03/-0.04	**4.42/4.23/5.16/4.56**	-0.12/-0.44/-0.12/-0.12	**2.24/1.94/2.25/2.14**	**3.29/3.06/3.66/3.56**	**3.14/2.96/3.49/2.58**	**2.90/2.64/1.96/2.33**	0.58/0.79/0.47/0.63
NG10	0.97/0.83/0.97/0.89	**1.68**/1.27/**1.88**/1.36	**3.45/3.26/3.45/3.56**	1.27/1.00/1.27/1.21	**2.83/2.51/3.16/2.37**	**3.11/3.09/3.83/3.53**	**3.05/2.79/3.05/1.93**	**3.39/3.22/2.76/2.74**	0.58/0.94/0.49/0.55
NG11	-0.80/-0.93/-0.77/-0.85	**2.63/2.24/1.96/1.98**	0.57/0.44/0.54/0.51	0.38/0.03/0.38/0.35	**1.94/1.71/1.94/1.97**	1.28/0.99/1.19/1.32	**2.30/2.38/1.73/1.86**	**2.53/2.49/1.84/2.20**	0.97/0.83/0.97/0.92
NG12	**2.95/2.82/2.95/2.78**	**-3.36/-3.48/-2.45/-2.76**	**1.74**/1.45/**2.08/1.69**	**-1.79/-2.05/-1.80**/-1.59	0.36/0.04/0.36/0.35	**2.24/1.94/2.25/2.14**	1.63/1.42/1.39/1.41	**1.71**/1.47/**1.71**/1.55	**2.25/1.97/2.18/2.08**
VG1	**-1.76/-2.18/-2.24/-1.75**	0.08/0.29/0.07/0.07	**4.78/4.66/5.14/4.11**	**3.09/2.87/2.91/3.76**	**2.78/2.57/3.20/3.13**	**3.96/3.90/5.15/3.48**	1.03/0.85/1.03/0.92	-0.07/-0.24/-0.07/-0.07	**2.10/2.06/2.74/2.15**
VG2	**-2.45/-2.90/-2.72/-2.64**	**1.67/1.65**/1.42/1.43	**5.14/5.21/4.04/4.51**	**4.70/4.56/5.71/5.34**	**3.29/3.06/3.66/3.56**	**4.73/4.66/5.44/4.14**	**1.87/1.83/1.97/1.84**	-0.11/-0.18/-0.09/-0.11	**1.71/1.92/1.75/1.79**
VG3	-0.65/-0.95/-1.15/-0.66	0.56/0.76/0.50/0.58	**2.14/2.14/2.21/2.18**	**4.44/4.39/4.76/4.69**	**3.11/3.09/3.83/3.53**	**2.40/2.19/2.40/2.55**	**2.02/2.06/1.83/1.95**	0.65/0.82/0.47/0.65	0.34/0.65/0.28/0.33
VG4	-1.40/**-1.74**/-1.42/-1.41	**2.25/2.20/2.63/2.18**	**2.61/2.18/2.61/1.95**	**4.78/4.73/5.16/4.03**	**3.96/3.90/5.15/3.48**	**2.83/2.51/3.16/2.37**	**3.15/3.22/2.95/2.86**	1.49/1.34/1.63/1.47	**3.47/3.06/3.47/2.82**
VG5	-1.50/**-1.94/-1.74/-1.74**	**2.85/2.84/2.85/2.52**	**1.92/1.75/2.04/1.72**	**5.99/5.79/4.52/6.01**	**4.73/4.66/5.44/4.14**	**1.94/1.71/1.94/1.97**	**2.00/2.18/2.24/1.92**	0.80/0.89/0.79/0.73	**2.45/2.29/2.36/2.42**
VG6	0.64/0.40/0.78/0.60	0.63/0.84/0.67/0.71	**2.94/2.88/3.36/2.60**	**2.52/2.34/2.74/2.30**	**2.40/2.19/2.40/2.55**	**1.69/1.75**/1.58/1.36	0.43/0.65/0.45/0.43	1.13/1.40/1.16/1.13	**1.75/1.90/2.16/1.73**
VG7	-0.38/-0.62/-0.32/-0.40	**1.68**/1.62/1.56/1.54	**2.85/2.97/2.50/2.45**	**1.91/1.74/2.14/1.90**	**1.69/1.75/1.58/1.36**	**3.08/3.03/3.08/2.99**	**2.27/2.36/3.24/2.20**	**1.95/2.01/2.26/1.74**	1.51/**1.76**/1.64/1.55
VG8	0.43/0.19/0.59/0.41	0.12/0.19/0.13/0.12	**2.34/2.30/2.33/2.43**	**4.05/3.94/3.97/3.74**	**3.08/3.03/3.08/2.99**	1.22/1.11/1.30/1.22	**1.99/2.09/2.16/1.72**	1.44/1.63/1.67/1.27	0.59/0.75/0.62/0.62
VG9	-0.10/-0.14/-0.11/-0.09	**2.70/2.61/2.77/2.93**	-0.57/-0.80/-0.55/-0.54	**2.49/2.26/2.45/2.62**	1.22/1.11/1.30/1.22	0.36/0.04/0.36/0.35	0.42/0.69/0.41/0.40	0.62/0.91/0.62/0.61	1.17/0.86/1.43/1.05
VG10	**2.59/2.55/3.59/2.90**	-0.97/-1.26/-0.85/-0.87	-1.27/-1.63/-1.21/-1.17	**-3.92/-4.25/-3.42/-3.74**	-1.02/-1.23/-1.15/-1.04	-1.02/-1.23/-1.15/-1.04	**1.69**/1.57/**1.93**/1.37	**2.37/2.29/2.37/2.12**	**1.98/1.98/1.91/1.85**
VG11	**-2.36/-1.98/-1.91/-2.20**	**3.90/3.66/4.43/4.17**	0.42/0.40/0.46/0.36	0.21/0.11/0.36/0.20	-0.63/-0.58/-0.72/-0.60	-0.63/-0.58/-0.72/-0.60	-0.17/0.01/-0.16/-0.15	-0.13/-0.19/-0.13/-0.13	1.55/1.57/**1.93/1.69**
VG12	0.42/0.41/0.40/0.39	0.43/0.29/0.43/0.44	-0.66/-0.81/-0.68/-0.60	**-2.11/-2.20/-2.33/-2.02**	-0.11/0.08/-0.11/-0.10	-0.11/0.08/-0.11/-0.10	1.07/1.26/1.03/0.94	0.57/0.60/1.07/0.58	1.41/1.47/3.57/1.56
VG13	1.09/1.00/0.86/0.84	1.55/1.46/**1.80/1.67**	-1.02/-1.12/-1.00/-0.86	-0.95/-1.18/-1.04/-0.95	-0.33/-0.42/-0.33/-0.30	-0.33/-0.42/-0.33/-0.30	0.34/0.34/0.38/0.31	-0.16/-0.39/-0.18/-0.15	0.87/0.90/0.98/0.91
VG14	**2.35/2.38/1.94/2.34**	0.20/-0.15/0.20/0.22	-1.17/-1.41/-1.17/-1.10	**-1.92/-2.22/-1.93/-1.71**	-1.42/-1.54/-1.42/-1.28	-1.42/-1.54/-1.42/-1.28	0.13/0.13/0.13/0.11	1.35/1.27/1.35/1.24	0.87/0.94/0.87/0.79
VG15	-0.08/-0.01/-0.09/-0.08	1.00/0.75/1.10/1.07	0.37/0.31/0.41/0.35	0.37/0.23/0.71/0.38	-0.22/-0.27/-0.41/-0.21	-0.22/-0.27/-0.41/-0.21	0.73/0.69/0.74/0.66	0.21/0.28/0.20/0.23	**1.75/1.74/2.53/1.85**
VG16	-1.37/-1.17/-1.21/-1.31	**2.53/2.29/3.29/2.43**	0.16/0.07/0.18/0.15	0.81/0.69/0.64/0.86	-0.31/-0.27/-0.31/-0.30	-0.31/-0.27/-0.31/-0.30	-1.21/-1.01/-1.11/-1.10	-1.36/-1.33/-2.56/-1.46	0.63/0.69/0.97/0.67

Table A7. Z statistics of rainfall extremes for monsoon season of pre-1950

Grid Id	CDD	CWD	PRCPTOT	R10	R20	R40	R95	1Day	5day
	MK1/MK2/MK3/MK4	MK1/MK2/MK3/MK4	MK1/MK2/MK3/MK4	MK1/MK2/MK3/MK4	MK1/MK2/MK3/MK4	MK1/MK2/MK3/MK4	MK1/MK2/MK3/MK4	MK1/MK2/MK3/MK4	MK1/MK2/MK3/MK4
NG1	0.01/-0.28/0.01/0.01	**1.99/1.72/1.83/1.85**	-0.03/-0.66/-0.03/-0.04	-0.34/-0.59/-0.44/-0.35	0.15/-0.27/0.15/0.16	0.15/-0.27/0.15/0.16	-0.84/-1.15/-0.84/-0.94	-0.22/-0.78/-0.22/-0.25	-0.08/-0.51/-0.06/-0.09
NG2	-0.04/-0.62/-0.05/-0.05	**3.46/3.09/3.46/3.25**	-0.77/-1.27/-1.03/-0.91	0.59/0.23/0.94/0.69	-0.90/-1.70/-0.85/-1.10	-0.90/-1.70/-0.85/-1.10	-3.77/-4.32/-2.90/-3.60	**-3.59/-3.97/-5.07/-3.65**	-1.16/-1.35/-1.11/-1.17
NG3	0.73/0.43/0.73/0.67	-0.65/-0.55/-0.65/-0.55	-0.24/-0.68/-0.24/-0.26	-0.37/-0.74/-0.37/-0.39	0.00/-0.34/0.00/0.00	0.00/-0.34/0.00/0.00	-1.11/-1.42/-3.07/-1.13	-0.82/-1.25/-1.96/-0.89	-0.13/-0.46/-0.18/-0.13
NG4	-0.35/-0.70/-0.35/-0.28	-0.82/-0.79//-0.87	-0.64/-1.09/-0.64/-0.71	0.03/-0.37/0.02/0.03	-0.68/-1.32/-0.68/-0.75	-0.68/-1.32/-0.68/-0.75	-0.62/-0.67/-0.62/-0.58	-1.21/-1.35/-1.21/-1.15	-0.91/-0.91/-0.91/-1.01
NG5	0.05/-0.34/0.06/0.05	0.81/0.76/0.92/0.90	-0.03/-0.37/-0.03/-0.04	1.10/0.84/1.10/1.19	-0.19/-0.54/-0.19/-0.22	-0.19/-0.54/-0.19/-0.22	-1.85/-2.71/-1.45/-1.24	**-1.63/-2.13/-2.36/-1.92**	-0.53/-0.78/-0.53/-0.59
NG6	0.73/0.36/0.73/0.82	1.33/0.94/1.33/1.43	-0.17/-0.47/-0.17/-0.19	0.13/-0.15/0.13/0.15	0.34/-0.03/0.34/0.32	0.34/-0.03/0.34/0.32	-1.06/-0.91/-3.04/-1.02	-1.12/-1.41/-2.01/-1.28	-0.84/-1.22/-1.13/-0.88
NG7	-0.57/-1.07/-0.80/-0.67	1.07/1.11/1.07/1.08	-0.29/-0.66/-0.29/-0.34	0.15/-0.23/0.20/0.19	0.48/0.08/0.48/0.52	0.48/0.08/0.48/0.52	-1.57/-1.19/-1.57/-1.54	**-1.70/-2.01/-1.60/-1.54**	-1.14/-1.15/-1.55/-1.16
NG8	-0.33/-0.60/-0.33/-0.40	1.53/1.28/1.75/1.20	0.01/-0.27/0.01/0.01	1.14/0.68/1.49/1.20	-0.13/-0.35/-0.13/-0.15	-0.13/-0.35/-0.13/-0.15	-1.03/-1.74/-1.03/-1.19	**-1.86/-2.39/-1.86/-2.06**	-1.26/-1.73/-1.26/-1.47
NG9	-0.70/-0.63/-0.70/-0.66	0.69/0.43/0.69/0.58	0.12/-0.18/0.17/0.15	0.88/0.72/0.88/1.00	-0.03/-0.28/-0.03/-0.03	-0.03/-0.28/-0.03/-0.03	-1.70/-2.73/-1.70/-1.85	**-1.96/-2.46/-1.96/-2.10**	-1.29/-1.56/-1.29/-1.41
NG10	0.31/0.31/0.31/0.26	-0.61/-1.03/-0.61/-0.60	-0.57/-0.61/-0.57/-0.69	0.95/0.61/0.95/1.01	0.34/-0.02/0.34/0.38	0.34/-0.02/0.34/0.38	-2.11/-3.24/-2.11/-2.32	**-2.21/-2.51/-2.21/-2.31**	-1.30/-1.63/-1.30/-1.48
NG11	-0.67/-0.60/-0.67/-0.64	0.65/0.38/0.65/0.55	0.03/-0.25/0.05/0.04	0.88/0.62/0.88/0.99	0.31/0.24/0.31/0.36	0.31/0.24/0.31/0.36	-1.27/-2.00/-1.27/-1.47	**-1.82/-2.22/-1.82/-1.94**	-1.33/-1.65/-1.33/-1.49
NG12	-0.81/-0.73/-0.81/-0.78	0.64/0.27/0.64/0.66	0.33/-0.39/0.37/0.25	0.76/0.42/0.76/0.66	0.20/-0.45/0.19/0.17	0.20/-0.45/0.19/0.17	-0.64/-0.76/-0.95/-0.60	-0.79/-1.20/-1.13/-0.77	-0.72/-1.13/-0.72/-0.69
VG1	-0.21/-0.65/-0.21/-0.24	**-2.40/-1.98/-2.10/-2.91**	-0.38/-0.84/-0.43/-0.50	-0.48/-0.91/-0.58/-0.65	0.56/0.38/1.04/0.69	0.56/0.38/1.04/0.69	-1.77/-1.50/-1.69/-1.62	**-2.07/-2.28/-2.36/-1.90**	-1.27/-1.18/-1.27/-1.38
VG2	-0.27/-0.79/-0.27/-0.31	**-2.39/-2.18/-2.39/-2.81**	-0.28/-0.47/-0.31/-0.36	-0.96/-1.01/-1.14/-1.26	0.05/-0.31/0.05/0.06	0.05/-0.31/0.05/0.06	-1.25/-1.23/-1.19/-1.19	**-1.79/-2.06/-1.97/-1.68**	-0.98/-0.87/-0.98/-1.10
VG3	-0.62/-0.92/-0.62/-0.74	-1.62/-1.42/-1.62/-1.74	-0.54/-0.75/-0.60/-0.62	-1.05/-1.32/-1.23/-1.09	-0.21/-0.17/-0.29/-0.24	-0.21/-0.17/-0.29/-0.24	-1.78/-1.98/-1.48/-1.88	**-1.74/-1.37/-2.01/-1.92**	-1.28/-0.80/-1.28/-1.49
VG4	-1.11/-1.93/-0.94/-1.24	1.17/1.42/1.17/1.38	-0.03/-0.46/-0.03/-0.04	0.37/0.07/0.58/0.41	0.41/0.28/0.41/0.46	0.41/0.28/0.41/0.46	-1.22/-1.51/-1.47/-1.31	**-1.81/-1.96/-1.69/-1.77**	-0.95/-0.96/-0.95/-0.98
VG5	-0.14/-0.44/-0.19/-0.18	-0.89/-0.72/-0.89/-0.90	-0.74/-1.09/-0.79/-0.90	-0.42/-0.94/-0.57/-0.51	-0.60/-0.91/-0.60/-0.69	-0.60/-0.91/-0.60/-0.69	**-2.78/-1.85/-2.31/-2.43**	-2.07/-1.75/-2.58/-2.22	-1.41/-1.22/-1.41/-1.72
VG6	1.84/1.71/1.84/2.17	-0.75/-0.55/-0.75/-0.85	**-1.92/-1.87/-1.92/-2.10**	-1.29/-1.82/-1.29/-1.18	-1.10/-1.35/-1.61/-1.10	-1.10/-1.35/-1.61/-1.10	-1.19/-0.40/-1.19/-1.14	-1.25/-0.80/-1.12/-1.31	**-1.66/-1.72/-1.66/-1.89**
VG7	0.01/-0.47/0.01/0.01	1.34/1.45/1.34/1.51	0.30/-0.08/0.30/0.34	1.28/0.96/1.40/1.43	-0.63/-0.67/-0.66/-0.65	-0.63/-0.67/-0.66/-0.65	-2.18/-2.78/-2.18/-2.29	**-1.93/-1.92/-1.90/-1.93**	-1.08/-0.75/-1.08/-1.25
VG8	0.82/0.30/0.82/0.81	0.05/0.22/0.05/0.05	**-1.66/-1.75/-1.66/-2.09**	-0.50/-1.00/-0.50/-0.53	-0.95/-1.13/-0.95/-1.04	-0.95/-1.13/-0.95/-1.04	-2.47/-0.97/-2.08/-2.29	-1.36/-1.06/-1.88/-1.46	**-1.79/-1.51/-1.79/-2.10**
VG9	1.26/0.84/1.26/1.43	0.10/0.20/0.10/0.12	**-1.79/-1.80/-1.93/-2.17**	-0.70/-1.11/-0.70/-0.88	**-1.93/-2.19/-2.03/-2.14**	**-1.93/-2.19/-2.03/-2.14**	-1.50/-0.61/-1.41/-1.42	-1.42/-0.97/-1.55/-1.43	-1.47/-1.32/-1.47/-1.65
VG10	0.77/0.56/1.18/0.74	0.26/-0.15/0.28/0.26	0.22/-0.15/0.22/0.22	0.00/-0.48/0.00/0.00	0.83/0.58/0.83/0.88	0.83/0.58/0.83/0.88	0.22/0.27/0.22/0.22	-0.16/-0.34/-0.17/-0.16	-0.68/-0.65/-0.85/-0.71
VG11	0.39/0.34/0.54/0.33	0.76/0.72/0.71/0.92	-0.10/-0.35/-0.11/-0.11	-0.03/-0.47/-0.03/-0.04	0.03/0.22/0.03/0.03	0.03/0.22/0.03/0.03	0.03/-0.12/0.03/0.03	0.00/0.41/0.00/0.00	-0.67/-0.28/-0.67/-0.79
VG12	0.23/0.30/0.69/0.20	1.27/0.87/1.27/1.53	0.01/-0.30/0.01/0.01	0.18/-0.09/0.27/0.19	0.38/0.32/0.38/0.37	0.38/0.32/0.38/0.37	0.23/0.17/0.23/0.27	0.03/0.30/0.03/0.03	-0.65/-0.25/-0.85/-0.77
VG13	0.44/0.72/0.44/0.35	1.07/0.87/1.07/1.27	-0.03/-0.32/-0.03/-0.03	0.03/-0.50/0.03/0.03	0.44/0.03/0.44/0.43	0.44/0.03/0.44/0.43	-0.19/-0.41/-0.21/-0.20	0.20/-0.03/0.22/0.22	-0.88/-0.61/-0.88/-0.94
VG14	0.61/0.57/0.61/0.54	0.02/-0.54/0.02/0.02	0.85/0.37/1.13/0.76	-0.34/-0.72/-0.50/-0.30	1.36/1.06/1.43/1.26	1.36/1.06/1.43/1.26	0.90/1.15/0.90/0.90	0.61/0.37/0.61/0.60	0.02/-0.01/0.02/0.02
VG15	0.65/0.68/0.82/0.63	-0.18/-0.56/-0.18/-0.21	0.38/0.03/0.62/0.40	0.74/0.37/0.75/0.75	-0.29/-0.49/-0.29/-0.31	-0.29/-0.49/-0.29/-0.31	0.31/0.30/0.33/0.32	0.47/0.80/0.51/0.54	-0.58/-0.28/-0.65/-0.65
VG16	1.11/1.13/1.11/1.25	0.00/-0.12/0.00/0.00	0.00/-0.06/0.00/0.00	0.28/0.31/0.28/0.27	0.05/-0.11/0.05/0.05	0.05/-0.11/0.05/0.05	-0.18/-0.24/-0.18/-0.20	0.08/0.32/0.15/0.09	-0.53/0.15/-0.82/-0.62

Table A8. Z statistics of rainfall extremes for monsoon season of post-1950

Grid Id	CDD	CWD	PRCPTOT	R10	R20	R40	R95	1Day	5day
	MK1/MK2/MK3/MK4	MK1/MK2/MK3/MK4	MK1/MK2/MK3/MK4	MK1/MK2/MK3/MK4	MK1/MK2/MK3/MK4	MK1/MK2/MK3/MK4	MK1/MK2/MK3/MK4	MK1/MK2/MK3/MK4	MK1/MK2/MK3/MK4
NG1	0.30/0.56/0.30/0.29	**-1.76/-1.80/-1.59/-1.76**	0.12/0.11/0.07/0.07	-1.61/-1.57/-0.97/-0.96	0.53/0.78/0.28/0.34	0.53/0.78/0.28/0.34	0.17/0.29/0.14/0.10	1.03/1.01/0.80/0.64	1.73/1.98/1.36/1.10
NG2	0.40/0.30/0.53/0.40	**-2.13/-2.21/-2.13/-1.96**	-0.84/-1.00/-0.84/-0.60	-0.79/-0.71/-0.79/-0.66	0.44/0.41/0.44/0.38	0.44/0.41/0.44/0.38	-0.12/0.26/-0.15/-0.07	-0.18/0.03/-0.16/-0.13	-0.68/-0.33/-1.30/-0.50
NG3	**2.57/2.94/2.57/2.32**	**-2.92/-2.81/-2.92/-2.34**	**-3.35/-3.91/-3.39/-2.16**	**-2.59/-2.74/-1.79/-1.64**	**-2.22/-2.28/-2.22/-1.77**	**-2.22/-2.28/-2.22/-1.77**	**-2.57/-1.75/-1.80/-1.93**	**-3.17/-3.33/-3.17/-2.79**	**-3.09/-3.24/-3.27/-2.72**
NG4	-1.22/-1.05/-2.85/-1.09	1.21/0.79/1.00/1.00	1.11/1.57/1.11/0.80	**1.92/2.28/1.92/1.75**	0.60/0.84/0.49/0.47	0.60/0.84/0.49/0.47	**-2.11/-0.35/-1.96/-1.61**	**-1.76/-1.27/-1.86/-1.42**	-1.07/-0.87/-1.14/-0.86
NG5	0.20/0.48/0.20/0.19	**-2.23/-2.29/-2.73/-1.82**	-1.20/-1.26/-0.87/-1.10	-1.02/-0.88/-1.28/-1.13	-0.34/-0.33/-0.34/-0.36	-0.33/-0.33/-0.33/-0.36	-1.29/-0.61/-1.19/-0.97	-0.84/-0.93/-1.01/-0.72	-0.68/-0.77/-0.68/-0.57
NG6	0.23/0.49/0.22/0.17	**-3.73/-3.92/-3.98/-3.41**	**-2.69/-2.55/-2.69/-2.28**	**-2.57/-2.52/-2.57/-2.74**	-0.31/-0.37/-0.31/-0.28	-0.31/-0.37/-0.31/-0.28	-0.08/-0.33/-0.08/-0.07	-0.06/-0.39/-0.06/-0.05	**-1.95/-2.18/-1.95/-1.80**
NG7	**-2.79/-2.46/-2.79/-2.40**	0.56/0.27/0.56/0.54	0.20/-0.01/0.25/0.19	1.77/1.63/1.77/1.46	-0.64/-0.71/-0.58/-0.54	-0.64/-0.71/-0.58/-0.54	-1.49/-2.46/-1.94/-1.54	-0.96/-1.29/-0.94/-0.97	-0.92/-1.32/-0.99/-0.95
NG8	0.04/0.00/0.06/0.04	**-3.22/-3.50/-3.22/-2.82**	-1.64/-1.56/-1.36/-1.31	-1.17/-0.99/-1.40/-1.21	0.15/0.09/0.15/0.15	0.15/0.09/0.15/0.15	-0.05/0.02/-0.05/-0.03	-0.24/-0.43/-0.24/-0.23	-0.87/-0.86/-0.87/-0.80
NG9	-0.03/-0.30/-0.04/-0.02	**-2.30/-2.68/-1.29/-1.69**	**-1.81/-2.06/-1.81/-1.71**	**-2.67/-2.46/-2.67/-2.76**	-0.70/-0.84/-0.70/-0.62	-0.70/-0.84/-0.70/-0.62	0.42/0.27/0.45/0.35	0.40/0.28/0.44/0.33	-1.17/-1.50/-1.23/-1.13
NG10	0.42/0.37/0.42/0.41	**-1.85/-2.05/-1.83/-1.61**	-0.33/-0.51/-0.34/-0.23	-1.64/-1.40/-1.64/-1.54	0.72/0.25/0.73/0.54	0.72/0.25/0.73/0.54	2.05/0.77/1.65/1.11	**2.01/1.72/2.01/1.62**	0.81/0.68/0.81/0.63
NG11	0.05/0.09/0.05/0.06	**-3.24/-3.26/-4.04/-3.15**	-1.12/-1.29/-1.14/-0.88	**-2.35/-2.19/-2.35/-2.18**	-0.37/-0.61/-0.40/-0.35	-0.37/-0.61/-0.40/-0.35	1.44/1.17/1.44/1.28	1.01/0.93/0.82/0.85	-0.06/-0.41/-0.06/-0.06
NG12	**3.23/3.16/4.42/3.28**	**-4.25/-4.32/-3.75/-3.70**	-0.23/-0.36/-0.23/-0.23	**-2.95/-2.76/-2.95/-2.90**	0.35/0.14/0.42/0.37	0.35/0.14/0.42/0.37	**2.59/1.67/2.59/2.19**	**2.50/2.15/2.50/2.31**	1.42/1.20/1.42/1.29
VG1	-0.64/-0.16/-1.35/-0.50	0.78/0.99/1.05/0.65	0.87/0.86/0.94/0.75	**1.75/1.63/1.75/1.96**	0.70/0.86/0.61/0.74	0.70/0.86/0.61/0.74	-0.83/-0.43/-0.83/-0.67	0.72/0.52/0.72/0.68	0.54/0.50/0.54/0.50
VG2	**-2.52/-2.17/-2.52/-2.47**	1.46/1.69/1.46/1.31	1.38/1.01/1.49/1.35	1.43/1.36/1.43/1.64	0.87/0.83/0.87/0.88	0.87/0.83/0.87/0.88	0.09/-0.44/0.09/0.10	0.90/0.56/0.90/0.93	0.11/-0.04/0.11/0.12
VG3	0.12/0.52/0.10/0.10	0.07/0.05/0.06/0.08	**1.70/1.50/1.70/1.70**	**2.80/2.62/2.80/3.30**	1.62/1.98/1.62/1.85	1.62/1.98/1.62/1.84	1.01/0.91/1.18/0.95	1.24/1.10/1.24/1.21	0.80/0.96/0.76/0.69
VG4	-1.41/-1.15/-1.46/-1.30	-0.20/-0.09/-0.23/-0.18	1.22/1.08/1.15/0.93	0.81/0.65/0.77/0.63	0.56/0.17/0.72/0.45	0.56/0.17/0.72/0.45	0.42/0.33/0.42/0.40	0.58/0.21/0.58/0.61	0.41/0.08/0.45/0.43
VG5	-1.37/-1.13/-1.37/-1.37	0.33/0.04/0.30/0.29	**2.14/1.80/2.39/1.70**	**2.19/1.97/1.60/2.21**	**2.24/2.09/1.97/1.83**	**2.24/2.09/1.97/1.83**	1.60/1.01/1.60/1.42	**1.87/1.84/2.05/1.72**	**1.73/1.45/1.93/1.74**
VG6	0.53/0.68/0.60/0.47	0.35/0.51/0.35/0.40	**1.87/1.84/2.50/1.98**	**2.51/2.47/2.67/2.57**	**1.94/2.18/1.94/2.19**	**1.94/2.18/1.94/2.19**	-0.20/-0.80/-0.20/-0.22	0.61/0.38/0.61/0.62	0.52/0.50/0.52/0.48
VG7	-0.35/-0.03/-0.35/-0.39	-0.37/-0.75/-0.37/-0.32	1.51/1.19/1.69/1.20	0.18/0.02/0.18/0.17	1.63/1.57/1.47/1.13	1.63/1.57/1.47/1.13	1.58/1.17/1.58/1.35	**2.32/2.09/2.32/2.17**	1.63/1.34/1.79/1.57
VG8	-0.37/0.01/-0.43/-0.34	0.51/0.47/0.67/0.55	**2.51/2.49/2.51/2.01**	**2.53/2.32/2.53/2.28**	**2.11/2.08/2.31/1.99**	**2.11/2.08/2.31/1.99**	1.71/1.29/1.71/1.55	1.57/1.46/1.57/1.37	**2.04/1.74/2.08/2.12**
VG9	0.74/0.90/0.70/0.59	0.09/0.21/0.09/0.09	**2.05/1.95/2.05/2.08**	**2.54/2.70/2.44/2.51**	1.57/1.58/1.57/1.65	1.57/1.57/1.57/1.65	-0.23/-0.70/-0.23/-0.28	0.51/0.55/0.51/0.51	0.41/0.27/0.41/0.43
VG10	**1.74/1.66/1.74/2.08**	**-3.27/-3.45/-3.74/-2.97**	0.30/0.17/0.39/0.27	**-2.38/-2.29/-2.38/-2.36**	0.15/-0.21/0.16/0.15	0.15/-0.21/0.16/0.15	**3.13/3.23/3.13/2.55**	**3.29/2.98/3.29/2.95**	**2.00/1.71/2.00/1.84**
VG11	-1.14/-1.05/-1.63/-1.14	1.38/1.25/1.47/1.42	1.46/1.34/1.23/1.10	0.05/-0.24/0.06/0.04	1.15/0.79/1.46/1.12	1.15/0.78/1.45/1.12	1.68/1.15/1.68/1.58	1.39/1.21/1.39/1.39	**2.10/1.68/2.10/2.19**
VG12	-0.72/-0.42/-0.72/-0.66	-0.78/-0.79/-0.78/-0.69	**1.78/1.76/1.78/1.59**	0.16/0.15/0.15/0.15	1.60/1.46/1.60/1.46	1.60/1.46/1.60/1.46	0.92/0.93/1.65/0.86	1.49/1.60/2.29/1.45	1.51/1.29/1.97/1.60
VG13	0.17/0.31/0.23/0.13	-0.44/-0.51/-0.49/-0.46	1.38/1.26/1.38/1.06	0.83/0.63/0.83/0.76	0.85/0.62/0.85/0.77	0.85/0.62/0.85/0.77	1.18/0.85/1.18/1.16	0.97/1.23/0.97/0.83	1.45/1.46/1.45/1.50
VG14	**2.02/1.95/1.62/2.12**	**-2.16/-2.02/-1.93/-2.28**	-1.53/-1.38/-1.53/-1.49	-2.64/-2.82/-2.64/-2.56	-0.94/-0.81/-0.94/-0.85	-0.94/-0.81/-0.94/-0.85	1.81/1.50/1.81/1.53	1.45/1.65/1.45/1.29	0.52/0.54/0.52/0.44
VG15	-0.28/-0.14/-0.28/-0.28	-1.01/-1.06/-1.12/-1.05	-0.45/-0.18/-0.45/-0.38	-0.39/-0.30/-0.39/-0.40	-0.26/-0.09/-0.32/-0.23	-0.26/-0.09/-0.32/-0.22	-0.36/-0.08/-0.36/-0.33	-0.66/-0.57/-0.66/-0.68	-0.07/-0.23/-0.07/-0.07
VG16	-1.19/-0.79/-1.19/-1.04	-1.25/-1.39/-1.03/-1.20	0.69/0.40/0.99/0.67	1.16/1.03/1.16/1.33	0.52/0.27/0.67/0.49	0.52/0.27/0.67/0.49	-0.63/-0.64/-0.63/-0.67	-0.89/-0.76/-0.84/-0.89	-0.39/-0.55/-0.57/-0.37

Table A9. Z statics of monthly rainfall trend analysis from January to December

Grid Id	Jan	Feb	March	April	May	June	July	Aug	Sep	Oct	Nov	Dec
	MK1/MK2/MK3/MK4	MK1/MK2/MK3/MK4	MK1/MK2/MK3/MK4	MK1/MK2/MK3/MK4	MK1/MK2/MK3/MK4	MK1/MK2/MK3/MK4	MK1/MK2/MK3/MK4	MK1/MK2/MK3/MK4	MK1/MK2/MK3/MK4	MK1/MK2/MK3/MK4	MK1/MK2/MK3/MK4	MK1/MK2/MK3/MK4
NG1	-0.43/-0.49/-0.45/-0.43	-1.58/-0.98/-1.23/-1.49	0.94/1.32/0.90/0.98	-0.32/-0.37/-0.32/-0.37	-0.08/0.25/-0.11/-0.09	1.01/0.95/1.42/0.94	**2.67/2.90/3.10/2.44**	0.85/0.56/0.97/0.70	-0.04/-0.11/-0.04/-0.03	-0.65/-0.71/-0.65/-0.67	-0.72/-0.77/-3.88/-0.65	0.01/-0.64/0.01/0.01
NG2	-0.16/-0.03/-0.19/-0.16	**-1.77/-1.17/-1.74/-1.66**	0.82/1.23/1.09/0.90	-0.02/0.04/-0.02/-0.03	0.26/0.50/0.36/0.28	1.04/0.74/1.00/0.94	**1.83/2.25/3.25/1.78**	-0.13/-0.35/-0.21/-0.12	-0.89/-1.05/-0.74/-0.77	-0.34/-0.30/-0.32/-0.35	0.02/0.12/0.03/0.02	-0.04/-0.08/-0.03/-0.04
NG3	-0.55/-0.41/-0.71/-0.56	**-1.76**/-0.63/-1.56/-1.57	0.76/1.07/0.80/0.80	-1.21/-1.27/-1.27/-1.32	0.28/0.30/0.28/0.31	-1.24/-1.49/-1.45/-1.13	-0.99/-1.02/-0.99/-1.17	**-2.62/-2.97/-2.43/-2.51**	**-2.01/-2.06/-2.01/-1.72**	-0.51/-0.51/-0.48/-0.50	0.11/0.41/0.14/0.10	0.53/0.66/0.52/0.55
NG4	0.04/0.26/0.06/0.04	-0.59/-0.43/-0.69/-0.58	1.43/**1.95**/1.52/1.44	**1.95/1.68/1.67/2.04**	**1.71/1.96**/1.54/**1.86**	**2.18/1.93/2.43/2.24**	**2.48/2.76/3.07/2.46**	1.18/0.86/1.43/1.15	-0.40/-0.45/-0.42/-0.40	0.39/0.35/0.41/0.41	0.75/1.23/0.76/0.72	1.02/0.93/1.02/1.06
NG5	-0.39/-0.35/-0.56/-0.40	-1.30/-0.88/-1.60/-1.22	1.01/1.46/1.03/1.07	-0.81/-0.67/-1.74/-0.86	-1.04/-0.58/-1.30/-1.17	0.65/0.39/0.56/0.64	1.44/1.55/1.44/1.23	-1.03/-1.35/-0.90/-1.12	0.27/0.11/0.29/0.25	-0.26/-0.22/-0.25/-0.25	-0.51/-0.28/-0.66/-0.51	0.53/0.24/0.53/0.57
NG6	-0.72/-1.04/-0.80/-0.74	-1.49/-0.96/-1.36/-1.34	0.63/1.05/0.59/0.67	-0.71/-0.68/-0.81/-0.77	0.16/0.33/0.16/0.18	0.33/0.11/0.40/0.30	**1.88/2.09/1.88**/1.60	-1.14/-1.43/-1.14/-1.10	-1.25/-1.50/-1.22/-1.12	0.03/0.05/0.03/0.04	-0.38/-0.14/-0.51/-0.35	-0.08/-0.28/-0.08/-0.09
NG7	-0.76/-0.26/-0.78/-0.74	-0.52/-0.32/-0.67/-0.46	1.36/**1.74**/1.36/1.44	1.23/1.23/1.51/1.33	1.30/**1.68**/1.42/1.51	**1.94/1.80/2.17/1.83**	**3.02/3.44/2.63/2.91**	1.30/1.02/3.17/1.39	-0.11/-0.20/-0.12/-0.10	0.50/0.46/0.61/0.53	-0.70/-0.05/-0.70/-0.63	-0.54/-0.46/-0.44/-0.56
NG8	-0.49/-0.24/-0.53/-0.52	-1.50/-0.93/-1.54/-1.39	1.44/1.60/**1.70**/1.49	-0.34/-0.27/-0.66/-0.38	**-2.09/-1.92/-2.84/-2.24**	0.53/0.42/0.46/0.48	**2.41/2.59/2.07/2.29**	0.02/-0.19/0.02/0.02	-0.39/-0.43/-0.48/-0.34	-0.68/-0.59/-0.62/-0.66	-1.01/-0.80/-1.47/-1.02	0.27/-0.03/0.24/0.29
NG9	-0.74/-0.70/-0.98/-0.76	-1.63/-1.24/-1.70/-1.49	1.27/1.38/1.28/1.29	0.48/0.48/0.58/0.52	0.30/0.56/0.35/0.33	0.90/0.69/0.90/0.85	**3.86/3.79/4.31/3.65**	0.53/0.29/0.56/0.51	**-1.91/-2.07/-2.02/-1.70**	-0.94/-0.86/-0.94/-0.94	-0.73/-0.39/-1.02/-0.72	-0.44/-0.74/-0.63/-0.48
NG10	-0.13/0.08/-0.15/-0.13	**-1.80**/-1.38/-2.73/-1.64	0.94/0.99/0.97/0.85	0.00/0.13/0.00/0.00	**-2.44/-2.31/-4.04/-2.44**	0.76/0.51/0.65/0.71	**4.05/4.48/4.41/3.99**	1.48/1.20/1.23/1.02	-0.41/-0.53/-0.46/-0.37	-1.54/-1.37/-1.42/-1.41	-1.27/-1.06/-1.66/-1.28	-0.10/-0.54/-0.10/-0.11
NG11	-0.15/0.11/-0.23/-0.16	-1.08/-0.78/-1.08/-0.98	**1.82/1.96/2.42/1.80**	0.50/0.61/0.72/0.56	-0.16/0.03/-0.29/-0.16	1.00/0.95/1.00/0.93	**3.55/3.54/3.55/3.33**	1.25/0.99/1.34/1.11	-1.53/-1.69/-1.53/-1.43	-0.96/-0.89/-0.96/-0.94	-0.67/-0.29/-0.91/-0.66	0.07/-0.06/0.07/0.07
NG12	-0.67/-0.09/-0.67/-0.65	**-2.72/-2.04/-3.50/-2.23**	0.29/0.31/0.38/0.25	0.31/0.68/0.31/0.29	0.79/0.97/0.99/0.79	-1.08/-1.34/-1.08/-1.15	0.15/0.14/0.15/-0.11	-1.52/-1.61/-1.52/-1.26	-0.15/-0.25/-0.18/-0.16	-0.41/-0.29/-0.45/-0.39	-1.51/-0.71/-**1.98**/-1.44	**-1.65/-2.63/-1.65/-1.77**
VG1	-0.30/0.44/-0.35/-0.28	-0.14/0.10/-0.26/-0.14	0.42/0.22/0.42/0.38	1.16/0.92/1.18/1.22	1.45/**1.91/1.82/1.69**	**1.77**/1.62/**1.77/1.70**	**2.11/2.55/1.81/2.24**	1.80/1.62/2.05/1.89	0.13/0.13/0.18/0.13	0.54/0.48/0.56/0.54	0.55/0.94/0.55/0.51	0.29/0.10/0.23/0.30
VG2	0.26/0.47/0.26/0.24	0.03/0.14/0.03/0.03	1.23/0.87/1.08/1.21	1.54/1.35/1.58/1.64	**2.04/2.44/2.04/2.36**	**2.35/2.21/2.35/2.18**	**3.91/4.69/3.42/3.72**	**3.08/2.90/2.77/3.23**	1.08/1.17/1.35/1.11	0.50/0.46/0.52/0.51	0.20/0.81/0.20/0.18	-0.40/-0.54/-0.44/-0.42
VG3	0.39/0.46/0.39/0.38	-0.99/-0.55/-0.99/-0.90	0.86/0.45/0.90/0.85	0.55/0.40/0.44/0.59	1.35/**1.83/2.17**/1.49	1.64/1.50/1.64/1.62	**2.63/3.10/2.63/2.75**	**1.92**/1.62/1.60/1.60	0.72/0.96/0.97/0.77	0.63/0.53/0.65/0.64	0.41/0.69/0.41/0.38	0.19/0.15/0.18/0.20
VG4	0.05/0.30/0.04/0.04	-0.44/-0.33/-0.41/-0.37	**2.48/2.53/2.18/2.29**	**2.52/2.48/2.91/2.62**	**3.06/3.18/3.15/3.28**	**3.33/3.10/3.16/3.02**	**4.58/4.32/3.86/4.47**	**2.20/1.94/2.54/2.17**	-0.12/-0.16/-0.11/-0.12	0.34/0.37/0.35/0.34	-0.50/0.01/-0.50/-0.46	-0.50/-0.66/-0.42/-0.52
VG5	0.15/0.50/0.15/0.15	-0.36/0.01/-0.39/-0.31	**2.38/2.46/1.86/2.16**	**2.45/2.09/1.99/2.77**	**2.82/2.89/2.82/2.91**	**3.11/3.13/3.11/2.84**	**4.33/4.29/6.58/4.19**	**3.25/3.05/3.25/2.93**	0.71/0.84/0.78/0.77	0.47/0.40/0.49/0.48	-0.36/0.02/-0.36/-0.34	-1.09/-1.49/-1.81/-1.15
VG6	0.49/0.46/0.49/0.48	-1.43/-0.58/-1.43/-1.23	0.50/0.67/0.50/0.52	-0.14/-0.77/-0.11/-0.15	0.70/1.08/0.89/0.76	0.89/0.79/1.11/0.97	1.51/1.59/1.51/1.37	**1.67**/1.37/**1.79**/1.51	-0.25/-0.06/-0.25/-0.27	0.45/0.37/0.58/0.48	0.13/0.43/0.13/0.13	-0.61/-1.02/-0.58/-0.65
VG7	-0.29/-0.52/-0.23/-0.31	-0.96/-0.90/-0.82/-0.98	**1.98/1.94/1.93/1.79**	1.26/1.31/1.16/1.28	**2.58/2.72/2.64/2.58**	**1.80/1.66/2.28/1.77**	**2.78/2.62/3.22/2.88**	1.58/1.33/1.58/1.58	-0.88/-0.90/-0.97/-0.96	-0.07/-0.18/-0.07/-0.07	-0.91/-0.41/-0.91/-0.82	-1.11/-1.57/-1.11/-1.18
VG8	-0.30/-0.57/-0.27/-0.31	-1.02/-0.63/-0.86/-0.94	**2.53/2.70/2.46/2.31**	1.26/0.99/1.07/1.33	**2.07/2.21**/1.56/**2.05**	1.48/1.38/1.55/1.57	**2.38/2.22/2.55/2.26**	**1.79**/1.58/**1.92/1.69**	-0.23/0.12/-0.25/-0.25	0.06/-0.04/0.06/0.06	-1.00/-0.73/-1.00/-0.97	-0.99/-**1.97**/-0.99/-1.06
VG9	0.43/0.57/0.44/0.39	-0.96/-0.31/-0.81/-0.79	1.61/1.58/1.61/1.60	0.71/0.36/0.66/0.82	1.57/**1.90/2.27/1.70**	**1.65**/1.46/**2.00/1.80**	**1.96/1.74/2.11/1.86**	1.59/1.38/**1.72/1.65**	-0.64/-0.43/-0.84/-0.72	0.26/0.06/0.27/0.28	-0.19/0.05/-0.19/-0.19	-0.65/-1.20/-0.63/-0.70
VG10	-0.41/-0.42/-0.42/-0.44	-1.33/-0.71/-1.33/-1.26	0.86/0.76/1.37/0.74	0.07/0.30/0.07/0.06	0.60/0.64/0.73/0.58	-1.49/-**1.74**/-1.49/-1.56	0.01/0.01/0.01/-0.07	-0.97/-1.25/-0.93/-0.85	-1.16/-1.30/-1.16/-1.22	-0.50/-0.46/-0.52/-0.51	-0.76/-0.47/-1.00/-0.74	-1.14/-**1.73**/-1.14/-1.23
VG11	-0.28/-0.53/-0.27/-0.29	-0.98/-0.87/-0.81/-1.07	1.61/1.53/**1.80**/1.43	0.42/0.49/0.37/0.41	1.51/**1.63/1.64**/1.50	-0.12/-0.40/-0.13/-0.12	0.90/0.84/1.01/0.92	0.25/0.10/0.25/0.25	-1.02/-1.04/-1.41/-1.03	-0.19/-0.22/-0.20/-0.20	-1.11/-0.76/-1.11/-1.06	-1.09/-**1.78**/-0.93/-1.17
VG12	-0.07/0.87/-0.07/-0.07	-0.98/-1.05/-0.81/-1.06	1.53/1.28/**1.81**/1.37	0.16/0.21/0.14/0.15	**1.87/1.95/1.66/1.86**	-0.48/-0.76/-0.48/-0.53	-0.25/-0.24/-0.27/-0.19	-0.69/-0.86/-0.75/-0.69	-0.69/-0.70/-1.06/-0.73	0.23/0.15/0.23/0.24	-1.24/-0.92/-1.24/-1.22	-1.12/-**1.90**/-1.00/-1.21
VG13	-0.30/0.44/-0.32/-0.28	-1.41/-2.00/-1.23/-1.62	0.47/0.27/0.54/0.43	-1.07/-1.07/-0.99/-1.07	0.74/0.83/0.86/0.77	-0.61/-0.78/-0.61/-0.60	-0.49/-0.44/-0.53/-0.41	-0.29/-0.45/-0.31/-0.29	-0.76/-0.78/-1.04/-0.75	0.16/0.23/0.17/0.18	-0.97/-0.82/-1.18/-0.96	-0.87/-**1.63**/-0.75/-0.94
VG14	-0.49/-0.60/-0.47/-0.51	**-1.88**/-1.50/-**2.33**/-1.63	-0.38/-0.33/-0.36/-0.32	-0.05/0.35/-0.06/-0.05	0.46/0.64/0.46/0.46	**-1.93/-2.21/-1.93/-2.05**	-0.21/-0.22/-0.19/-0.16	-0.65/-0.82/-0.65/-0.66	-0.84/-0.88/-1.05/-0.90	-0.27/-0.15/-0.27/-0.29	-1.40/-0.97/-1.72/-1.37	-1.48/-**2.18**/-1.21/-1.55
VG15	-0.27/-0.54/-0.25/-0.29	-0.94/-0.94/-0.94/-1.06	1.04/0.89/1.17/0.94	0.31/0.53/0.26/0.30	1.23/1.34/1.07/1.22	-0.43/-0.80/-0.43/-0.46	-0.15/-0.14/-0.17/-0.08	0.31/0.17/0.31/0.31	-0.44/-0.51/-0.39/-0.46	0.16/0.14/0.16/0.17	-1.24/-1.08/-1.24/-1.27	-0.99/-1.64/-0.82/-1.05
VG16	-0.23/-0.42/-0.20/-0.23	-0.82/-1.13/-0.82/-0.94	1.16/1.02/1.34/1.10	-0.05/0.29/-0.04/-0.04	0.96/1.05/1.23/0.94	-0.52/-0.70/-0.58/-0.54	-0.04/-0.04/-0.05/0.20	-0.06/-0.19/-0.06/-0.05	-0.51/-0.65/-0.64/-0.52	0.04/0.07/0.04/0.04	-1.08/-0.80/-1.08/-1.06	-0.99/-**1.81**/-0.90/-1.05

Table A10. Trends in Rainfall Extremes of July Month

Grid Id	CDD	CWD	PRCPTOT	R10	R20	R40	R95	1Day	5Day
NG1	**-2.85/-2.64/-3.55/-2.81**	0.74/0.40/0.71/0.69	**2.74/2.46/2.76/2.98**	1.59/1.56/**1.82/1.66**	0.94/0.83/1.01/0.99	**1.83/2.26/1.75/1.85**	1.22/1.50/1.36/1.31	0.79/0.59/1.06/0.85	1.40/1.19/1.60/1.40
NG2	**-2.05**/-1.64/**-1.83/-2.01**	0.89/0.93/0.89/0.97	**1.99/1.97/3.39/2.44**	**2.67/2.56/2.68/3.24**	**1.81/1.97/1.86/2.07**	-0.17/-0.64/-0.17/-0.19	0.54/0.43/0.69/0.65	0.80/0.66/0.80/0.93	1.52/1.36/1.52/**1.79**
NG3	0.96/0.55/1.02/0.82	**-1.65**/-1.18/-1.52/-1.52	-0.66/-0.84/-0.66/-0.70	-0.31/-0.50/-0.31/-0.32	-0.91/-1.02/-0.91/-0.94	-0.21/-0.52/-0.21/-0.23	-0.60/-0.89/-0.79/-0.72	-0.71/-0.69/-0.90/-0.87	-1.05/-0.87/-1.05/-1.19
NG4	**-1.90**/-1.38/**-1.90/-1.72**	**1.80**/1.56/**1.90/1.71**	**2.44/2.41/2.96/2.71**	**3.25/3.10/5.55/3.20**	**2.03/2.30/2.03/2.13**	-0.73/-0.92/-0.68/-0.75	-0.67/-0.74/-0.70/-0.74	0.20/0.18/0.23/0.23	1.12/1.12/1.28/1.25
NG5	-1.47/-1.54/**-1.84**/-1.52	0.07/-0.25/0.06/0.06	1.45/1.25/1.45/1.55	1.22/1.12/1.27/1.24	0.81/0.66/0.71/0.93	1.37/1.11/1.53/1.37	0.58/0.28/0.53/0.57	0.98/1.11/0.91/1.01	0.94/0.91/1.15/0.96
NG6	-0.84/-1.19/-0.70/-0.88	0.35/0.33/0.31/0.33	**2.16/1.77/2.16/2.46**	**2.11/1.82/1.85/2.35**	**2.28/1.85/2.28/2.16**	0.89/1.01/0.77/1.00	1.12/0.89/1.12/1.23	1.19/1.10/1.33/1.29	1.16/0.97/1.16/1.32
NG7	-0.81/-0.70/-0.88/-0.81	-0.74/-0.44/-0.90/-0.67	**3.10/3.00/2.46/3.55**	**3.43/3.44/3.09/3.81**	**3.03/3.02/2.82/2.90**	**1.87/2.32/1.28/1.92**	1.64/**1.88**/1.44/**1.72**	**1.91/1.71/1.91/2.10**	**2.32/2.24/2.32/2.54**
NG8	-1.17/-1.39/-1.00/-1.39	**2.01/1.95/1.74/2.02**	**2.36/2.30/2.02/2.55**	**2.37/2.21/2.39/2.62**	**1.92/1.88/1.92/2.01**	1.23/0.96/1.44/1.19	**1.65**/1.37/**1.91**/1.57	**1.80/1.67/2.49/2.07**	**2.44/2.29/2.44/2.72**
NG9	-1.08/-1.16/-1.01/-1.23	0.15/0.02/0.17/0.13	**3.94/3.76/4.40/3.89**	**1.89/1.70**/1.53/**2.09**	**3.60/3.51/3.60/3.52**	**3.15/2.59/2.20/2.65**	**3.39/3.38/3.20/2.70**	**4.02/3.99/4.96/3.64**	**3.83/3.75/4.49/3.60**
NG10	**-2.43/-2.52/-2.43/-2.61**	0.61/0.45/0.61/0.62	**4.07/4.07/4.43/4.53**	**2.26/2.16/1.95/2.48**	**4.14/3.86/3.23/4.10**	**3.25/2.43/2.63/2.94**	**3.41/3.68/4.26/3.35**	**3.69/3.90/3.83/4.03**	**4.18/4.11/4.69/4.60**
NG11	-1.48/**-1.69**/-1.09/-1.50	1.42/1.10/1.40/1.22	**3.63/3.43/3.63/3.64**	**2.14/1.94/1.80/2.22**	**2.93/2.63/2.55/3.07**	**2.31/1.65/1.96/2.17**	**2.65/2.12/2.37/2.35**	**2.50/2.57/2.91/2.46**	**2.99/2.94/3.11/3.11**
NG12	0.92/1.09/0.92/0.85	**-3.37/-3.25/-3.37/-2.83**	0.27/0.00/0.29/0.26	-0.73/-0.82/-0.67/-0.67	0.12/-0.11/0.12/0.11	1.32/1.16/1.12/1.30	**1.97**/1.40/**1.97/1.82**	**1.66/1.67/1.66/1.76**	1.01/0.87/1.25/1.00
VG1	-1.35/-1.27/-1.21/-1.21	-0.51/-0.17/-0.86/-0.42	**2.23/2.29/1.90/2.68**	**1.97/2.12/1.93/2.25**	**2.52/2.92/2.52/2.59**	1.25/1.20/1.25/1.25	0.95/0.68/1.05/1.06	1.00/0.87/1.41/1.14	**1.74/1.91/2.26/2.09**
VG2	**-1.97/-1.93/-2.02/-2.05**	1.56/1.61/1.43/1.46	**3.89/3.78/3.41/4.60**	**3.64/3.77/3.15/4.10**	**3.15/3.10/3.15/3.35**	**2.28/2.94/2.28/2.79**	**2.02/2.22/2.02/2.28**	1.55/1.49/1.64/**1.70**	**2.78/2.82/3.16/3.24**
VG3	-1.62/-1.59/-1.50/**-1.67**	0.82/1.26/0.84/0.88	**2.58/2.74/2.58/3.01**	**2.76/2.76/3.11/3.12**	**2.93/2.84/2.72/3.43**	1.42/**1.86/2.90/1.69**	1.52/**1.83**/1.43/**1.66**	1.16/1.01/1.21/1.24	**2.20/2.29/2.20/2.41**
VG4	**-2.90/-2.78/-3.74/-3.04**	**2.13/2.33/1.83/2.06**	**4.69/4.54/3.39/4.41**	**4.12/4.28/2.98/3.69**	**3.76/3.70/3.26/3.75**	**3.50/2.03/1.93/3.06**	**3.23/2.10/2.06/2.98**	**3.00/2.97/4.68/3.15**	**3.43/3.38/6.18/3.62**
VG5	**-2.48/-2.28/-2.19/-2.50**	**2.01/2.10/2.41/1.76**	**4.34/4.21/6.57/4.30**	**4.12/4.04/5.30/4.16**	**4.25/4.07/4.25/4.38**	1.37/0.82/1.68/1.33	1.38/0.94/1.61/1.30	**1.81**/1.63/**2.55/1.82**	**3.29/3.28/5.31/3.43**
VG6	-0.94/-0.72/-0.94/-0.92	-0.17/0.11/-0.17/-0.18	1.52/1.39/1.52/1.60	1.26/0.99/1.26/1.13	**2.64/2.40/2.64/2.80**	1.17/1.31/1.49/1.23	1.09/1.10/1.12/1.12	1.13/0.76/1.41/1.20	1.55/1.44/1.42/1.53
VG7	-1.03/-1.19/-1.03/-1.07	1.00/0.97/1.06/0.91	**2.85/2.89/3.30/2.68**	**2.32/2.35/2.50/2.40**	**2.06/1.73/2.04/2.02**	**1.87**/1.39/1.37/**1.84**	**1.66**/1.50/1.42/1.57	1.26/1.49/1.35/1.23	**2.53/2.62/2.58/2.45**
VG8	-0.21/-0.17/-0.18/-0.20	1.05/1.17/1.25/1.13	**2.39/2.21/2.39/2.23**	**2.22/2.11/2.16/2.09**	**2.28/2.65/1.95/2.40**	**2.77/1.76/2.66/2.47**	**2.32/1.72/2.32/2.14**	**1.70/1.64/1.93/1.70**	**2.33/2.36/3.35/2.28**
VG9	-1.02/-1.16/-1.22/-1.08	**2.37/2.42/2.36/2.69**	**1.94/1.82/2.08/1.74**	**1.90/1.79/2.42/1.78**	**2.20/1.77/1.78/1.87**	0.89/0.58/0.86/0.82	0.52/0.43/0.55/0.51	0.11/0.15/0.11/0.10	**1.67/1.69/2.07/1.53**
VG10	1.22/1.01/1.42/1.18	-1.42/-1.52/-1.23/-1.36	0.08/0.06/0.11/0.10	-1.41/-1.64/-1.32/-1.51	0.15/0.13/0.16/0.17	0.65/0.61/0.56/0.71	0.58/0.58/0.46/0.56	0.60/0.69/0.54/0.60	0.55/0.73/0.52/0.57
VG11	-1.41/-1.14/-1.41/-1.31	**2.72/2.52/2.93/2.74**	0.95/0.94/1.06/0.90	1.07/0.87/1.45/0.99	0.64/0.85/0.73/0.75	-0.46/0.03/-0.59/-0.43	-0.76/-0.41/-0.70/-0.69	-1.04/-0.91/-1.12/-1.02	0.76/0.90//0.78
VG12	-0.23/-0.51/-0.21/-0.25	0.27/0.05/0.43/0.29	-0.23/-0.15/-0.25/-0.22	-0.67/-0.73/-0.84/-0.64	0.66/0.81/0.63/0.68	0.72/0.91/0.81/0.65	0.64/0.75/0.59/0.59	-0.38/-0.29/-0.35/-0.38	0.62/0.91/0.54/0.68
VG13	1.06/0.66/1.17/1.04	0.41/0.12/0.39/0.40	-0.37/-0.35/-0.50/-0.34	0.21/0.23/1.51/0.20	-0.82/-0.57/-0.82/-0.80	0.44/0.51/0.54/0.42	0.20/0.39/0.22/0.19	-0.23/-0.35/-0.22/-0.22	-0.01/0.10/-0.01/-0.01
VG14	-0.06/-0.21/-0.07/-0.06	0.05/-0.15/0.05/0.05	-0.12/-0.16/-0.12/-0.13	-0.67/-0.62/-0.70/-0.65	-0.24/-0.41/-0.24/-0.24	-0.09/-0.19/-0.09/-0.09	0.66/0.57/0.66/0.67	0.20/0.31/0.18/0.20	0.36/0.51/0.36/0.39
VG15	0.66/0.59/0.62/0.70	0.56/0.35/0.41/0.47	-0.12/-0.06/-0.18/-0.11	0.59/0.61/0.61/0.55	0.25/0.33/0.38/0.23	-0.22/-0.16/-0.25/-0.22	-0.22/0.36/-0.21/-0.22	-0.98/-0.92/-0.73/-0.96	0.21/0.37/0.25/0.22
VG16	-0.52/-0.52/-0.52/-0.51	**2.74/2.47/2.74/2.36**	0.03/0.25/0.04/0.03	0.49/0.59/0.51/0.47	0.53/0.54/0.64/0.50	-1.27/-0.75/-1.18/-1.22	-1.27/-0.77/-2.30/-1.25	**-1.94/-1.79/-3.90/-1.97**	-0.37/-0.18/-0.37/-0.39

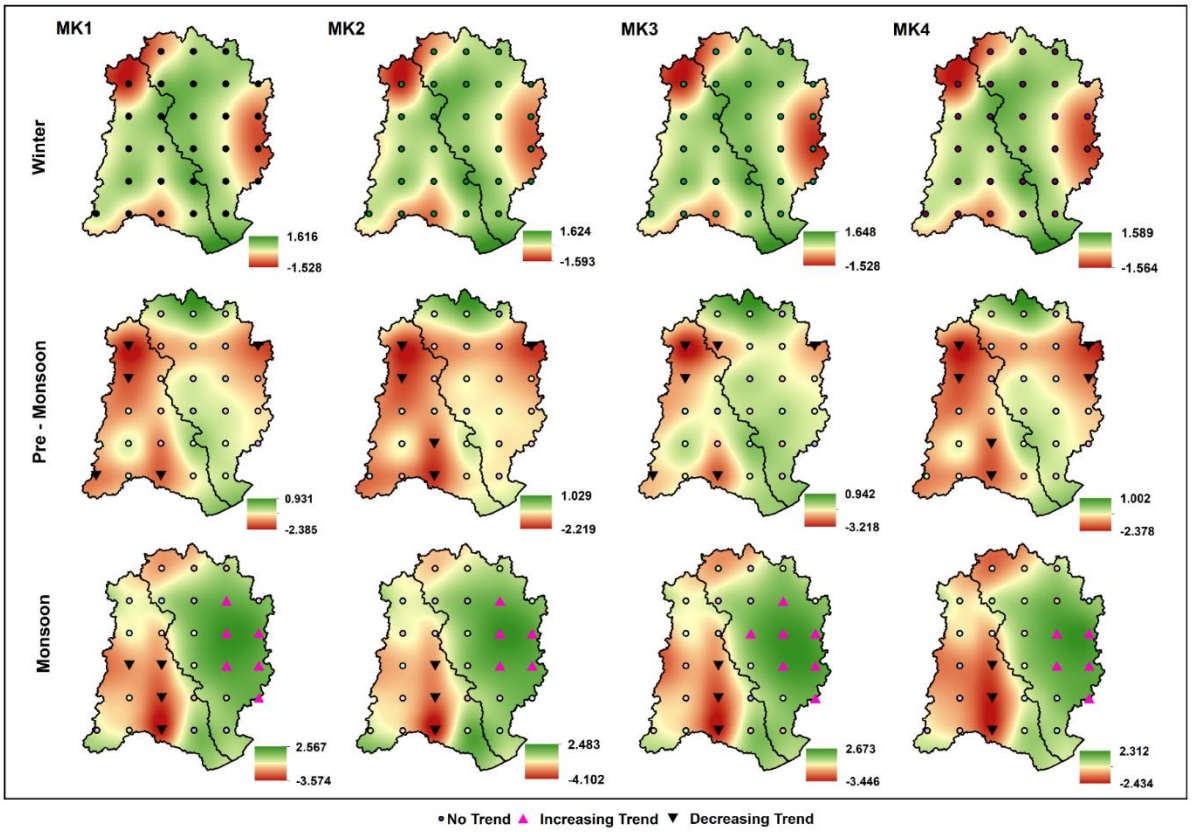

Figure A1. Spatial plots of trends in rainfall during winter pre-monsoon and monsoon seasons of post-1950

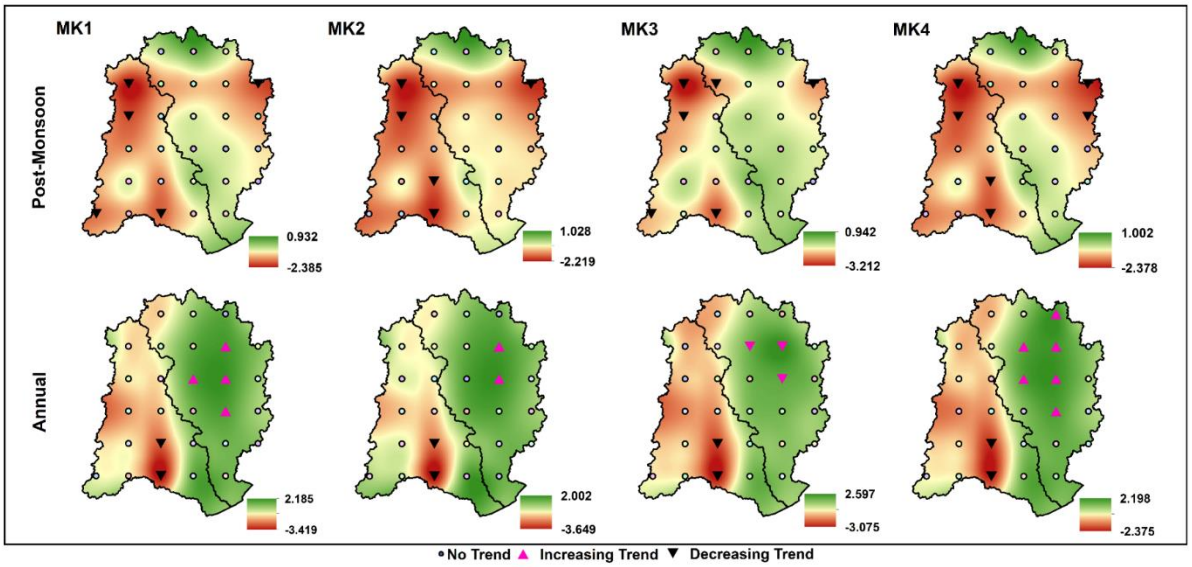

Figure A2. Spatial plots of trends post-monsoon and annual rainfall of post-1950.

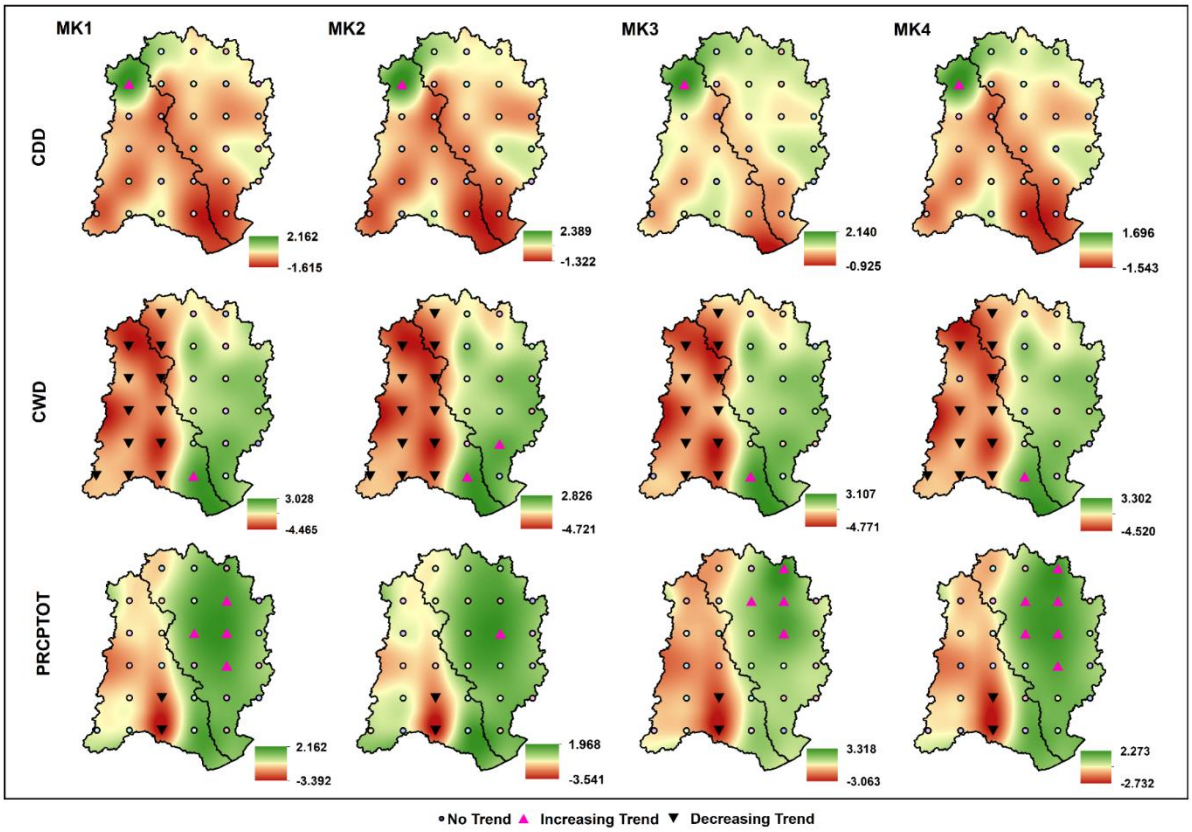

Figure A3. Spatial plot of trends in annual rainfall extremes (CDD, CWD, and PRCPTOT) of post-1950

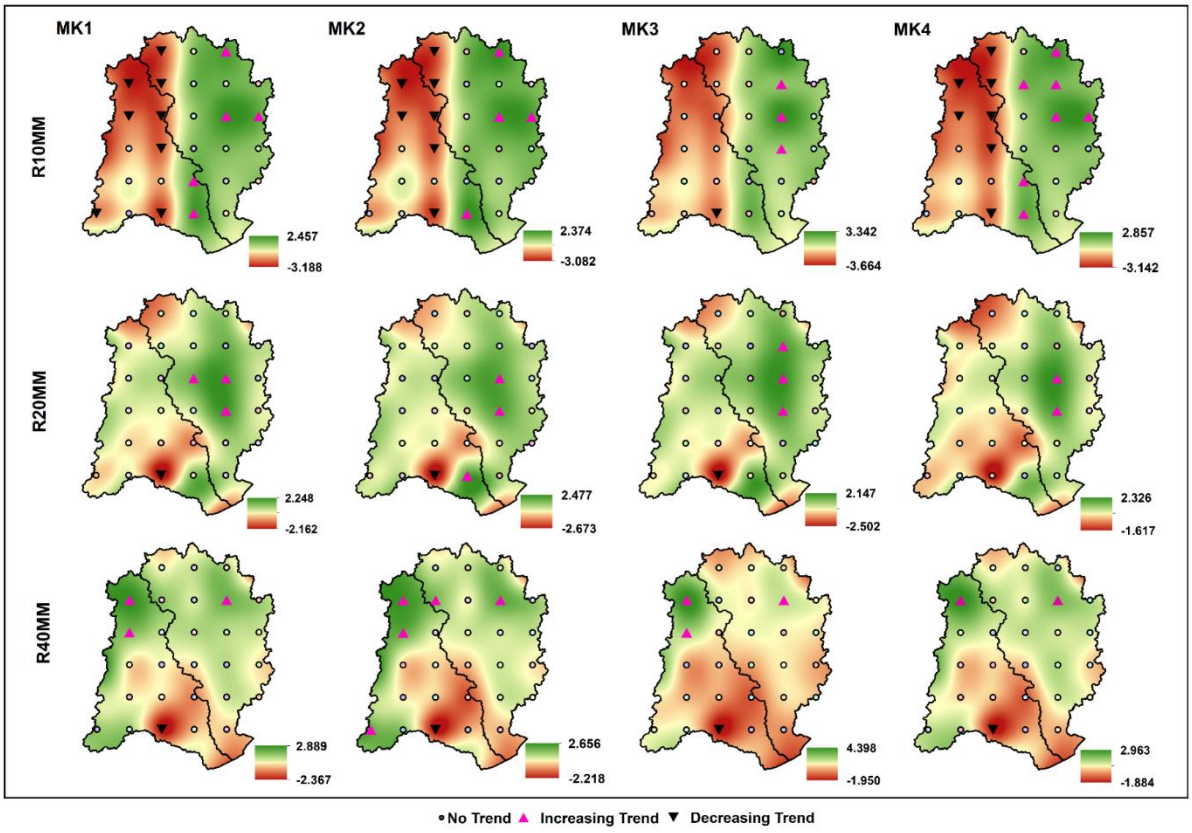

Figure A4. Spatial plot of trends annual rainfall extremes (R10MM, R20MM, and R40MM) of post-1950

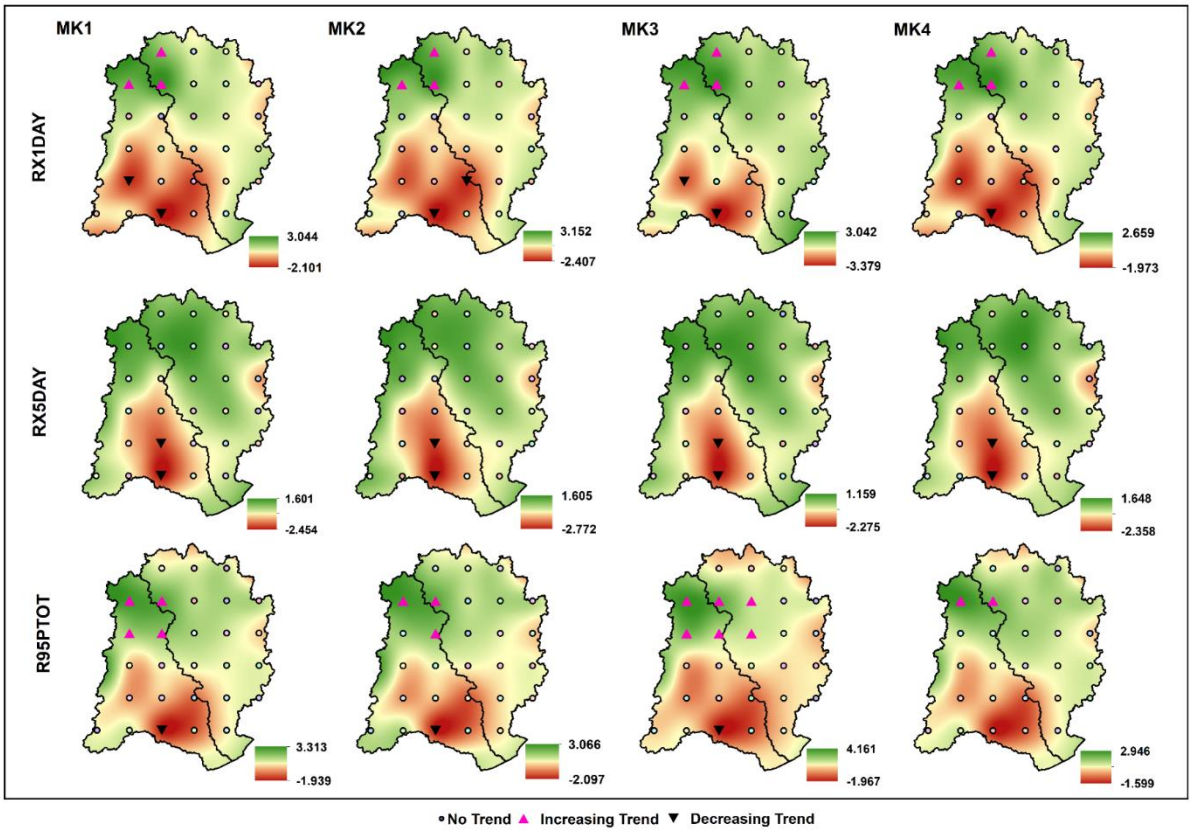

Figure A5. Spatial plot of trends in annual rainfall extremes (RX1DAY, RX5DAY, and R95PTOT) of post-1950

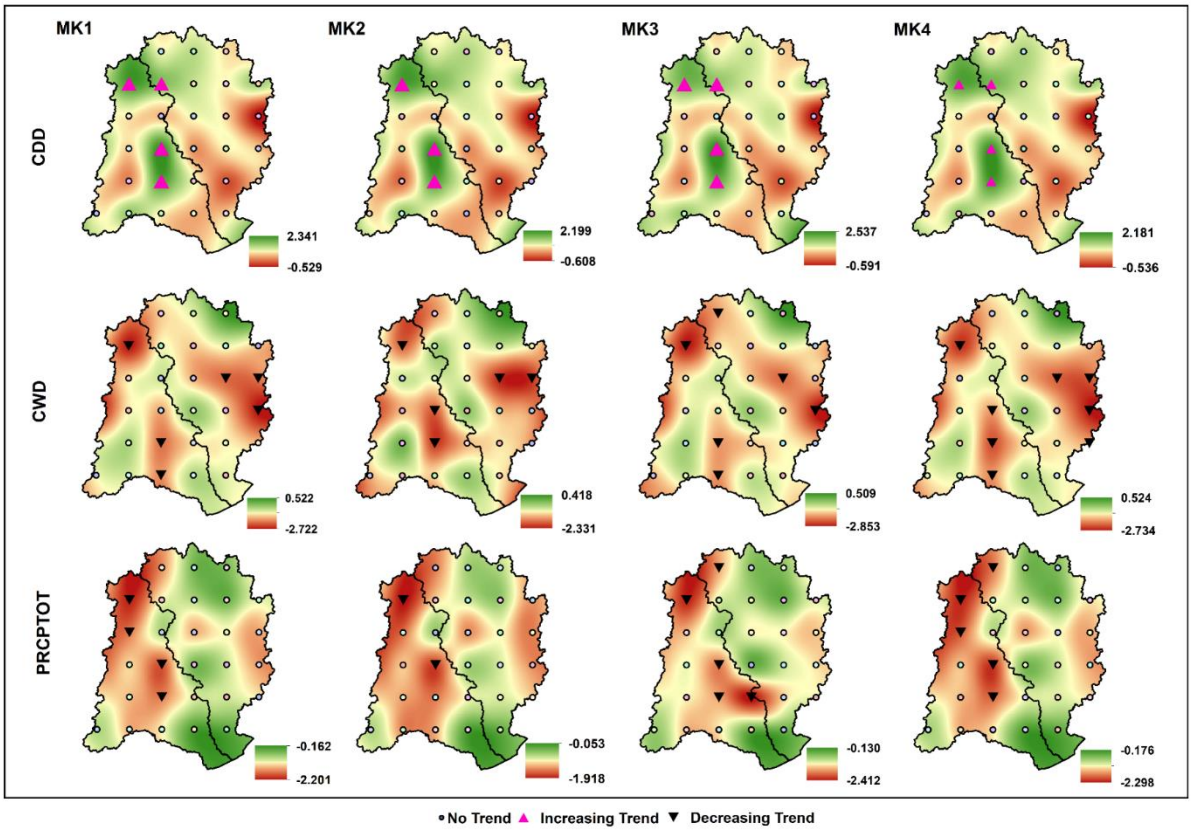

Figure A6. Spatial plot of trends rainfall extremes (CDD, CWD, and PRCPTOT) during winter season

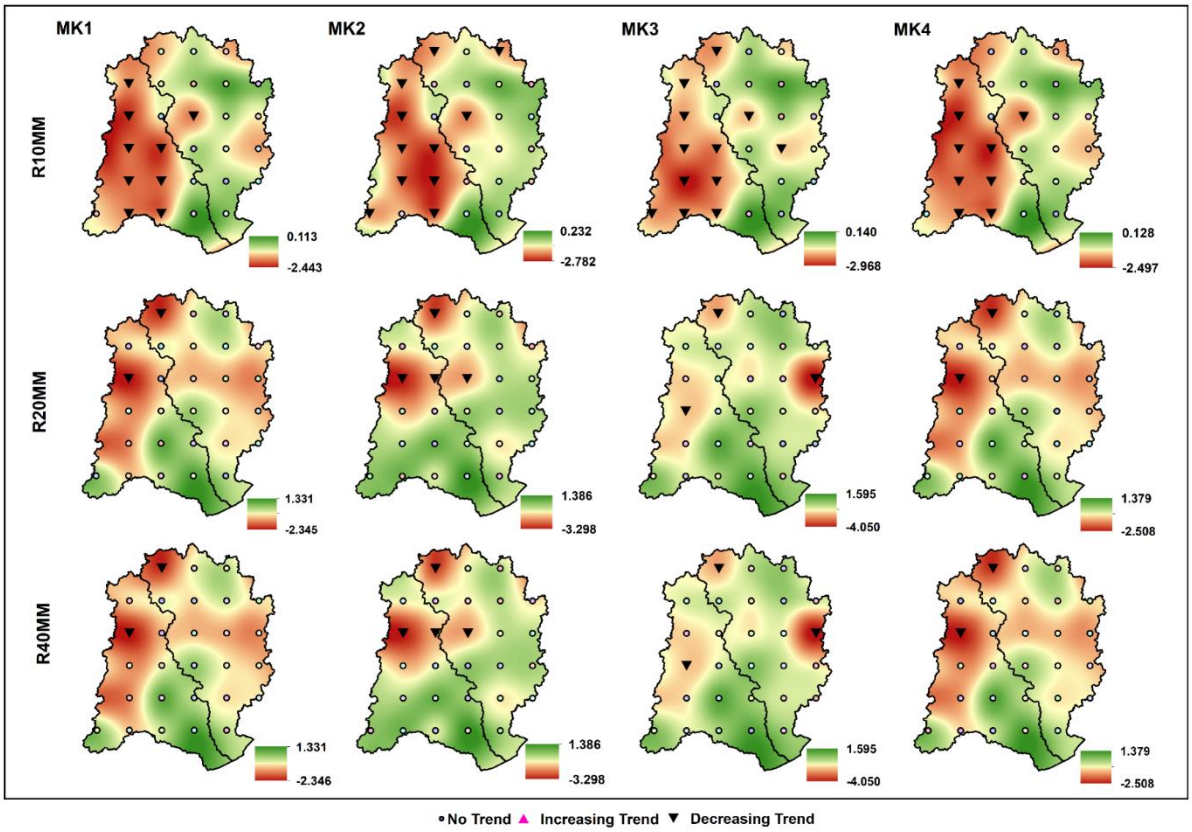

Figure A7. Spatial plot of trends rainfall extremes (R10MM, R20MM and R40MM) during winter season

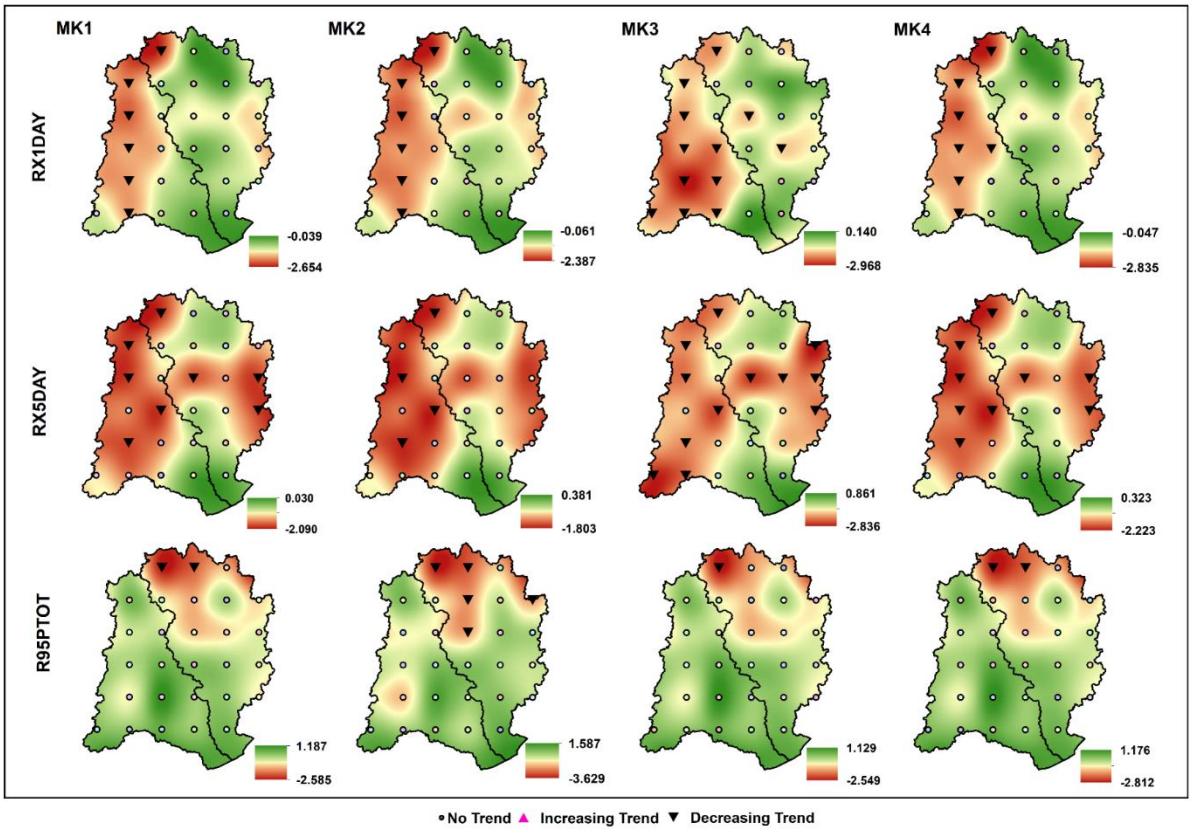

Figure A8. Spatial plot of trends rainfall extremes (RX1DAY, RX5DAY, and R95PTOT) during winter season

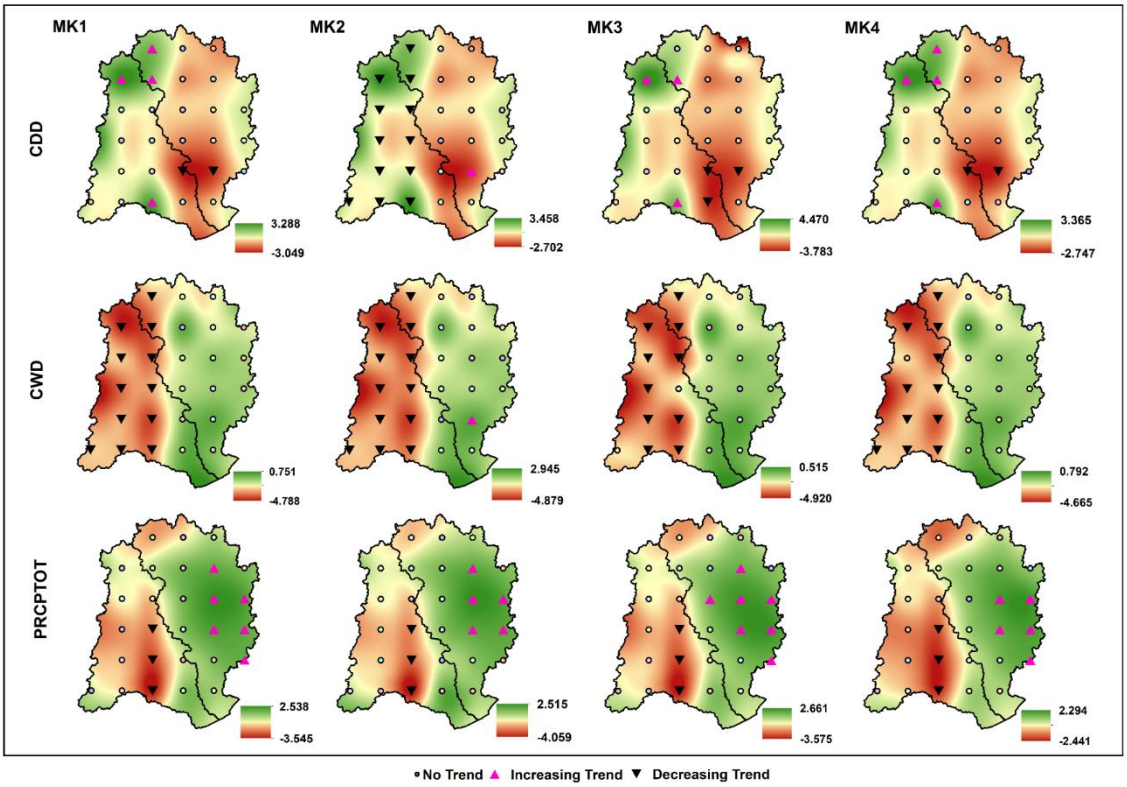

Figure A9. Spatial plot of trends rainfall extremes (CDD, CWD, and PRCPTOT) during monsoon season of post-1950

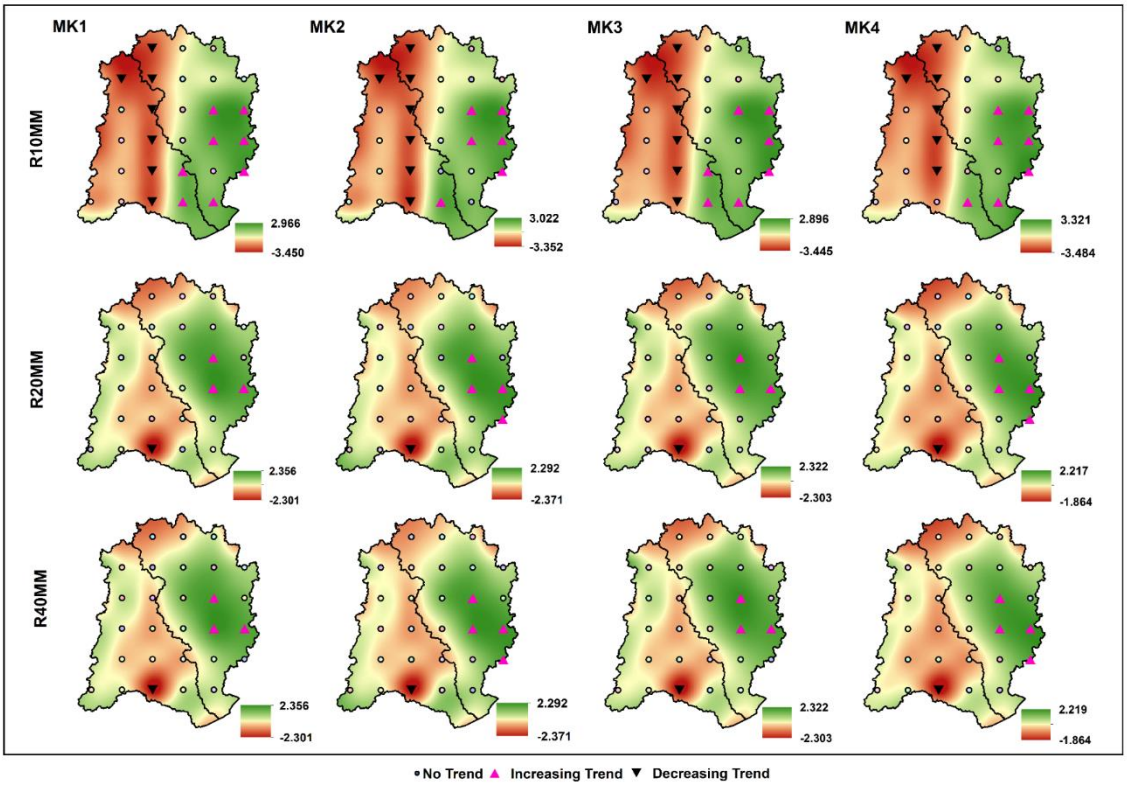

Figure A10. Spatial plot of trends rainfall extremes (R10MM, R20MM and R40MM) during monsoon season of post-1950

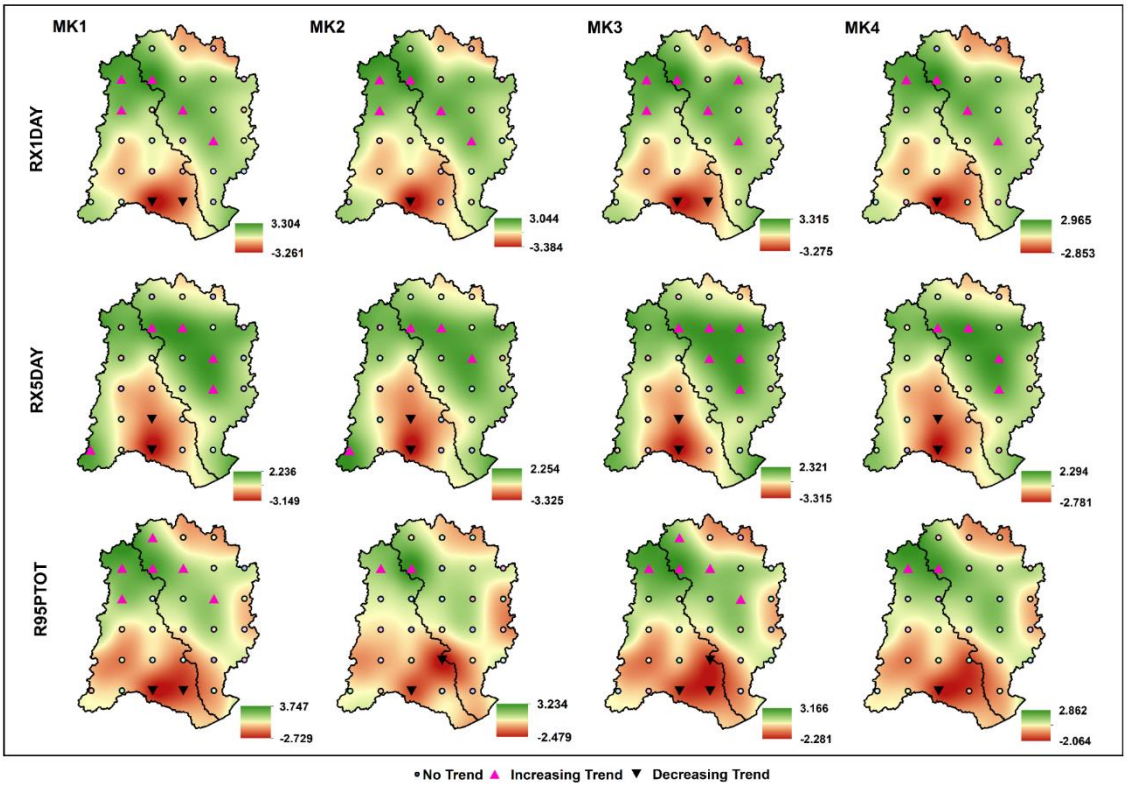

Figure A11. Spatial plot of trends rainfall extremes (RX1DAY, RX5DAY, and R95PTOT) during monsoon season of post-1950

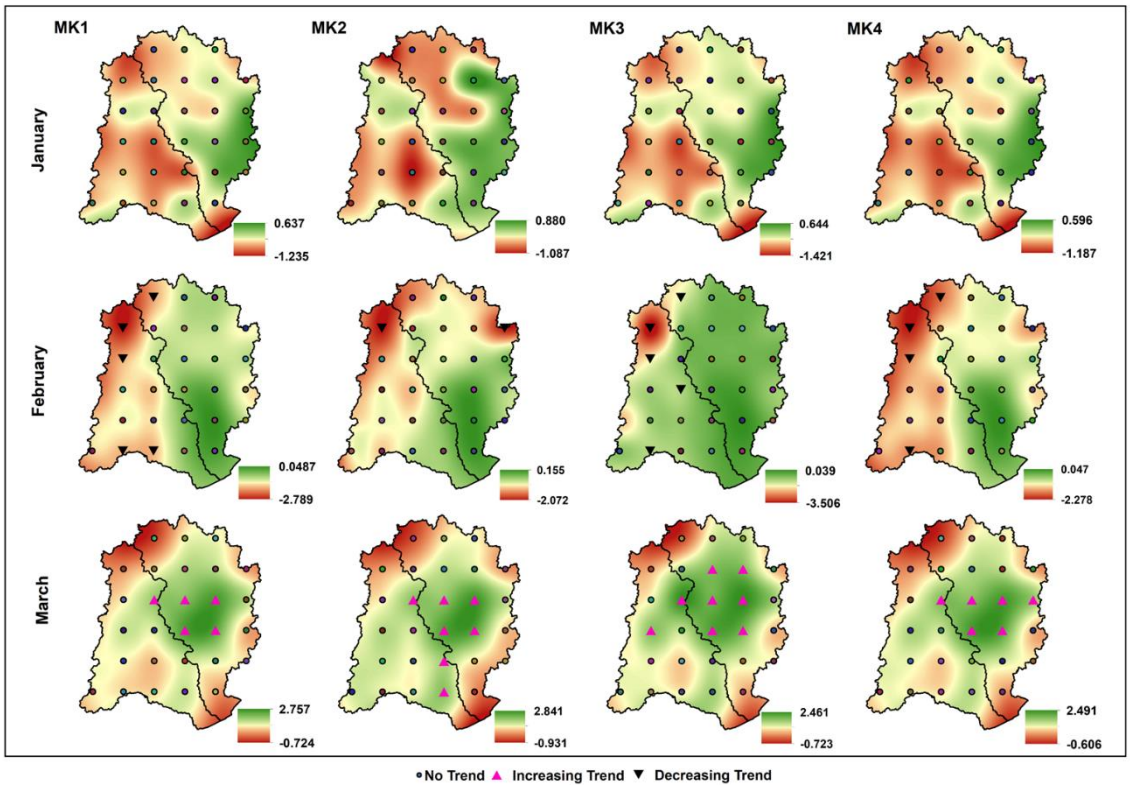

3

Figure A12. Spatial Plot of Trend in Rainfall in January, February, and March Months

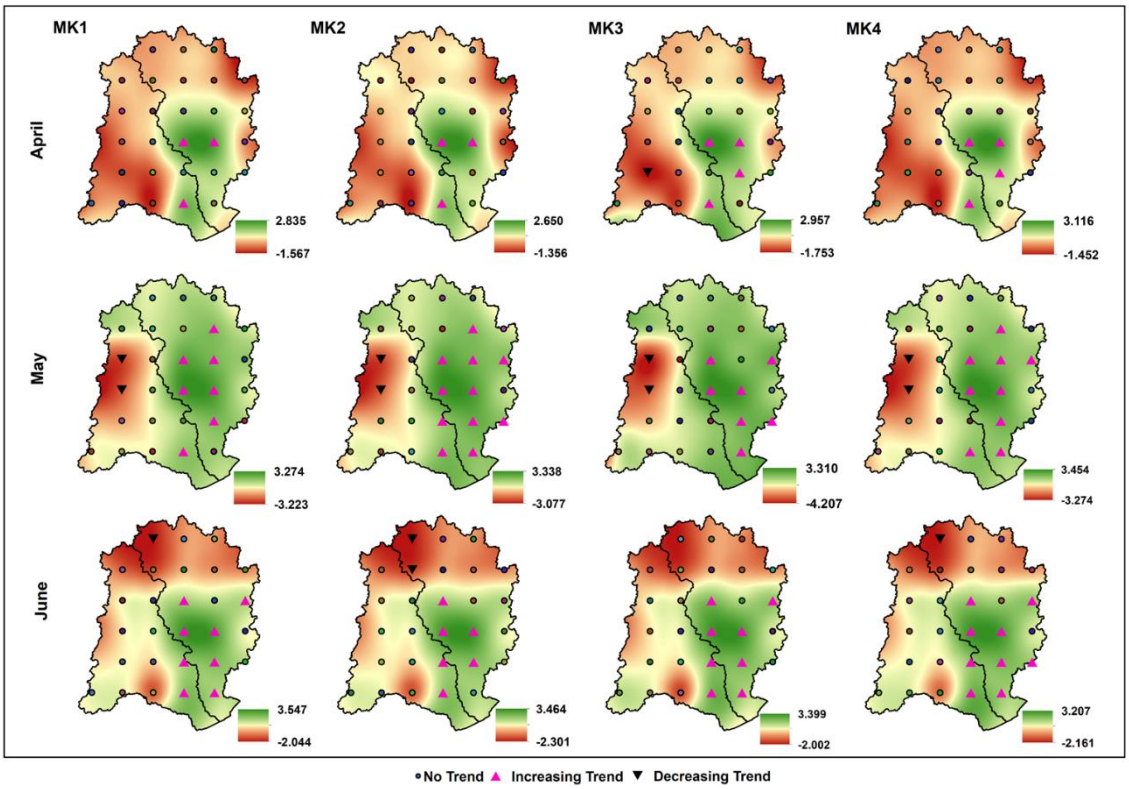

Figure A13. Spatial Plot of Trend in Rainfall in April, May, June Months

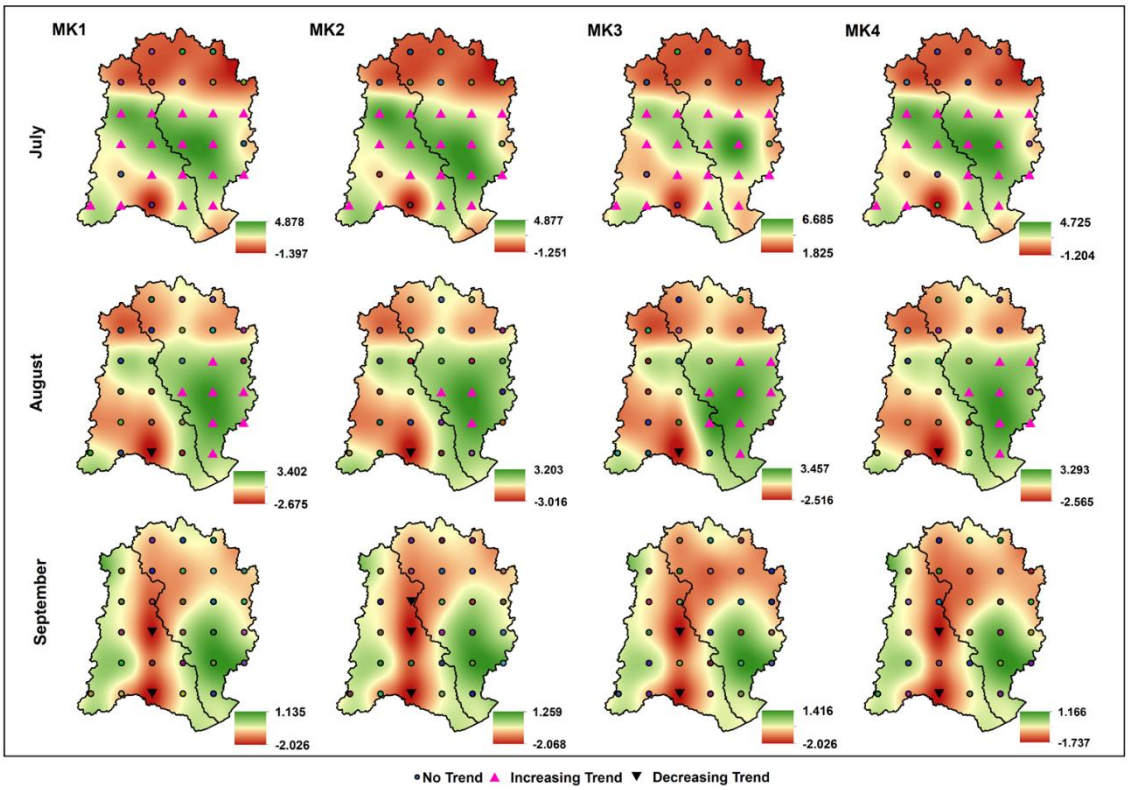

Figure A14. Spatial Plot of Trend in Rainfall in July, August, September Months

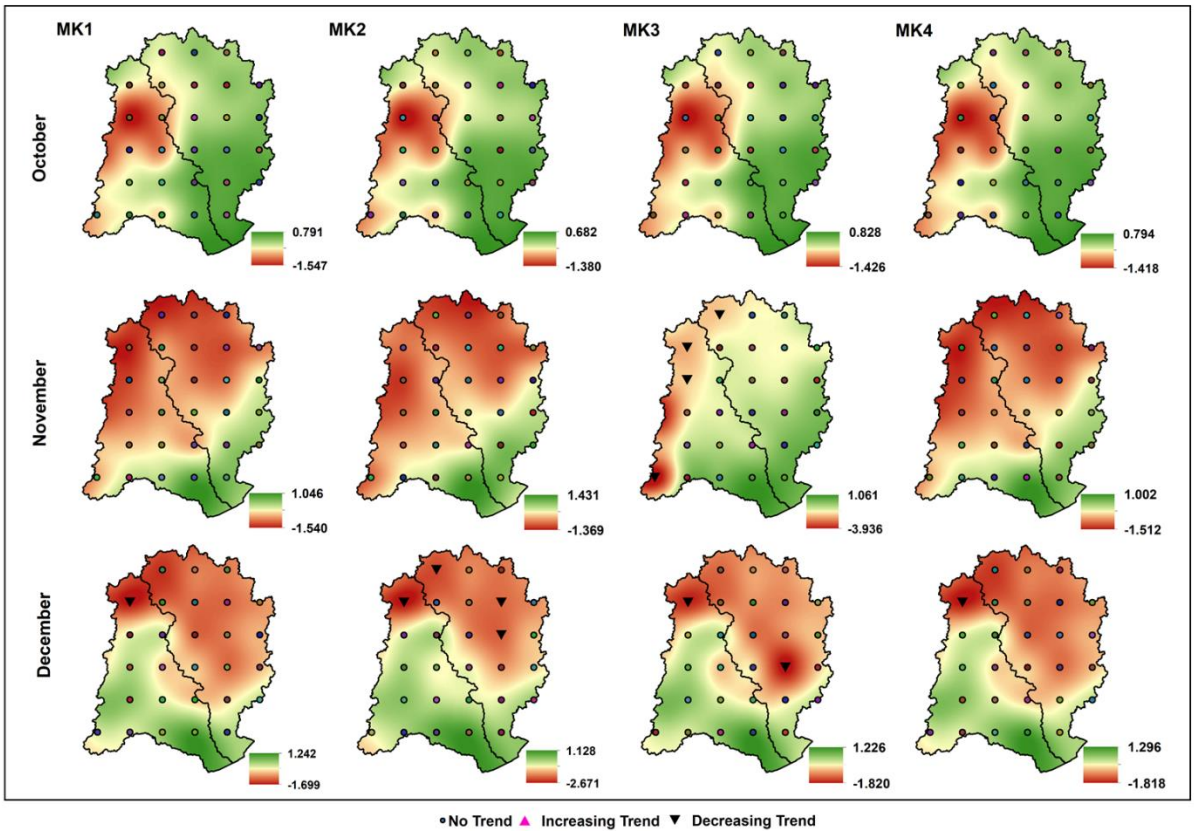

Figure A15. Spatial Plot of Trend in Rainfall in October, November, and December

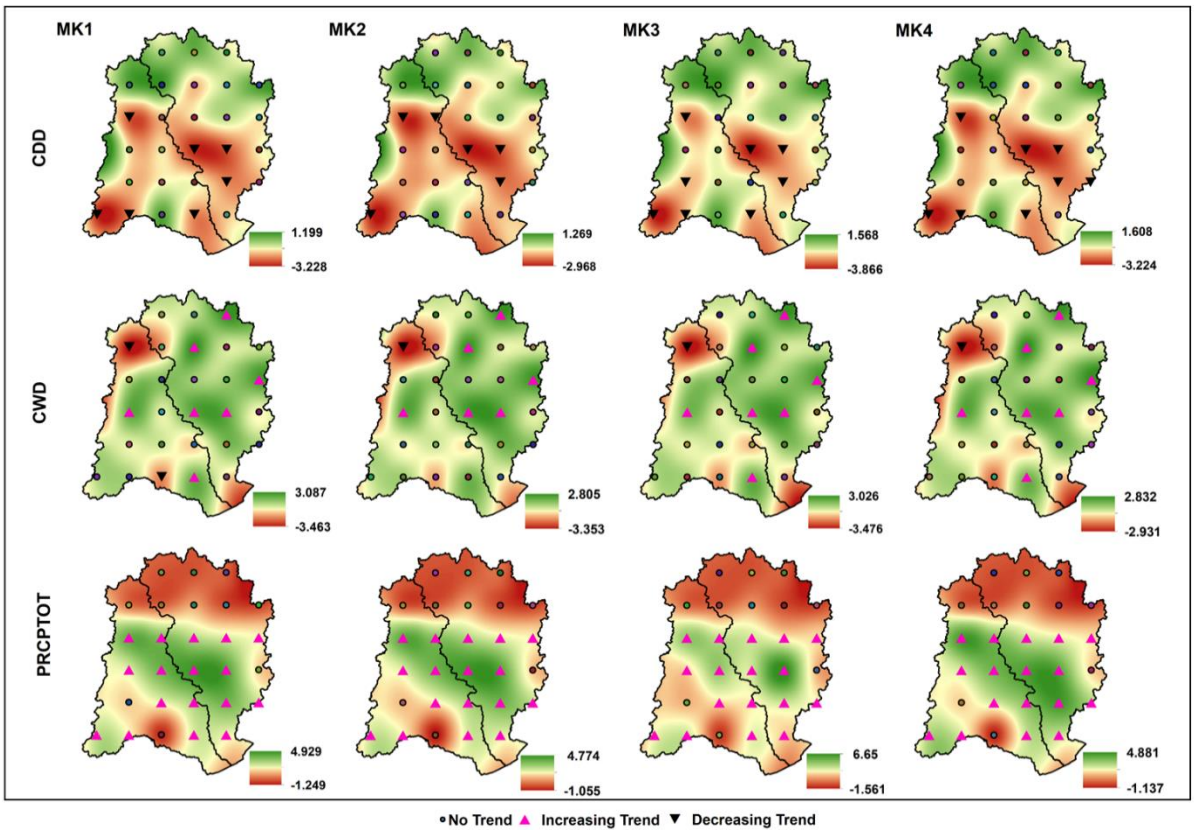

Figure A16. Spatial Plot of Trend Rainfall Extremes (CDD, CWD, and PRCPTOT) in July Month

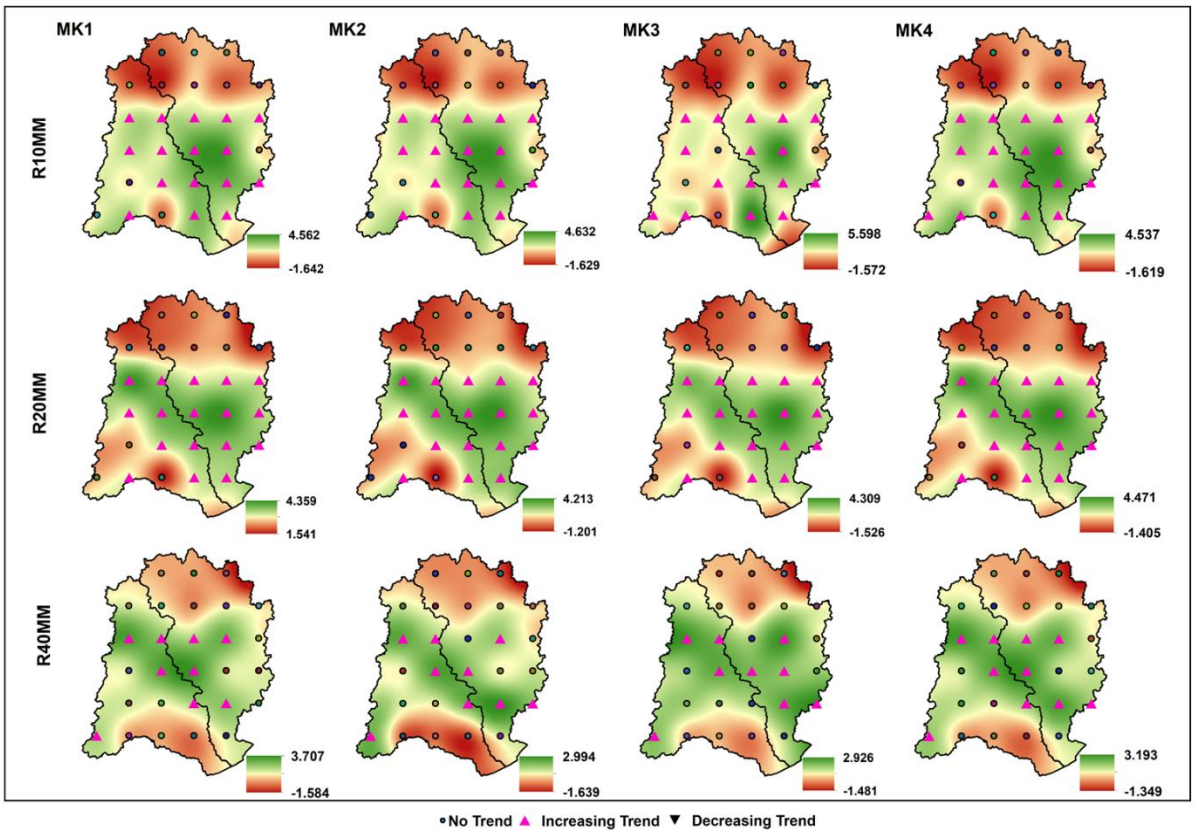

Figure A17. Spatial Plot of Trend Rainfall Extremes (R10MM, R20MM, and R40MM) in July Month

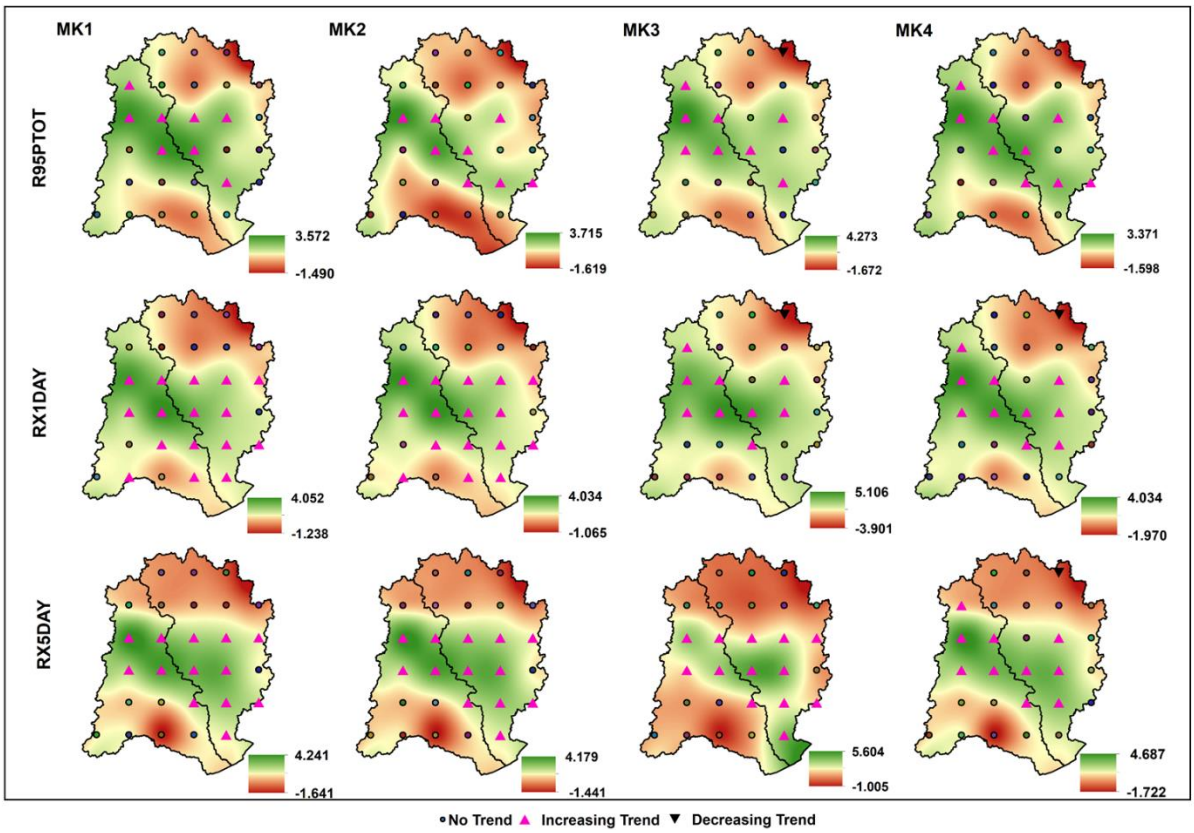

Figure A18. Spatial Plot of Trend Rainfall Extremes (R95PTOT, RX1DAY, and RX5DAY) in July Mont

Appendix-B

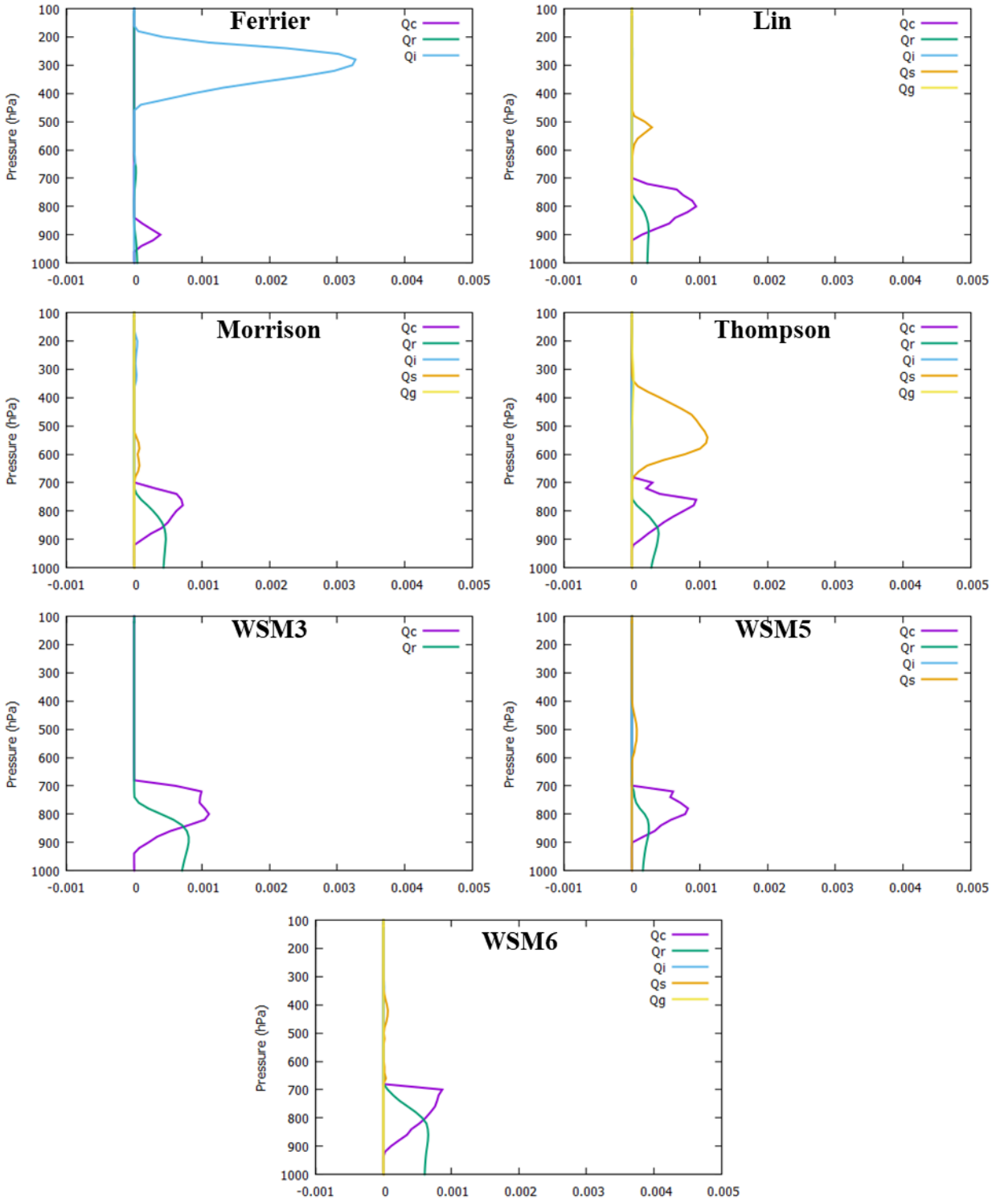

Figure B1. Time evolution of area averaged mixing ratios (g/kg) for cyclone Daye

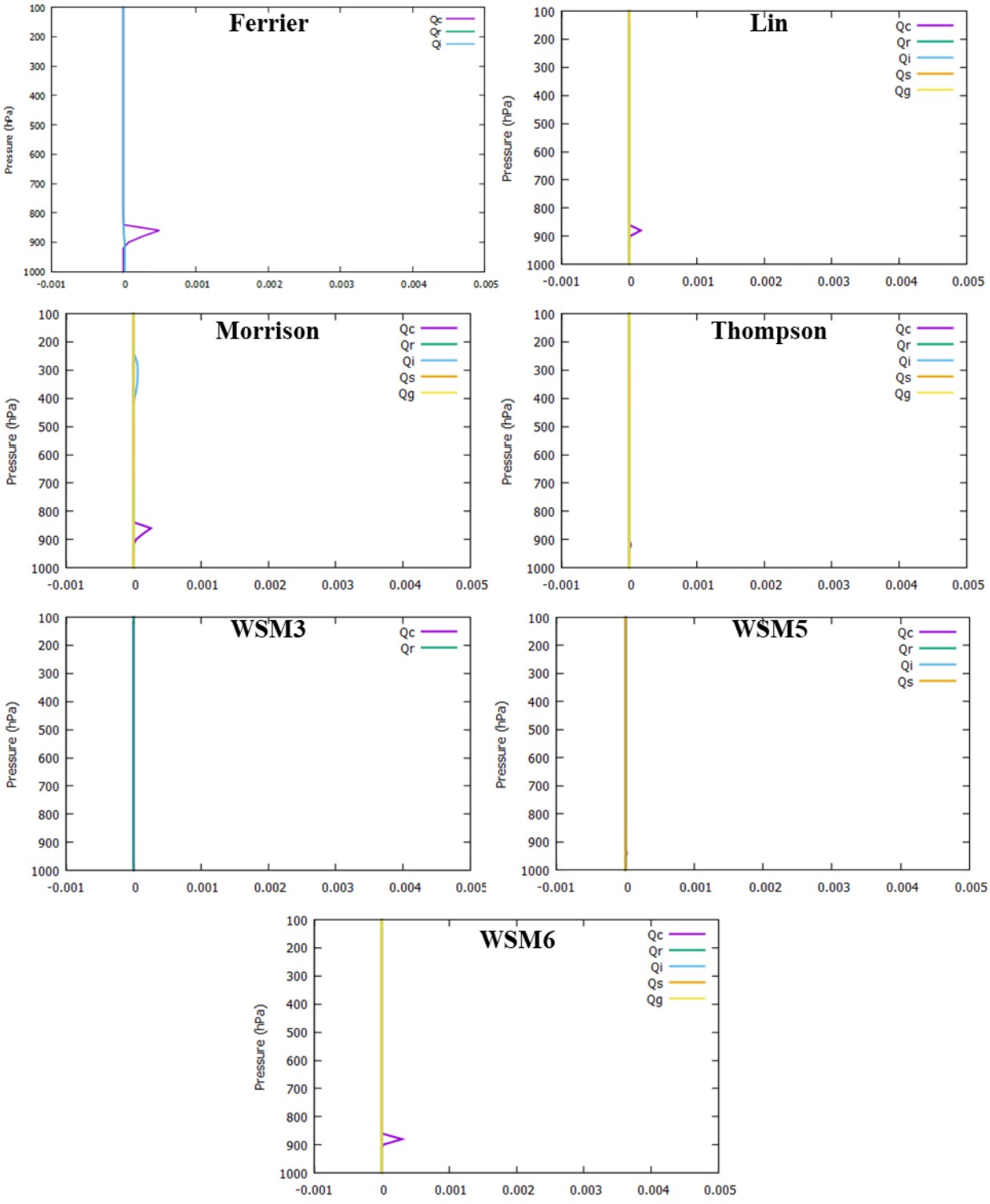

Figure B2. Time evolution of area averaged mixing ratios (g/kg) for cyclone Gaja

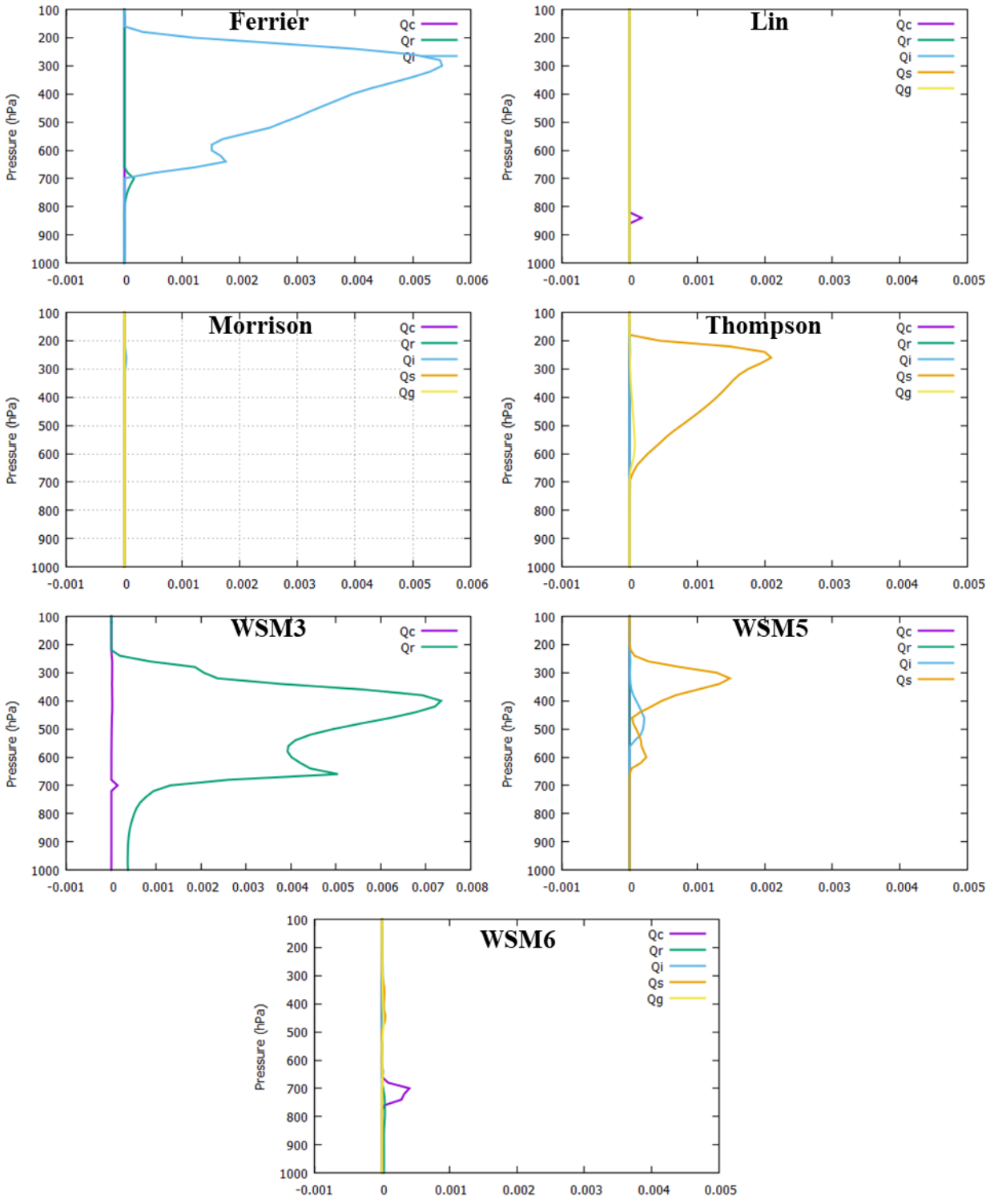

Figure B3. Time evolution of area averaged mixing ratios (g/kg) for cyclone Kyant

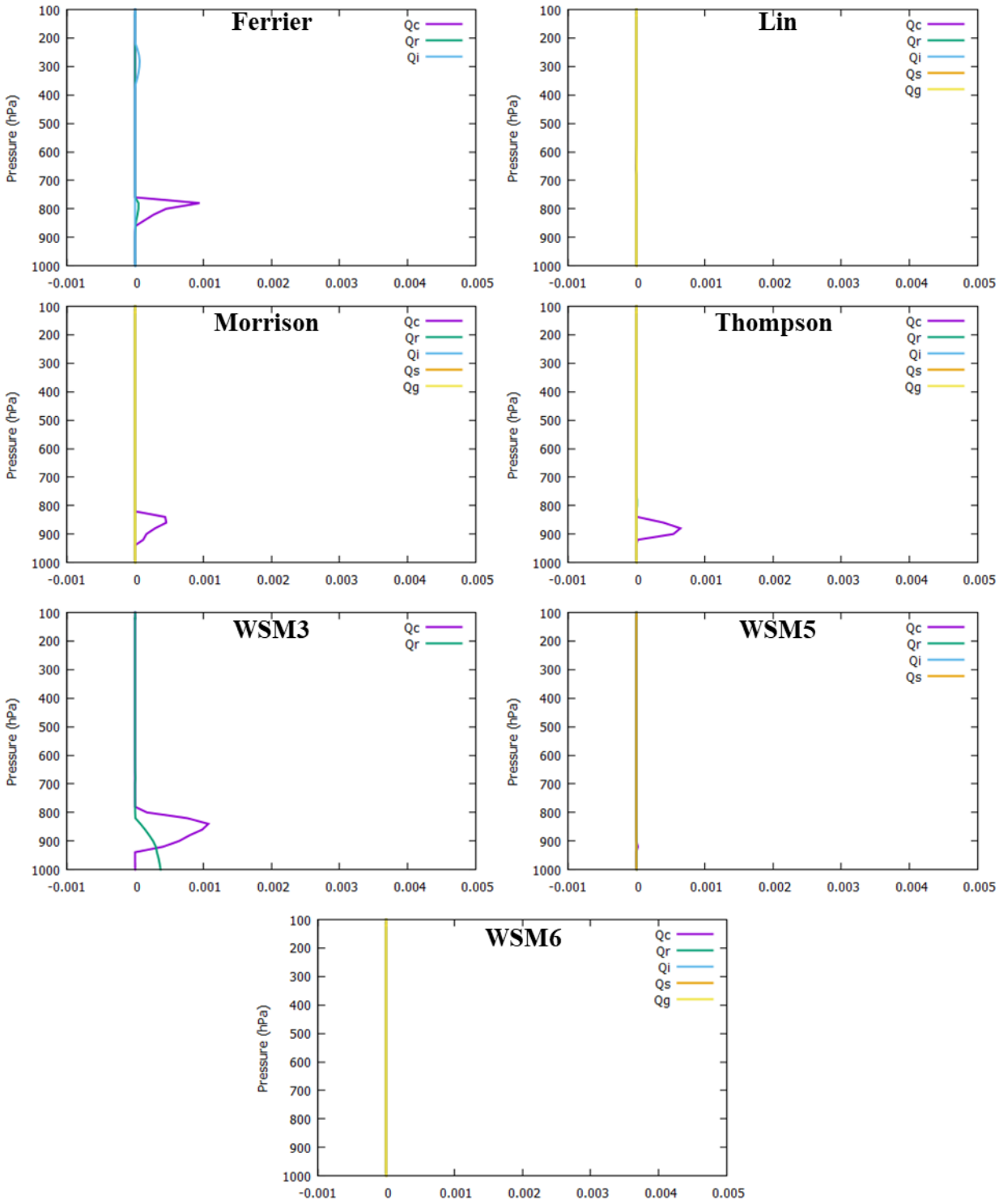

Figure B4. Time evolution of area averaged mixing ratios (g/kg) for cyclone Nilofar

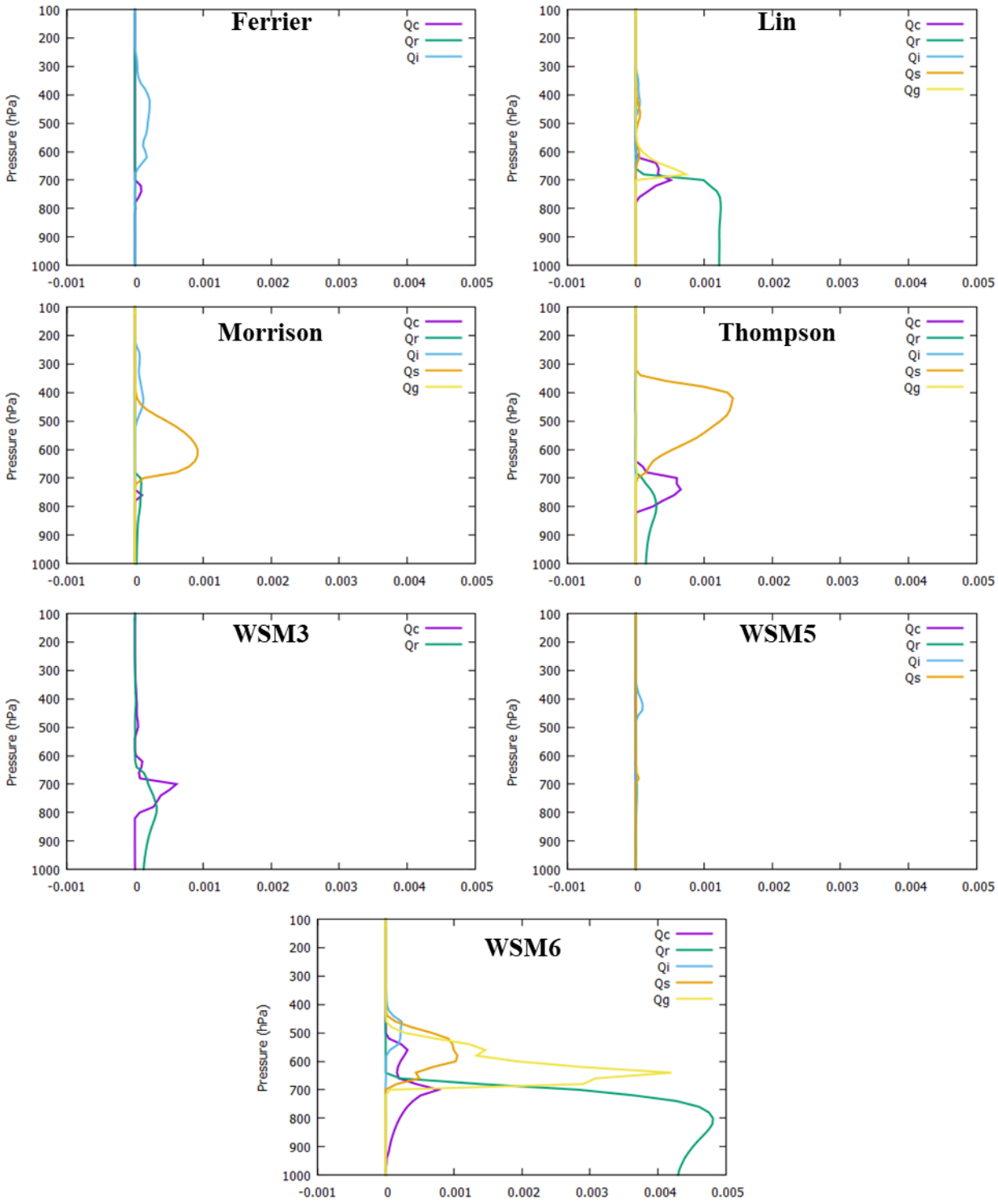

Figure B5. Time evolution of area averaged mixing ratios (g/kg) for cyclone Ockhi

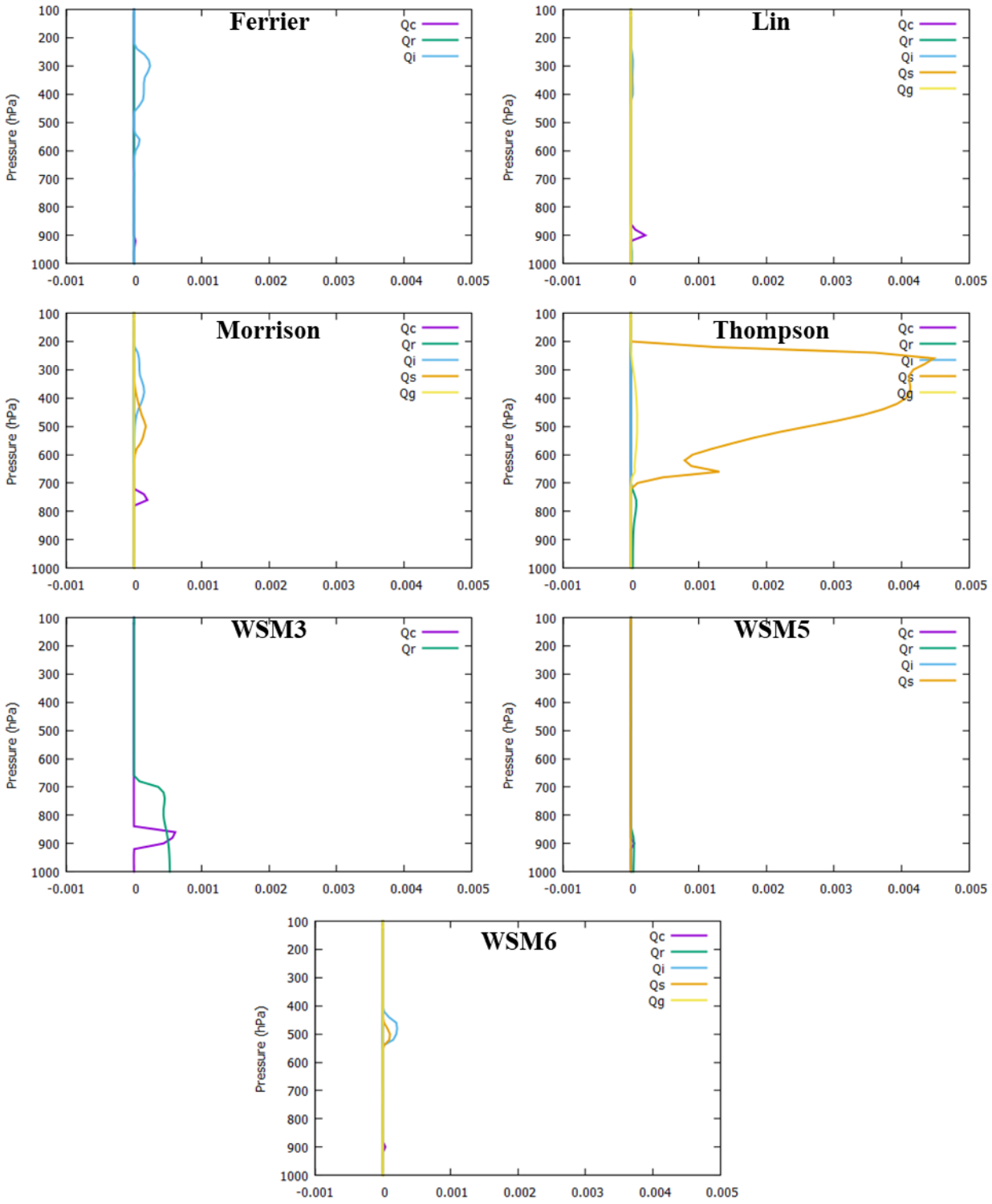

Figure B6. Time evolution of area averaged mixing ratios (g/kg) for cyclone Phethai

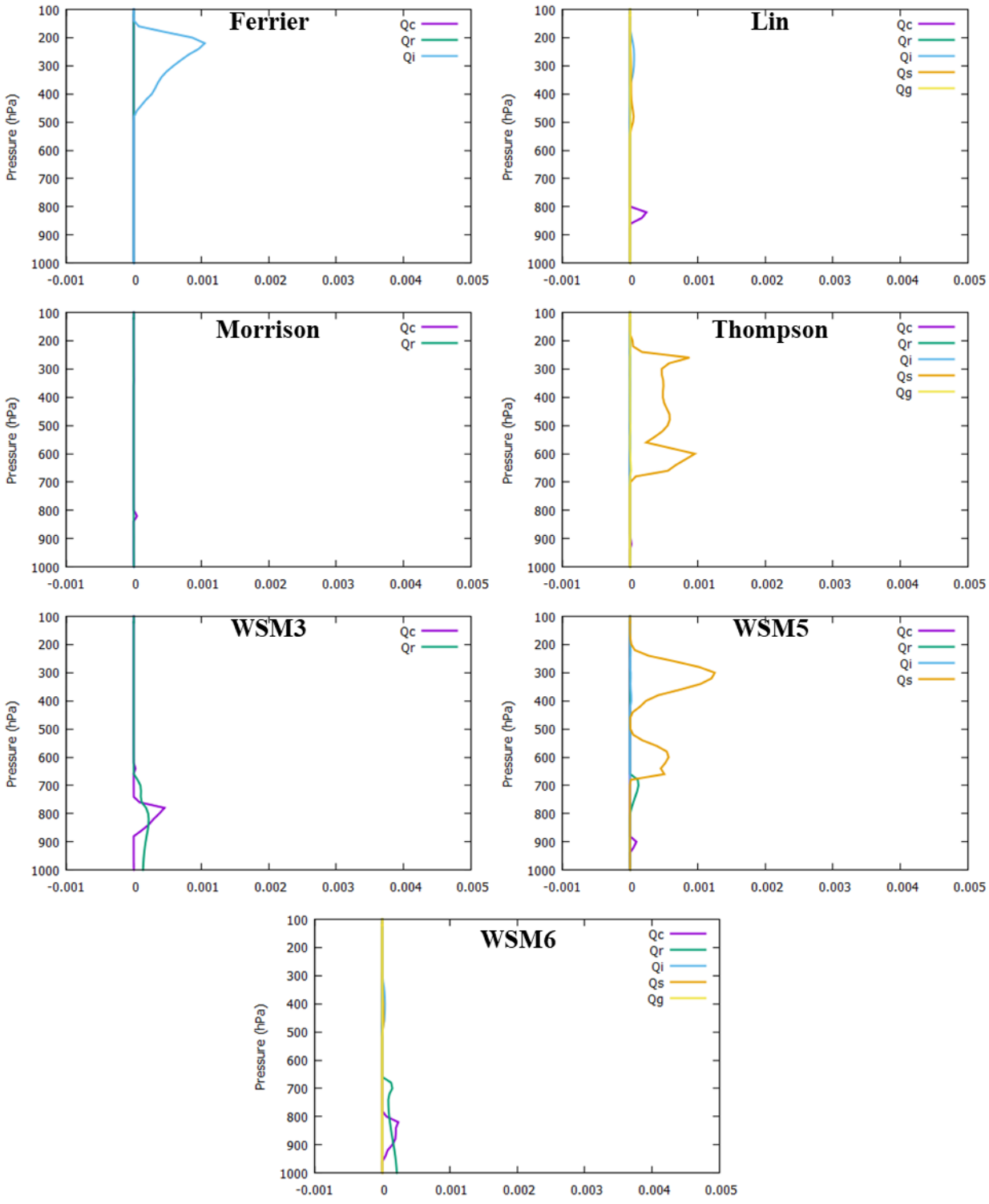

Figure B7. Time evolution of area averaged mixing ratios (g/kg) for cyclone Titli

Appendix-C

 # load external library to read grib data

```
library(rgdal)
library(gdata)
library(lubridate)
library(RCurl)
library(stringr)
library(SWATplusR)
library(sf)
library(ggplot2)
library(tidyr)
library(dplyr)
```

#Downloading GFS Forecasts for the next five days

```
h <- format(Sys.Date(),"%Y%m%d")
f <- as.numeric(h)
setwd("H:\\GFS_Data")
path <- "H:\\GFS_Data"
files <- list.files()
for ( i in 1: length(files))
  file.remove(files[i])
url =
"https://nomads.ncep.noaa.gov/pub/data/nccf/com/gfs/prod/gfs.20210607/00/atmos/gfs.t00z.pgrb2.0p25.f024"
k <- as.vector(url)
str_sub(k,61,68) <- paste0(h)
destfile = file.path(path, "gfs.t00z.pgrb2.0p25.f024")
download.file(k, destfile,method="curl")
url =
"https://nomads.ncep.noaa.gov/pub/data/nccf/com/gfs/prod/gfs.20210607/00/atmos/gfs.t00z.pgrb2.0p25.f048"
k <- as.vector(url)
str_sub(k,61,68) <- paste0(h)
destfile = file.path(path, "gfs.t00z.pgrb2.0p25.f048")
```

```
download.file(k, destfile,method="curl")

url =
"https://nomads.ncep.noaa.gov/pub/data/nccf/com/gfs/prod/gfs.20210607/00/atmos/gfs.t00z.pgrb2.0p25.f072"

k <- as.vector(url)

str_sub(k,61,68) <- paste0(h)

destfile = file.path(path, "gfs.t00z.pgrb2.0p25.f072")

download.file(k, destfile,method="curl")

url =
"https://nomads.ncep.noaa.gov/pub/data/nccf/com/gfs/prod/gfs.20210607/00/atmos/gfs.t00z.pgrb2.0p25.f096"

k <- as.vector(url)

str_sub(k,61,68) <- paste0(h)

destfile = file.path(path, "gfs.t00z.pgrb2.0p25.f096")

download.file(k, destfile,method="curl")

url =
"https://nomads.ncep.noaa.gov/pub/data/nccf/com/gfs/prod/gfs.20210607/00/atmos/gfs.t00z.pgrb2.0p25.f120"

k <- as.vector(url)

str_sub(k,61,68) <- paste0(h)

destfile = file.path(path, "gfs.t00z.pgrb2.0p25.f120")

download.file(k, destfile,method="curl")
```

 # now load the data (assuming the data is in the current working directory)

```
#datain1 <- readGDAL("H:\\GFS_Data\\gfs.t00z.pgrb2.0p25.f024")

#datain2 <- readGDAL("H:\\GFS_Data\\gfs.t00z.pgrb2.0p25.f048")

#datain3 <- readGDAL("H:\\GFS_Data\\gfs.t00z.pgrb2.0p25.f072")

#datain4 <- readGDAL("H:\\GFS_Data\\gfs.t00z.pgrb2.0p25.f096")

#datain5 <- readGDAL("H:\\GFS_Data\\gfs.t00z.pgrb2.0p25.f120")

#Code testing for TITLI cyclone data

datain1 <- readGDAL("H:\\GFS_Data\\gfs.0p25.2021092700.f024.grib2")

datain2 <- readGDAL("H:\\GFS_Data\\gfs.0p25.2021092700.f048.grib2")

datain3 <- readGDAL("H:\\GFS_Data\\gfs.0p25.2021092700.f072.grib2")

datain4 <- readGDAL("H:\\GFS_Data\\gfs.0p25.2021092700.f096.grib2")
```

datain5 <- readGDAL("H:\\GFS_Data\\gfs.0p25.2021092700.f120.grib2")

bfact = read.csv("H:\\GFS_Data\\input_files\\bias_factors.csv", header = T) **#bfact is bias factors csv file**

nlatlong = read.csv("H:\\GFS_Data\\input_files\\latlong_nagavali.csv", header = F) **#Nagavali Basin Lat long file**

vlatlong = read.csv("H:\\GFS_Data\\input_files\\latlong_vamsadhara.csv", header = F) **#Vamsadhara Basin Lat long file**

 # extract the data we want to plot and cell centres, e.g. surface air temp

 # bands from https://nomads.ncep.noaa.gov/pub/data/nccf/com/gfs/prod/gfs.20220105/00/atmos/gfs.t00z.pgrb2.0p25.f025.idx

 # Band586: Maximum Precipitation

 # Band587: Minimum Precipitation

 # Band597: Cumulative Precipitation

#Reading Precipitation, Maximum Temperature and Minimum Temperature Data from GFS grib files

day1_precip <- matrix(datain1$band597, 1440, 721)

day2_precip <- matrix(datain2$band597, 1440, 721)

day3_precip <- matrix(datain2$band597, 1440, 721)

day4_precip <- matrix(datain4$band597, 1440, 721)

day5_precip <- matrix(datain5$band597, 1440, 721)

day1_maxt <- matrix(datain1$band586, 1440, 721)

day2_maxt <- matrix(datain2$band586, 1440, 721)

day3_maxt <- matrix(datain2$band586, 1440, 721)

day4_maxt <- matrix(datain4$band586, 1440, 721)

day5_maxt <- matrix(datain5$band586, 1440, 721)

day1_mint <- matrix(datain1$band587, 1440, 721)

day2_mint <- matrix(datain2$band587, 1440, 721)

day3_mint <- matrix(datain2$band587, 1440, 721)

day4_mint <- matrix(datain4$band587, 1440, 721)

day5_mint <- matrix(datain5$band587, 1440, 721)

x <- seq(0.125, by = 0.25, length.out = 1440)

y <- seq(90 - 0.125, by = -0.25, length.out = 721)

 # now put it onto a different grid going -180 to 180 and -90 to 90 # and not the default 0 to 360 and 90 to -90

```
x <- x[c(721:1440,1:720)]
x <- ifelse( x > 180, x - 360, x)
y <- rev(y)
day1_precip = day1_precip[c(721:1440,1:720),721:1]
day2_precip = day2_precip[c(721:1440,1:720),721:1]
day3_precip = day3_precip[c(721:1440,1:720),721:1]
day4_precip = day4_precip[c(721:1440,1:720),721:1]
day5_precip = day5_precip[c(721:1440,1:720),721:1]
day1_maxt = day1_maxt[c(721:1440,1:720),721:1]
day2_maxt = day2_maxt[c(721:1440,1:720),721:1]
day3_maxt = day3_maxt[c(721:1440,1:720),721:1]
day4_maxt = day4_maxt[c(721:1440,1:720),721:1]
day5_maxt = day5_maxt[c(721:1440,1:720),721:1]
day1_mint = day1_mint[c(721:1440,1:720),721:1]
day2_mint = day2_mint[c(721:1440,1:720),721:1]
day3_mint = day3_mint[c(721:1440,1:720),721:1]
day4_mint = day4_mint[c(721:1440,1:720),721:1]
day5_mint = day5_mint[c(721:1440,1:720),721:1]
```

#Extracting the Precipitation Maximum Temperature and Minimum Temperature data over the Nagavali and Vamsadhara Basins

```
nv_precipday1 = day1_precip[1051:1060,433:442]
nv_precipday2 = day2_precip[1051:1060,433:442]
nv_precipday3 = day3_precip[1051:1060,433:442]
nv_precipday4 = day4_precip[1051:1060,433:442]
nv_precipday5 = day5_precip[1051:1060,433:442]
nv_maxtday1 = day1_maxt[1051:1060,433:442]
nv_maxtday2 = day2_maxt[1051:1060,433:442]
nv_maxtday3 = day3_maxt[1051:1060,433:442]
nv_maxtday4 = day4_maxt[1051:1060,433:442]
nv_maxtday5 = day5_maxt[1051:1060,433:442]
```

```
nv_mintday1 = day1_mint[1051:1060,433:442]
nv_mintday2 = day2_mint[1051:1060,433:442]
nv_mintday3 = day3_mint[1051:1060,433:442]
nv_mintday4 = day4_mint[1051:1060,433:442]
nv_mintday5 = day5_mint[1051:1060,433:442]
precipday1 = unmatrix(nv_precipday1,byrow=T)
precipday2 = unmatrix(nv_precipday2,byrow=T)
precipday3 = unmatrix(nv_precipday3,byrow=T)
precipday4 = unmatrix(nv_precipday4,byrow=T)
precipday5 = unmatrix(nv_precipday5,byrow=T)
precipday1 = t(precipday1)
precipday2 = t(precipday2)
precipday3 = t(precipday3)
precipday4 = t(precipday4)
precipday5 = t(precipday5)
precipitation = rbind(precipday1,precipday2, precipday3, precipday4, precipday5)
maxtday1 = unmatrix(nv_maxtday1,byrow=T)
maxtday2 = unmatrix(nv_maxtday2,byrow=T)
maxtday3 = unmatrix(nv_maxtday3,byrow=T)
maxtday4 = unmatrix(nv_maxtday4,byrow=T)
maxtday5 = unmatrix(nv_maxtday5,byrow=T)
maxtday1 = t(maxtday1)
maxtday2 = t(maxtday2)
maxtday3 = t(maxtday3)
maxtday4 = t(maxtday4)
maxtday5 = t(maxtday5)
MaxT = rbind(maxtday1,maxtday2, maxtday3, maxtday4, maxtday5)
mintday1 = unmatrix(nv_mintday1,byrow=T)
mintday2 = unmatrix(nv_mintday2,byrow=T)
mintday3 = unmatrix(nv_mintday3,byrow=T)
mintday4 = unmatrix(nv_mintday4,byrow=T)
mintday5 = unmatrix(nv_mintday5,byrow=T)
```

```
mintday1 = t(mintday1)
mintday2 = t(mintday2)
mintday3 = t(mintday3)
mintday4 = t(mintday4)
mintday5 = t(mintday5)
MinT = rbind(mintday1,mintday2, mintday3, mintday4, mintday5)
```

#Applying Bias Correction to Precipitation data

```
Bc_precip = precipitation * bfact[,1]
```

#Extracting rainfall and temperature data over the Nagavali basin

```
ng1 = rowMeans(Bc_precip[,c(52,53,62,63)])
ng2 = rowMeans(Bc_precip[,c(13,14,23,24)])
ng3 = rowMeans(Bc_precip[,c(23,24,33,34)])
ng4 = rowMeans(Bc_precip[,c(33,34,43,44)])
ng5 = rowMeans(Bc_precip[,c(43,44,53,54)])
ng6 = rowMeans(Bc_precip[,c(24,25,34,35)])
ng7 = rowMeans(Bc_precip[,c(34,35,44,45)])
ng8 = rowMeans(Bc_precip[,c(44,45,54,55)])
ng9 = rowMeans(Bc_precip[,c(25,26,35,36)])
ng10 = rowMeans(Bc_precip[,c(35,36,45,46)])
ng11 = rowMeans(Bc_precip[,c(26,27,36,37)])
ng12 = rowMeans(Bc_precip[,c(36,37,46,47)])
ng13 = rowMeans(Bc_precip[,c(27,28,37,38)])
```

#Maximum Temperature

```
ngmax1 = rowMeans(MaxT[,c(52,53,62,63)])
ngmax2 = rowMeans(MaxT[,c(13,14,23,24)])
ngmax3 = rowMeans(MaxT[,c(23,24,33,34)])
ngmax4 = rowMeans(MaxT[,c(33,34,43,44)])
ngmax5 = rowMeans(MaxT[,c(43,44,53,54)])
ngmax6 = rowMeans(MaxT[,c(24,25,34,35)])
ngmax7 = rowMeans(MaxT[,c(34,35,44,45)])
ngmax8 = rowMeans(MaxT[,c(44,45,54,55)])
ngmax9 = rowMeans(MaxT[,c(25,26,35,36)])
```

```
ngmax10 = rowMeans(MaxT[,c(35,36,45,46)])
ngmax11 = rowMeans(MaxT[,c(26,27,36,37)])
ngmax12 = rowMeans(MaxT[,c(36,37,46,47)])
ngmax13 = rowMeans(MaxT[,c(27,28,37,38)])
```

##Minimum Temperature

```
ngmin1 = rowMeans(MinT[,c(52,53,62,63)])
ngmin2 = rowMeans(MinT[,c(13,14,23,24)])
ngmin3 = rowMeans(MinT[,c(23,24,33,34)])
ngmin4 = rowMeans(MinT[,c(33,34,43,44)])
ngmin5 = rowMeans(MinT[,c(43,44,53,54)])
ngmin6 = rowMeans(MinT[,c(24,25,34,35)])
ngmin7 = rowMeans(MinT[,c(34,35,44,45)])
ngmin8 = rowMeans(MinT[,c(44,45,54,55)])
ngmin9 = rowMeans(MinT[,c(25,26,35,36)])
ngmin10 = rowMeans(MinT[,c(35,36,45,46)])
ngmin11 = rowMeans(MinT[,c(26,27,36,37)])
ngmin12 = rowMeans(MinT[,c(36,37,46,47)])
ngmin13 = rowMeans(MinT[,c(27,28,37,38)])
```

#Comibing all the grids into single file

```
ngrain = cbind(ng1,ng2,ng3,ng4,ng5,ng6,ng7,ng8,ng9,ng10,ng11,ng12,ng13)
ngmaxt = cbind(ngmax1,ngmax2,ngmax3,ngmax4,ngmax5,ngmax6,ngmax7,ngmax8,
         ngmax9,ngmax10,ngmax11,ngmax12,ngmax13)
ngmint = cbind(ngmin1,ngmin2,ngmin3,ngmin4,ngmin5,ngmin6,ngmin7,ngmin8,
         ngmin9,ngmin10,ngmin11,ngmin12,ngmin13)
ngrain = round(ngrain, digits = 0)
ngmaxt = round(ngmaxt, digits = 0)
ngmint = round(ngmint, digits = 0)
colnames(ngrain) = NULL
colnames(ngmaxt) = NULL
colnames(ngmint) = NULL
nrainfall = rbind(nlatlong,ngrain)
nmaxt = rbind(nlatlong,ngmaxt)
```

```
nmint = rbind(nlatlong,ngmint)

ntemp =
cbind(nmaxt$V1,nmint$V1,nmaxt$V2,nmint$V2,nmaxt$V3,nmint$V3,nmaxt$V4,nmint$V4,
nmaxt$V5,nmint$V5,nmaxt$V6,nmint$V6,nmaxt$V7,nmint$V7,nmaxt$V8,nmint$V8,
nmaxt$V9,nmint$V9,nmaxt$V10,nmint$V10,nmaxt$V11,nmint$V11,nmaxt$V12,nmint$V1
2,nmaxt$V13,nmint$V13,nmaxt$V14,nmint$V14,nmaxt$V15,nmint$V15,nmaxt$V16,nmint
$V16)

vg1 = rowMeans(Bc_precip[,c(53,54,63,64)])

vg2 = rowMeans(Bc_precip[,c(54,55,64,65)])

vg3 = rowMeans(Bc_precip[,c(64,65,74,75)])

vg4 = rowMeans(Bc_precip[,c(45,46,55,56)])

vg5 = rowMeans(Bc_precip[,c(55,56,65,66)])

vg6 = rowMeans(Bc_precip[,c(65,66,75,76)])

vg7 = rowMeans(Bc_precip[,c(46,47,56,57)])

vg8 = rowMeans(Bc_precip[,c(56,57,66,67)])

vg9 = rowMeans(Bc_precip[,c(66,67,76,77)])

vg10 = rowMeans(Bc_precip[,c(37,38,47,48)])

vg11 = rowMeans(Bc_precip[,c(47,48,57,58)])

vg12 = rowMeans(Bc_precip[,c(57,58,67,68)])

vg13 = rowMeans(Bc_precip[,c(67,68,77,78)])

vg14 = rowMeans(Bc_precip[,c(38,39,48,49)])

vg15 = rowMeans(Bc_precip[,c(48,49,58,59)])

vg16 = rowMeans(Bc_precip[,c(58,59,68,69)])
```

#Maximum Temperature

```
vgmax1 = rowMeans(MaxT[,c(53,54,63,64)])

vgmax2 = rowMeans(MaxT[,c(54,55,64,65)])

vgmax3 = rowMeans(MaxT[,c(64,65,74,75)])

vgmax4 = rowMeans(MaxT[,c(45,46,55,56)])

vgmax5 = rowMeans(MaxT[,c(55,56,65,66)])

vgmax6 = rowMeans(MaxT[,c(65,66,75,76)])

vgmax7 = rowMeans(MaxT[,c(46,47,56,57)])

vgmax8 = rowMeans(MaxT[,c(56,57,66,67)])

vgmax9 = rowMeans(MaxT[,c(66,67,76,77)])

vgmax10 = rowMeans(MaxT[,c(37,38,47,48)])
```

```
vgmax11 = rowMeans(MaxT[,c(47,48,57,58)])
vgmax12 = rowMeans(MaxT[,c(57,58,67,68)])
vgmax13 = rowMeans(MaxT[,c(67,68,77,78)])
vgmax14 = rowMeans(MaxT[,c(38,39,48,49)])
vgmax15 = rowMeans(MaxT[,c(48,49,58,59)])
vgmax16 = rowMeans(MaxT[,c(58,59,68,69)])
```

#Minimum Temperature

```
vgmin1 = rowMeans(MinT[,c(53,54,63,64)])
vgmin2 = rowMeans(MinT[,c(54,55,64,65)])
vgmin3 = rowMeans(MinT[,c(64,65,74,75)])
vgmin4 = rowMeans(MinT[,c(45,46,55,56)])
vgmin5 = rowMeans(MinT[,c(55,56,65,66)])
vgmin6 = rowMeans(MinT[,c(65,66,75,76)])
vgmin7 = rowMeans(MinT[,c(46,47,56,57)])
vgmin8 = rowMeans(MinT[,c(56,57,66,67)])
vgmin9 = rowMeans(MinT[,c(66,67,76,77)])
vgmin10 = rowMeans(MinT[,c(37,38,47,48)])
vgmin11 = rowMeans(MinT[,c(47,48,57,58)])
vgmin12 = rowMeans(MinT[,c(57,58,67,68)])
vgmin13 = rowMeans(MinT[,c(67,68,77,78)])
vgmin14 = rowMeans(MinT[,c(38,39,48,49)])
vgmin15 = rowMeans(MinT[,c(48,49,58,59)])
vgmin16 = rowMeans(MinT[,c(58,59,68,69)])
vgrain = cbind(vg1,vg2,vg3,vg4,vg5,vg6,vg7,vg8,vg9,vg10,vg11,
        vg12,vg13,vg14,vg15,vg16)
vgmaxt = cbind(vgmax1,vgmax2,vgmax3,vgmax4,vgmax5,vgmax6,vgmax7,
vgmax8,vgmax9,vgmax10,vgmax11,vgmax12,vgmax13,vgmax14,vgmax15,vgmax16)
vgmint = cbind(vgmin1,vgmin2,vgmin3,vgmin4,vgmin5,vgmin6,vgmin7,
        vgmin8,vgmin9,vgmin10,vgmin11,vgmin12,vgmin13,vgmin14,vgmin15,vgmin16)
vgrain = round(vgrain,digits = 0)
vgmaxt = round(vgmaxt,digits = 0)
vgmint = round(vgmint,digits = 0)
```

```
colnames(vgrain) = NULL

colnames(vgmaxt) = NULL

colnames(vgmint) = NULL

vrainfall = rbind(vlatlong,vgrain)

vmaxt = rbind(vlatlong,vgmaxt)

vmint = rbind(vlatlong,vgmint)

vtemp =
cbind(vmaxt$V1,vmint$V1,vmaxt$V2,vmint$V2,vmaxt$V3,vmint$V3,vmaxt$V4,vmint$V4,
vmaxt$V5,vmint$V5,vmaxt$V6,vmint$V6,vmaxt$V7,vmint$V7,vmaxt$V8,vmint$V8,
vmaxt$V9,vmint$V9,vmaxt$V10,vmint$V10,vmaxt$V11,vmint$V11,vmaxt$V12,vmint$V1
2,vmaxt$V13,vmint$V13,vmaxt$V14,vmint$V14,vmaxt$V15,vmint$V15,vmaxt$V16,vmint
$V16)
```

#Converting Precipitation data into SWAT (.pcp)for Nagavali basin

```
nagavalirain<-nrainfall[-(1:2),]

testnrain = rbind(nagavalirain,nagavalirain)

nagavalirain = testnrain

for (i in 1:nrow(nagavalirain)) {

  print(i)

  kdays<-nagavalirain[i,]

  kdays[which(nchar(as.numeric(round(as.numeric(kdays))))==2)]<-
paste0('0',kdays[which(nchar(as.numeric(round(as.numeric(kdays))))==2)])

  kdays[which(nchar(as.numeric(round(as.numeric(kdays))))==1)]<-
paste0('00',kdays[which(nchar(as.numeric(round(as.numeric(kdays))))==1)])

  kdays[which(nchar(as.numeric((as.numeric(kdays))))==1)]<-
paste0(kdays[which(nchar(as.numeric((as.numeric(kdays))))==1)],'.0')

  kdays[which(nchar(as.numeric((as.numeric(kdays))))==2)]<-
paste0(kdays[which(nchar(as.numeric((as.numeric(kdays))))==2)],'.0')

  kdays[which(as.numeric(kdays)==0)]<-'000.0'

  nagavalirain[i,]<-kdays

}

ltt<-sprintf("%1.1f",nrainfall[1,])

loo<-sprintf("%1.1f",nrainfall[2,])

dttt<-(as.numeric('001'):(as.numeric('001')+nrow(nagavalirain)-1))

jdays<-dttt

jdays[which(nchar(jdays)==2)]<-paste0('0',jdays[which(nchar(jdays)==2)])
```

```
jdays[which(nchar(jdays)==1)]<-paste0('00',jdays[which(nchar(jdays)==1)])

r1<-c('Station  ',paste0('X',(loo),'Y',ltt,','))

lt<-c('Lati    ',paste0((ltt),' '))

lo<-c('Long    ',paste0((loo),' '))

el<-c('Elev   ',paste0('    ',rep(0,ncol(nrainfall))))

dtl<-paste0(2021,jdays)

rs<-cbind(dtl,nagavalirain)

rs<-rbind(r1,lt,lo,el,rs)

#write.table(rs,'pcp1.pcp',row.names = F,col.names = F,quote = F,sep = "")

write.table(rs,'F:\\SPARC\\Inundation_Maps\\SWAT_RES\\Nagavali_Res\\Scenarios\\N_RS
WAT\\TxtInOut\\pcp1.pcp',row.names = F,col.names = F,quote = F,sep = "")
```

#Converting Temperature data into SWAT (.tmp)for Nagavali basin

```
nagavalitemp<-ntemp[-(1:2),]

testntemp = rbind(nagavalitemp,nagavalitemp)

nagavalitemp = testntemp

for (i in 1:nrow(nagavalitemp)) {

  print(i)

  kdays<-nagavalitemp[i,]

  kdays[which(nchar(as.numeric(round(as.numeric(kdays))))==2)]<-
paste0('0',kdays[which(nchar(as.numeric(round(as.numeric(kdays))))==2)])

  kdays[which(nchar(as.numeric(round(as.numeric(kdays))))==1)]<-
paste0('00',kdays[which(nchar(as.numeric(round(as.numeric(kdays))))==1)])

  kdays[which(nchar(as.numeric((as.numeric(kdays))))==1)]<-
paste0(kdays[which(nchar(as.numeric((as.numeric(kdays))))==1)],'.0')

  kdays[which(nchar(as.numeric((as.numeric(kdays))))==2)]<-
paste0(kdays[which(nchar(as.numeric((as.numeric(kdays))))==2)],'.0')

  kdays[which(as.numeric(kdays)==0)]<-'000.0'

  nagavalitemp[i,]<-kdays

}

dttt<-(as.numeric('001'):(as.numeric('001')+nrow(nagavalitemp)-1))

jdays<-dttt

jdays[which(nchar(jdays)==2)]<-paste0('0',jdays[which(nchar(jdays)==2)])

jdays[which(nchar(jdays)==1)]<-paste0('00',jdays[which(nchar(jdays)==1)])

ltt<-sprintf("%1.1f",ntemp[1,])
```

```
loo<-sprintf("%1.1f",ntemp[2,])
ctl1<-c()
ctl2<-c()
ct1<-1
while (ct1<=length(ltt)) {
 ctl1<-c(ctl1,ct1)
 ctl2<-c(ctl2,ct1+1)
 ct1<-ct1+2
}
loo[ctl2]<-'    '
ltt[ctl2]<-'    '
ell<-paste0('    ',rep(0,ncol(ntemp)))
ell[ctl2]<-'     '
stn<-paste0('X',(loo),'Y',ltt,',')
stn[ctl2]<-''
r1<-c('Station  ',stn)
lt<-c('Lati         ',paste0((ltt),' '))
lo<-c('Long         ',paste0((loo),' '))
el<-c('Elev        ',ell)
dtl<-paste0('2021',jdays)
rs<-cbind(dtl,nagavalitemp)
rs<-rbind(r1,lt,lo,el,rs)
#write.table(rs,'Tmp1.Tmp',row.names = F,col.names = F,quote = F,sep = "")
write.table(rs,'F:\\SPARC\\Inundation_Maps\\SWAT_RES\\Nagavali_Res\\Scenarios\\N_RS
WAT\\TxtInOut\\Tmp1.Tmp',row.names = F,col.names = F,quote = F,sep = "")
```

#Converting Precipitation data into SWAT (.pcp) for Vamsadhara basin

```
vamsdhararain<-vrainfall[-(1:2),]
testvrain = rbind(vamsdhararain,vamsdhararain)
vamsdhararain = testvrain
for (i in 1:nrow(vamsdhararain)) {
 print(i)
 kdays<-vamsdhararain[i,]
```

```
  kdays[which(nchar(as.numeric(round(as.numeric(kdays))))==2)]<-
paste0('0',kdays[which(nchar(as.numeric(round(as.numeric(kdays))))==2)])

  kdays[which(nchar(as.numeric(round(as.numeric(kdays))))==1)]<-
paste0('00',kdays[which(nchar(as.numeric(round(as.numeric(kdays))))==1)])

  kdays[which(nchar(as.numeric((as.numeric(kdays))))==1)]<-
paste0(kdays[which(nchar(as.numeric((as.numeric(kdays))))==1)],'.0')

  kdays[which(nchar(as.numeric((as.numeric(kdays))))==2)]<-
paste0(kdays[which(nchar(as.numeric((as.numeric(kdays))))==2)],'.0')

  kdays[which(as.numeric(kdays)==0)]<-'000.0'

  vamsdhararain[i,]<-kdays

}

ltt<-sprintf("%1.1f",vrainfall[1,])

loo<-sprintf("%1.1f",vrainfall[2,])

dttt<-(as.numeric('001'):(as.numeric('001')+nrow(vamsdhararain)-1))

jdays<-dttt

jdays[which(nchar(jdays)==2)]<-paste0('0',jdays[which(nchar(jdays)==2)])

jdays[which(nchar(jdays)==1)]<-paste0('00',jdays[which(nchar(jdays)==1)])

r1<-c('Station  ',paste0('X',(loo),'Y',ltt,','))

lt<-c('Lati    ',paste0((ltt),' '))

lo<-c('Long    ',paste0((loo),' '))

el<-c('Elev   ',paste0('    ',rep(0,ncol(vrainfall))))

dtl<-paste0(2021,jdays)

rs<-cbind(dtl,vamsdhararain)

rs<-rbind(r1,lt,lo,el,rs)

write.table(rs,'F:\\SPARC\\Inundation_Maps\\SWAT_RES\\VAMSADHARA_RES\\Scenario
s\\V_RSWAT\\TxtInOut\\pcp1.pcp',row.names = F,col.names = F,quote = F,sep = "")
```

#Converting Temperature data into SWAT (.tmp) for Vamsadhara basin

```
vamsdharatemp<-vtemp[-(1:2),]

testvtemp = rbind(vamsdharatemp,vamsdharatemp)

vamsdharatemp = testvtemp

for (i in 1:nrow(vamsdharatemp)) {

  print(i)

  kdays<-vamsdharatemp[i,]
```

```
  kdays[which(nchar(as.numeric(round(as.numeric(kdays))))==2)]<-
paste0('0',kdays[which(nchar(as.numeric(round(as.numeric(kdays))))==2)])
  kdays[which(nchar(as.numeric(round(as.numeric(kdays))))==1)]<-
paste0('00',kdays[which(nchar(as.numeric(round(as.numeric(kdays))))==1)])
  kdays[which(nchar(as.numeric((as.numeric(kdays))))==1)]<-
paste0(kdays[which(nchar(as.numeric((as.numeric(kdays))))==1)],'.0')
  kdays[which(nchar(as.numeric((as.numeric(kdays))))==2)]<-
paste0(kdays[which(nchar(as.numeric((as.numeric(kdays))))==2)],'.0')
  kdays[which(as.numeric(kdays)==0)]<-'000.0'
  vamsdharatemp[i,]<-kdays
}
dttt<-(as.numeric('001'):(as.numeric('001')+nrow(vamsdharatemp)-1))
jdays<-dttt
jdays[which(nchar(jdays)==2)]<-paste0('0',jdays[which(nchar(jdays)==2)])
jdays[which(nchar(jdays)==1)]<-paste0('00',jdays[which(nchar(jdays)==1)])
ltt<-sprintf("%1.1f",vtemp[1,])
loo<-sprintf("%1.1f",vtemp[2,])
ctl1<-c()
ctl2<-c()
ct1<-1
while (ct1<=length(ltt)) {
  ctl1<-c(ctl1,ct1)
  ctl2<-c(ctl2,ct1+1)
  ct1<-ct1+2
}
loo[ctl2]<-'    '
ltt[ctl2]<-'    '
ell<-paste0('    ',rep(0,ncol(vtemp)))
ell[ctl2]<-'     '
stn<-paste0('X',(loo),'Y',ltt,',')
stn[ctl2]<-''
r1<-c('Station  ',stn)
lt<-c('Lati         ',paste0((ltt),' '))
```

```
lo<-c('Long         ',paste0((loo),' '))

el<-c('Elev        ',ell)

dtl<-paste0('2021',jdays)

rs<-cbind(dtl,vamsdharatemp)

rs<-rbind(r1,lt,lo,el,rs)

write.table(rs,"F:\\SPARC\\Inundation_Maps\\SWAT_RES\\VAMSADHARA_RES\\Scenarios\\V_RSWAT\\TxtInOut\\Tmp1.Tmp",row.names = F,col.names = F,quote = F,sep = "")
```

#Running SWAT Model

```
q_sim_nag <- run_swat2012(project_path = 'F:\\SPARC\\Inundation_Maps\\SWAT_RES\\Nagavali_Res\\Scenarios\\N_RSWAT\\TxtInOut',
                          output = define_output(file = "rch",
                                                 variable = "FLOW_OUT",
                                                 unit = 1:34),
                          start_date = "2021-01-01",
                          end_date = "2021-01-10")

print(q_sim_nag)

nag_dis = rbind(q_sim_nag$FLOW_OUT_7,q_sim_nag$FLOW_OUT_27,(q_sim_nag$FLOW_OUT_2+q_sim_nag$FLOW_OUT_12))

nag_dis = t(nag_dis)

nag_dis = nag_dis[-(1:5),]

q_sim_vam <- run_swat2012(project_path = 'F:\\SPARC\\Inundation_Maps\\SWAT_RES\\VAMSADHARA_RES\\Scenarios\\V_RSWAT\\TxtInOut',
                          output = define_output(file = "rch",
                                                 variable = "FLOW_OUT",
                                                 unit = 1:30),
                          start_date = "2021-01-01",
                          end_date = "2021-01-10")

print(q_sim_vam)

vam_dis = rbind(q_sim_vam$FLOW_OUT_4,(q_sim_vam$FLOW_OUT_16+q_sim_vam$FLOW_OUT_17))

vam_dis = t(vam_dis)
```

```
vam_dis = vam_dis[-(1:5),]
```

#Updating SWAT simulated discharge into HEC-RAS model for Nagavali Basin

```
dt<-Sys.Date()
mtl<-c('JAN','FEB','MAR','APR','MAY','JUN','JUL','AUG','SEP','OCT','NOV','DEC')
yr<-substr(dt,1,4)
mt<-substr(dt,6,7)
dy<-substr(dt,9,10)
dt2<-paste0(dy,mtl[as.numeric(mt)],yr)
if (as.numeric(yr)%%4==0){
  mtl2<-c(31,29,31,30,31,30,31,31,30,31,30,31)
}else{
  mtl2<-c(31,29,31,30,31,30,31,31,30,31,30,31)
}
stdate<-dt2
dy2<-as.numeric(dy)+5
if (dy2>=mtl2[as.numeric(mt)]){
  dy2<-mtl2[as.numeric(mt)]-dy2
  mtk<-as.numeric(mt)+1
  if (mtk>=12){
    mtk<-as.numeric(mtk)-12
    yrk<-as.numeric(yr)+1
    mt<-mtk
    yr<-yrk
  }
}
if (nchar(dy2)<2){
  dy2<-paste0(0,dy2)
}
enddate<-paste0(dy2,mtl[as.numeric(mt)],yr)
a<-readLines("F:\\SPARC\\Inundation_Maps\\Nagavali_2d_1d -
Copy\\Nagavali_2d_1d.u01")
xt13<-paste0('Fixed Start Date/Time=',stdate,',00:00')
```

```
xt25<-paste0('Fixed Start Date/Time=',stdate,',00:00')
xt37<-paste0('Fixed Start Date/Time=',stdate,',00:00')
a[13]<-xt13
a[25]<-xt25
a[37]<-xt37
bl<-nag_dis
bl<-t(bl)
for (i in 1:3) {
  pt<-a[(12*(i-1))+7]
  bb<-bl[i,]
  kz<-c()
  for (j in 1:length(bb)) {
    if (nchar(as.numeric(bb[j]))!=8){
      gp<-abs(nchar(as.numeric(bb[j]))-8)
      gpp<-paste0(rep(' ',gp),collapse = "")
      kz<-c(kz,paste0(gpp,as.numeric(bb[j])))
    }else{
      kz<-c(kz,paste0(as.numeric(bb[j])))
    }
  }
  stt<-paste0(kz,collapse = "")
  a[(12*(i-1))+7]<-stt
}
writeLines(a,"F:\\SPARC\\Inundation_Maps\\Nagavali_2d_1d - Copy\\Nagavali_2d_1d.u01")
```

#Updating the Simulation Time for Nagavali Basin

```
dt<-Sys.Date()
mtl<-c('JAN','FEB','MAR','APR','MAY','JUN','JUL','AUG','SEP','OCT','NOV','DEC')
yr<-substr(dt,1,4)
mt<-substr(dt,6,7)
dy<-substr(dt,9,10)
dt2<-paste0(dy,mtl[as.numeric(mt)],yr)
if (as.numeric(yr)%%4==0){
```

```
 mtl2<-c(31,29,31,30,31,30,31,31,30,31,30,31)
}else{
 mtl2<-c(31,29,31,30,31,30,31,31,30,31,30,31)
}
stdate<-dt2
dy2<-as.numeric(dy)+3
if (dy2>=mtl2[as.numeric(mt)]){
 dy2<-dy2-mtl2[as.numeric(mt)]
 mtk<-as.numeric(mt)+1
 if (mtk>=12){
  mtk<-as.numeric(mtk)-12;
  yr<-as.numeric(yr)+1
 }
 mt<-mtk
 yr<-yr
}
if (nchar(dy2)<2){
 dy2<-paste0(0,dy2)
}
enddate<-paste0(dy2,mtl[as.numeric(mt)],yr)
a<-readLines("F:\\SPARC\\Inundation_Maps\\Nagavali_2d_1d -
Copy\\Nagavali_2d_1d.p01")
xt<-paste0('Simulation Date=',stdate,',00:00,',enddate,',00:00')
a[4]<-xt
writeLines(a,"F:\\SPARC\\Inundation_Maps\\Nagavali_2d_1d - Copy\\Nagavali_2d_1d.p01")
```

#Updating SWAT Simulated discharge into HEC-RAS model for Vamsadhara Basin

```
dt<-Sys.Date()
mtl<-c('JAN','FEB','MAR','APR','MAY','JUN','JUL','AUG','SEP','OCT','NOV','DEC')
yr<-substr(dt,1,4)
mt<-substr(dt,6,7)
dy<-substr(dt,9,10)
dt2<-paste0(dy,mtl[as.numeric(mt)],yr)
```

```
if (as.numeric(yr)%%4==0){
  mtl2<-c(31,29,31,30,31,30,31,31,30,31,30,31)
}else{
  mtl2<-c(31,29,31,30,31,30,31,31,30,31,30,31)
}
stdate<-dt2
dy2<-as.numeric(dy)+5
if (dy2>=mtl2[as.numeric(mt)]){
  dy2<-mtl2[as.numeric(mt)]-dy2
  mtk<-as.numeric(mt)+1
  if (mtk>=12){
    mtk<-as.numeric(mtk)-12
    yrk<-as.numeric(yr)+1
    mt<-mtk
    yr<-yrk
  }
}
if (nchar(dy2)<2){
  dy2<-paste0(0,dy2)
}
enddate<-paste0(dy2,mtl[as.numeric(mt)],yr)
a<-readLines("F:\\SPARC\\Inundation_Maps\\V_2d_1d - Copy\\v_1d_2d.u01")
xt13<-paste0('Fixed Start Date/Time=',stdate,',00:00')
xt25<-paste0('Fixed Start Date/Time=',stdate,',00:00')
a[13]<-xt13
a[25]<-xt25
bl<-vam_dis
bl<-t(bl)
for (i in 1:2) {
  pt<-a[(12*(i-1))+7]
  bb<-bl[i,]
  kz<-c()
```

```
  for (j in 1:length(bb)) {
    if (nchar(as.numeric(bb[j]))!=8){
      gp<-abs(nchar(as.numeric(bb[j]))-8)
      gpp<-paste0(rep(' ',gp),collapse = "")
      kz<-c(kz,paste0(gpp,as.numeric(bb[j])))
    }else{
      kz<-c(kz,paste0(as.numeric(bb[j])))
    }
  }
  stt<-paste0(kz,collapse = "")
  a[(12*(i-1))+7]<-stt
}
writeLines(a,"F:\\SPARC\\Inundation_Maps\\V_2d_1d - Copy\\v_1d_2d.u01")
```

#Updating Simulation Time for Vamsadhara Basin

```
dt<-Sys.Date()
mtl<-c('JAN','FEB','MAR','APR','MAY','JUN','JUL','AUG','SEP','OCT','NOV','DEC')
yr<-substr(dt,1,4)
mt<-substr(dt,6,7)
dy<-substr(dt,9,10)
dt2<-paste0(dy,mtl[as.numeric(mt)],yr)
if (as.numeric(yr)%%4==0){
  mtl2<-c(31,29,31,30,31,30,31,31,30,31,30,31)
}else{
  mtl2<-c(31,29,31,30,31,30,31,31,30,31,30,31)
}
stdate<-dt2
dy2<-as.numeric(dy)+3
if (dy2>=mtl2[as.numeric(mt)]){
  dy2<-dy2-mtl2[as.numeric(mt)]
  mtk<-as.numeric(mt)+1
  if (mtk>=12){
    mtk<-as.numeric(mtk)-12;
```

```
  yr<-as.numeric(yr)+1
 }
 mt<-mtk
 yr<-yr
}
if (nchar(dy2)<2){
 dy2<-paste0(0,dy2)
}
enddate<-paste0(dy2,mtl[as.numeric(mt)],yr)
a<-readLines("F:\\SPARC\\Inundation_Maps\\V_2d_1d - Copy\\v_1d_2d.p01")
xt<-paste0('Simulation Date=',stdate,',00:00,',enddate,',00:00')
a[4]<-xt
writeLines(a,"F:\\SPARC\\Inundation_Maps\\V_2d_1d - Copy\\v_1d_2d.p01")
```

#Running HEC-RAS Model

```
import win32com.client
from osgeo import gdal
RC = win32com.client.Dispatch("RAS610.HECRASController")
RC.ShowRAS()
```

#Nagavali HEC-RAS File

```
RC.Project_Open(r"F:\SPARC\Inundation_Maps\Nagavali_2d_1d - Copy\Nagavali_2d_1d.prj")
Simulation=RC.Compute_CurrentPlan(None,None,True)
RC.Project_Save()
RC.QuitRAS()
src = gdal.Open(r"F:\SPARC\Inundation_Maps\Nagavali_2d_1d - Copy\N_1d_2d\Depth (Max).Nagavali_SRTM_DEM.tif")
src1 = r"F:\SPARC\Inundation_Maps\data_dir\Inundation_Maps\Nagavali_FIM.tif"
ds = gdal.Translate(src1,src)
ds = None
```

#Vamsadhara HEC-RAS File

```
RC.ShowRAS()
RC.Project_Open(r"F:\SPARC\Inundation_Maps\V_2d_1d - Copy\v_1d_2d.prj")
```

```
Simulation=RC.Compute_CurrentPlan(None,None,True)

RC.Project_Save()

RC.QuitRAS()

src = gdal.Open(r"F:\SPARC\Inundation_Maps\V_2d_1d - Copy\2d1d\Depth
(Max).Vamsadhara_SRTM_DEM.tif")

src1 = r"F:\SPARC\Inundation_Maps\data_dir\Inundation_Maps\Vamsadhara_FIM.tif"

ds = gdal.Translate(src1,src)

ds = None
```

Appendix-D

HTML Script

```
<!DOCTYPE html>
<html>
  <head>
    <meta charset="utf-8" />
    <title>Real-time Flood Forecastig</title>
    <meta
      name="viewport"
      content="initial-scale=1.0, user-scalable=no, width=device-width"
    />
```

#Connecting CSS and JavaScript files to HTML Script

```
    <link rel="stylesheet" href="https://openlayers.org/en/v6.12.0/css/ol.css" />
    <link rel="stylesheet" href="./dist/ol-style.css" />
    <link rel="stylesheet" href="style.css" />
  </head>
  <body>
    <div id="header">
      <div id="row1">
        <div id="column1">
          <a href="https://www.nitw.ac.in/" target="_blank">
            <img src="./img/NITW.png" alt="NITW" style="width: 100%;">
        </a>
        </div>
        <div id="column1">
          <a href="https://sparc.iitkgp.ac.in/" target="_blank">
              <img src="./img/SPARC1.png" alt="SPARC" style="width: 100%;">
          </a>
        </div>
        <div id="column2">
          <h2><b>Real-time Flood Forecasting Over the
            Nagavali and Vamsadhara Basins</b></h2>
        </div>
        <div class="column1">
          <a href="https://vt.edu/" target="_blank">
              <img src="./img/VT1.png" alt="VT" style="width: 100%;">
          </a>
        </div>
        <div class="column">
          <a href="https://www.tamu.edu/" target="_blank">
              <img src="img/TAMU.png" alt="TAMU" style="width: 100%;">
          </a>
        </div>
      </div>
```

```
  </div>
  <div id="map">
   <div id="Legend">
    <h4>Depth (m)</h4>
    <img
src="http://localhost:8080/geoserver/wms?REQUEST=GetLegendGraphic&VERSION=1.0.0
&FORMAT=image/png&WIDTH=20&HEIGHT=20&LAYER=SPARC:Nagavali_FIM"
alt="">
   </div>
  </div>
  <script src="https://openlayers.org/en/v6.12.0/build/ol.js"></script>
  <script src="./dist/ol-main.js"></script>
  <script src="main.js"></script>
  <hr>
   <p><u><b>Project Details</b></u></p>
   <p>The work has been carried out as a part of on-going SPARC projecrt titled <b>Real-
time Flood Forecastig using SWAT model</b> over
   the <a href="https://en.wikipedia.org/wiki/Nagavali_River">Nagavali</a> and <a
href="https://en.wikipedia.org/wiki/Vamsadhara_River">
   Vamsadhara</a> Basins funded by MoE. The work has been carried out at
   National Institute of Technology Waranagal (NITW) in collaboration with Virginia Tech
   (VT), Blacksburg, VA, USA and Texas A&M University (TAMU), College Station, TX,
USA. The project is carried out with fund by Ministry of Education (MoE) (erstwhile MHRD),
   <i><b> GoI under Scheme for Promotion of Academic and Research Collaboration
(SPARC) </b></i>
   with projetc number P270.</p>
  <hr>
  <div id="footer">
   <div id="frow">
    <div id="fcol1">
     <p><u><b>Scholars Involved in the Project</b></u></p>
     <p>1. Mr. G Venkata Rao, Research Scholar, Civil Engineering Dept., NITW</p>
     <p>2. Mr. N Nageswara Reddy, Research Scholar, Civil Engineering Dept., NITW</p>
    </div>
    <div id="fcol2">
     <p><u><b>Faculty Involaved in the Project</b></u></p>
     <p>1. <a href="https://www.nitw.ac.in/faculty/id/16214/">Dr. K Venkata Reddy</a>,
Associate Professor, Civil Engineering Dept., NITW (Indian PI) </p>
     <p>2. <a href="https://ssl.tamu.edu/people/r-srinivasan/">Dr. Raghavan
Srinivasan</a>, Director of the Texas A&M AgriLife Blackland Research & Extension Center,
TAMU, College Station, TX, USA (Foreign PI)</p>
     <p>3. <a href="https://www.bse.vt.edu/people/faculty/venkat-sridhar.html">Dr.
Venkataramana Sridhar</a>, Associate Professor, Department of Biological Syatems
Engineering, VT, Blacksburg, VA, USA (Foreign Co-PI)</p>
     <p>4. <a href="https://www.nitw.ac.in/faculty/id/16195/">Dr. N V Umamahesh</a>,
Professor, Civil Engineering Dept., NITW (Indian Co-PI)</p>
```

```
        <p>5. <a href="https://www.nitw.ac.in/faculty/id/16205/">Dr. Deva Pratap</a>, Professor, Civil Engineering Dept., NITW (Indian Co-PI)</p>
      </div>
      </div>
  </body>
</html>
```

JavaScript

#Importing OpenLayers to JavaScript

```
(function () {
  var fullScreenControl = new ol.control.FullScreen();
  var zoomSliderControl = new ol.control.ZoomSlider();
  var scaleLineControl = new ol.control.ScaleLine();
  var updateLegend = function (resolution) {
    var graphicUrl = wmsSource.getLegendUrl(resolution);
    var img = document.getElementById('legend');
    img.src = graphicUrl;
  };
  var mousePositionControl = new ol.control.MousePosition();
  var map = new ol.Map({
    target: 'map',
    keyboardEventTarget: document,
    controls: ol.control.defaults().extend([
      fullScreenControl,
      //mousePositionControl,
      scaleLineControl,
      zoomSliderControl
    ]),
    layers: [
      new ol.layer.Group({
        title: 'Base maps',
        layers: [
          new ol.layer.Group({
            title: 'Bing Maps',
            type: 'base',
            combine: true,
            visible: true,
            layers: [
              new ol.layer.Tile({
                source: new ol.source.BingMaps({
                  key:                                    "AvcmFjEs4wUeEgcoyiNcImmFiKaHQA6-
yWGPH5cEV4Sru8tQwjyOutXchQ_QLyX-",
                  imagerySet: "AerialWithLabels",
                })
              }),
            ]
```

```
        }),
        new ol.layer.Tile({
          title: 'OSM',
          type: 'base',
          visible: false,
          source: new ol.source.OSM()
        })
      ]
    }),
```

#Importing layers from GeoServer to JavaScript

```
    new ol.layer.Group({
      title: 'Base Layers',
      fold: 'open',
      layers: [
        new ol.layer.Group({
          title: 'Nagavali',
          fold: 'open',
          layers: [
            new ol.layer.Tile({
              title: 'Nagavali Boundary',
              visible: false,
              source: new ol.source.TileWMS({
                url: 'http://localhost:8080/geoserver/SPARC/wms',
                params: {'LAYERS': 'SPARC:Nagavali-Boundary-line', 'TILED': true},
                serverType: 'geoserver',
                transition: 0,
              })
            }),
            new ol.layer.Tile({
              title: 'Nagavali River Network',
              visible: false,
              source: new ol.source.TileWMS({
                url: 'http://localhost:8080/geoserver/SPARC/wms',
                params: {'LAYERS': 'SPARC:Nagavali_streams', 'TILED': true},
                serverType: 'geoserver',
                transition: 0
              })
            }),
            new ol.layer.Image({
              title: 'Inundation Area',
              visible: true,
              source: new ol.source.ImageWMS({
                url: 'http://localhost:8080/geoserver/SPARC/wms',
                params: {'LAYERS': 'SPARC:Nagavali_FIM'},
                serverType: 'geoserver',
                transition: 0,
```

```
        transparent:true,
        format: 'image/png',
        ratio: 1
      })
    })
  ]
}),
new ol.layer.Group({
  title: 'Vamsadhara',
  fold: 'open',
  layers: [
    new ol.layer.Tile({
      title: 'Vamsadhara Boundary',
      visible: false,
      source: new ol.source.TileWMS({
        url: 'http://localhost:8080/geoserver/SPARC/wms',
        params: {'LAYERS': 'SPARC:Vamsadhara-Boundary-line', 'TILED': true},
        serverType: 'geoserver',
        transition: 0
      })
    }),
    new ol.layer.Tile({
      title: 'Vamsadhara River Network',
      visible: false,
      source: new ol.source.TileWMS({
        url: 'http://localhost:8080/geoserver/SPARC/wms',
        params: {'LAYERS': 'SPARC:Vamsadhara_Streams', 'TILED': true},
        serverType: 'geoserver',
        transition: 0
      })
    }),
    new ol.layer.Image({
      title: 'Inundation Area',
      visible: true,
      source: new ol.source.ImageWMS({
        url: 'http://localhost:8080/geoserver/SPARC/wms',
        params: {'LAYERS': 'SPARC:Vamsadhara_FIM'},
        serverType: 'geoserver',
        transition: 0,
        //transparent:true,
        //format: 'image/png',
        ratio: 1
      })
    })
  ]
})
```

```
        ]
      })
    ],
    view: new ol.View({
      center: ol.proj.transform([84, 18.5], 'EPSG:4326', 'EPSG:3857'),
      zoom: 10,
    })
  });
  var layerSwitcher = new ol.control.LayerSwitcher({
    tipLabel: 'Légende', // Optional label for button
    groupSelectStyle: 'children' // Can be 'children' [default], 'group' or 'none'
  });
  map.addControl(layerSwitcher);
  var resolution = map.getView().getResolution();
  updateLegend(resolution);
  map.addLayer(updateLegend);
})();
```

CSS Script

```
html,
body {
  height: 100vh;
  padding: 0;
  margin: 0;
  font-family: sans-serif;
  font-size: small;
}
#header {
  padding: 10px;
  background-color: beige;
}
#map {
  width: 98.7vw;
  height: 80vh;
}
#footer {
  background-color: bisque;
}
/* Limit the width of the layer-switcher */
.layer-switcher {
  max-width: 300px;
}
h3 {
  text-align: center;
  color: goldenrod;
```

```
}
h2{
  text-align: center;
  margin: 0%;
  padding: 0px;
}
hr {
  margin: 0px;
  padding: 2px;
}
p {
  text-align: justify;
  padding-left: 1%;
  padding-right: 1%;
  padding-top: 0%;
  padding-bottom: 0%;
}
#footer {
  text-align: justify;
}
#Legend {
  z-index: 10;
  padding: 8px 8px;
  border: 6px solid grey;
  position: absolute;
  bottom: 100px;
  height: 28%;
  overflow: scroll;
  width: 6%;
  right: 0%;
  background-color: #ffffff;
  font-weight: bold;
}
#column1 {
  float: left;
  width: 15%;
  padding: 0px;
  height: 30px;
}
#column2 {
  float: left;
  width: 40%;
  padding: 10px;
  height: 30px;
  text-align: center;
  color: royalblue;
```

```
}
#row1{
  content: "";
  display: flex;
  clear: both;
}
#fcol1 {
  float: left;
  width: 40%;
  padding: 0px;
 background-color: lightblue;
}
#fcol2 {
  float: left;
  width: 60%;
  padding: 0px;
  background-color: lightblue;
}
#frow {
  content: "";
  display: flex;
  clear: both;
}
```